HEAT WAVES IN THE WEST AFRICAN SAHEL: NATURE, DRIVERS AND PREDICTABILITY

Kiswendsida Guigma

UNIVERSITY OF SUSSEX

Thesis submitted for the degree of Doctor of Philosophy

DEPARTMENT OF GEOGRAPHY
UNIVERSITY OF SUSSEX
UNITED KINGDOM

February 2021

Abstract

The Sahel in West Africa is a vast semi-arid region stretching from the Atlantic coast to the Red Sea and marks a transition between the Guinean forests and the Sahara desert, home to several millions of people. It is a climatologically hot region with a peak of heat observed in boreal spring before the summer monsoon. However, heatwave research in the region is still in its infancy despite that, as in most regions of the globe, high temperatures have escalated over recent decades as a result of climate change. This thesis builds knowledge on the characteristics, physical understanding and predictability of heatwaves in the Sahel at the weather and intraseasonal scales. These timescales have received little attention from previous work despite being important for operational risk management. The analyses are built on two main datasets including the fifth generation of the European reanalyses (ERA5) and the hindcast of the ECMWF ensemble extended-range forecasting system (ENS-ext).

Sahelian intraseasonal heatwaves are overall short-lived with mean duration between three and five days. Record-breaking events can nonetheless last up to two weeks in some locations. Heatwaves in the Sahel are also characterised by low frequencies of occurrence with typically one to two events a year across most of the region. On the other hand, they are very severe in intensity given that the mean state of the atmosphere is already hot. The eastern and central parts of the Sahel are the most affected by heatwaves in terms of duration, frequency and intensity whereas the proximity to the Atlantic Ocean attenuates extreme heat events in western Sahel.

The physical quantification of heat can be done in considering temperature only or adding other environmental variables to build multivariate thermal indices. The upstream choice of thermal index for heatwave study is important in the Sahel. Indeed, heatwaves sampled using different indices show only moderate synchronicity between them. Besides, the Sahel is characterised by a low concomitance between daytime and nighttime heatwave events, which is a relieving factor when it comes to the impact on health.

Regarding the thermodynamic processes, heat advection and greenhouse effect of moisture are found to be the main underlying causes. Both these processes are made possible by a significant perturbation of the low-level flow, favouring a transport of hotter or more humid air masses towards Sahelian locations. At the large-scale, this circulation anomaly is often associated with convective anomalies in the Guinean region of West Africa, where convection is at its peak during the spring

season. Consequently, the link between heatwaves in the Sahel and tropical modes of variability including the Madden Julian Oscillation (MJO) and the equatorial Rossby (ER) and Kelvin waves (EK), which are important drivers of the Guinean convection, was investigated. The examination reveals that the probability and, to a lesser extent, intensity of Sahelian heatwaves are significantly modulated by the passage of tropical modes over the West African domain. Depending on their convective phases, i.e. either enhanced or suppressed, they can increase or decrease heatwave probability in the region. The modulation is sensitive to the diurnal period and geographical location with nighttime heatwaves more impacted by the modes over eastern Sahel and daytime heatwaves more affected over western Sahel. Among the investigated modes, the MJO was found to have the greatest impact on heatwaves owing to its larger spatial extension and longer periodicity.

The skill of Sahelian heatwave prediction by numerical models was assessed using ENS-ext which is regularly considered as one of the best forecasting systems at the intraseasonal scales. Significant skill was found in the first two to three weeks of the forecast. Longer predictability can be achieved using a "flexible" evaluation i.e. tolerating errors within a given temporal window, especially at the longest lead-times, where even approximate indication of heatwave occurrence is valuable for targeted anticipatory actions. With increasing lead-times, heatwaves are found to be more predictable at night than at day. Interestingly, ENS-ext is able, on one hand, to relatively well predict the local activity of tropical modes over West Africa and, on the other hand, to simulate their observed impact on Sahelian heatwaves. Furthermore, heatwave prediction skill is higher when tropical modes are active, implying that they are good sources of heatwave predictability. As a result, in the future, more precision and longer predictability can be obtained for heatwave prediction in the Sahel in view of the continual improvement in the representation of convection and tropical modes by models.

Given its findings, this thesis has many implications for heatwave risk management in the Sahel across a range of sectors including, but not limited to, health, labour productivity, water and energy.

Supervisors

Prof. Martin Todd
Department of Geography, University of Sussex, United Kingdom

Dr. Yi Wang
Department of Geography, University of Sussex, United Kingdom

Funding
This thesis was generously sponsored by Mr. Peter Carpenter through the African Climate Scholarship at the University of Sussex. Without this funding, this research would not have been possible.

Declaration
I declare that this thesis is my own work, both in concept and execution and that apart from the normal guidance and advice from my supervisors and external collaborators, I have received no assistance except from what has been acknowledged. I declare that neither the ideas nor any particular part of my thesis has been submitted in the past, or is currently being, or is to be submitted for a degree at the University of Sussex or at any other university. Chapters 2, 3 and 4 of this manuscript have been published in Climate Dynamics. I confirm that this above declaration holds true for the publication too, and the co-authorship of my two supervisors and external collaborators (Francoise Guichard, Philippe Peyrille and Dave MacLeod) represent their assistance in improving the papers and advising me through the peer-review process.

Brighton, 11 February 2021

Kiswendsida Guigma

Dedication

This thesis is dedicated to Françoise Guichard and to the victims of terrorism and violence in the Sahel.

List of acronyms

ACASIS - Project on Heatwave Early Warning and their Impact on Health

AMMA – African Monsoon Multidisciplinary Analysis

AEJ – African Easterly jet

AEW - African Easterly Wave

AIRS - Atmospheric Infrared Sounder

AMJ - April-May-June

AT - Apparent Temperature

BEST - Berkeley Earth Surface Temperature

CERES - Clouds and Earth's Radiant Energy System

CMIP – Coupled Model Inter-comparison Project

CORDEX - Coordinated Regional Downscaling Experiment

ECMWF - European Centre for Medium-range Weather Forecasts

EK - Equatorial Kelvin wave

ENS-ext - ECMWF ensemble extended range forecasting system

ENSO - El Niño-Southern Oscillation

EOF - Empirical Orthogonal Function

ER - Equatorial Rossby wave

ERA5 - Fifth generation of the European Reanalyses

FbF/FbA - Forecast-based Financing/ Forecast-based Action

FM - February-March

GHCN - Global Historical Climatology Network

GPCP - Global Precipitation Climatology Project

GSOD - Global Summary of the Day

HEWS - Heat Early Warning System

HI - Heat Index

ITCZ - Intertropical Convergence Zone

ITF – Intertropical Front

LSHW - Large-Scale Heatwave

MJO - Madden-Julian Oscillation

NCEP - National Centers for Environmental Prediction

NET - Net Effective Temperature

OLR - Outgoing Longwave Radiation

SEB - Surface Energy Budget

SEDI - Symmetric Extremal Dependency Index

UTCI - Universal Thermal Comfort Index

WAHL – West African Heat Low

WAM - West African Monsoon

WHO - World Health Organisation

WMO - World Meteorological Organisation

Contents

Chapter 1. Introduction

1.1. Generalities about heatwaves

1.1.1 Emergence of heatwaves in the literature

Climate change has become one of the hottest topics over recent decades at the global level. As early as the 1980s, an emerging consensus was already pointing to a major role of man-made carbon dioxide causing an increase of temperature beyond the natural climate variability (Hansen et al. 1981; WMO N°661). The increasing trend of global temperature has remained on track, with the latest annual report from the US National Oceanic and Atmospheric Administration (NOAA) showing that 2020 has been the second hottest year on record with the global temperature 0.98°C above the twentieth-century average (NOAA 2021). The consequences of this warming on the climate system itself are important and include ice melting especially at the poles (Stammerjohn et al. 2008) and glacial retreat (Xu et al. 2009), sea-level rise (Nerem et al. 2018), changes of oceanic circulation (Meredith et al. 2012) and precipitation patterns (Dore 2005). Furthermore, extreme weather and climate events are more and more frequent (Meehl et al. 2000) and are increasingly linked to climate change (Moore et al. 2015; Mann et al. 2017; Diffenbaugh et al. 2017). The most recurrent extremes include tropical cyclones, heavy rainfall events and sustained periods of extreme heat or heatwaves. The latter are the focus of this PhD research.

Heatwaves are a growing concern for countries worldwide and the literature abounds of cases that have been particularly disastrous. The recent deadliest reported heatwaves are that of Russia in 2010 with more than 55,000 deaths (Barriopedro et al. 2011), Europe in 2003 with about 40,000 deaths (García-Herrera et al. 2010) and India in 2015 with more than 2,200 deaths (Sarath Chandran et al. 2017). Many regions of the world now suffer from heatwaves with events in Australia, South Asia and the Middle East, Europe and Northern America regularly making the headlines. Heatwaves, despite not having a universally accepted definition, are characterised by heat levels significantly higher than usual with the potential to harm human's health and comfort. They can be confined to small areas (of the scale of a city for example), or spread over many countries (Keellings et al. 2018). In terms of observed trend, heatwaves have increased in frequency, spatial extent and duration across most places of the globe (Sharma and Mujumdar 2017; Perkins-Kirkpatrick and Lewis 2020). Likewise, in agreement with global warming, heatwave intensity has also increased over recent years (Perkins et al. 2012). The future evolution of these extremes is also worrying. Several published works indeed warn of more frequent, wider spread and more severe heatwaves in decades to come (e.g.

Russo et al. 2014; Cowan et al. 2014; Im et al. 2017; Rohini et al. 2019). This challenges governments and non-governmental organisations across the globe to undertake actions that will help mitigate heatwave harmful impacts.

1.1.2 Negative impacts of heatwaves

These impacts are primarily seen in the health sector. Severe heatwaves are often associated with increased mortality, which in the most extreme cases, can turn to become public health disasters (Keatinge 2003; Gasparrini and Armstrong 2011). Besides the mortality, heatwaves can cause a surge of hospital admissions putting a strain on medical services (Toloo et al. 2014; Gronlund et al. 2014; Goldie et al. 2017; van Loenhout et al. 2018; Davis and Novicoff 2018). The diagnoses reveal that these admissions are related to heatstroke and sunstroke (Hopp et al. 2018), respiratory (Anderson et al. 2013), cardiovascular (Yin and Wang 2017) and renal diseases (Borg et al. 2017) as well as mental disorders (Trang et al. 2016). Even though heat affects almost everyone, some social groups are more vulnerable than others. Thus, the elderly (Oudin Åström et al. 2011; Liss et al. 2017; Cheng et al. 2018) and young children (Johnson et al. 2005; Xu et al. 2014; Nicholls and Strengers 2018) are generally the most at risk during heatwave events. It should also be noted that the period of the day during which heatwaves occur has differential impacts on health, with concurrent daytime and nighttime events being the most dangerous since they do not allow any respite to the body (Fischer and Schär 2010; Kueh et al. 2017; Mukherjee and Mishra 2018).

Besides health, a handful of other socio-economic sectors can be impacted. Extreme heat events are indeed associated with an increased strain on the power (Pechan and Eisenack 2014; Cook et al. 2015; Añel et al. 2017), water (van der Velde et al. 2010) and transport infrastructures (Lemonsu et al. 2015). Ecosystem services (Depietri et al. 2013) and tourism (Moreno 2010; Koutroulis et al. 2018) can also be perturbed. Efforts should therefore be dedicated to these different sectors in order to keep to minimum the heat-related disturbances especially in the least developed countries where they are in a relatively fragile state.

1.1.3 Insufficient heatwave studies in the least developed countries

Unfortunately it is precisely in these countries that heatwaves have received the least attention. From a global review by Campbell et al. (2018), it appears that, in addition to the fragility of their

economies, they are likely to experience the most extreme heatwaves in the future, and yet they are under (or not) represented in the current heatwave literature. This urges the scientific community to have more regard for heatwaves in these regions. Almost all heatwave research areas need to be addressed or deepened: evidentiating the very existence of heatwaves, describing their statistical characteristics from historical records, understanding their physical mechanisms, analysing their short to medium term predictability as well as their future evolution under different greenhouse gas emission pathways. How (much) heatwaves impact societies and economies in the least developed countries should also be meticulously investigated as this might differ from the findings in high-income countries.

Of these least developed countries, those in Africa (sub-Saharan Africa in particular) are regularly cited as hotspots of present and future climate with heatwaves likely to worsen in the coming decades (Russo et al. 2016). Surprisingly, despite evidence from historical records that several severe heatwaves have hit sub-Saharan Africa in the past, they are overlooked in the global emergency events database (EM-DAT) with only two events reported between 1900 and 2019, to be compared with 83 events in Europe just between 1980 and 2019 (Harrington and Otto 2020). Various reasons may explain this omission of African heatwaves in the global literature. Africa has a relatively warm climate with high levels of heat all year round, which may make periods of exceptionally hotter situations perhaps less striking. In addition, many heat-related casualties go unreported at the national levels as a result of a lack of strong institutional policy in that regard. Local expertise is also missing in many countries, making heat-related studies tributary to western countries for both funding and human resources.

One African region which has been particularly affected by climate shocks is the West African Sahel. The region has indeed been plagued by prolonged droughts resulting in famines (Meillassoux 1974; Charney 1975; Janicot et al. 1996; Cook 2008), torrential rains leading to devastating floods and damages to the built and natural environments (Lafore et al. 2017; Taylor et al. 2017; Salack et al. 2018; Tazen et al. 2019), as well as severe dust storms (Middleton 1985; Tulet et al. 2008; Klose et al. 2010). The Sahel is also characterised by the high variability of its seasonal rainfall at various time scales (Sultan et al. 2003; Parker et al. 2005; Nicholson and Webster 2007; Poan et al. 2016) which occurs in boreal summer. These three main thematics (drought, rainfall variability and dust) have retained the largest part of climate-related publications over the region. As a result, despite being among the hottest regions of the globe, the Sahel has not benefited from numerous studies on heatwaves. This thesis therefore intends to contribute to filling this knowledge gap.

1.2. General presentation of the Sahel

There is no consensual physical delimitation of the Sahel. It is generally regarded as the semi-arid region marking the transition between the Sudanian Savanna and the Sahara desert, stretching from the Atlantic Ocean to the Red Sea. In this study, it is taken as the continental domain delimited by the coordinates 20°W, 30°E, 10°N and 20°N. It is characterised by an overall flat topography, with mean altitude typically between 200 and 500 m (Sylla et al. 2012).

Lying between the equatorial and subtropical zones, the Sahel has a relatively complex climate system. A brief description of this system is made here, starting from the global circulation, before focusing on more local features. At the global scale, solar heating is known as the primary source of the energy found on earth. This energy is however received differentially at the earth surface, with the equatorial regions being more heated than the poles. Atmospheric (and oceanic) motions are thus triggered to evenly redistribute this energy across the earth. Given its buoyancy, the warm (and humid) equatorial air rises, whereas off-equatorial air masses converge at the surface toward the equator to replace the rising air (by continuity). The large-scale convergence and the uplifting near the equator engender an area of deep convection where the earth maximum precipitation is observed: the Intertropical Convergence Zone (ITCZ). As the air rises, near the tropopause (about 10-15 km in the tropics), it loses buoyancy and is thus constrained poleward. The poleward motion progressively cools the air, and given the increasing effect of the Coriolis force[1] away from the equator, it is deflected eastward, forming the subtropical jets (approximately at the 30° parallel of each hemisphere -horse latitudes-). As the air is by then cold (heavy), it descends and warms up adiabatically, leading to a decrease of its relative humidity. This subsidence inhibits convection, engendering some of the world largest deserts (e.g. the Sahara). At the surface, the dry and cold air diverges given the subsidence, and is directed back toward the equatorial zone, closing the loop. This surface equatorward motion is also affected by the Coriolis force, leading to a northeasterly flow (trade wind). The overall circulation is thus made up of two "twin loops", one in each hemisphere. They are called Hadley cells, and comprise each an ascending branch near the equator and a descending branch located near 30° (Fig. 1.1).

[1] Coriolis force: An apparent force created by the earth's rotation, which, as seen by an observer on the earth, deflects moving air to the right in the northern hemisphere and to the left in the southern hemisphere.

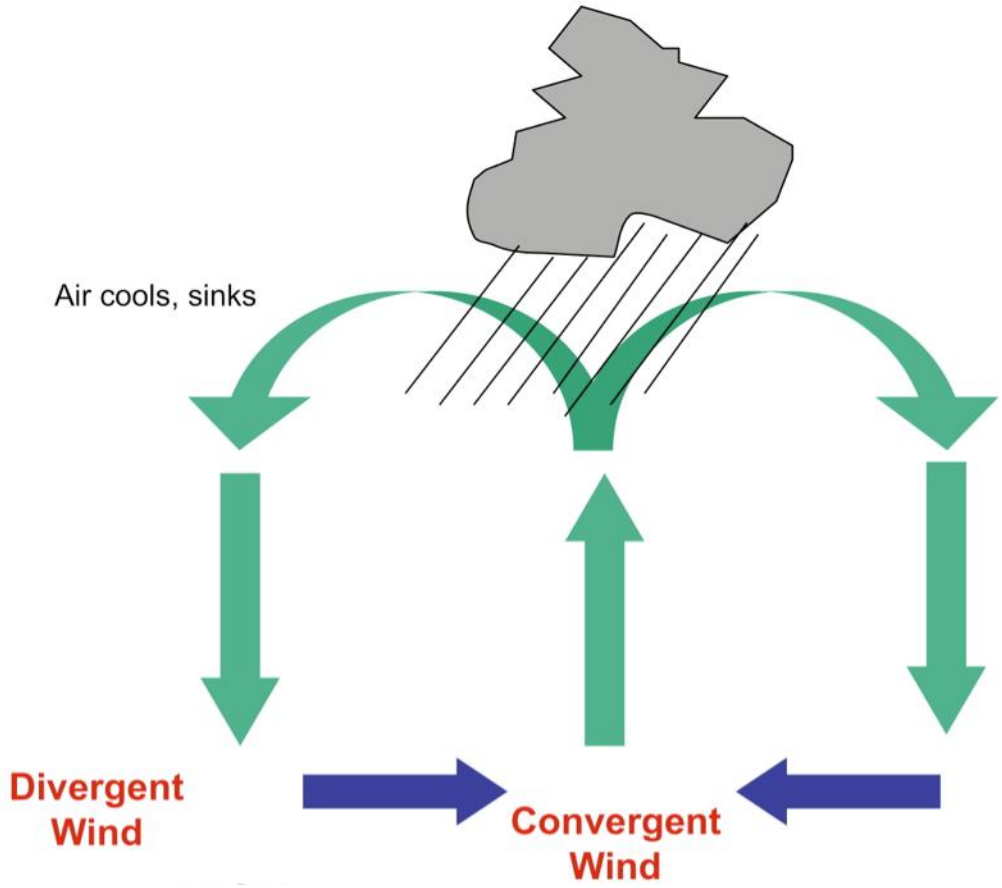

Fig. 1.1 Schematic of the Hadley cells.

The Hadley cells and the ITCZ are less well defined over lands, as in addition to surface convergence, other regional features such as local atmospheric jets and waves, proximity to the oceans, terrain-induced convective systems, moisture recycling, and spatiotemporal variability of land cover and albedo distort the expected patterns (Dezfuli 2017). As a result, over Africa, the notion of Intertropical Front (ITF, also called Intertropical Discontinuity ITD) is often used instead to clearly designate the surface convergence (Lele and Lamb 2010). The ITF, over West Africa, corresponds to the frontline between the trade winds from the northern hemisphere (northeasterly winds, called Harmattan) and those from the southern hemisphere, which are originally southeasterly but progressively turn southwesterly after crossing the equator, as a result of a directional change of the Coriolis force. The southwesterly flow is termed as monsoon wind as it brings large quantities of moisture from the Gulf of Guinea into continental West Africa. The area of maximum convection and rainfall is located 400 to 500 km south to the ITF, since moisture is moderate near the ITF (given the Harmattan winds).

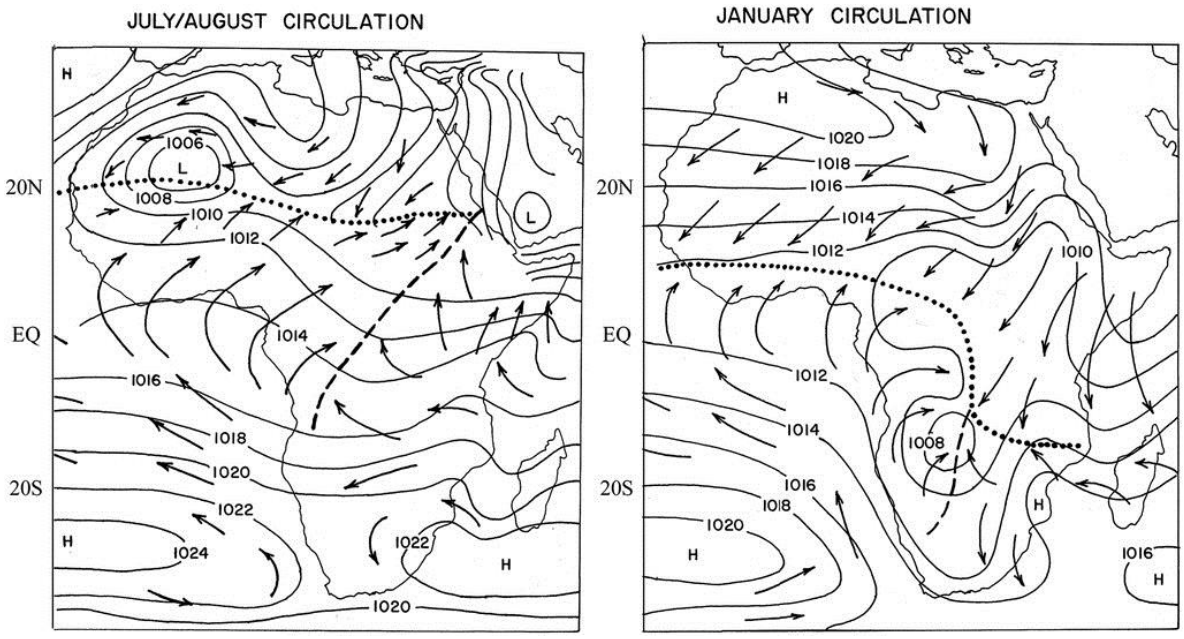

Fig. 1.2 The ITF (dotted line) over Africa in July–August and January. Arrows represent near surface wind flow and contours mean sea level pressure. Source: Nicholson 2011.

As already mentioned, the general circulation described above is a consequence of the differential heating of the earth by the sun. Given the revolution of the earth in orbit around the sun, this differential heating changes throughout the year, and this also affects the atmospheric circulation and the ITCZ (and ITF over West Africa). In boreal winter, because of the earth's axis tilt, the southern (northern) hemisphere receives its maximum (minimum) heating. As a result, the ITCZ is located at its southernmost position. Over West Africa, the ITF is found near 5°N (Fig. 1.2). Consequently, the Sahel is under the influence of the Harmattan winds which carry cool, dry and dusty air masses from the Sahara toward the Gulf of Guinea. It is the driest and coolest season of the year in the Sahel, with monthly average minimum (maximum) temperature near 15C (30C) across most of the Sahel (Figs. 1.3 & 1.4). These values are relatively high, implying a quasi-permanent warm state all year round.

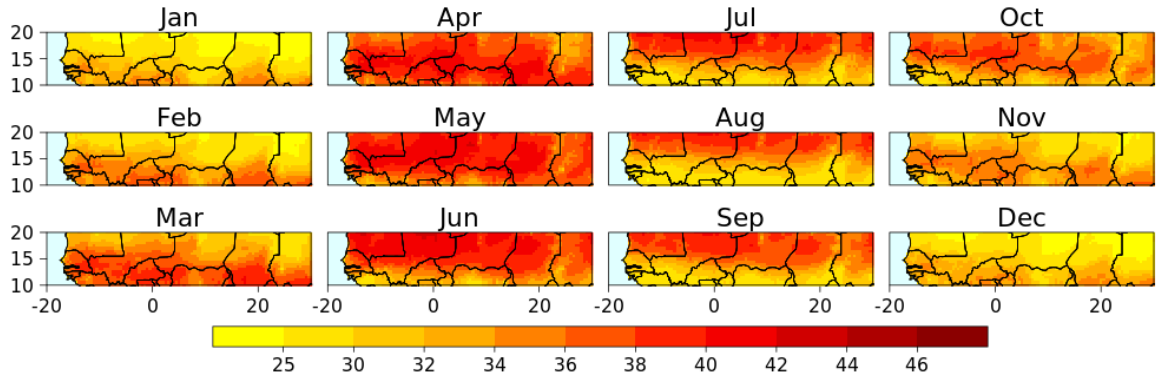

Fig. 1.3 Annual cycle of daily maximum temperature in the Sahel using ERA5 reanalysis. Units in C.

In spring, the earth inclination focalises the solar heating between 10 and 15°N (Lavaysse et al. 2009), which, combined with favourable albedo, ranks the Sahel as the hottest area of West Africa. The Sahel therefore coincides with the West African Heat Low (WAHL), a dynamic feature highlighting areas of high surface temperatures and low pressures (Lavaysse et al. 2009). Temperatures then often exceed 40C during the day (Fig. 1.3) and 25C during the night (Fig. 1.4). The ITF also shifts northward to reach the Sahel such that rainfall is maximum in the Guinean sector of West Africa: this marks the Guinean phase of the West African Monsoon (WAM). Given that the ITF lies within the Sahel, near surface winds are generally weak (Guichard et al. 2009), but an important variability is observed as monsoonal winds often surge into the Sahel (Couvreux et al. 2010), advecting moisture in the Sahel, with a potential greenhouse effect to further heat up the region. A comparison of Fig. 1.3 vs Fig. 1.4 reveals that maximum temperatures reach their peak (in April-May) before minimum temperatures (May-June). The main reason is the higher sensitivity of minimum temperatures to moisture, which becomes important in the Sahel only in late spring as the ITF progresses northward.

In summer, the WAHL and the ITF migrate to Saharan latitudes (Fig. 1.2). The large thermal gradient between the Sahara and the Gulf of Guinea generates the African Easterly Jet (AEJ) in the mid-tropospheric levels (Cook 1999). In its turn, through instability, the AEJ causes westward propagating weather disturbances called African Easterly Waves (AEWs), which are responsible for organised convection in the form of squall lines (Burpee 1972, Reed et al. 1988, Fink and Reiner 2003). The exact origin of AEWs is however still the subject of ongoing research. The Sahel therefore becomes the region of maximum precipitation in West Africa (Sahelian phase of the WAM), with rainfall totals increasing from 200 mm at the Sahara border to 600 mm in the south (Nicholson 2013). Finally, in autumn, the WAHL and ITF withdraw back to Sahelian latitudes. Subsequently, the Sahel experiences its second thermal peak of the year, which is however much less pronounced than that observed in spring (Figs. 1.3 & 1.4). Likewise, a second rainy season is observed over the Guinean sector.

Summarily, the climate of the Sahel consists of two main seasons engendered by the meridional oscillation of the ITF: a relatively short rainy season in summer and a dry season over the rest of the year. The dry season comprises a relatively cool period in winter and two thermal peaks observed just prior to and after the summer rainy season with the first peak being the most important. Given the large reliance of the Sahelian populations on rainfall for agriculture (the main activity in the region) and the large variability of the rainy season at all timescales, most scientific projects in the region

have focused on the WAM, the most important to date being the African Monsoon Multidisciplinary Analysis (AMMA). However, hot conditions are quasi-permanent over the Sahel, especially in spring, where days during which temperatures soar largely above their mean values are potentially harmful. The situation is worsened when these days are consecutive, forming heatwave events. These events were, however, practically absent from Sahelian literature until the 2010s. It was to fill this gap, and inspired by the growing evidence of the negative impacts of heatwaves in Europe, that the French-led Sahelian Heatwave Early Warning and their Impact on Health (ACASIS) project was initiated. Thanks to this project and other isolated works, a comprehensive study of Sahelian heatwaves has been undertaken leading to the first scientific insights on these hazards.

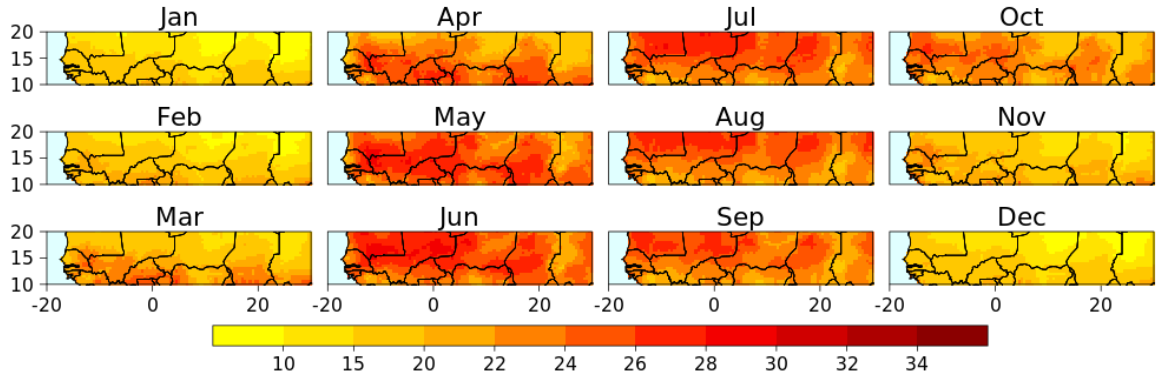

Fig. 1.4. Same as Fig. 1.3 but for daily minimum temperature.

1.3. Review of Sahelian heatwave literature

The existing literature on extreme heat over the Sahel can be categorised into three major areas: characterisation, physical mechanisms and future projections.

1.3.1 Characteristics of heatwaves in the Sahel

Most papers discussing the long-term evolution of temperature over the Sahel agree on a significant warming over the last decades. New et al. (2006), examining observed temperature timeseries over West Africa between 1961 and 2000, claimed that a large proportion of stations showed statistically significant upward trends for both minimum and maximum temperatures. Moreover, they found that the increase of very hot days is accompanied by a similar decrease of very cold days inducing a stationarity of the diurnal temperature range. The outcome of this is then a global hotter climate. Guichard et al. (2012) from observational and reanalyses datasets also concluded of a warming in the Sahel over the last 60 years. Considering the diurnal cycle, the increase is differential, with nights

warming faster than days. They also made the point that during the warmest season (boreal spring), the variability at inter-annual scale is weaker than at multi-decadal scale. A similar result is achieved by Fontaine et al. (2013), who evaluate to 1°–3C the warming appearing by the mid-1960s over the Sahara and Sahel. Furthermore, this warming goes with higher (lesser) frequency of warm (cold) temperatures as mentioned by New et al. (2006). In addition, Fontaine et al. (2013) defined heatwaves at regional scale over the eastern and western Sahel, and realized that over recent decades, they are becoming longer lasting and more frequent. Rising trends of the maximum and minimum temperature anomalies, which have been also more and more pronounced since the past 60 years, are what Ringard et al. (2016) also found over the entire West Africa at both regional and local scales. Their analysis is built on station-based indices over the 1900–2012 period. Additionally, they further supported the larger intensification of nocturnal temperature warming over the second half of the 20th century as compared to that of daytime temperature. With different data, in occurrence NCEP and ERA-Interim reanalyses, as well as outputs from CORDEX models, Adeniyi and Oyekola (2017) confirm that the magnitude of heatwaves is increasing. The conclusions of Oueslati et al. (2017) also abide by the upward trend of heatwave frequency. They however used a different heat measure than that of other studies, the US heat-index (HI) which includes the effect of moisture in the perception of heat. As a result, it appears interesting to widen this approach by incorporating other environmental variables that also affect heat perception (radiation and wind for example). In a spatiotemporal point of view, Oueslati et al. (2017) also found Sahelian heatwaves to become longer lasting, covering larger areas, and reaching higher intensities. This is consistent with Ceccherini et al. (2017) which made use of the daily Heat Wave Magnitude Index (HWMId). They suggested that, between 2006 and 2015 especially, an increase of the frequency and the spatial coverage of extreme heatwaves has been evident. Concatenating the Global Historical Climatology Network (GHCN) and Global Surface Summary of the Day (GSOD) databases, Moron et al. (2016) also concluded of an increase of the daily minimum and maximum temperature. They also mentioned that heat spells tend to last longer, with almost constantly positive anomalies since the mid-1990s. This paper also tried to explain this evolution at different timescales. Thus, the low-frequency (>8 years) variations are attributed to the regional-scale mark of global warming, whilst the high-frequency (<8 years) variations are linked to a delayed remote impact of El Niño–Southern Oscillation (ENSO) events over the region, with warm (cold) anomalies tending to follow warm (cold) ENSO events. Finally, through a special filtering method, Barbier et al. (2018) were able to retain synoptic and intraseasonal scale heatwaves and showed that during spring and early summer, the deeper one gets into the season, the shorter and less frequent are heatwaves. This is however a paradoxical finding since temperatures are higher closer to

the monsoon season than at the beginning of spring. Unfortunately, no other work has focused on these timescales to discuss these findings.

Summarily, the characterisation studies largely agree on the increasing threat that heatwaves pose to Sahelian populations through the increase of their frequency, the amplification of their magnitude, their increasingly large spatial extent and lasting nature. Sahelian heatwaves have been even more threatening over recent decades.

1.3.2 Physical mechanisms

The literature on physical mechanisms shaping heatwaves in the Sahel is less abounding than that on statistical characteristics. Fontaine et al. (2013) is a precursor in this area. Through compositing weather patterns over regional-scale heatwave events, they established that Sahelian heatwaves are associated with positive low-level temperature anomalies over the Sahel and Sahara as well as a low and mid-level cyclonic rotation over Morocco. This large-scale dynamics is associated with a Rossby wave pattern which mitigates low-level northeasterlies (Harmattan). Additionally, in terms of moisture, wetter and dryer patterns are found respectively west and east to 0°, while the vertical velocity shows an upward (downward) anomaly above the western (eastern) regions associated with the Rossby wave pattern. Short Rossby waves would therefore, according to the authors, play an important role given the coherence of these patterns with a potential jet stream deformation. Sambou et al. (2020) showed that heatwaves in Senegal, the westernmost part of the Sahel, are associated with a positive sea-level pressure anomaly centred near the strait of Gibraltar. This anomalous pressure system promotes easterly and northeasterly wind anomaly which carries continental hot air towards the coast. The thermodynamic causes of Sahelian heatwaves have been investigated by Oueslati et al. (2017) through a case study (of the April 2010 event). Their main finding is that the greenhouse effect of moisture is important especially for nighttime heatwaves. Atmospheric circulation plays an important role by advecting this moisture from the Gulf of Guinea. In addition, they supported the ENSO modulation of heatwaves at the interannual timescales (initially claimed by Moron et al. (2016)), by showing that warm ENSO events increase water vapour feedback in the region. The dominant role of water vapour in the April 2010 nighttime heatwave is further proved by Largeron et al. (2020) through a modelling study. They furthermore pointed to the early northward incursion of monsoonal winds and the well-known tropical plume phenomenon (which is connected to extratropical Rossby waves) as being the dynamical causes through which important moisture was brought into the Sahel.

So, the main conclusions of these studies are the potential impact of mid-latitude weather systems on Sahelian heatwaves and the leading role played by water vapour mostly on nighttime events. They remained relatively evasive on the leading mechanisms of daytime heatwaves and did not systematically assess the differences across different subregions of the Sahel. In addition, in terms of large-scale dynamics, besides extra-tropical weather systems, previous non-heatwave-related research suggests other potential drivers which have not been explored.

The spring season, during which temperatures reach their maximum in the Sahel, also corresponds to the Guinean phase of the WAM as shown in Section 1.2. Actually, the variability of the Sahel is intrinsically linked to that of Equatorial Africa, especially just before and after the monsoon season. Thus, Kalapureddy et al. (2010) found that the synoptic variability over the Sahel during the pre- (April to June) and post-monsoon (October and November) is controlled by monsoon surges with a periodicity similar to that of the well-known AEWs (3-5 days). According to Couvreux et al. (2010), these monsoon surges may be stationary or westward moving along with the AEWs. In the same order of ideas, Mera et al. (2014) also showed that synoptic and subseasonal circulation disturbances lead to an influx of moisture from the Gulf of Guinea into the Sahel (and could therefore lead to a similar greenhouse effect as the April 2010 nighttime heatwave). These circulations are essentially controlled by extratropical cyclones, but also by equatorial Kelvin (EK) and Rossby (ER) waves, and possibly the Madden-Julian oscillation (MJO). These waves could serve as connectors between Sahelian heatwaves and the Guinean phase of the WAM, since they are the main drivers of the monsoon at the intraseasonal scale, as stressed by Berhane et al. (2015). There is also a benefit in these modes contributing to heatwaves in the Sahel, as they have the potential to provide intraseasonal predictability.

1.3.3 Heatwave prediction

The last area of scientific research on extreme heat in the Sahel addresses their prediction at different timescales. At weather through to seasonal scales, the literature is extremely scarce. Only one single paper with a total focus on the Sahel has been published on the topic. This paper (Batté et al. 2018) evaluated two coupled forecasting systems (one operational and the other experimental used in the WMO's S2S project) both based on the CNRM-CM coupled global climate model at seasonal and intraseasonal scales. Using the ERA-Interim reanalysis as reference, they found their models, at the seasonal scale, to have a significant (low) skill in predicting interannual anomalies when the evaluation is conducted regional (gridpoint)-wise. As for the intraseasonal predictability, it showed

skill only for the deterministic range (up to seven days). Additionally, although not Sahel-focused, the results of Perez et al. (2018) revealed that the ECMWF model has a good skill at predicting heatwaves in the Sahel in the short term (first week of the forecast).

The evolution of Sahelian heatwaves at climate timescales has benefited from more attention. According to CMIP5 projections analysed by Ringard et al. (2016), in any scenario, Sahelian heatwaves will have a significant increasing trend in the future. Russo et al. (2016) postulated that in the most severe scenario, by 2040, unusual heatwave events will occur on a regular basis in the Sahel. Dosio (2017), under the same scenario and using the 1981-2010 period as a reference estimates to +3.5 to +6C the increase of temperature over the region starting from around 2060. Another study by Déqué et al. (2017) claimed that, under a global warming by 2C, the occurrence of heatwaves in the Sahel will increase by a factor 10 if defined with the same temperature threshold in the reference climate and in the scenario.

From these studies as well as those with a more global scope, there is a relatively good level of certainty that heatwaves across the Sahel will be worse in intensity, frequency and duration in the very next decades. Countries of the region and their partners are therefore urged to undertake both strategic and tactical actions to relieve their populations from the burden of these extremes. This requires a deep knowledge on the hazard itself, which is not yet satisfactorily achieved, given the numerous research gaps that need to be filled.

1.4. Research questions

Many research gaps not (or not fully) addressed by the existing literature can be highlighted below. At first instance, one global objective in climate research is to have a holistic understanding of the climate system across all timescales in order to deliver seamless predictions of the earth system (Palmer et al. 2008). In this way, the intraseasonal scale has attracted much attention in recent years and offers new opportunities for climate risk management (Webster and Jian 2011). The existing literature on Sahelian heatwaves has however not delved much on the topic, prioritising the interannual and climate scales. This then calls for a deeper investigation of heatwaves at the intraseasonal scale in the region.

Besides, as in many regions, the vast majority of studies have used temperature as a heat measure with only two (Oueslati et al. 2017; Sambou et al. 2020) taking into account the effect of moisture. However, other environmental parameters, such as wind and solar radiation, play an important role

in the perception of heat, and it would be interesting to see how complexifying the heat definition with these parameters affects the nature of heatwaves.

There has also been no sufficient exploration of the physical causes of heatwaves. For example, there is no clear evaluation of how the physics change between different sub-domains of the Sahel (e.g. the western vs eastern Sahel) as well as their seasonality. In addition, the physical causes of daytime heatwaves remain elusive and should therefore be more assessed. Furthermore, in terms of large-scale dynamics, no paper has addressed the impact that the Guinean phase of the WAM could play on Sahelian heatwaves, despite a potential connection between the two, suggested by anterior literature (see Section 1.3.2). Research in this route is interesting as it could add predictability to Sahelian heatwaves. The predictability itself has not been widely investigated, especially at the intraseasonal horizons. It will therefore be important to strengthen research on the topic, taking care to consider potential sources of predictability.

Because of the above complication, the present thesis seeks to answer the following main question: ***How predictable are Sahelian heatwaves from weather to intraseasonal timescales?***

Although seeming simplistic, answering this research question is not straightforward. It indeed raises new questions that need to be addressed in order to give more clarity to the final answer. From the outset, it is necessary to clearly delineate the object of the study (i.e. intraseasonal-scale heatwaves) and apprehend its nature in terms of both statistical and physical properties. Hence the first research sub-question: ***What are intraseasonal-scale heatwaves in the Sahel and what are their underpinning thermodynamics?***

Then, it is important to explore their drivers, i.e. the large-scale conditions that sustain their thermodynamic ingredients for prolonged periods. This leads to the question: ***What are the large-scale drivers of Sahelian heatwaves?***

Finally, since the ultimate interest is in the prediction of heatwaves, it is necessary to assess the skill of the state-of-the-art models in predicting them. This step benefits from the answers provided to the two previous sub-questions, in a view of extending the current limits of the prediction skill, based on the knowledge on the drivers of the hazard. The question is thus: ***what is the prediction skill of heatwaves and is there a potential for improvement considering their physical drivers?***

1.5. How significant is the contribution of this thesis to knowledge?

The Sahel is home to dozens of millions of people who have one of the fastest growth rates of the planet (May et al. 2017). With extreme heat being a growing threat in this already hot region, mitigation actions are urgently required. Preventive actions should be taken at different timescales. This study paves the way for heatwave risk management in the region at the short and medium terms i.e. from a few days to a few months. These timeframes are especially relevant for humanitarian preventive interventions, but their effectiveness is contingent on sound understanding and skilful predictions of the hazards themselves. Very few is however known about Sahelian heatwaves at weather and intraseasonal timescales. The present thesis builds knowledge on this issue. It has a thorough approach to the physical science of heatwaves by examining their nature, drivers and predictability. It also makes connections between each of these aspects, such that they are well sequenced with a logical interdependence. In addition, it helps in closing the knowledge gap in tropical and low-income regions' heatwaves and therefore in a more general way, contributes to a better understanding of the earth's climate system.

1.6. Description of each chapter

Each of the three research sub-questions is addressed in the form of a research paper.

The first question (*what are intraseasonal-scale heatwaves in the Sahel and what are their underpinning thermodynamics?*) is addressed in chapter 2. Five distinct heat measures, combining different environmental variables including temperature, moisture, wind and solar radiation, have been used. Previous studies in the Sahel have focused mainly on temperature alone, while there is evidence from other regions that the choice of heat measure (also termed as thermal index) has important implications for the downstream results (Heo and Bell 2019). It is therefore important to assess the extent to which the nature of Sahelian heatwaves (characteristics and thermodynamics) is sensitive to the very measure of the heat itself. As the focus of this research is on the intraseasonal scale, the timeseries of the thermal indices as well as that of the physical variables were high-pass filtered to retain intraseasonal variability. A statistical analysis of heatwaves detected from these intraseasonal signals was then conducted to characterise them in terms of intensity, duration and frequency. Likewise, an energy budget analysis was used to determine the thermodynamic processes that locally shape these extremes at the intraseasonal scale. Special attention was paid to the difference of both statistical and thermodynamic characteristics of heatwaves across the five thermal indices. This provided a hint into their potential large-scale drivers (Chapter 3).

The identified local thermodynamic processes were used to inform the investigation of the second issue of the thesis (*what are the large-scale drivers of Sahelian heatwaves?*), developed in Chapter 3. The large-scale drivers question was partly addressed by previous work, which suggested a potential role of mid-latitude weather systems (Fontaine et al. 2013). However, considering previous literature on the WAM, further supported by the findings on heatwave thermodynamics, it appeared that the intraseasonal drivers of the Guinean phase of the WAM could also, by extension, exert a control on Sahelian heatwaves. These drivers, also active in other tropical regions (hence their name tropical modes of variability), include the MJO and the convectively coupled equatorial waves. The task in this part of the thesis thus consisted in assessing whether tropical modes significantly impact Sahelian heatwaves. To carry out this task, tropical modes were first identified based on a method pioneered by Riley et al. (2011), which allows to estimate their activity at a given location. Then, the statistical study of the occurrence and intensity of heatwaves versus the activity of tropical modes allowed the assessment of the relationship between the two. A case study of a major heatwave event was also conducted to bolster the findings. The understanding of the drivers was then used to inform the assessment of the skill of numerical models at predicting heatwaves.

The third research question (*what is the prediction skill of heatwaves and is there a potential for improvement considering their physical drivers?*) was lastly addressed in Chapter 4 using the ECMWF ensemble extended-range forecasting system (ENS-ext) hindcast, as this model is regularly reckoned as the best model in many model-intercomparison studies (de Andrade et al. 2019). The hindcast covers the past 20 years with a forecast horizon of 46 days. The evaluation was performed through three major steps. The first step consisted in a simple evaluation of how good the model is at predicting Sahelian heatwaves. Given the extreme nature of heatwaves, a special evaluation metric, the Symmetric Extremal Dependency Index (SEDI) was used as more generic metrics degenerate when it comes to rare events. The second step of the evaluation looked at the quality of the representation by the model of (i) the physical drivers on the one hand and (ii) the relationship between these drivers and heatwaves on the other hand. It is indeed demonstrated that one prerequisite for a model to be able to draw predictability of a hazard from its physical drivers is to first be able to simulate both the driver and its link to the hazard (Marshall et al. 2013). Finally, to test whether a given driver of heatwave variability is also a source of predictability, the skill of heatwave prediction was compared between instances where the model forecasts this driver to be active versus instances where it was forecast to be inactive. The conclusions were reinforced through the case study of the prediction skill of a heatwave event.

Chapter 5 brings the findings of all these papers together and elaborates on their implication for operational risk management before discussing the next steps for heatwave research in the Sahel.

Chapter 2. Characteristics and thermodynamics of Sahelian heatwaves analysed using various thermal indices

Reproduced with the permission of Springer (https://link.springer.com/article/10.1007/s00382-020-05438-5)

Characteristics and thermodynamics of Sahelian Heatwaves analysed using various thermal indices

Kiswendsida H. Guigma[1*], Martin Todd[1], Yi Wang[1*]

[1]University of Sussex, Brighton. UK

[*]Corresponding authors:

Email addresses: k.guigma@sussex.ac.uk (K. Guigma), Yi.Wang@sussex.ac.uk (Y. Wang)

Abstract

Prolonged periods of extreme heat also known as heatwaves are a growing concern in a changing climate. Over the Sahel, a hot and semi-arid region in West Africa, they are still relatively poorly understood and managed. In this research, five multivariate thermal indices derived from the ERA5 database were used to characterize Sahelian heatwaves for statistical analysis and as a sampling basis to investigate their underlying thermodynamic causes. Results show that on average most locations in the Sahel suffer from one or two heatwaves a year, lasting three to five days, but with severe magnitude. The eastern Sahel is more at risk than the west, experiencing more frequent and longer lasting events. Despite similar statistics of intensity, duration and frequency across the heatwave indices, for a given diurnal phase, there is surprisingly low agreement in the timing of events. Furthermore daytime and nighttime heatwaves have little synchronicity. In terms of associated thermodynamic processes, heat advection and the greenhouse effect of moisture are identified as the main causes of Sahelian heatwaves. The processes are nevertheless sensitive to the indices, consequence of the distinctness of their respective samples. Therefore, attention should be given to the choice of either index in operational monitoring and forecasting of heatwaves. This will allow to effectively target different exposed socio-economic groups and resultantly enhance the efficiency of early warning systems.

Keywords: heatwaves, Sahel, thermal indices, simultaneousness, thermodynamic processes.

2.1. Introduction

Heatwaves, extended periods of extreme heat (Gasparrini and Armstrong 2011), are increasingly recognised as a major hazard to the society, with impacts directly on human health (e.g. Guirguis et al. 2013; Arbuthnott and Hajat 2017) and important socio-economic sectors, including agriculture (Smoyer-Tomic et al. 2003), energy (Añel et al. 2017), transport (Palin et al. 2013), infrastructure (Chapman et al. 2013) and tourism (Perry 2000). Recent illustrative examples of heatwaves that have caused major loss of life and global impacts through commodity supply chains include Russia in 2010 (estimated 55,000 deaths, Barriopedro et al. 2011) and Europe in 2003 (estimated 40,000 deaths, García-Herrera et al. 2010; Miralles et al. 2014). Indeed, in Australia, heatwaves have been identified as the deadliest natural hazard (Coates et al. 2014). Under a warming climate there is clear evidence that heat extremes have been increasing in recent decades (Hartmann et al. 2013), and are likely to continue to do so under all plausible greenhouse gas emission trajectories (Collins et al. 2013).

The Sahel region of West Africa is especially vulnerable to heatwaves with mean temperatures and heatwave risks peaking in the spring and autumn seasons immediately prior to and following the summer monsoon (Guichard et al. 2009). In addition, the population of the Sahel is extremely vulnerable to climate shocks due to dependence on climate sensitive sectors (e.g. agriculture), widespread poverty and inadequate provision of health services amongst others (e.g. Davidson et al. 2003; Tschakert 2007). However, the literature on the Sahel's climate and society focuses overwhelmingly on rainfall variability and its societal impact, and much less on the causes and impacts of extreme heat. Yet, like other regions, there are clear upward trends in Sahelian temperatures (e.g. Guichard 2014; Moron et al. 2016), most notably during nighttime. Recent studies have shown upward trends in duration, frequency and intensity of heatwave events over the past decades (Fontaine et al. 2013; Moron et al. 2016; Ceccherini et al. 2017; Barbier et al. 2018) and future projections also show a growing risk of extreme heat in the region (e.g. Nangombe et al. 2019; Rohat et al. 2019). However, some contradictory evidence of unchanged frequency exists (Adeniyi and Oyekola 2017), which may be related to the choice of heatwave index.

The negative impacts of extreme heat can, nevertheless, be mitigated, based on skilful forecasts (e.g. Ebi et al. 2004; Masato et al. 2015; Lee et al. 2016). Heatwave-health early warning systems are being developed in a number of countries, guided by the WMO-WHO (2015). Further, complementing national government systems, in the humanitarian sector, systematic approaches to using weather/climate forecasts in risk management called Forecast-Based Action (FbA) and Financing (FbF) are being developed and implemented by the Red Cross/Red Crescent Society amongst others (Perez et al. 2018; Wilkinson et al. 2018), and are being applied to heatwave hazards. The relevant meteorological timescales for an efficient implementation of these plans are the synoptic and

intraseasonal scales. In the Sahel, the ACASIS (Sahelian heatwave early warning and their impacts on health) project advanced the scientific evidence of drivers and impacts of heatwaves (https://acasis.locean-ipsl.upmc.fr/). Heatwaves have been routinely monitored by two national meteorological services in the Sahel, namely in Burkina Faso and Senegal. Effective forecasting and risk management require nevertheless a clear definition and understanding of heatwave processes, especially at the short (synoptic and intraseasonal) timescales.

There is no conventionally accepted definition of a heatwave (Souch and Grimmond 2006). Various heatwave indices have been proposed, which often combine various environmental variables (humidity, wind and solar radiation) to represent the link between the physical phenomenon (heat) and the physiological issues (health or comfort) (e.g. Macpherson 1962; Cheng et al. 2012; de Freitas and Grigorieva 2015, 2017). Further, the selection of thresholds of index intensity, duration and spatial extent varies across the literature and operational systems (e.g. Nairn and Fawcett; Robinson 2001; Zhang et al. 2012; Perkins and Alexander 2012; Smith et al. 2013; Perkins 2015; Gachon et al. 2016; Xu et al. 2016, 2017). However, multiple heatwave indices complicate both 1) Scientific analysis as the heatwave event samples and underpinning thermodynamic processes may vary. 2) Monitoring and prediction and early warning under conditions where predictability and the link to health outcomes varies between indices.

Because of above complication, this paper has two main scientific objectives: (1) to compare the statistical characteristics of high-frequency heatwaves in the Sahel using diverse multivariate thermal indices (see methods in Section 2.2.2.1-2.2.2.2, results in Section 2.3.1) and (2) based on these indices, to assess and compare for the first time the underlying thermodynamic processes driving the heatwaves (see methods in Section 2.2.2.3, results in Section 2.3.3). The variability of the thermodynamics across heatwave indices will give an insight as to their robustness and, by implication, their potential predictability. Note that the large-scale dynamical drivers of heatwave events are not considered here since they will be explored in a companion paper later.

The novelty of this research is that through its approach, it makes a connection between pure atmospheric physics and proved health outcomes (e.g. Black 2010) through the use of multivariate thermal indices. In addition, the comparative study of heatwave characteristics sampled from different thermal indices is in itself original, since over this region, to the best of the authors' knowledge, such analysis has not yet been conducted. This study is also the first to investigate the thermodynamics of heatwaves at the synoptic to intraseasonal scale, and is thus relevant for FbA/FbF plans.

The makeup of the paper is as follows. Section 2.2 details the methodology used. Section 2.3 presents the results both in terms of statistical characteristics and thermodynamic processes. Section 2.4

discusses the findings of this paper with respect to other published works and elaborates on the potential dynamical large scale drivers. Section 2.5 summarizes the study.

2.2. Data and Methods

2.2.1. Data and derivation of thermal indices

To meet the research aims of comparing multivariate heatwave indices and determining the associated thermodynamic processes, a self-consistent multivariate dataset is desirable. The Sahel is a data-sparse region and so, the fifth generation of the European reanalysis (ERA5 hereafter) dataset is used, regridded at 0.5° x 0.5° resolution and covering the 1979-2018 period (C3S, 2017). The limitations of reanalyses data as a modelled dataset are acknowledged. However, Barbier et al. (2018) have demonstrated greater agreement with observed temperatures over the Sahel for ERA-Interim (Dee et al., 2011). ERA5 is an improvement of ERA-Interim when compared to observations and other reanalysis products. Furthermore, Oueslati et al. (2017) have reported that the ERA-Interim reanalysis is able to very well capture the annual cycle and the interannual variability of the US heat-index (an index which is used in the present study over the Sahel). There is additional evidence that ERA5 is the reanalysis that offers the best representation of various near surface meteorological products, including near surface moisture and wind speed (e.g. Olauson 2018; Ramon et al. 2019), which are used in this paper (see Table 2.1). ERA5 is therefore well suited to this research. The study domain of the Sahel is defined as the continental area located between 20°W-30°E and 10°-20°N.

Five distinct formulations of heat measures (hereafter thermal indices) have been selected from over 100 currently existing indices (Pappenberger et al. 2015) to characterise Sahelian heatwaves (specified in Table 2.1). They include Temperature (T), the Heat Index (HI), the Steadman non radiant Apparent Temperature (AT), the Net Effective Temperature (NET) and the Universal Thermal Comfort index (UTCI). Since this study aims at targeting the effective impacts on comfort, the criteria for the choice are essentially how they simulate the exposure of Sahelian populations to diverse extreme heat-related environmental conditions. This follows a joint WMO-WHO recommendation on heatwaves and health early warning systems (WMO-No.1142, 2015). The exposure conditions represented by the thermal indices are also summarised in Table 2.1. Note that they have all been used in other semi-arid regions.

For each day over the period 1979-2018, daytime and nighttime indices are derived from each thermal index. For T, HI, AT and NET, daytime (nighttime) values are obtained by combining the daily maximum (minimum) temperature and the averages over the daytime (nighttime) time steps of 09,

Table 2.1. Description of thermal indices used in this paper.

Index name (abbreviation)	References	Formula	Variables	Environmental characteristics
1-Temperature (T)	(Fischer and Schär (2010); Perkins and Alexander (2012); Panda et al. (2017)	T	T: temperature	Classic heat measure; shielded indoor conditions
2-Heat Index (HI)	Steadman (1979); Oueslati et al. (2017)	$HI = -42.37 + 2.04T + 10.14RH - 0.22\,T.RH\ - 6.83\ * 10^{-3}T^2\ \ - 5.48 * 10^{-2}RH^2 + 1.22 * 10^{-3}T^2.RH + 8.52 * 10^{-4}T.RH^2 - 1.99 * 10^{-6}T^2.RH^2$	(i)T: temperature (ii) RH: relative humidity	Shielded indoor conditions integrating moisture effect
3-Apparent temperature (AT)	Steadman (1994); Willett and Sherwood (2012); Krstić (2011)	$AT = T + 0.33e - 0.7V - 4$	(i) T: temperature in C, (ii) e: water vapour pressure in hPa. (iii) V: wind speed at 10m height in ms^{-1}.	Shielded outdoor conditions
4-Net Effective Temperature (NET)	Hentschel (1987); Li and Chan (2000); Blazejczyk et al. (2012)	$NET = 37 - \frac{37 - T}{0.68 - 0.0014RH + \frac{1}{1.76 + 1.4V^{0.75}}} - \frac{0.29T}{1 - 0.001RH}$	(i) T: temperature inC, (ii) RH: relative humidity in %, (iii) V:wind speed at 1.2m above the ground in ms^{-1}	Shielded Outdoor Conditions accounting for human physiology
5-Universal Thermal Comfort Index (UTCI)	Blazejczyk et al. (2012); Bröde et al. (2012)	Polynomial accessible at *http://james-ramsden.com/calculate-utci-c-code/*	(i)T: temperature in C (ii)RH: relative humidity in %; (iii) V: wind speed at 10 m above the ground in ms^{-1} (iv)Tmrt: mean radiant temperature C.	Exposed outdoor conditions accounting for human physiology

12, 15 and 18 UTC (21, 0, 3, and 6 UTC) of the other variables involved. The computation of UTCI is relatively complex (Bröde et al. 2012). The data are however now directly available on the ERA5 portal (Di Napoli et al. 2020) at an hourly resolution. For this index, the daytime (nighttime) component is taken as the maximum (minimum) over the period between 07 and 18 UTC (19 and 06 UTC), respectively, which introduces a small inconsistency with the other indices.

Considering separately the diurnal phases, there is thus a total of ten thermal indices, namely: Tday, Tnight, HIday, HInight, ATday, ATnight, NETday, NETnight, UTCIday and UTCInight. These short names will consistently be used in the paper.

Table 2.2. Heatwave types under investigation.

	FM	AMJ	
	Day	Day	Night
East Sahel	Ed-FM	Ed-AMJ	En-AMJ
West Sahel	Wd-FM	Wd-AMJ	Wn-AMJ

2.2.2. Methods for heatwave characteristics inter-comparison

The first step in answering the two research objectives is to define a heatwave day at each data grid-cell across the Sahel. The following method is used to achieve this.

2.2.2.1. Heatwave definition

The analysis covers the months of February to June corresponding to the hot period in between the cool winter season and the monsoon season, and during which the first and most important peak of the temperature annual cycle is observed (Guichard et al. 2009; Nicholson 2018). For a given grid-cell and a given thermal index, several steps are followed to detect heatwaves.

First of all, from the raw data of the thermal index, the 75^{th} percentile of the total distribution is computed and is considered as a locally fixed threshold, which will allow to discard non-absolutely hot days.

Then considering that the synoptic to intraseasonal timescales are the most relevant for heatwave prediction and risk management plans, the thermal index values are converted into anomaly values by removing the daily climatology (itself smoothed through a 31-day centred running averaging). These anomalies are further high-pass filtered using Lanczos weights (Duchon 1979) with a cut-off

frequency of 90 days, to retain variability in the synoptic and intraseasonal timescales. As data is lost at the edges of the input timeseries, the subsequent analysis is built on years 1980 to 2017 which are complete. From these filtered anomalies, the 90th percentile value of each calendar day is derived using a 31-day centred window to remove noise associated with a relatively short 38-year dataset.
Heatwaves are finally defined as sequences of at least three consecutive days passing both magnitude constraints simultaneously: (i) The 75th percentile of the raw data total distribution and (ii) The calendar day 90th percentile of the high-pass filtered data.
Note that the calendar day threshold has been used by previous studies (e.g. Schoof et al. 2017; Perkins-Kirkpatrick and Gibson 2017).

2.2.2.2. Inter-comparison of thermal index-based heatwaves at the grid-cell scale

In order to answer research question one, a comparison is made between the statistics of heatwaves across the various thermal indices used on a gridcell basis. This includes specifically:
(i) The heatwave duration, frequency and intensity. The duration corresponds to the length, i.e. the number of days of an event. The frequency is defined as the average number of events per year over the 1980-2017 period. The intensity is defined as the average value of the index high-pass filtered anomaly during the heatwave. To allow comparison between different indices, the intensity values are standardised (divided by their standard deviation). The results of heatwave duration, frequency and intensity are presented in map formats in Section 2.3.1.1.

(ii) The 'synchronicity' of heatwave detection. For each grid-cell the binary timeseries of heatwave occurrences for different indices is compared using the coefficient of similarity or Jaccard coefficient (Jaccard 1901). Given two sets of data X and Y, the Jaccard coefficient is the ratio between their intersection and their union:

$J(X,Y) = \frac{X \cap Y}{X \cup Y}$ (1) with $0 \leq J(X,Y) \leq 1$ (1).

If $X = Y$, $J(X,Y) = 1$. If X and Y have no common elements $J(X,Y) = 0$.

For binary signals, the formula is:

$J(X,Y) = \frac{M_{11}}{M_{10}+M_{01}+M_{11}}$ (2).

M_{00}: total number of attributes where both timeseries X and Y have a value of 0

M_{10}: total number of attributes where the attribute of X is 1 and the attribute of Y 0

M_{01}: total number of attributes where the attribute of X is 0 and the attribute of Y 1

M_{11}: total number of attributes where X and Y both have a value of 1.

The results of this analysis are presented in Section 2.3.1.2.

A direct comparison between the thermal indices over all days of the February to June period (irrespective of the presence of heatwaves) is also made through computing the correlation coefficients between them. Furthermore, the importance of the three main constituting variables (i.e. temperature, relative humidity and wind speed) in the thermal indices is assessed. This is done by analysing the coefficients of determination of the linear regression of each thermal index on each variable, following Berman et al. (2016). The coefficients of determination in the present context are statistical measures of the portions of variances of the thermal indices attributable to the constituting variables. The diurnal phases of the variables are the same as described in Section 2.2.1, i.e. daily maximum (minimum) for temperature, and averages over the time steps 09, 12, 15 and 18 UTC (21, 0, 3, and 6 UTC) for relative humidity and wind speed at daytime (nighttime). Both correlation and determination coefficients are computed at each grid-cell before spatially averaging over the Sahel domain and are presented in Section 2.3.1.3.

2.2.3. Methods for understanding the thermodynamic processes underpinning heatwaves

2.2.3.1. Definition of arealy extensive large-scale heatwave events

To address the second research objective, the thermodynamic processes are analysed, only on days where major, arealy extensive, large-scale heatwave events (hereafter, LSHWs), i.e. events extending over a large number of contiguous grid-cells occurred. Focusing on the LSHWs allows to identify clear signals in the thermodynamic processes, minimising small-scale 'noise' in these data.

For each day over the February to June period, binary masks are obtained over the Sahel domain using occurrence/non-occurrence of heatwaves at each grid-cell (grid-cell heatwaves are defined in Section 2.2.2.1 above). Then, a hierarchical clustering (Anderberg 1973; Everitt et al. 2011) is applied to these grid-cells based on the spatial distances between them using the average linkage method. The ultimate aim is to identify days where LSHWs were observed. This method initially considers all grid-cells as clusters, merges the closest two, recalculates the distance between the clusters, merges again the closest two and so forth. The distance between two clusters is defined as the average distance between each grid-cell of one cluster to every grid-cell of the other cluster. The clustering process ends when the distance between the closest two clusters is larger than a subjective cut-off distance defined in this paper as 1,000 km, characteristic of the synoptic scale in meteorology. Then, the areas of the clusters are calculated, and only those extending over at least 600,000 km^2 (consistently with Barbier et al. 2018) are considered as LSHWs. The algorithmic of this method is summarised in the

supplemental material to this paper (see the flowchart in Fig. S2.1 and an illustration of a real case in Fig. S2.2).

Sensitivity tests have been carried out on both the cut-off distance (initially set to 1,000 km) and the minimum areal extension of the LSHWs (600,000 km^2 initially). Reducing the latter leads to an increase of the number of events by the same order than the change of areal threshold (50% decrease of the areal threshold leads to a doubling of the sample size), and reversely when it is increased. On the other hand, the increase of the cut-off distance between clusters leads to wider clusters and then a higher number of LSHWs. The order of the increase of the cut-off level is also conserved in terms of change of sample size (with decreasing values of cut-off level, LSHW events become rarer). However, these changes of both areal extent thresholds and cut-off distances have no significant impacts on the spatial structures of LSHWs or the identified thermodynamic processes (see Section 2.2.3.2).

Because the minimum 3-day temporal constraint (see Section 2.2.2.1) is applied prior (at grid-cell level) to the minimum areal extent threshold (as in Schoetter et al., 2015), the LSHW event samples exclude any very fast moving events. This is consistent with the goal of detecting the likely most harmful events as it is assumed the longer the duration the greater the impact is. The resulting maps show the occurrence and location of LSHWs that allow the analysis of the characteristics patterns of LSHW occurrence (see Section 2.3.2) and provide the sampling basis to composite the fields of thermodynamic processes (see description in Section 2.2.3.4 and results in Section 2.3.3). For this subsequent analysis, the samples of LSHW events (see Table 2.3) are separated into appropriate seasons, consistent with previous work (e.g. Kalapureddy et al. 2010; Moron et al. 2018): (i) The dry season (February-March, hereafter, FM) and (ii) The pre-monsoon season (April to June, hereafter, AMJ). The pre-monsoon is the hottest season of the year and obviously the most active in terms of heatwave occurrence. The FM season stands as a transition between the coolest and the hottest seasons and carries a risk of thermal ‘shocks’ associated with the thermo-physiological strain of rapid adjustment (de Freitas and Grigorieva, 2015)

2.2.3.2. Spatio-temporal partitioning of heatwaves

The LSHW maps are analysed as follows. First, an empirical orthogonal function (EOF) decomposition is used to determine the patterns of spatial variability in LSHWs. These EOFs are calculated separately for each index, each season and for night and day (excluding the FM season for all nighttime indices as well as daytime indices of AT-day and HI-day, due to the small LSHW sample sizes) on all dates where a LSHW event is detected over the Sahel domain (see Table 2.3 for the exact

input sample sizes of each index). The input data consist of the high-pass filtered anomaly values of the thermal index over the whole domain (including grid-cells which are not part of the LSHW event). Sensitivity tests of the EOF results were carried out and are discussed in Section 2.3.2.

The resulting EOF loading patterns broadly show a dipolar structure indicative of preferred occurrence of LSHW events over the eastern versus the western Sahel (see Section 2.3.2). On the basis of these EOF loading patterns, six characteristic heatwave types are identified (see Table 2.2 for the abbreviations used), accounting for the two subregions of the eastern (E) and western (W) Sahel domains, two seasons (FM and AMJ), and the diurnal cycle of day ('d') and night ('n'). The major LSHW event days of each of the six characteristic types are identified as instances where the standardised EOF time coefficients absolutely exceed one (the sign is combined with the spatial loadings to decide whether they correspond to the eastern or western Sahel). These samples of major characteristic LSHW events form the basis of the analysis of thermodynamic processes (methods described below, results in Section 2.3.2).

2.2.3.3. Thermodynamic processes causing large-scale heatwave events

To quantify the thermodynamic processes driving LSHW events, as in Oueslati et al. (2017), the surface energy budget (hereafter, SEB) is derived from ERA5 data:

$$\frac{c_s \Delta T}{\Delta t} = SWR + LWR + SHF + LHF \qquad (3).$$

Where SWR is the net shortwave radiation, LWR is the net longwave radiation, SHF is the sensible heat flux, LHF is the latent heat flux and c_s is the specific heat at constant pressure of the surface. Note that the ground fluxes are neglected in this study. To assess the role of clouds during some heatwave types, the cloud radiative effect (CRE) was derived from the ERA5 data as the difference between the (longwave and shortwave) radiation of a cloud-free atmosphere and that of the real atmosphere. As a convention, the radiative fluxes are counted negatively when directed away from the surface to the atmosphere. The radiative fields are relatively well represented in ERA5 over land (Martens et al. 2020), and can thus be trusted in the present study.

The SEB considers only diabatic processes since it is derived from the first law of thermodynamics at the surface level, where processes are frequently non-adiabatic. It also accounts only for the skin temperature (temperature at levels of a few centimetres high above the ground). However, people live in the boundary layer where adiabatic processes including air advection may also play an important role (e.g. Foken 2008; Leuning et al. 2012; Cuxart et al. 2015). Therefore, using the 925 hPa level as

a proxy for the boundary layer, the horizontal temperature advection is analysed during heatwave events to complement the SEB:

$$A = -\vec{V}\vec{\nabla}T = -u\frac{\partial T}{\partial x} - v\frac{\partial T}{\partial y} \quad (4).$$

Where T is temperature and $\vec{V}$ is the horizontal wind which is decomposed into its zonal (u) and meridional (v) components.

To account for moisture, the second most common parameter to the indices, near surface relative humidity data are investigated. Cloud cover data are also examined to describe the synoptic conditions during heatwaves.

Similarly to the thermal indices, all the physical quantities are first high-pass filtered to retain variability at the synoptic and intraseasonal scales (see Section 2.2.1). Their composite mean anomalies for the major LSHW event days and preceding days were derived for each of the six LSHW types. The statistical significance at the 0.05 probability level of each composite mean departure from zero was determined by a Student's t-test. These anomalies are standardised and the magnitude of the anomalies indicates their likely contribution to causing the heatwave.

To compare the magnitude of the thermodynamic processes driving various heatwave indices directly, they are spatially averaged over grid-cells where the EOF spatial coefficient has a normalised amplitude larger than 0.3 (results shown in Section 2.3.3).

2.3. Results

2.3.1. Heatwave characteristics and statistics across thermal indices

2.3.1.1. Heatwave characterization

The three most important measures of heatwaves are assessed: duration, frequency and intensity (defined in Section 2.2.2.2). In terms of duration (Figs. 2.1a & 2.2a) it is seen that:

(i) Sahelian heatwaves are typically not especially long lasting, with a mean duration not much in excess of the three-day minimum threshold and with little apparent sensitivity to the various thermal indices. Overall, the mean duration is quite low compared to other regions (e.g. Australia, Cowan et al. 2014) and other definitions over the Sahel (Oueslati et al. 2017; Barbier et al. 2018). However, the longest lasting daytime heatwaves on record (Figs. S2.3.a & S2.4.a) persist for up to two weeks over some locations (central Burkina Faso, Northwestern Nigeria and across the Chad-Niger border).

(ii) Daytime events are longer lasting than nocturnal events (Fig. 2.1a vs Fig. 2.2a), persisting on average up to 4.5 days (Fig. 2.2a) notably over the Central Sahel.

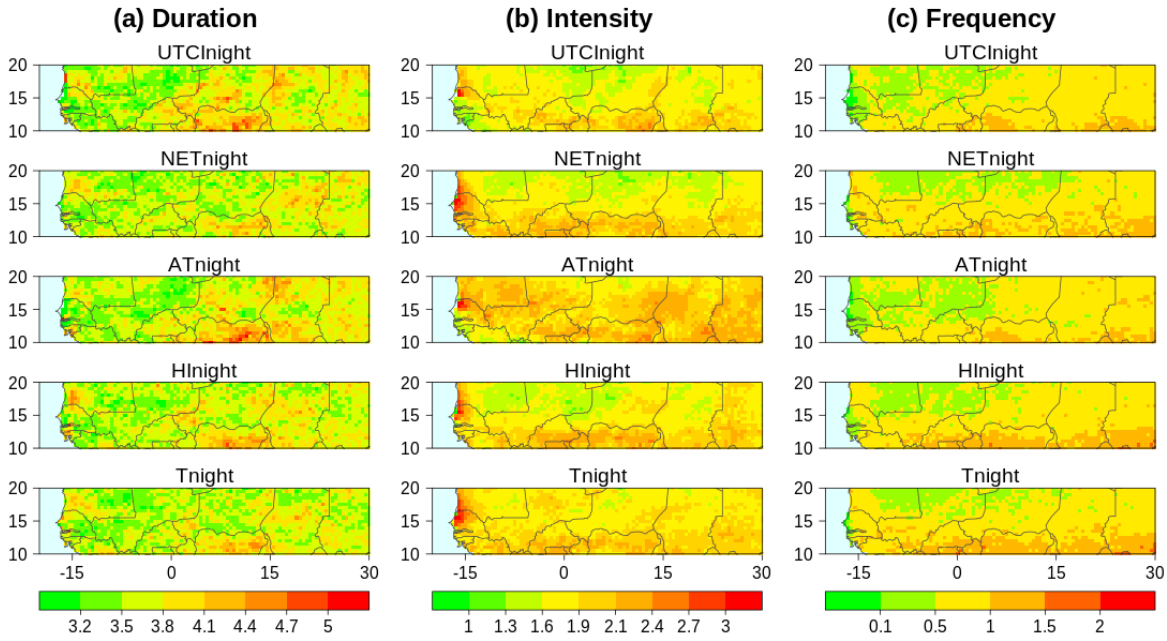

Fig. 2.1 Characteristics of nighttime heatwaves: (a) average duration in number of days per event, (b) average intensity in standardised units and (c) frequency in number of events per year. See Section 2.2.2.2 for the computation method.

(iii) Although the spatial variability in duration is not pronounced, broadly the central and eastern Sahel experiences longer lasting events than the western Sahel during both day and night across most indices (Figs. 2.1a & 2.2a).

(iv) Across the thermal indices, although differences are relatively small, over the eastern Sahel, AT presents the longest events at night (AT-night) but has some of the shortest events during the day (AT-day). This may be caused by the strong diurnal cycle of wind speed and its 'cooling' effect in the AT index formulae (Table 2.1). Surface wind speeds are highest during the day when boundary layer mixing is greatest and lowest at night, when the surface-atmosphere decoupling is pronounced and nocturnal low-level jets commonly form (Parker et al. 2005; Washington and Todd 2005; Fiedler et al. 2013).

Regarding heatwave intensity it can be noticed that:

(i) Nighttime events are slightly more intense than daytime (the magnitude of the differences between them is mostly below 0.3 standard deviation) (Fig. 2.1b vs Fig. 2.2b).

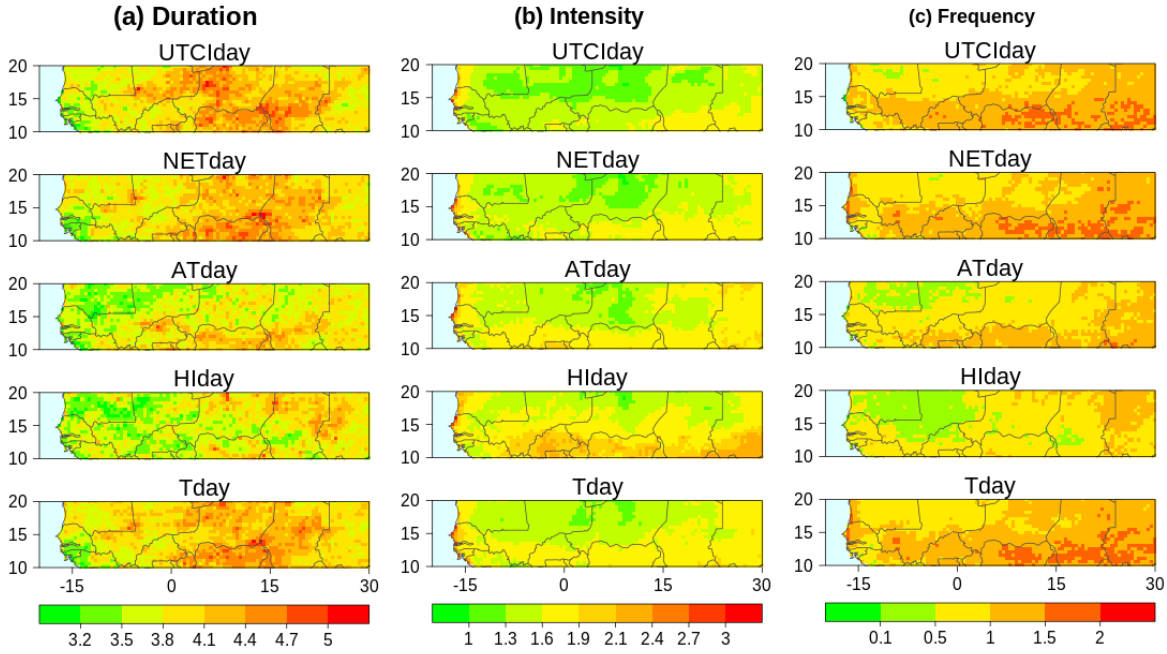

Fig. 2.2 Same as Fig. 2.1 but for daytime heatwaves.

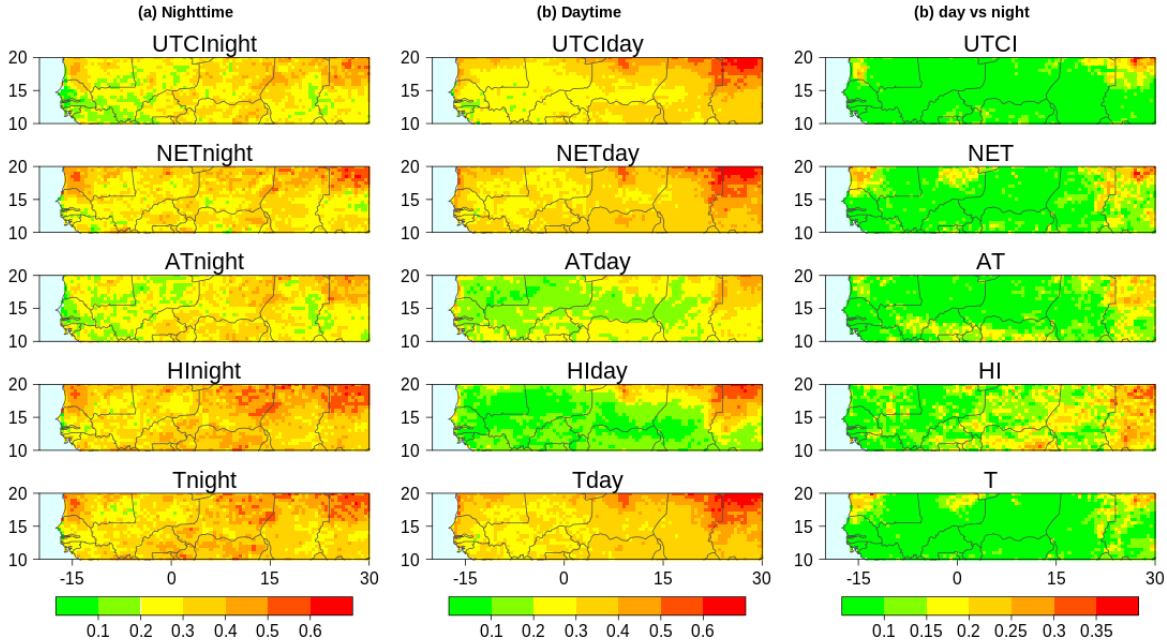

Fig. 2.3 Average Jaccard similarity coefficients between each thermal index and the other four of the same diurnal phase at (a) Nighttime and (b) daytime, and (c) between the daytime and the nighttime components of the same index.

(ii) There is a higher intensity in the eastern, the extreme western and the southernmost parts (Sudan belt) of the Sahel compared to the centre for most indices.

(iii) There is considerable variability in intensity with the most extreme events exceeding 5 (3) standard deviations in the eastern (western) Sahel (Figs. S2.3b & S2.4b). Such events are likely to be very harmful in terms of health.

Regarding heatwave frequency, most grid-cells experience between one and two events per year (Figs. 2.1c & 2.2c), with increasing values from the western to the eastern Sahel, for both day and night events - a similar structure to that of duration and intensity. Daytime events are slightly more frequent than nighttime events.

These contrasts in the diurnal cycle and the spatial distribution are mostly explained by the constraints of the heatwave definition and the spatio-temporal variability of the thermal indices. A sensitivity test on the minimum duration constraint reveals that extreme hot events persist longer in daytime than nighttime over the dry eastern Sahel whereas over the western Sahel, nighttime heatwaves last longer. The locally fixed intensity threshold (75^{th} percentile of the total distribution of the raw indices) also amplifies the day/night and East/West disparities through highlighting the differential annual cycle. The distributions of indices during the nighttime and over and the western Sahel are more clustered around the average values (Figs. S2.5 & S2.6), resulting in lesser heatwave probabilities especially during the transitional months (February and March). In fact, for most indices (UTCI being the exception), the variances are larger during the daytime and over the eastern Sahel than at nighttime and over the western Sahel (Fig. S2.7).

It should also be noted that the 75^{th} percentile of the total distribution is very determinant in ensuring that the intraseasonal events that are detected are hot indeed. March is a transition month in the Sahel and without this constraint most heatwaves would have been detected in this month given its strong intraseasonal variability.

In summary, the statistics show the eastern Sahel (especially Chad and Sudan) to be the most affected by heatwaves, hosting the longest lasting, most intense and most frequent events. Heatwaves are more frequent and longer-lasting during the daytime compared to the nighttime, while there is little diurnal difference in intensities. For the same diurnal period, the differences in heatwave statistics between indices are not especially important.

2.3.1.2. Synchronicity of heatwaves defined by the various thermal indices

The previous section suggests that the choice of thermal index does not greatly affect the characteristics and basic statistics of the detected heatwaves. However, does this mean the indices identify the same events? The analysis of the Jaccard coefficient of similarity suggests quite surprising results. The average Jaccard coefficient (i.e. the average Jaccard coefficient for a given thermal index versus the other four indices) for nighttime (Fig. 2.3a) and daytime (Fig. 2.3b) separately is typically less than 0.5 across the vast majority of the domain grid-cells. No clear spatial consistency is observed in the similarity index patterns across the pairs of indices, although the northeast of the domain centred on the Chad-Sudan border repeatedly depicts the maximum similarity between indices. Even for the most similar two indices, the Jaccard coefficients are only quite moderate with almost all the domain experiencing values less than 0.7 during the day, and lower for nighttime. The probable reasons for this dissimilarity are discussed in Section 2.3.1.3, and in Section 2.4 the potential implications for heatwave risk management in the Sahel are discussed.

The similarity between day and nighttime events is lower still (Fig. 2.4c), with typically less than 10% of all heatwave days being common to both day and night for most indices and grid-cells. The HI index has the greatest similarity across day and night, such that daily average of this index would yield the most robust combined indicator. So, in the Sahel, daytime and nighttime heatwaves do not usually occur simultaneously, a finding consistent with Barbier et al. (2018). This also has profound implications which are explored in Section 2.4.

Table 2.3. Sample sizes of daytime and nighttime LSHWs over the 1980-2017 period.

	T		HI		AT		NET		UTCI	
	night	day	night	day	night	day	night	day	night	day
Feb	7	43	0	6	0	7	10	41	0	19
Mar	49	160	33	34	9	70	66	162	6	134
Apr	182	238	163	169	105	222	183	235	113	247
May	224	202	212	199	204	212	190	191	217	208
Jun	137	128	136	124	116	150	137	134	139	164
FM	56	203	33	40	9	77	76	203	6	153
AMJ	543	568	511	492	425	584	510	560	469	619
Total	599	771	544	532	434	661	586	763	475	772

2.3.1.3. Factors of the low co-occurrence across heatwave samples

In this section, the reason for the low Jaccard coefficients between heatwaves sampled from different indices over the same diurnal phase (Figs. 2.3a & 2.3b) is investigated. Two main factors could be seen to exert a control on the coincidence of heatwaves sample from different indices: (i) the upstream constraints imposed on heatwave definition (duration and intensity thresholds) and (ii) the interaction between the constituting variables of the thermal indices.

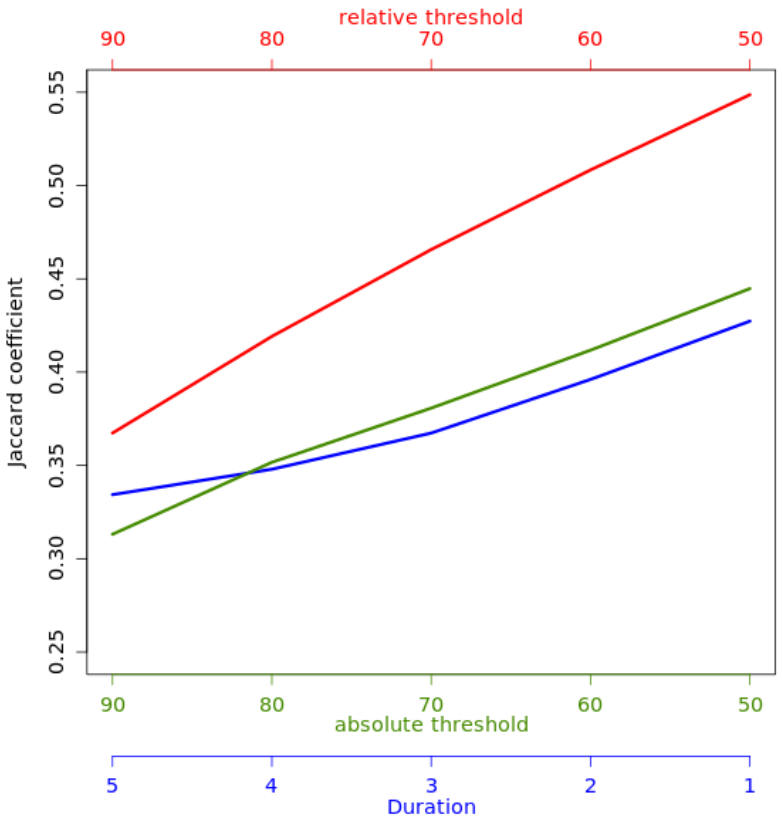

Fig. 2.4 Sensitivity of Sahel-wide average Jaccard coefficients between T-day and the four other daytime heatwave indices (HI-day, AT-day, NET-day and UTCI-day) to changes of heatwave definition thresholds. The red line represents averages of the Jaccard coefficients when the relative threshold is varied between the 90th and the 50th percentile of calendar day distribution (keeping the absolute threshold to 75th percentile of the total distribution and the minimum duration to three days); likewise for the blue (green) lines but changing the absolute threshold and keeping the calendar day threshold to the 90th percentile and the duration to three days (changing the duration between five days and one day and keeping the relative threshold to the 90th percentile of calendar distribution and the absolute threshold to the 75th percentile of the total distribution)

A sensitivity analysis on the impact of the duration, absolute and calendar day magnitude thresholds is presented in Fig. 2.4 using Tday as an example (the rates of the changes are similar for the other heatwave indices). Thus, lowering the magnitude thresholds induces an increase of the Jaccard coefficient between the heatwave samples. As an illustration, the average Sahel-wide Jaccard coefficient between Tday and the four other daytime heatwave indices is approximately 1.5 times higher if the calendar day threshold is set to the 50^{th} percentile rather than the 90^{th} percentile (without changing the other constraints). Similar (but slightly lower) variations are observed for the absolute intensity threshold. The coincidence between heatwave samples also increases with decreasing heatwave duration thresholds. There is indeed an average increase (Sahel-wide) of 0.04 of the Jaccard coefficient when the duration threshold is shortened by a day. This means that, if at the outset the minimum duration was set to two consecutive days, the absolute intensity threshold to the 60^{th} percentile of the total distribution, and the relative intensity threshold to the 80^{th} percentile of calendar day distribution, the average Jaccard coefficient of Tday would have been 0.5 instead of 0.36 (not shown). Consequently the more extreme the constraints for heatwave detection, the lower the co-occurrence of heatwave events across different thermal indices. Note that the variation of the different thresholds does not affect the spatial patterns of the Jaccard coefficients illustrated in Fig. 2.3.

The correlation coefficients between the thermal indices are relatively high (black solid lines in Fig. S2.8) but the proportions of the thermal index variance explained by temperature, relative humidity and wind speed (method described in Section 2.2.2.2) varies significantly from an index to another, and also contributes to the low inter-index Jaccard coefficients, especially during the AMJ season. Out of these constituents, wind speed (green dashed lines in Fig. S2.8) is generally the least important to the index variance. It however shows a relatively important portion of explained variability during the dry season (FM) where its annual cycle is at its peak with daytime more affected than nighttime. The daytime components of AT and UTCI are the most impacted by wind speed. Wind almost has no impact on HI, and therefore with increasing ventilation, a moist and hot air is more likely to lead to a HI-heatwave.

Since all indices have temperature as their principal variable (Table 2.1), it explains most of their variance (above 80% in most indices, red dashed lines in Fig. S2.8). However, its importance varies with the season, the diurnal cycle and the indices themselves. In FM, the influence of temperature is the largest and slightly decreases gradually in AMJ as the role of relative humidity (blue dashed lines in Fig. S2.8) increases due to moisture surges (Couvreux et al. 2010). It should be noted that temperature itself is strongly associated with moisture in AMJ at daytime (due to clouds; Fig. S2.8b). Consequently, an anomalously clearer (cloudier) sky than usual increases (decreases) the probability of T-day heatwaves (the same conclusion cannot be straightforwardly drawn for HI, AT and UTCI

heatwaves probabilities as shown below). NET is the index with the strongest links with temperature, especially at daytime with the coefficient of determination close to 1 (Fig. S2.8h), leading to high Jaccard coefficients between T-day and NET-day. The thermal indices with the weakest links with temperature are HI-day, AT-day, AT-night and UTCI-night (Fig. S2.8d, S2.8f, S2.8e and S2.8i respectively). The causes are not the same however. For HI-day and AT-day, it is due to the opposed daytime evolution of temperature versus moisture (Gounou et al. 2012): an increase of moisture may be associated with an increase of clouds (e.g. mid-level altocumulus, Bourgeois et al. 2018), and thus cause a decrease of temperature. For AT-night and UTCI-night, the wind speed, although with low determination coefficients, tends to counteract both the moisture and temperature effects. UTCI-day on the other hand maintains a relatively important link with temperature, given that it takes solar radiation into account in its formulation, the latter being itself well correlated with temperature (Blazejczyk et al. 2012).

Summarily the choice of various constraints for heatwave definition and the interactions between the constituting variables of thermal indices are two important factors for the (a)synchronicity of heatwaves samples. The second factor also affects the underpinning thermodynamic causes as will be described in Section 2.3.3.

2.3.2. Thermodynamic processes: spatial structures of Sahelian heatwaves

From this section, the focus is on LSHW events as defined in Section 2.2.3.1. Table 2.3 presents the input sample sizes of each index for each month and season of interest over the 1980-2017 period. T (HI) has the largest (smallest) sample size. Regarding the temporal distribution, the smallest heatwave sample is recorded in February across all indices, mainly as a consequence of the absolute threshold (75^{th} percentile). The months with the largest heatwave occurrences are April for the daytime (except HI-day) and May for the nighttime (Table 2.3).

The spatial structures of variability associated with LSHWs are assessed through an EOF analysis (see Section 2.2.3.2). To ensure robust results, the sensitivity of the technique to the sampling domain (Hannachi et al. 2007) is tested by using two imbricated regions consistent with Richman (1986): A small domain covering the Sahel only (20°W-30°E and 10°-20°N), and a larger domain extending over the entire Northern Africa domain (20°W-50°E and 0°-35°N). The resulting EOF loading patterns are very similar within their overlapping area and only the larger domain is retained for further analyses since the EOF loadings of the smaller domain peak towards the boundaries of the Sahel box, suggesting processes of larger spatial scale. The EOF loading patterns are also insensitive to the choice of minimum areal threshold or cut-off distance (see Section 2.2.3.1).

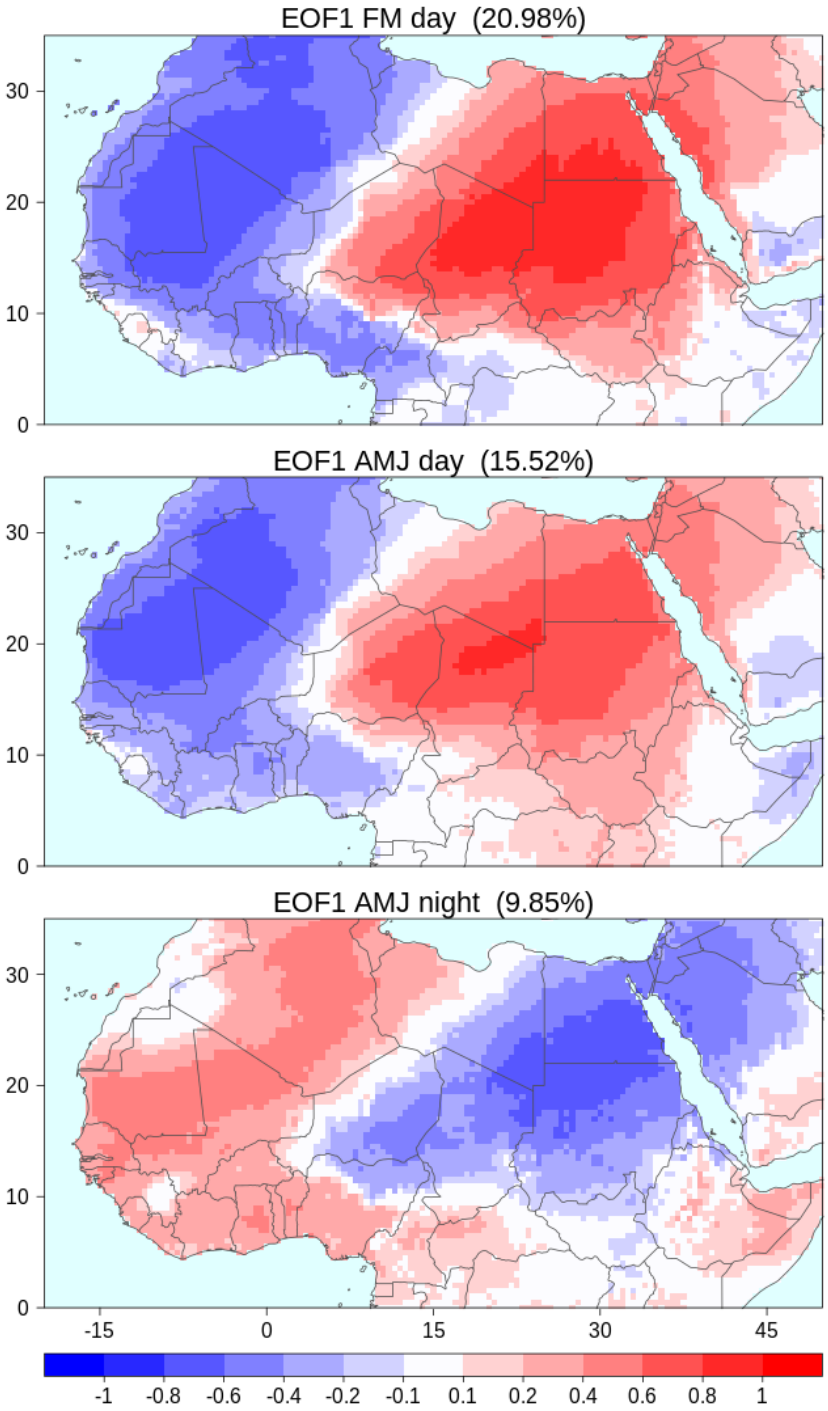

Fig. 2.5 Leading EOF loadings for different LSHW types using the T index. Numbers in brackets are the portions of variance explained (see Section 2.2.3.2 for the method description).

The results indicate that the leading mode of each heatwave type, which explains around 15% of the total variance, has a zonally dipolar structure (Fig. 2.5, illustrated using the results from the T index). This means that LSHW events over the western (eastern) Sahel are associated with a relative cooling (warming) in the eastern (western) Sahel. Note that the temperature anomalies associated with several weather type patterns over the northern tropical Africa domain also present the dipolar structure (Moron et al. 2018). The percentages of variance of LSHWs explained by the EOFs are relatively low but the method in itself is a robust and objective approach to capture the natural patterns of variability and has extensively been used in climate studies (e.g. Hannachi et al. 2006).

2.3.3. Thermodynamic processes: energy budget and moisture analyses

In this section, the underlying thermodynamics associated with each heatwave type are assessed using the terms of the SEB (equation 3) and the heat advection (equation 4) presented in Section 2.2.3.3. Before describing the details of each heatwave type, it is important to mention some general observations. All heatwave types are associated with an increase of temperature, and most of them see a significant decrease of wind speed. In terms of magnitude, the eastern Sahel heatwave processes are generally larger than their western Sahel counterparts. Similarly, in FM the magnitude of the processes are more important than in AMJ, in agreement with Moron et al. (2018). The analysis of the SEB on days leading to the heatwave reveals that for most heatwave types the anomalies of the processes keep the same sign as during the heatwave or are null. A progressive increase of their magnitude is however observed towards the onset of the heatwaves (except during the FM season), meaning that the heating is not sudden but is a gradual process.

The latent heat flux is generally the least important of the SEB terms, with relatively small anomalies, hence its omission hereafter.

For conciseness purposes, to indicate the origins of hot air in cases where heat advection is important, only wind anomalies associated with T are shown (Fig. 2.12).

The key results presented by heatwave type in the following discussion are summarised in Table 2.4, where information on the diagnostic and leading processes as well as the agreement between the indices is presented.

Daytime heatwaves in the FM season over the western Sahel (Wd-FM). Fig. 2.6. They are characterised by a decrease of surface relative humidity and cloudiness for T and NET and reversely for UTCI. Regarding the underlying processes, T and NET agree on the leading role of heat advection

centred near the border between Mali and Mauritania, and originating from the region southeast to the heatwave area (i.e. Burkina Faso and Western Niger; Fig. 2.12a).

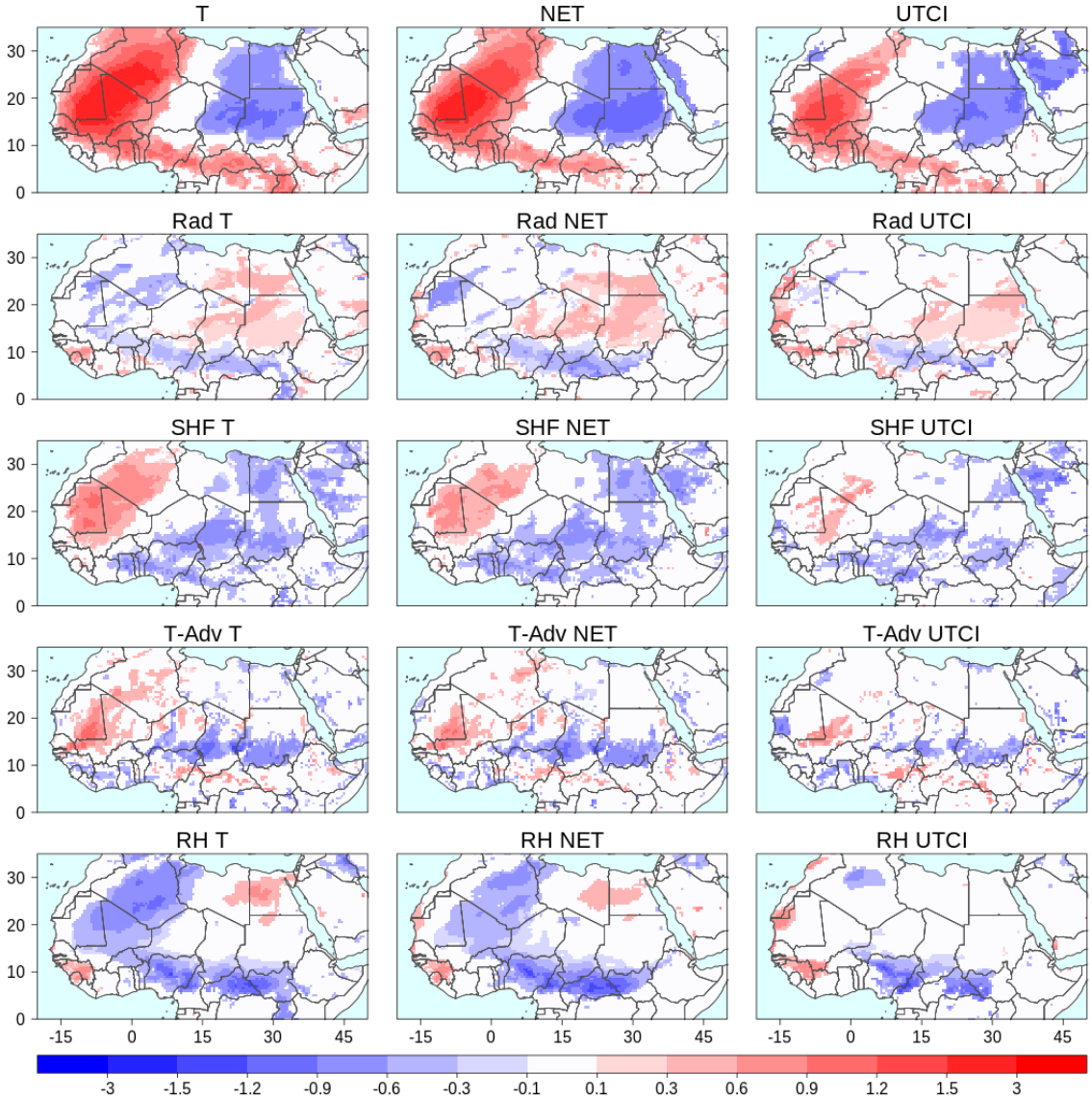

Fig. 2.6 Normalised anomalies associated with heatwaves occurring over the western Sahel at daytime during the FM season (Wd-FM). The top panel shows the anomalies of the indices themselves and the subsequent panels the anomalies of net radiation (Rad), sensible heat flux (SHF), temperature advection (T-Adv) and near surface relative humidity (RH) in that order. Shown from left to right are the anomalies associated with heatwaves detected using T, NET and UTCI respectively. White areas are not significant at the 0.05 probability level.

As shown in Fig. S2.9, the advection initiates up to three days prior to the heatwave and peaks the day before the onset with an intensity above 0.3 standard deviation. During UTCI events, the intensity of temperature advection is less important (less than 0.2). However the presence of low-level moisture favours a gain of thermal radiation amounting to around 0.1 that also contributes to the warming.

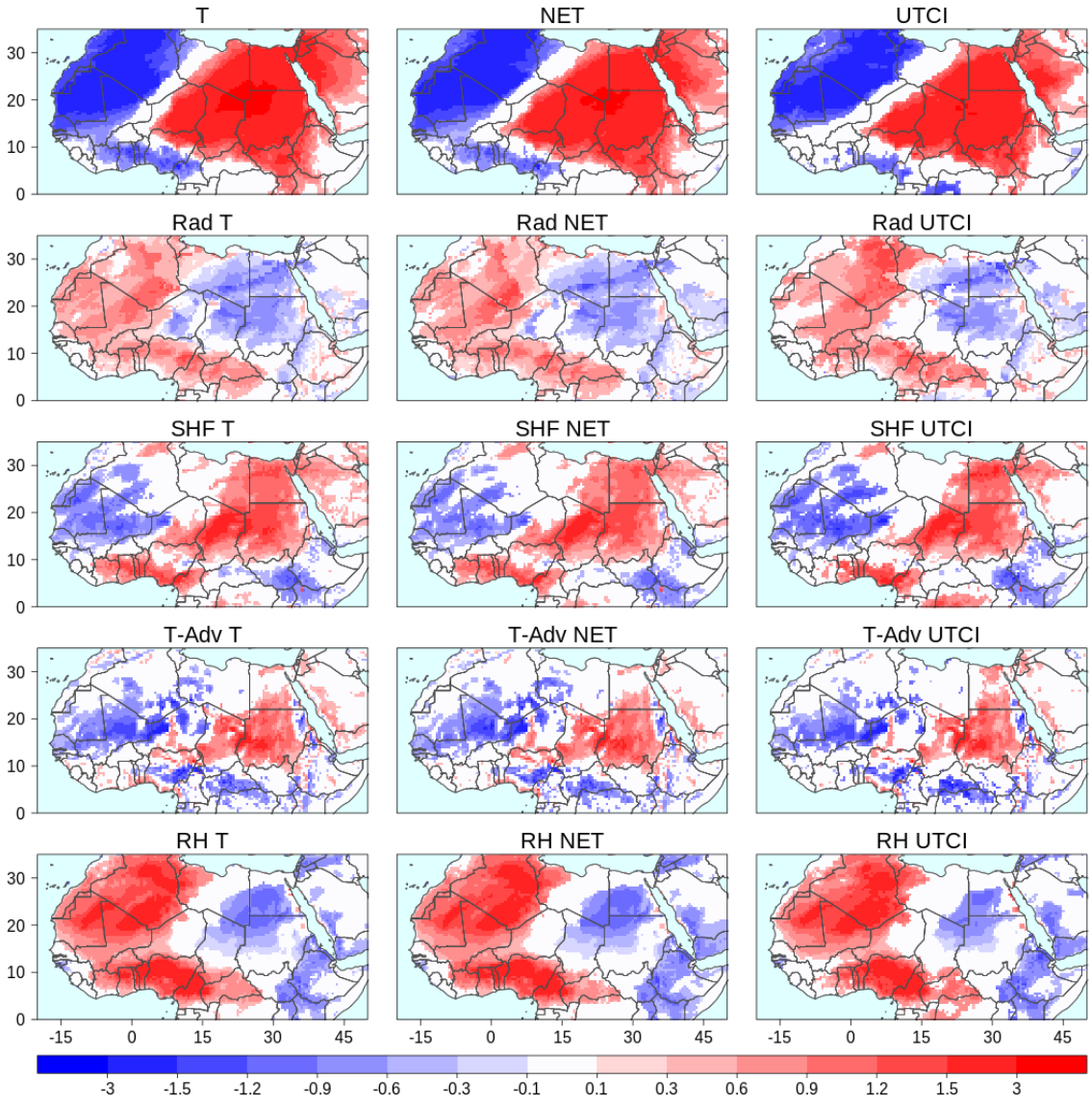

Fig. 2.7 Same as Fig. 2.6 but for heatwaves occurring over the eastern Sahel at daytime during the FM season (Ed-FM).

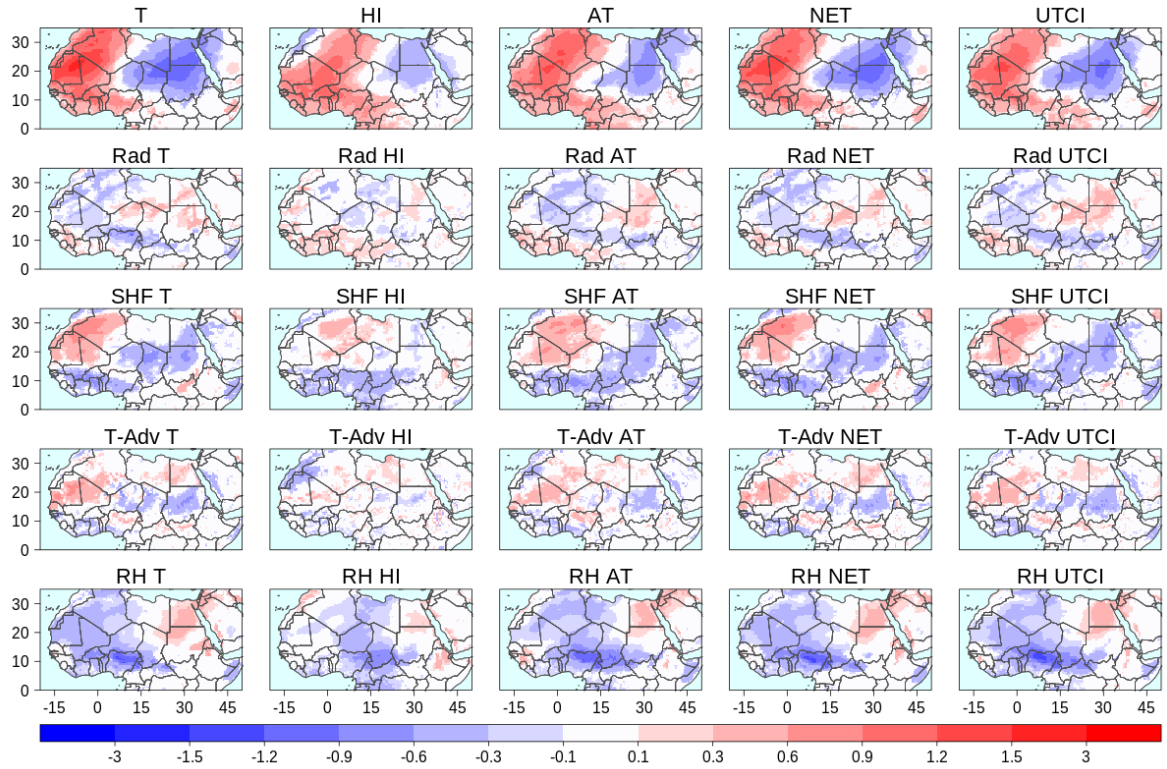

Fig. 2.8 Normalised anomalies associated with heatwaves occurring over the western Sahel at daytime during the AMJ season (Wd-AMJ). The top panel shows the anomalies of the indices themselves and the subsequent panels the anomalies of net radiation (Rad), sensible heat flux (SHF), temperature advection (T-Adv) and near surface relative humidity (RH) in that order. Shown from left to right are the anomalies associated with heatwaves detected using T, HI, AT, NET and UTCI respectively. White areas are not significant at the 0.05 probability level.

Daytime heatwaves in the FM season over the eastern Sahel (Ed-FM). Fig. 2.7. The characteristics of these events are consistent across the thermal indices. They are associated with a dipole of low-level moisture anomalies with the eastern Sahel (i.e. the heatwave region) hosting dryer air. There is also an increase of cloud cover whose structure has a southwest-northeast (SW-NE) orientation from the Gulf of Guinea toward the eastern Sahara (not shown). An important decrease of surface wind speed is also observed (the FM season corresponds to the annual peak of wind speed in the region, Guichard et al 2009). The leading thermodynamic process is (consistently across all indices) hot air advection from the equatorial West Africa to the eastern Sahel/Sahara (Fig. 2.12b). It starts up to five days before the heatwave (Fig. S2.9), increases gradually and reaches its maximum the day before the onset. It also leads to the surface sensible heat flux anomaly turning positive (as per the convention, this means less flux from the ground into the atmosphere). A particularity of this heatwave type is that, comparatively to the others, it is associated with large anomalies especially of

temperature (in excess of two standard deviations), wind speed (absolutely above 0.5 standard deviation), advection (above 0.5 standard deviation) and sensible flux (close to one standard deviation). The surface shortwave radiation follows the cloudiness pattern with negative anomalies oriented SW-NE from the Guinean countries through central Sahel to the eastern Sahara. As for the longwave anomalies, they match the low-level moisture, depicting a dipolar structure with radiative loss over the heatwave region.

Daytime heatwaves over the western Sahel in AMJ (Wd-AMJ). Fig. 2.8. These events extend over a broad sector from the countries of the Gulf of Guinea to the western Sahara, centred in northern Mali. They are consistently accompanied by a decrease of moisture and cloudiness (Fig. S2.10) over the region of interest. The decrease is the most important for T and NET. At the exception of AT, all heatwave indices show an increase of the surface ventilation (Fig. S2.10, consistent with Section 2.3.1.3).

The thermodynamic causes differ between the northern (Mauritania) and the southern (Burkina Faso, southern Mali) parts of the heatwave region. In the northern part, four out of five indices (T, AT, NET and UTCI) point to advection of hot air (with a magnitude around 0.2 standard deviation) from the area near the Algeria-Mali-Niger trijunction as cause of the heating. In HI events, the increase of incident solar radiation (following the decrease of cloudiness) stands as the leading cause of the heatwave in front of heat advection.

In the southern part of the heatwave region, all indices concord on an increase of sensible heat flux from the soil into the atmosphere as the process responsible for the heating. This process also extends to the Guinean band.

Daytime heatwaves over the eastern Sahel in AMJ (Ed-AMJ). Fig. 2.9. These heatwaves extend over a broad sector of the eastern Sahel, and appear to be an extension of heatwaves centred over the northeastern Sahara at the intersection between Libya, Egypt and Sudan. The meteorological conditions during this heatwave vary with the thermal indices, even if all show a significant decrease of wind speed, with AT having the maximum anomaly (above 0.5 standard deviation). On one hand, T, NET and UTCI see a decrease in moisture and cloudiness. On the other hand, in AT, and even more in HI, a substantial increase of moisture and cloudiness is observed in association with a low-level moisture convergence. Yet, regardless of the indices, all these heatwaves are driven primarily by the same process namely hot air advection from the southernmost Sahel (Fig. 2.12d), gradually increasing from approximately four days before the onset of the events (Fig. S2.9). This advection

dumps the sensible heat flux between the soil and the atmosphere over the region covered by the heatwave. Expectedly, the advective warming is the most important for indices with dry anomalies (T, NET and UTCI). The net radiation anomalies are small over all indices but for different reasons. In T, NET and UTCI, the decrease in cloudiness allows more solar radiation in, but the dryness of the low-level atmosphere also lets more thermal radiation out. On the other hand, there is less incoming solar radiation during HI and AT heatwaves due to the cloud cover whereas the increase of low-level moisture limits the thermal loss.

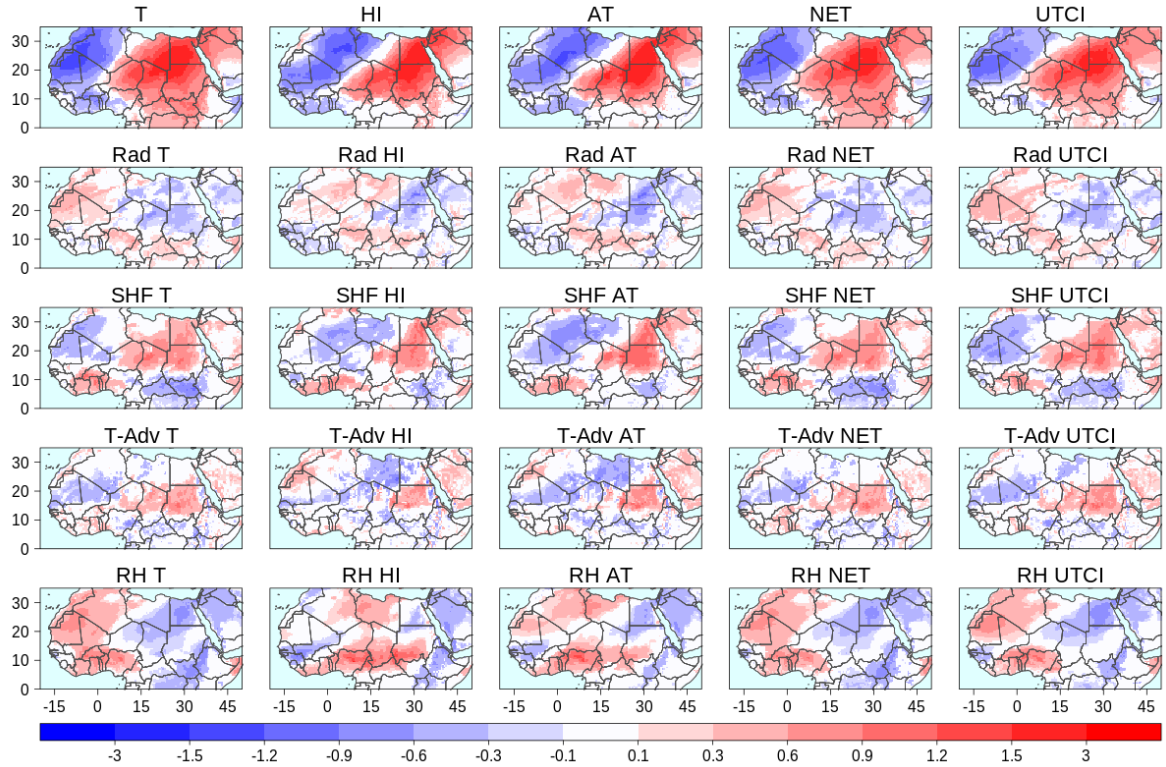

Fig. 2.9 Same as Fig. 2.8 but for heatwaves occurring at daytime over the eastern Sahel during the AMJ season (Ed-AMJ).

Nighttime heatwaves over the western Sahel in AMJ (Wn-AMJ). Fig. 2.10. They cover most of the western Sahel and Guinea but have intensity anomalies of only moderate magnitude (less than one standard deviation) in comparison with other heatwave types. The thermal indices can be categorised into two groups on the basis of the synoptic conditions during these heatwaves. T, HI and NET heatwaves occur along with an increase of wind speed and cloud cover (Fig. S2.10) over the region of interest, whilst the low-level moisture shows a small decrease. Reversely during AT and UTCI heatwaves, the low-level moisture increases significantly (a magnitude comparable to that of

temperature), whereas a decrease of wind speed is observed. Resultantly, the thermodynamics also vary with these two groups of indices. For T, HI and NET, the processes consist of small anomalies of longwave radiation. In AT and UTCI heatwaves, the increase of longwave radiation is well marked (in excess of 0.5 standard deviation). They also have two additional sources of heating: (i) sensible heat flux from the surface and (ii) small heat advection in the lower atmosphere. Therefore, unlike with Ed-AMJ events, the difference in synoptic conditions is also reflected in the thermodynamic quantities.

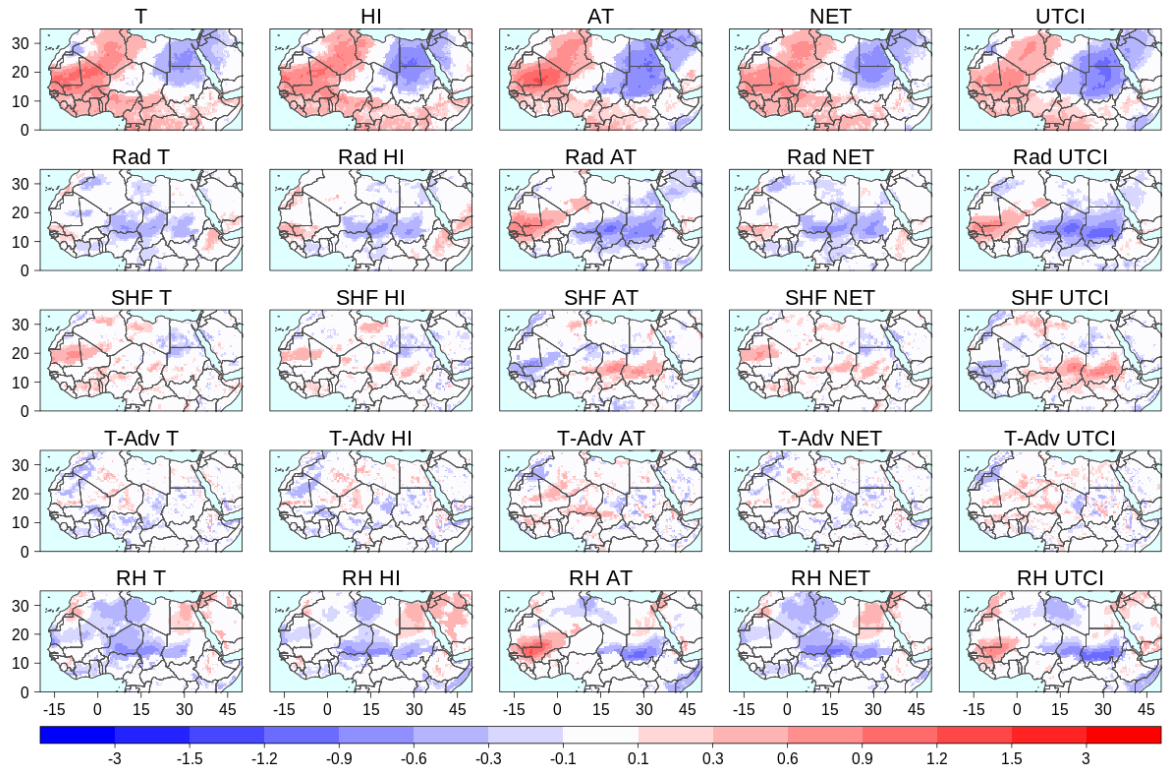

Fig. 2.10 Same as Fig. 2.8 but for heatwaves occurring over the western Sahel at nighttime during the AMJ season (Wn-AMJ).

Nighttime heatwaves over the eastern Sahel in AMJ (En-AMJ). Fig. 2.11. They extend in a southwest-northeast axis from the eastern Sahel to the northeast Sahara where the intensity is the greatest. As in Ed-FM, they show the highest agreement between the thermodynamic conditions sampled from the different heatwave indices. Indeed, all show a large increase of moisture and cloud cover which is the most important in AT and UTCI heatwaves where the magnitude of the moisture anomaly almost equates that of temperature. There is also a consistent decrease in wind speed across all indices (Fig. S2.10).

En-AMJ heatwaves occur as a result of (i) primarily longwave warming and (ii) sensible heat flux from the soil. The longwave warming extends from the equatorial West Africa region northeastwardly to the northeast coast of Africa, with magnitude peaking to above one standard deviation in AT and UTCI. The sensible heat flux is mainly confined within the southern half of the eastern Sahel, and its magnitude also goes up to 0.4 standard deviation.

Summarily the thermodynamics and synoptic conditions vary between daytime and nighttime and between the eastern and the western Sahel. Furthermore, there is a lower agreement between the FM and the AMJ daytime heatwaves over the western Sahel than over the eastern Sahel. However, there is an overall better consistency of the thermodynamic processes across heatwaves indices (Table 2.4) than what the low Jaccard coefficients suggest.

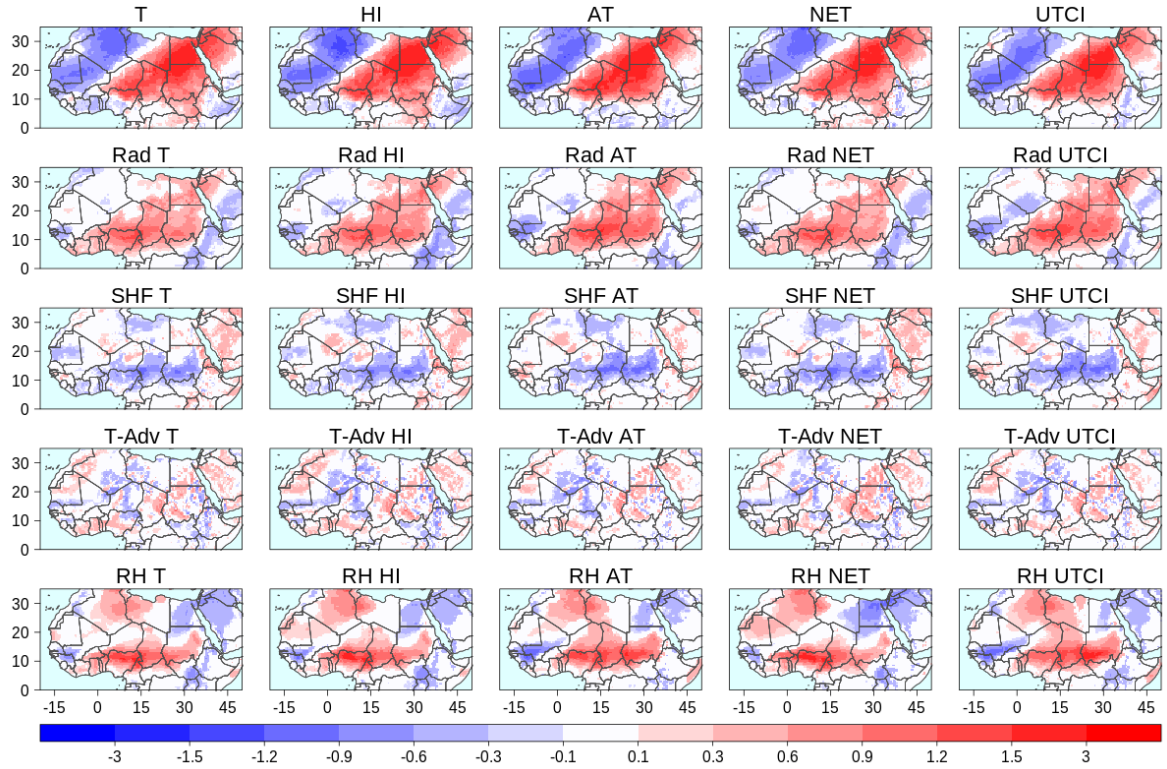

Fig. 2.11 Same as Fig. 2.8 but for heatwaves occurring over Eastern Sahel at nighttime during the AMJ season (En-AMJ).

2.4. Discussion

From an operational perspective, the low coincidence between heatwaves detected from different indices over the same diurnal period may have profound implications for heatwave prediction and

early warning, given that many countries (including in the Sahel) only consider a single index in their operational systems (WMO-No.1142, 2015). Using one particular index rather than another will necessarily lead to missing out heatwave events identified by the other indices, which could nonetheless be more relevant to a given group of vulnerable populations. It is thus recommended to monitor a range of indices in order to target various socio-economic groups of vulnerable populations with the most relevant index. Such an approach is relevant to the recent emphasis on multi-hazard impact-based forecasting (WMO-No. 1150, 2015) in which the warnings seek to indicate the potential damages of hydro-meteorological events on humans and their assets. For example, large proportions

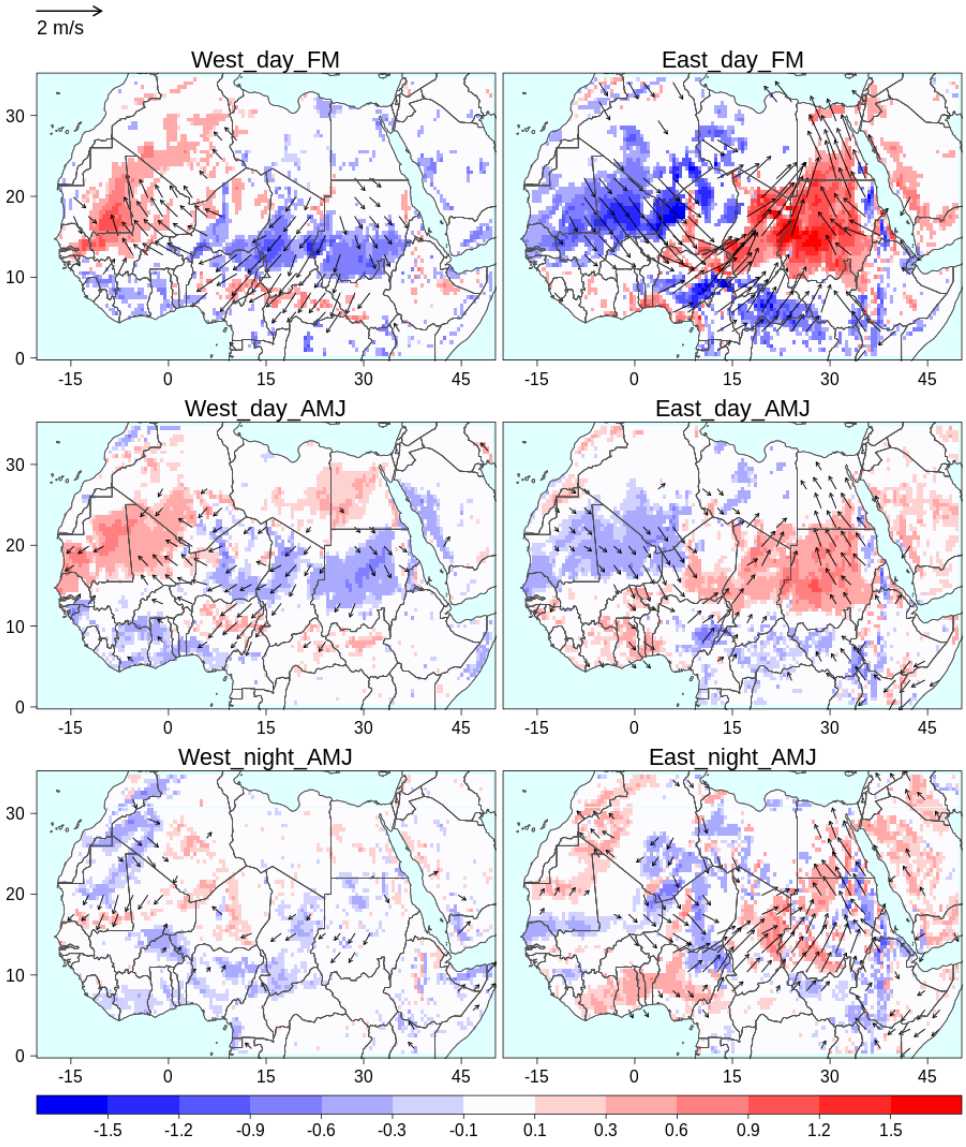

Fig. 2.12 Normalised anomalies of temperature advection (shades) and wind speed (vectors) associated with heatwaves detected using T. Only anomalies significant at the 0.05 probability level are plotted.

of Sahelian populations practice their economic activities outdoor and are exposed to relatively long hours of sunshine, including construction workers and street vendors in urban centres (Quak 2018 ; Balarabe and Sahin 2020), pastoralists and increasingly market gardeners (Woltering et al. 2011) and informal gold diggers (Ouedraogo and Mundler 2019) in rural areas. The UTCI index, which accounts for solar radiation (Table 2.1) may therefore be the most indicated for targeting these groups. From a spatial point of view, in the southernmost parts of the Sahel, where the similarity is the lowest, it is important to use indices which give much weight to humidity (HI, AT and UTCI), as this region also has the largest moisture variability, especially in AMJ. On the other hand, over the northeastern parts of the domain as well as the whole Sahel during the FM season, only little value will be added to heat warnings that use complex indices because of small variability of environmental variables (see Section 2.3.1.3). For these cases, mere temperature is a reasonably good choice.

The fact that only small proportions of heatwaves occur simultaneously at daytime and nighttime is an important information for risk management. There is evidence that hot days followed by hot nights indeed pose a greater threat to people (e.g. Schär 2016; Murage et al. 2017) because the body does not have a respite to the heat in such situations. As such, the lack of day/night synchronicity can be interpreted as a relieving factor for Sahelian populations. However, the few (but dangerous) cases where both heatwave types are synchronous should not be overlooked.

In terms of underlying thermodynamic processes, despite differences of the sampling bases, comparisons of the findings of this paper with that of previous publications can still be made. Most notably, the findings agree with Guichard (2014), Oueslati et al. (2017) and Sambou et al. (2020) on the leading role of greenhouse effect of moisture during Sahelian nighttime heatwaves. It should be noted that this process is not specific to the Sahel, but is also observed during nighttime heatwaves over other tropical regions (e.g. Oppermann et al. 2017; Chen et al. 2019). Likewise, the shortwave radiation at the southernmost part of the Sahel accompanying daytime heatwaves corroborates the findings of Oueslati et al. (2017) and is also found to drive some heatwaves in mid-latitude areas like Europe (e.g. Lhotka et al. 2018).

In addition, this paper clearly highlighted the key role played by thermal advection in the occurrence of Sahelian heatwaves, which was suggested by Moron et al. (2018) for weather types. Hot air is indeed conveyed from the continental eastern Sahel towards the cooler western coast on one hand and from the southernmost parts of the Sahel to its northernmost parts on the other hand (see Section 2.3.3). The importance of this process to heatwaves has also been proved over other regions (Cerne et al. 2007; Jacques-Coper et al. 2016; Sfîcă et al. 2017).

Table 2.4. Degree of agreement between the indices and diagnostic and major thermodynamic processes for each heatwave type.

HW type *(Degree of agreement between the indices)*	Diagnostic	Thermodynamic causes
West day FM *(Fair agreement)*	Decrease (increase) of moisture for T and NET (UTCI).	-Heat advection (T and NET) -Heat advection and LW (UTCI)
East day FM *(Large agreement)*	-dipole of moisture (dry in the HW region), weaker winds	Heat advection.
West day AMJ *(Fair agreement)*	Decrease of moisture and cloudiness in all indices. Increase of wind speed except in AT.	-Heat advection in the north and sensible flux in the south in T, AT, NET, UTCI. -shortwave radiation in the north and sensible flux in the south in HI.
East day AMJ *(Fair agreement on the diagnostic, large agreement on the thermodynamic causes)*	-decrease of moisture and cloudiness in T, NET, UTCI. -reversely in HI, AT.	Heat advection.
West night AMJ *(Fair agreement)*	-increase of wind speed and cloud cover, small decrease of moisture in T, HI, NET. -decrease of wind speed, increase of moisture in AT, UTCI.	-small LW (T, HI, NET). -LW, sensible flux and heat advection (AT, UTCI).
East night AMJ *(Large agreement)*	Increase of moisture and cloudiness, decrease of wind speed.	LW (primarily) and sensible flux.

The interpretation of the results on thermodynamic processes must however bear in mind the limitation of the ERA5 reanalysis data on which they are based. There is a considerable uncertainty in many meteorological fields between various reanalyses (Roberts et al. 2014, 2017) notably for some of the key radiative quantities of water vapour, clouds and dust. Dust is a crucial component of

the Sahelian atmosphere (Knippertz and Todd 2012) and its radiative contribution to the atmospheric heat budget (Alamirew et al. 2018) may then be an important parameter for heatwaves. Furthermore there is a clear need for improved observations across the Sahel to support assimilation into reanalyses and direct process analysis.

But notwithstanding this, the main findings of this paper along with that from previous research give a clue as to what can be the large-scale dynamical drivers of heatwaves over the Sahel. Thus, despite the dryness of the FM season, Ed-FM heatwaves are accompanied by important moisture anomalies in the western Sahel (Fig. 2.7), as well as positive rainfall anomalies over the Guinean region of West Africa (not shown). Additionally, the low-level circulation has a strong cyclonic anomaly (Fig. 2.12) causing moisture surges from the Atlantic. Such patterns recall the findings of studies (Fink and Knippertz 2003; Knippertz 2003; Knippertz and Martin 2005, 2007) investigating the causes of extra-monsoon precipitation over West Africa. The invasion of the Atlantic air masses from a dynamical point of view happens as a consequence of a southward penetration of mid-latitude Rossby waves, potentially leading to the well-known tropical plumes. It is therefore likely that the build-up stage of tropical plumes be favourable to heatwave occurrence over the Sahel.

During the AMJ season, heatwaves over the eastern Sahel are also associated with a cyclonic turning of the low-level wind over the Sahel with a strong southwesterly component (Fig. 2.12). Conversely, heatwaves over the western Sahel coincide with a reinforcement of the Harmattan winds. The AMJ season is also the period during which the Guinean region experiences the first peak of the West African Monsoon (WAM, Gu and Adler 2004; Nguyen et al. 2011; Thorncroft et al. 2011). This suggests a potential link between the monsoon and heatwaves, similarly to other tropical regions (Ghatak et al. 2017; Luo and Lau 2018).

In connection with the cyclonic and anticyclonic turning of low-level winds, there may be a substantial modulation by the West African Heat Low (WAHL). This major climatic feature is indeed located within the Sahel band during the AMJ season (Lavaysse et al. 2009). During Sahelian heatwaves, its occurrence oscillates zonally between the west and the east of the Sahel laying almost exactly within the heatwave region (Fig. S2.11). Consequently, a link may be found with heatwaves (at least statistically), but this requires deeper investigations.

So three large scale drivers including mid-latitude Rossby waves, the WAM over the equatorial region and the WAHL are likely to impact the occurrence of Sahelian heatwaves at the synoptic to intraseasonal timescales. The benefit in exploring such connections lies in the potential predictability which will be explored in future work. A companion paper (Guigma et al. 2020) examines the dynamical processes governing heatwaves, focusing on the role of the tropical modes of variability and their interaction with these circulation features.

2.5. Conclusion and prospects

This paper investigated synoptic to intraseasonal heatwaves in the West African Sahel. The purpose was to (i) derive and compare the statistical characteristics of these heatwaves in the Sahel using diverse multivariate thermal indices, and (ii) examine the underpinning thermodynamic processes. Consistently across the thermal indices used in this study, heatwaves in the Sahel are characterized by short-lasting events (3-5 day duration) which occur once to twice a year and are associated with large magnitude. However, different thermal indices sample different events, most particularly between daytime and nighttime events, but also perhaps surprisingly there can be notable differences in the events identified between indices for the same diurnal period. This may be very important given the preponderance of single indices in most heatwave early warning systems around the world (WMO-No.1142, 2015). The most spatially extended events are characterized by a (thermal) zonal polarisation of the Sahel. Their underpinning thermodynamic processes vary from one index to another, consistently with the differences in the samples. The most robust processes across all indices are hot air advection and longwave radiation.

The results suggest that the choice of thermal index is important with profound implications for: (i) The scientific understanding of heatwave phenomena such that synthesising research results should recognise the diversity of characteristics, causes and thus, potentially, predictability across different indices and (ii) Operational risk management, in that an appropriate choice of thermal index reflecting the risk to various exposed populations must be ensured. Thus, forecasters from Sahelian national meteorological services (NMSs) can target specific groups of the population (outdoor workers, farmers, and workers under shielded conditions etc) based on the typical features of each index. This will grant more efficiency and probably more trust to the heatwave warnings which is important for co-production.

Furthermore, a regional scale Early Warning-Early Action plan can make use of the definition and characterization of heatwaves of the present paper. Through the double magnitude constraint, there is a certitude of sampling only extremely hot events that may require humanitarian actions. However, there is a clear need to extend this scientific analysis towards understanding the actual impact on society and/or the environment. Appropriate thresholds of heatwave magnitude and duration should be defined in conjunction with relevant stakeholders, based on data and experience of the diverse impacts across differing levels of exposure and vulnerability. Such impact-based forecasting methods are being developed (Weyrich et al. 2018; Potter et al. 2018) and should be considered for heatwave risk management in the Sahel.

For example, in the health sector, there is a growing body of research into the link between heat and health (e.g. Lam et al. 2013; Herrmann and Sauerborn 2018; Campbell et al. 2018) at the global level. Using multiple thermal indices can lead to a better simulation of the heat-health relationship (e.g. Kim et al. 2011; Morabito et al. 2014). The present study provides a basis for such investigations over the Sahel through identifying and statistically characterising a variety of indices which simulate various heat hazards, as well as elaborating on the physical causes behind them. In fact, quantifying the link between heatwaves and health should now be a priority in future studies in the Sahel as this remains to date poorly explored.

Finally, in the logic of scaling FbA plans at the Sahel level, it is necessary to first assess the skill of forecast models in predicting relevant thermal indices. Given the differences in thermodynamic processes between indices identified in this paper, differing levels of predictability may be expected. This requires further analysis to build on existing work (e.g. Batté et al., 2018; Perez et al., 2018) to extend to all thermal indices in an LSHW approach. This is the subject of ongoing work by the authors.

Acknowledgements

KHG was supported by the Peter Carpenter Scholarship for African Climate Science at the University of Sussex, UK. Further support was provided through the (i) UK NERC/ESRC/DfID Science for Humanitarian Emergencies and Resilience (SHEAR) consortium project 'Towards Forecast-based Preparedness Action' (ForPAc, www.forpac.org), grant number NE/P000673/1 and (ii) Future Climate for Africa (FCFA) regional consortium project 'AMMA-2050', grant number NE/M02024X/1.

Supplemental materials

This supplement to the article provides additional results on heatwaves detection method, characteristics and driving processes.

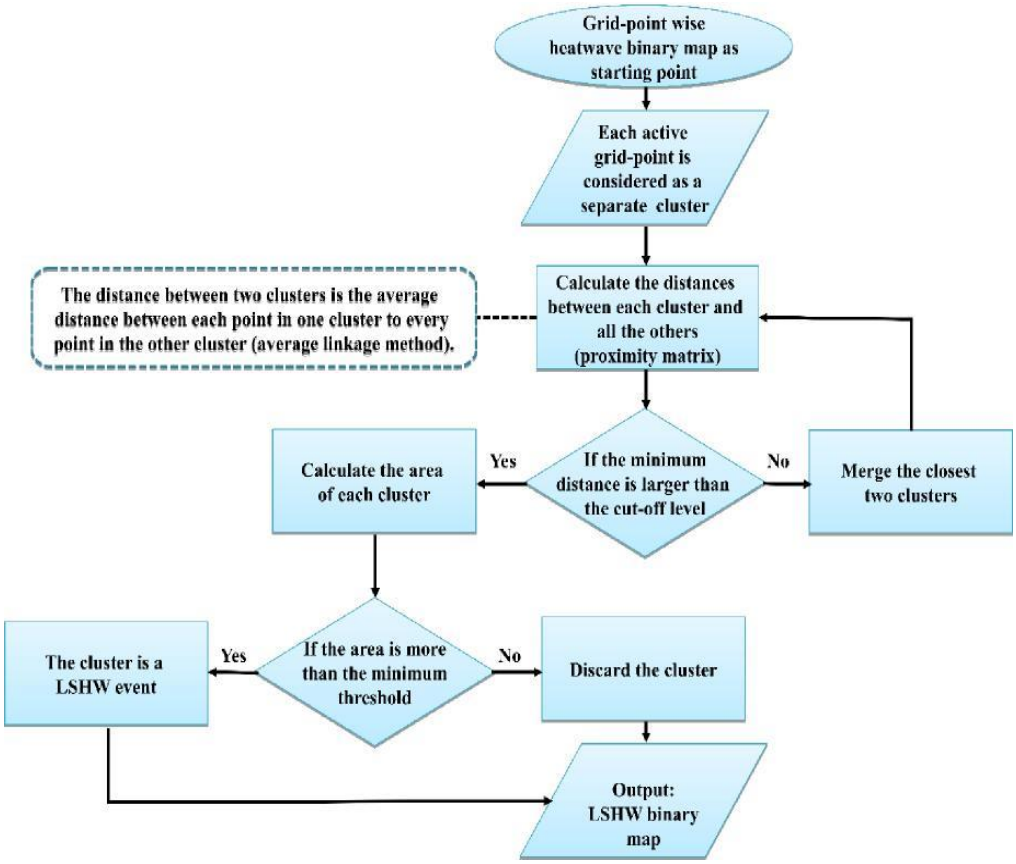

Fig. S2.1 Flow chart illustrating the detection of LSHWs (described in Section 2.2.3.1).

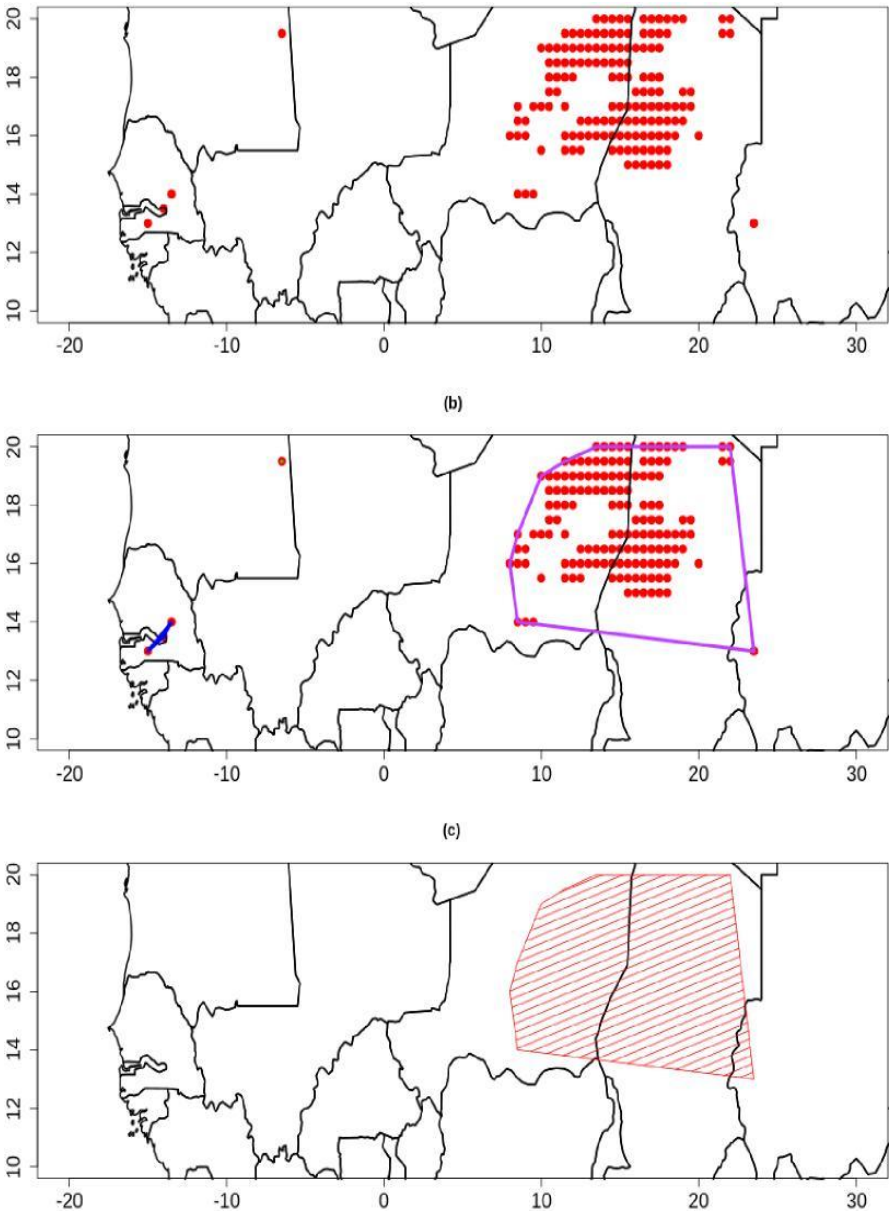

Fig. S2.2 Example of LSHW detection for T-night *on 22 June 1981*. *(a)* Initial grid-point wise binary map. (b) Three clusters detected after applying the average linkage method with cut-off level 1,000 km. (c) Final LSHW after applying the constraint on the spatial extent of clusters (600,000 km^2).

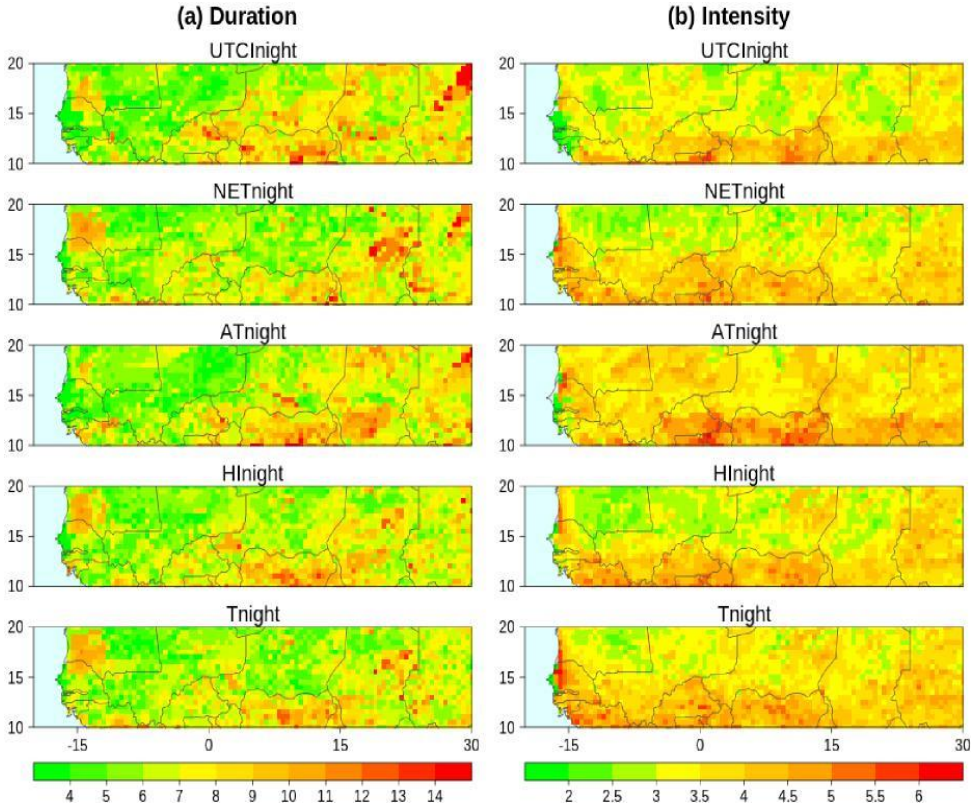

Fig. S2.3 (a) Longest durations and (b) Maximum intensities of nighttime heatwave events observed over the study period.

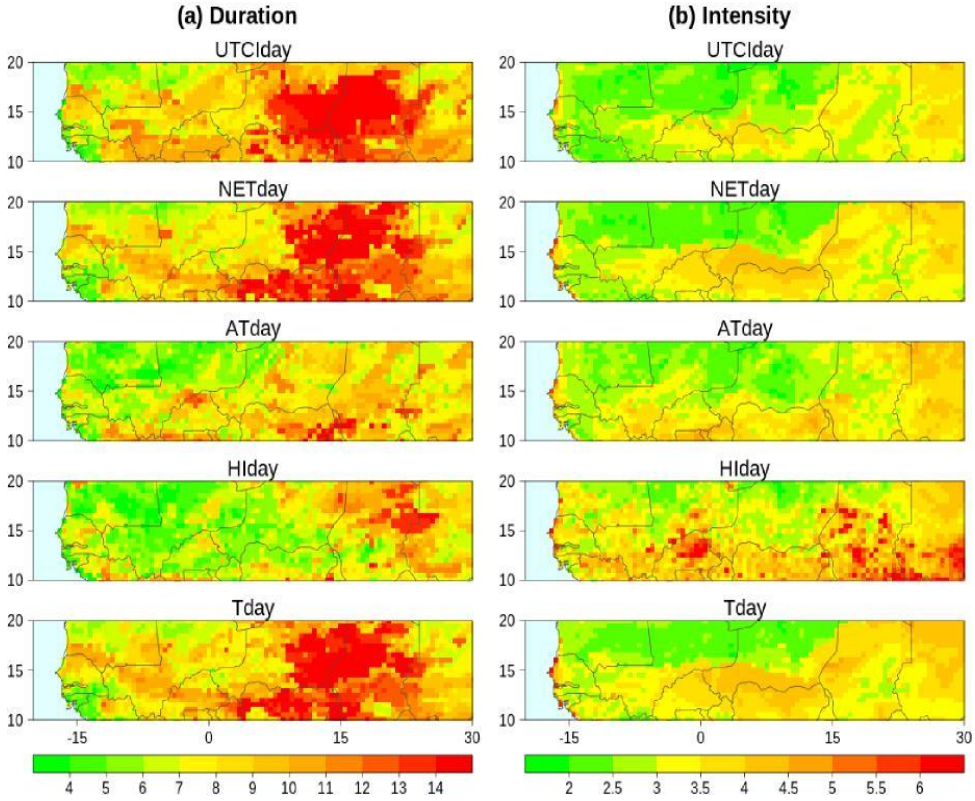

Fig. S2.4 Same as Fig. S2.3 but for daytime heatwaves.

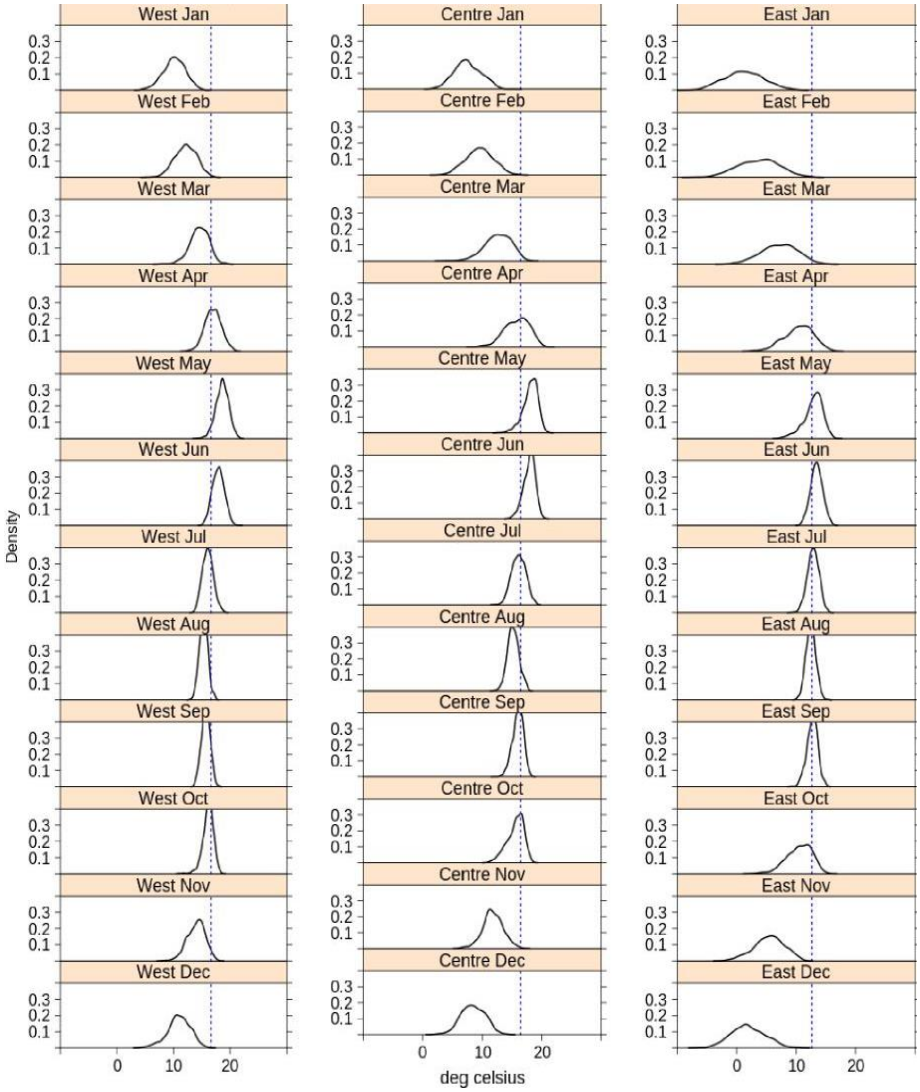

Fig. S2.5 Probability distribution of daily minimum temperature averaged over [14W-10W; 13N-17N] (West), [2W-2E; 13N-17N] (Centre) and [23E-27E; 13N-17N] (East) for each month of the year. The vertical dotted line represents the 75th percentile of the total distribution.

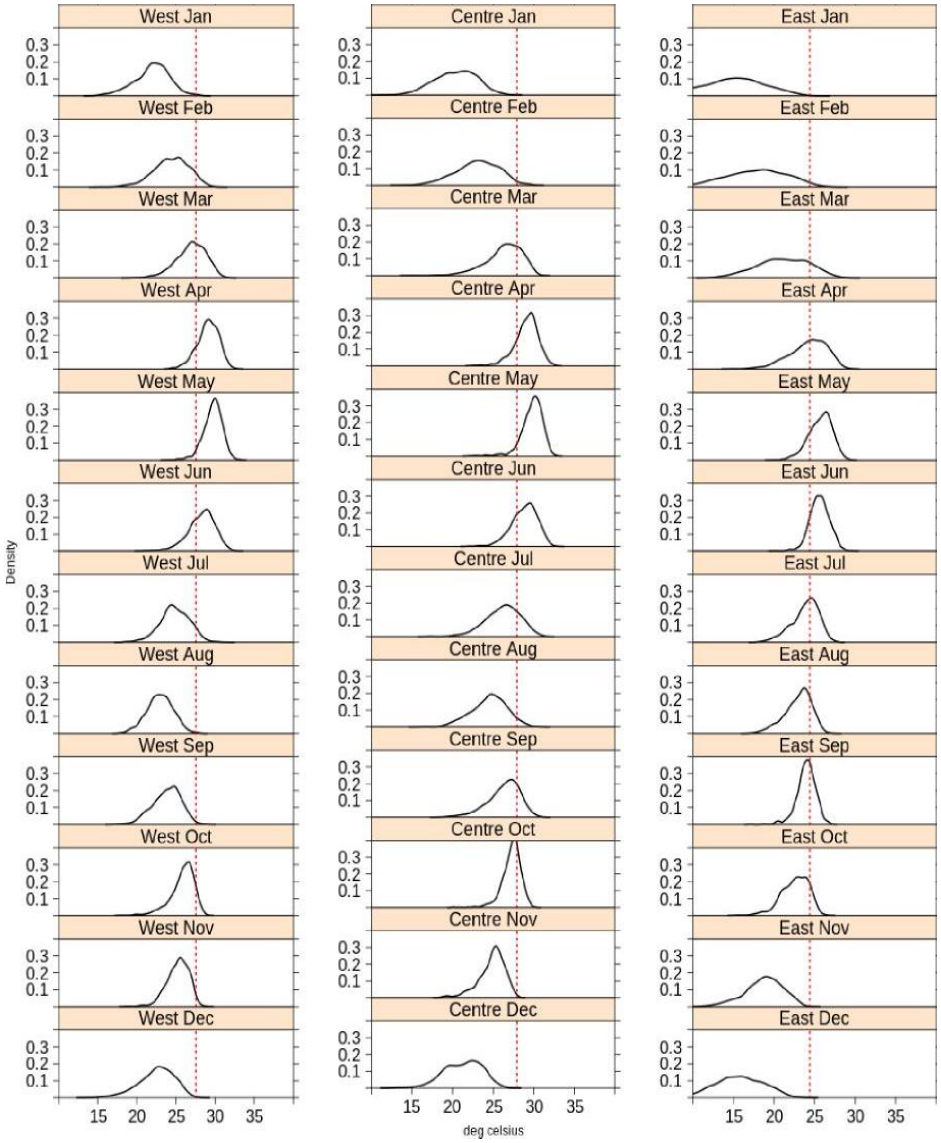

Fig. S2.6 same as Fig. S2.5 but for maximum temperature.

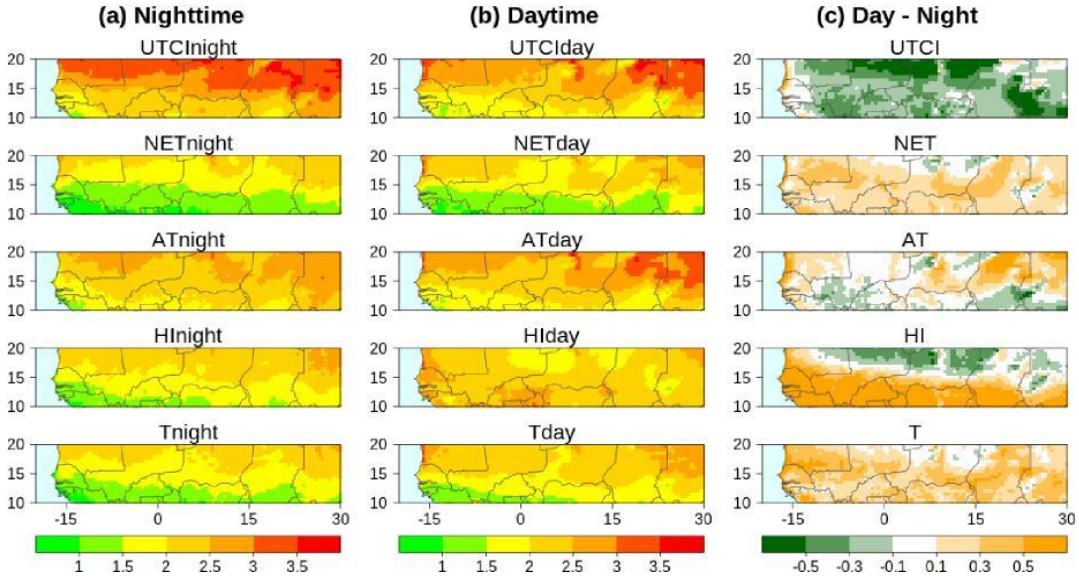

Fig. S2.7 Standard deviation of (a) nighttime indices, (b) daytime indices and the (c) difference between the both

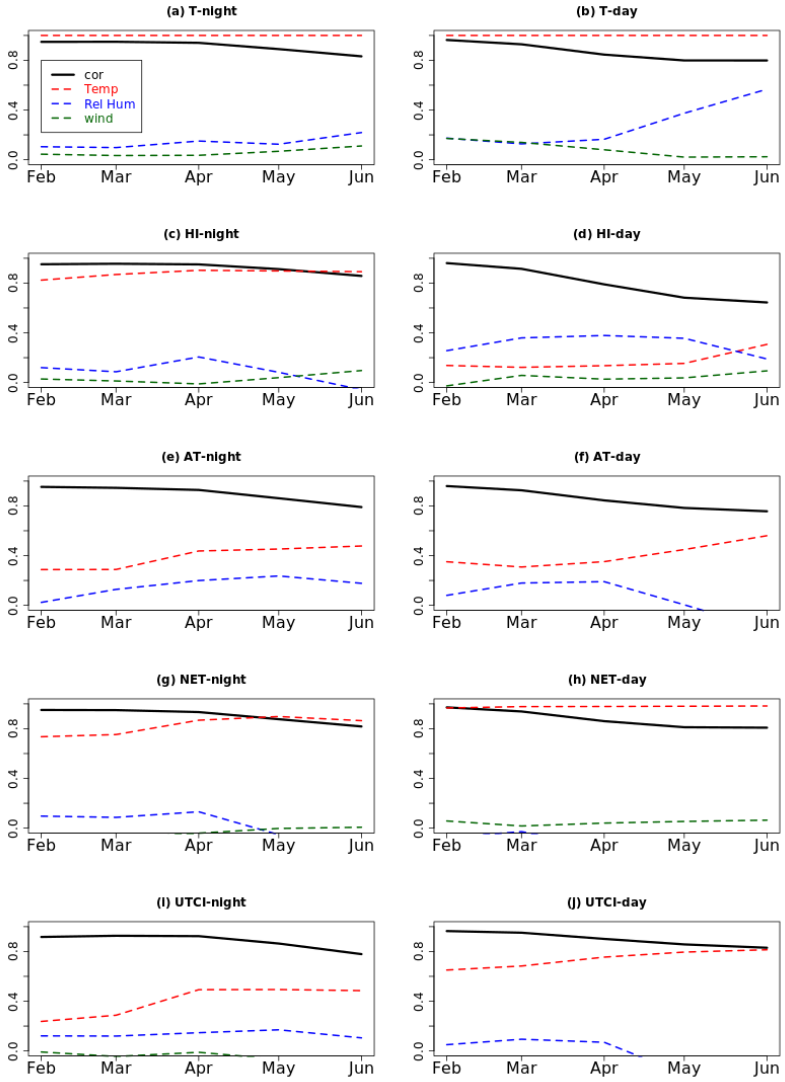

Fig. S2.8 Analysis of sources of uncertainty in heatwave statistics associated with thermal index parameterisation. Solid black lines: Coefficients of correlation between each thermal index and the other four of the same diurnal phase averaged for each month of the February to June period and over the Sahel domain. Dashed lines: coefficients of determination of the linear regression of each thermal index on temperature (red lines), near surface relative humidity (blue lines) and wind speed (green lines). See Section 2.2.2.2 for details on the computational method.

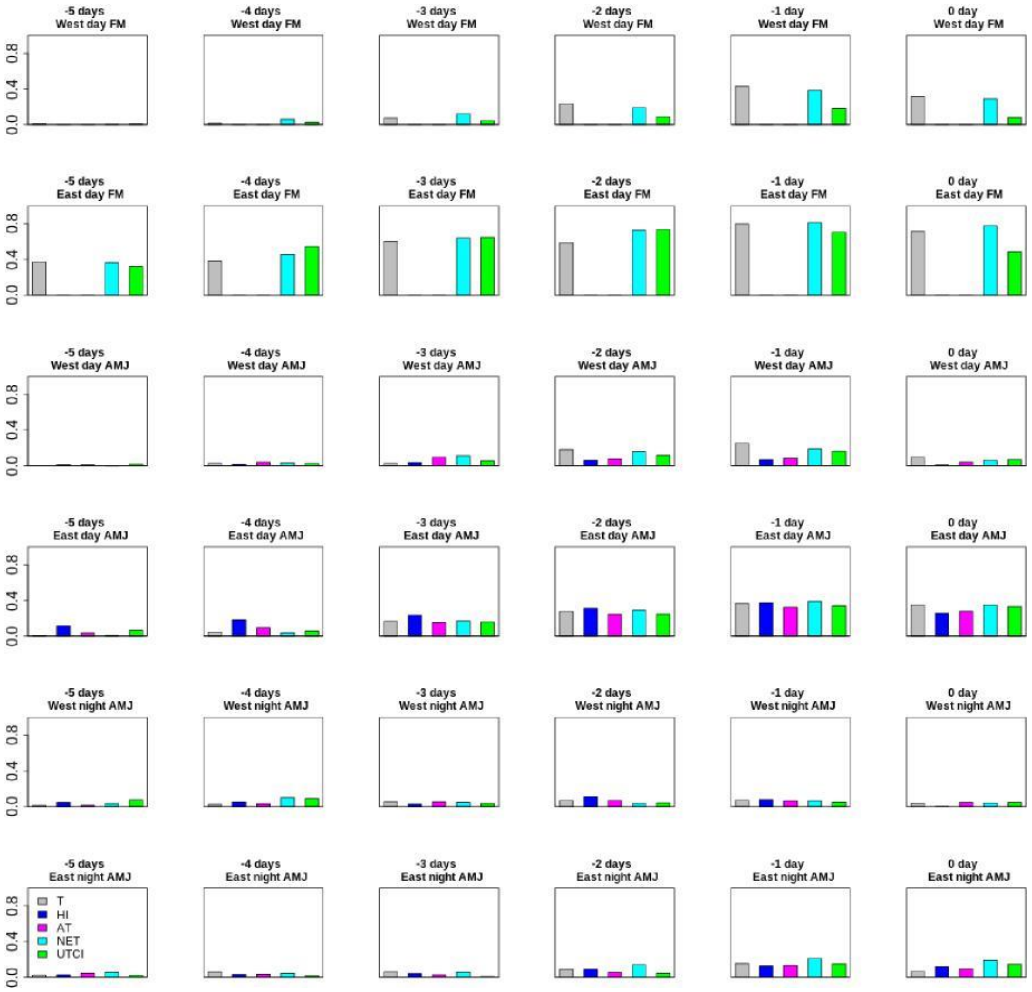

Fig. S2.9 EOF-based averages of standardised anomalies of temperature advection prior to and on the onset days for each thermal index. See Section 2.2.3.4 for computation methods. Only significant anomalies at the 0.05 probability level are considered.

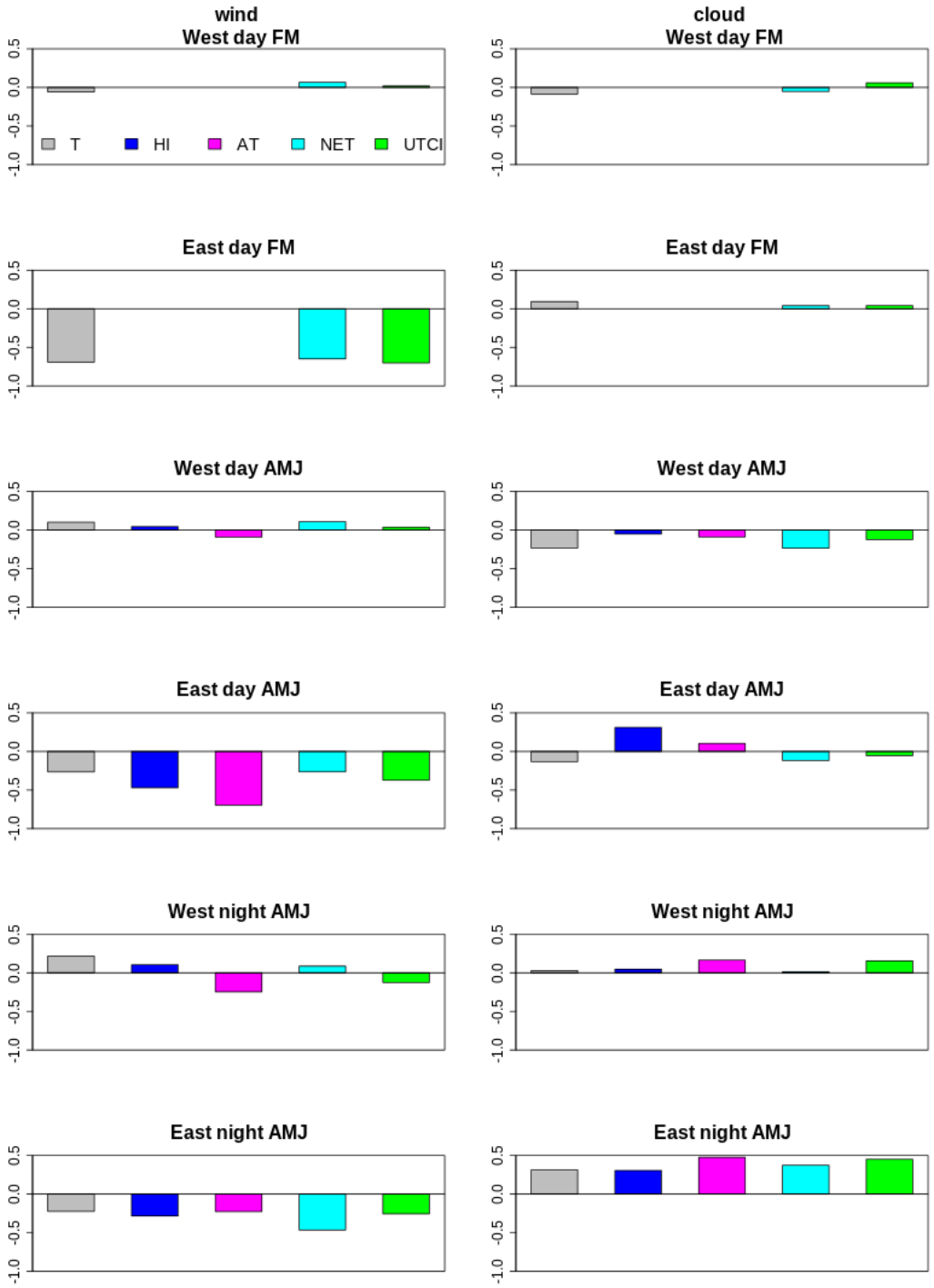

Fig. S2.10 EOF-based averages of standardised anomalies of 10m wind speed (left panel) and cloudiness (right panel) during heatwaves. Only significant anomalies at the 0.05 probability level are considered.

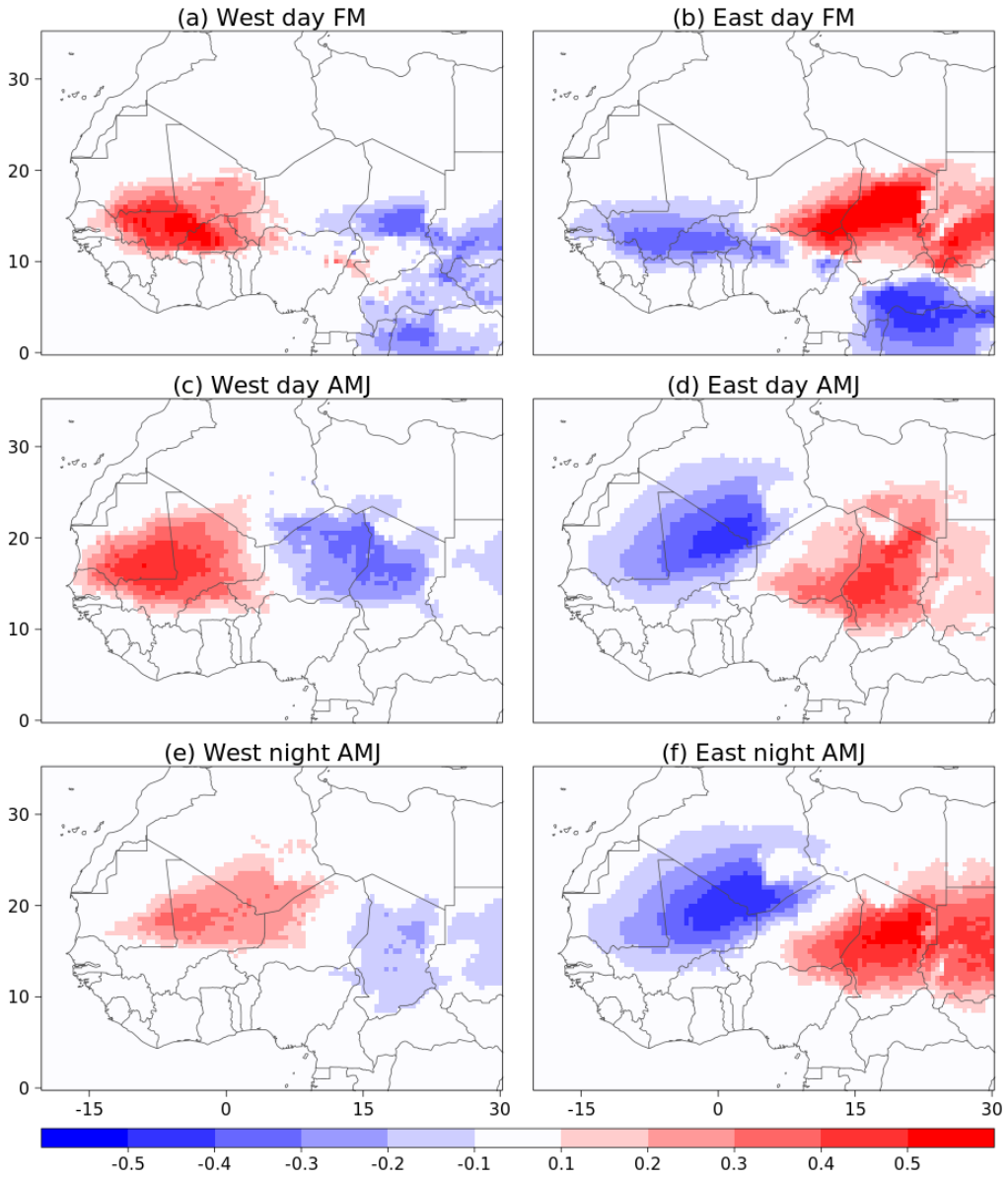

Fig. S2.11 Anomalies of occurrence of the WAHL during Sahelian heatwaves detected from the T index. The WAHL occurrence is defined as in Lavaysse et al. (2009).

Chapter 3. Atmospheric tropical modes are important drivers of Sahelian springtime heatwaves

Atmospheric tropical modes are important drivers of Sahelian springtime heatwaves

Kiswendsida H. Guigma[1*], Françoise Guichard[2], Martin Todd[1], Philippe Peyrille[2] and Yi Wang[1]

[1]University of Sussex, Brighton. UK

[2]Centre National de Recherches Météorologiques (CNRS) / Météo-France UMR 3589 Toulouse, Haute Garonne, France

[*]Corresponding author. Email address: k.guigma@sussex.ac.uk

Abstract

Heatwaves pose a serious threat to human health worldwide but remain poorly documented over Africa. This study uses mainly the ERA5 dataset to investigate their large-scale drivers over the Sahel region during boreal spring, with a focus on the role of tropical modes of variability including the Madden-Julian Oscillation (MJO) and the equatorial Rossby and Kelvin waves. Heatwaves were defined from daily minimum and maximum temperatures using a methodology that retains only intraseasonal scale events of large spatial extent. The results show that tropical modes have a large influence on the occurrence of Sahelian heatwaves, and, to a lesser extent, on their intensity. Depending on their convective phase, they can either increase or inhibit heatwave occurrence, with the MJO being the most important of the investigated drivers. A certain sensitivity to the geographic location and the diurnal cycle is observed, with nighttime heatwaves more impacted by the modes over the eastern Sahel and daytime heatwaves more affected over the western Sahel. The examination of the physical mechanisms shows that the modulation is made possible through the perturbation of regional circulation. Tropical modes thus exert a control on moisture and the subsequent longwave radiation, as well as on the advection of hot air. A detailed case study of a major event, which took place in April 2003, further supports these findings. Given the potential predictability offered by tropical modes at the intraseasonal scale, this study has key implications for heatwave risk management in the Sahel.

Keywords: heatwaves, tropical modes, Sahel, drivers, intraseasonal.

3.1. Introduction

The Sahel is a tropical semi-arid region located in West Africa that experiences high temperatures during the largest part of the year (Nicholson 2018), and especially in spring (March to June, MAMJ). Recent studies (Fontaine et al. 2013; Ringard et al. 2016; Moron et al. 2016; Oueslati et al. 2017; Guichard et al. 2017; Barbier et al. 2018) have highlighted an increase of extreme temperatures, and future projections predict even worse heatwave conditions (Russo et al. 2016; Dosio 2017; Déqué et al. 2017; Xu et al. 2020; Raymond et al. 2020).

Unfortunately, this region is also one of the least economically developed in the world (e.g. Davidson et al. 2003; Tschakert 2007), implying high levels of vulnerability. An efficient way of using the limited resources available to mitigate heatwave impacts, is to focus on preventive actions, based on skilful forecasts of these hazards as already implemented in other places (e.g. WMO N°1142; Wilkinson et al. 2018). The prevention however requires knowledge and understanding of the large-scale drivers of Sahelian heatwaves, which are both currently under-documented.

Greenhouse effect of moisture, hot air advection and incoming solar radiation (at daytime) appear as the dominant processes inducing extremely hot temperatures in spring over the Sahel (e.g. Slingo et al. 2009; Guichard et al. 2009; Oueslati et al. 2017; Guigma et al. 2020). The spring season also marks the peak of monsoon convection over the Guinean region of West Africa (i.e. south of 10°N; Nguyen et al. 2011), and, although not intuitive, there are potential links between convection and Sahelian heatwaves. Guigma et al. (2020) indeed found that large-scale heatwaves over the eastern Sahel are associated with a low-level cyclonic circulation anomaly over northern tropical Africa with an increase of precipitation over the Guinean band, versus an anticyclonic circulation anomaly and a decrease of Guinean precipitation for heatwaves over the western Sahel. When convection is weakened over the Guinean band, the associated northeasterly flow indeed allows the transport of hot air from the eastern Sahel/Sahara towards the coast of the western Sahel; conversely, a convective intensification conveys moisture from the Gulf of Guinea into the Sahel, through northward penetration of monsoon flow (e.g. Lothon et al. 2008; Couvreux et al. 2010), leading to longwave warming.

At the synoptic and intraseasonal scale, the Guinean convection is strongly modulated by tropical modes of variability, namely the Madden Julian Oscillation (MJO) and equatorial waves (e.g. Gu 2009; Kamsu-Tamo et al. 2014; Berhane et al. 2015). Can these modes of convective variability by extension modulate heatwaves in the Sahel? This is a plausible scenario in view of previous studies over West Africa. Moron et al. (2018a) for instance, using a weather type approach, found a

significant modulation of near surface temperature over northern tropical Africa by the MJO and equatorial Kelvin (EK) waves at the intraseasonal scale in spring. Advection of both hot air and moisture plays an important role in this modulation. Kalapureddy et al. (2010) also found that the synoptic variability over the Sahel, during the pre- (April to June) and post-monsoon (October and November) seasons, is controlled by monsoon surges with a periodicity similar to that of the African Easterly Waves (AEWs; 3-5 days). Furthermore, Couvreux et al. (2010) indicated that these surges can be stationary or westward moving, along with the AEWs. In the same logic, Mera et al. (2014) showed that synoptic and subseasonal circulation disturbances, driven by extratropical cyclones and also by EK and equatorial Rossby (ER) waves, and possibly by the MJO, lead to influx of moisture from the Gulf of Guinea into the Sahel.

Connections between heatwaves and atmospheric synoptic and intraseasonal modes of convective variability have already been evidenced in other regions. Murari et al. (2016), for example, found that the delay of the Indian monsoon onset weakens southwesterlies in the Arabian Sea, favouring clear sky days over India, and subsequently longer lasting and warmer heatwaves. In South America, the intraseasonal variability considerably modulates heatwaves in association with the Southern Atlantic Convergence Zone (Cerne and Vera 2011). In the southeastern part of Australia, Parker et al. (2014) showed that warm conditions are significantly associated with the phases 3-6 of the MJO. More recently, the summer 2018 long lasting heatwave over Northeast Asia was found by Hsu et al. (2020) to have been favoured by an unusually strong MJO over the western Pacific warm pool.

The present research aims at assessing the extent to which and in what ways Sahelian heatwaves are modulated by tropical modes during the MAMJ season. The reason for the focus on tropical modes is the potential for predictability at intraseasonal lead times. Tropical modes are indeed good sources of predictability at these scales (Moron et al. 2018b; Dias et al. 2018; Bengtsson et al. 2019; Li and Stechmann 2020; Judt 2020).

To the best of the authors' knowledge, this study is the first to use a systematic and comprehensive approach to investigate the impact of tropical modes on actual heatwaves in the Sahel. Two complementary methods are used for this purpose. The first consists of a statistical study over the 1979-2018 period while the second exemplifies the emerging overall processes with a detailed case study event in April 2003.

The rest of the manuscript is structured as follows. The data and the methods used are summarised in Section 3.2. Then, Section 3.3 presents the results obtained from the statistical study. In Section 3.4,

the case study of the 2003 heatwave event is analysed in detail. Finally, conclusions and perspectives are given in Section 3.5.

3.2. Methodology

The Sahel area is hereafter defined as the continental domain limited by the coordinates 20°W, 30°E, 10°N, 20°N. Since this work aims at depicting the large-scale drivers, the analysis however extends to the entire northern half of Africa, and sometimes to an even larger domain.

3.2.1. Data

The main dataset used in this paper is the fifth generation of the European reanalyses ERA5 (Hersbach et al. 2020) at a resolution of 0.5° x 0.5°, covering the period 1979-2018. The reason for the choice of this dataset is that it likely offers the best representation of near surface meteorological variables (Olauson 2018; Ramon et al. 2019) as well as radiative fields over land (Martens et al. 2020), and provides a comprehensive and self-consistent set of variables for diagnostic analysis.

This dataset is thus used in this research for (i) heatwave detection from daily minimum and maximum temperature at 2m (hereafter referred to as "Tmin" and "Tmax" respectively), (ii) tropical mode filtering from outgoing longwave radiation (OLR), and (iii) retrieving physical fields to understand the mechanisms of modulation. Previous studies (Oueslati et al. 2017; Barbier et al. 2018) have already shown the good quality of near surface thermal indices (including Tmin and Tmax) over the Sahel in ERA-Interim of which ERA5 is an improvement. OLR in ERA5 is taken as the negative of the net top-of-atmosphere (TOA) thermal radiation. Wang et al. (2017), Tall et al. (2019), Wright et al. (2020) and Hersbach et al. (2020) assessed radiative fluxes in different products and found that ERA5 shows TOA fluxes (including OLR) that are very consistent with the observed. Using observed OLR data such as the daily interpolated data from the NOAA (Liebmann and Smith 1996) does not significantly alter the results obtained with ERA5 (not shown), making it suitable for the present study.

Some of the physical variables used for analysing the mechanisms of heatwave modulation are directly available from ERA5: temperature, zonal and meridional components of wind, specific humidity, precipitable water and radiation data. As in Oueslati et al. (2017), the surface energy budget is derived from the radiation fields using the following equation:

$$\frac{c_s \Delta T}{\Delta t} = SWR + LWR + SHF + LHF \quad (1)$$

Where SWR is the net shortwave radiation, LWR is the net longwave radiation, SHF is the sensible heat flux, LHF is the latent heat flux and c_s is the surface heat capacity.

Radiative fluxes are hereafter counted positively when directed from the atmosphere to the surface.

Other meteorological variables necessary for understanding the physical mechanisms of heatwave modulation are not directly accessible from ERA5 and are thus derived. These include advection of heat (equation 2) and of specific humidity (equation 3) which are obtained from the horizontal components of wind speed, temperature and specific humidity:

$$A_T = -\vec{V}\vec{\nabla}T = -u\frac{\partial T}{\partial x} - v\frac{\partial T}{\partial y} \quad (2)$$

$$A_q = -\vec{V}\vec{\nabla}q = -u\frac{\partial q}{\partial x} - v\frac{\partial q}{\partial y} \quad (3)$$

Where T is temperature, q specific humidity and $\vec{V}$ horizontal wind which is decomposed into its zonal (u) and meridional (v) components.

All variables of the ERA5 database described in this section are available at an hourly frequency. The radiative variables are extracted as 12-hourly accumulations (0600 UTC to 1800 UTC for daytime and 1800 UTC to 0600 UTC of day +1 for nighttime) while the others as instantaneous entries at a 03-hourly resolution. For the latter, the daytime value is obtained by averaging over 0900, 1200, 1500 and 1800 UTC and the nighttime value over 2100, 0000, 0300 and 0600 UTC.

For the specific case of the derived variables (heat and moisture advection), they are first computed at the 03-hourly timescale before daily averaging.

In addition to the ERA5 reanalysis, various observational data have been utilised mainly for the case study (Section 3.4). Satellite estimates of radiative surface fields (incoming and outgoing shortwave and longwave radiation) were extracted from the Clouds and Earth's Radiant Energy System (CERES) Synoptic (SYN1deg) Product (Wielicki et al. 1996; Doelling et al. 2013, 2016) at a spatial resolution of 1° x 1° over the time period 2000-2018. The initial 03-hourly temporal resolution was aggregated to a daily frequency. Satellite estimates of precipitable water from the Atmospheric Infrared Sounder (AIRS, Teixeira et al. 2013) aboard NASA's second Earth Observing System polar-orbiting platform was also used for the case study at 1° x 1° spatial grid. Twice-daily data provided by the ascending and descending orbits were averaged to get daily estimates. This dataset runs from

2002 to 2016. To analyse the evolution of precipitation over the case study period, daily rainfall totals from the Global Precipitation Climatology Project (GPCP, Schamm et al. 2014) were used at a resolution of 1°x1°. Finally observed 2m temperature and specific humidity data at the Demokeya station in Sudan located at 30.5°E-13.3°N (Ardö 2013) were also investigated. The data cover the 2002-2012 period with a temporal resolution of 30 minutes. This provides a valuable in-situ observation over the eastern Sahel, a data sparse region, where the case study is mainly investigated.

3.2.2. Heatwave detection

Among the different definitions of heatwaves (Perkins 2015), a choice has been made on one allowing to capture major, large-scale events occurring over synoptic to intraseasonal scales during the spring season. Tropical modes are indeed planetary-scale disturbances and their effects are more likely to cover extensive areas than smaller isolated areas. Therefore, as in Guigma et al. (2020), Tmin and Tmax data are first 90-day highpass filtered to retain variability on the scales of interest. Then, potential heatwaves are defined at a given grid-point as spells of at least three consecutive days where the daily anomalies of Tmin or Tmax (taken separately) exceed the 90^{th} percentile of the distribution of the corresponding calendar days. The 90^{th} percentile for a given calendar day is derived, similarly to Russo et al. (2014) and Guigma et al. (2020), over a 31-day window centred on that day, to remove noise caused by the relative shortness of the dataset. After this step, to ensure sampling of only absolutely hot events regardless of the period of the year, potential heatwaves sampled on days where the raw data (i.e. data before deriving the anomalies) do not exceed the 75^{th} percentile of their total distribution are discarded (Guigma et al. 2020). Heatwave intensity is defined, at each grid-cell and for each heatwave day (not event), as the 90-day highpass filtered anomaly of Tmin (for a nighttime heatwave) or Tmax (for a daytime heatwave) on that day. Next, major large-scale events are defined by adding a minimum spatial extent threshold of 600,000 km^2 using a region growing technique as in Barbier et al. (2018). The outcome is a set of daily binary masks specifying the regions where these large-scale heatwaves occur, providing the final sample of heatwaves analysed in this study.

It should be noted that heatwaves can also be defined from other thermal indices than Tmin and Tmax, taking into account additional environmental variables (moisture, wind, solar radiation) as in Guigma et al. (2020). Only Tmin and Tmax are however retained for this study because of the consistency of the results across these indices (not shown).

3.2.3. Tropical mode detection

In this study, the expression “tropical modes" refers to the synoptic and intraseasonal modes of variability of the tropical atmosphere including the MJO and equatorially trapped waves. The MJO is the most important driver of intraseasonal variability of the tropical atmosphere (Madden and Julian 1971, 1972, 1994) and influences the West African Monsoon (e.g. Sossa et al. 2017). In this study, equatorial waves are explored in connection with convection (hence the expression convectively coupled equatorial waves CCEWs). Over West Africa, Kamsu-Tamo et al. (2014) and Schlueter et al. (2019, a,b) demonstrated statistically and dynamically that they have an impact on convection. In the present paper, the equatorial waves under investigation are the ER and EK waves. Other waves such as AEWs and mixed Rossby-gravity waves are not included as they are not so active in the region during the season of interest (MAMJ).

Table 3.1. Characteristics of each mode used in this study. The definition of each characteristic is given in Section 3.2.3.

Mode	Wavenumber band	Period band (days)	Equivalent depth (m)	References
MJO	0 to 9	20 to 100	Not specified	Kiladis et al. (2005)
ER	-10 to -1	9.7 to 72	1 to 90	Kiladis et al (2009)
EK	1 to 14	2.5 to 20	8 to 90	Straub & Kiladis (2002), (Mekonnen et al. 2008)

Each tropical mode is characterised by a range of wavenumbers, periods and equivalent depths summarised in Table 3.1. A wavenumber is the number of waves (each wave comprising one ridge and one trough) that it takes to zonally circumscribe the globe. The period of a wave measures the time separating the passage of two consecutive ridges at a given location. As for the equivalent depth, a more complex notion used for ER and EK wave filtering, it refers to the depth of the shallow layer of atmospheric fluid that is required (by theory) to get the appropriate values for the time-varying and horizontal components of their motion (Wheeler and Nguyen 2015).

Tropical modes are detected from the fields of OLR, which is a good proxy for tropical convection (Arkin and Ardanuy 1989), and has been extensively used in tropical mode investigation over West Africa (e.g. Lavender and Matthews 2009; Pearson et al. 2010; Yang et al. 2018). To extract a given

mode, the mean and first three harmonics of the OLR annual cycle are first removed to obtain intraseasonal anomalies. Then, the filtering in the wavenumber-frequency space consists of setting to zero any spectral coefficient outside the window corresponding to the mode of interest (Table 3.1), such that only the relevant coefficients are retained. The "kf_filter" function of the NCAR Command Language (NCL) was used for this operation. The output of the wavenumber-frequency decomposition is thus a three dimensional (time, longitude and latitude) filtered OLR field for each mode. The full explanation of the method can be found in Wheeler and Kiladis (1999) and Kiladis et al. (2006). No decomposition of the input data into asymmetric and symmetric components is done because the area of interest is fully located on one side of the Equator (northern hemisphere), as already done in several previous studies (e.g. Schreck et al. 2011; Lafore et al. 2017).

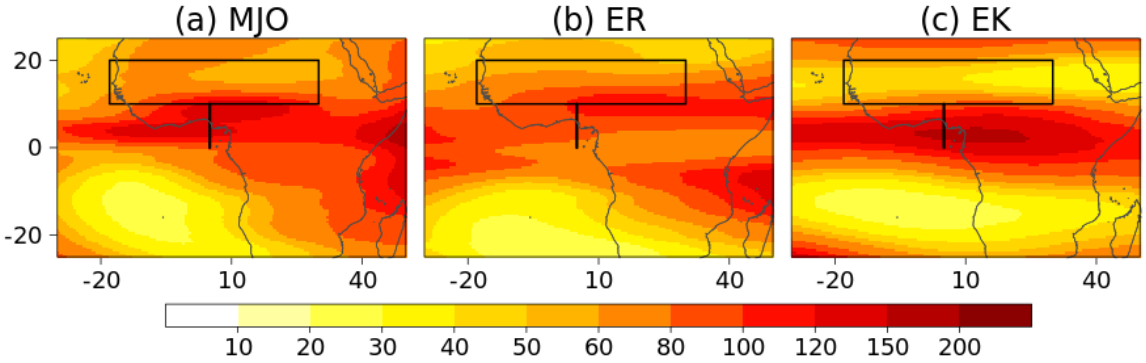

Fig. 3.1 Variance (in W^2m^{-4}) of mode-filtered OLR data during MAMJ. The rectangular box delimits the Sahel region. The vertical line marks the reference longitude (5°E) and latitudinal band over which the local activity of tropical modes is characterised (see Section 3.2.3).

In order to characterise the daily local activity of each mode, a phase and amplitude are determined as follows. Firstly, the 5°E longitude (centre of the Sahel domain) is arbitrarily set as reference longitude. Minor variations of the reference longitude do not significantly impact the results (not shown). Then, the daily mode-filtered OLR data at this longitude are averaged over the Guinean zone, i.e. for the latitudes between the Equator and 10°N (vertical line in Fig. 3.1), where convection is the most active in spring (Nguyen et al. 2011). Including latitudes up to 20°N does not make significant changes to the results. As in Riley et al. (2011), the resulting unidimensional timeseries and its (first order) local time derivative (both normalised by their respective standard deviations) are used to derive the trigonometric form of the corresponding mode, from which an angle and an amplitude are

extracted for each day. On a given day, a mode is considered active only if its amplitude is greater than one. Changes to this threshold do not affect the spatial structures of the impact of tropical modes on heatwaves but the magnitude of this impact is slightly modified and is discussed in Section 3.3.3. For the active days of each mode, the angles are further binned into eight 45° wide phases labelled 1 to 8 such that phase 1 represents instances where the mode is the most convectively suppressed (maximum of OLR), phase 5 the most convectively enhanced (minimum of OLR) and the six others are transitory phases (see the description of the full method in Riley et al. (2011)). Thus, a given active mode (active because passing the minimum amplitude threshold) can be either in a convectively suppressed or a convectively enhanced phase. It should be noted that, while the practice of setting a reference longitude effectively allows to detect the passage of tropical modes in the region, and to better characterise their local activity, it however comes with the caveat that, away from this longitude, the signal weakens progressively. As a consequence, towards the boundaries of the region, the modes with large wavenumbers are not as well accounted for as those with small wavenumbers.

3.2.4. Modulation of heatwaves by tropical modes and associated evolution of physical variables

The modulation of heatwave probability of occurrence and heatwave intensity is assessed, during the spring season, by modifying a method initially used by Xavier et al. (2014) for extreme rainfall and Hsu et al. (2017) for heatwaves. It consists of comparing heatwave probability/intensity when a given mode is active on a specific phase versus the climatological probability/intensity during the MAMJ season. The modulation of heatwave probability (MP) is thus given by the following formula:

$$MP = \frac{P_x - P_a}{P_a} \quad (4)$$

where P_x is heatwave probability given the mode is in phase x, i.e. the number of days where heatwaves occur during phase x over the total number of days where the mode is in this phase; P_a is the climatological probability of heatwaves, i.e. the number of heatwave days (regardless of the activity of the modes) over the total number of days. The probabilities are defined in terms of days rather than events, consistently with Hsu et al. (2017).

Likewise, the modulation of heatwave intensity (MI) is defined as follows:

$$MI = \frac{I_x - I_a}{I_a} \quad (5)$$

Where I_x is the average heatwave intensity (defined for each heatwave day and at each grid-cell as the highpass filtered anomaly of Tmin or Tmax on that day; Section 3.2.2) given the mode is in phase x and I_a the climatological intensity of heatwaves.

As will be shown in Section 3.3.1, heatwaves can be associated with distinct active tropical modes at different phases, in such a way that the superposition of two modes can lead to an amplified or reduced forcing on heatwaves. The modulation of heatwave probability by two superposed modes is investigated using the following formula:

$$MP = \frac{P_{xy} - P_a}{P_a} \quad (6)$$

P_{xy}: heatwave probability when the first mode is in phase x and the second mode in phase y.

P_a: heatwave climatological probability.

The significance of the modulation patterns is tested at each grid-point and for each phase of the modes through bootstrap resampling (Wang et al. 2008, Mazdiyasni and AghaKouchak 2015, Nissan et al. 2017, Harrington et al. 2019). Let N be the number of days where a given mode is in phase x (or one mode in phase x and another in phase y for the superposition case). Then, 1000 random samples, each of size N days are generated. Heatwave probability (or average intensity) is calculated for each sample. From these random probabilities (or average intensities), corresponding values of modulation of heatwave probability (intensity) are derived using equation (4), (5) or (6) accordingly. Significance is finally tested at a 5% probability level against these 1000 random modulation values.

The results of the modulation of heatwave probability are presented in Section 3.3.3, and that of heatwave intensity in Section 3.3.4.

To understand the physical mechanisms associated with the modulation of heatwaves, the composites of each of the diagnostic variables (presented in Section 3.2.1.) are derived over all active mode-phase days. To do this, the mean and the first three harmonics of the seasonal cycle for each variable are first removed. Then, they are passed to a Lanczos highpass filter (Duchon 1979) to retain variability at timescales shorter than 90 days. The filtering causes a loss of data at both edges of the input time series (also observed for heatwave detection and OLR filtering); therefore the analyses cover the 1980-2017 period. Finally, the composite mean of a given variable over a certain instance (e.g. phase x of a mode) corresponds to the average of this variable over all days of this instance. At each grid-

point, the significant departure of the average values from zero is tested using the Student's t-test at the 0.05 probability level. The results are shown in Section 3.3.5.

For the case study purpose, the activity of tropical modes is projected onto various physical fields, similarly to previous studies (e.g. Kiladis et al. 2006; Knippertz and Todd 2010). To do this, the daily mode-filtered OLR data are regressed onto the daily highpass filtered anomalies of the physical variables at each grid-point over the 1980-2017 period. Then, the influence of each tropical mode on the variable during the heatwave event is qualitatively estimated on a daily basis, using the predicted value of the diagnostic variable by the linear regression model. The advantage of this technique is that it allows on a given day to know the likely impact of a certain mode on a physical process (results in Section 3.4.4).

Table 3.2. General statistics associated with the activity of tropical modes at the reference longitude of 5°E. See Section 3.3.1 for the analysis.

Total number of MAMJ days over the 1980-2017 period	4636
Percentage of days where at least one mode is active	96.5%
Percentage of days where exactly one mode is active	19.0%
Percentage of days where the MJO is active **(and of which EK and ER are inactive)**	72.7 % **(9.3%)**
Percentage of days where the ER is active **(and of which MJO and ER are inactive)**	65.7 % **(6.6%)**
Percentage of days where the EK is active **(and of which MJO and ER are inactive)**	70.4% **(11.1%)**
Number of days where the MJO is active in phase 5 **(and where ER and EK are inactive)**	409 **(22)**
Number of days where the MJO is active in phase 1 **(and where ER and EK are inactive)**	458 **(41)**

Number of days where the ER is active in phase 5 **(and where MJO and EK are inactive)**	393 **(25)**
Number of days where the ER is active in phase 1 **(and where MJO and EK are inactive)**	409 **(42)**
Number of days where the EK is active in phase 5 **(and where MJO and ER are inactive)**	390 **(40)**
Number of days where the EK is active in phase 1 **(and where MJO and ER are inactive)**	443 **(38)**

3.3. Modulation of heatwaves by tropical modes: a statistical analysis

3.3.1. Activity of tropical modes over Africa during the spring season

Table 3.2 presents statistics associated with the activity of tropical modes over the Guinean region as detected at the reference longitude of 5°E (described in Section 3.2.3) focusing mainly on the most suppressed and the most enhanced phases (phases 1 and 5 respectively). During the MAMJ season, at least one mode is active 96% of the time irrespectively of the phase. Therefore, the spring season is intense in terms of tropical mode activity. For each of these modes, the activity is evenly distributed across the eight phases without a preference for any of them (not shown). The number of active days is not much different from one mode to another but it is apparent that the MJO has the largest sample. The occurrences of exactly one mode (whichever it is) at a given time exclusive of any other mode are quite infrequent (19% of the time). For a given active phase of any mode, merely 10% of its passages satisfy this configuration. Therefore, active tropical modes generally overlap. Consequently, an explicit analysis of the impact of these situations on Sahelian heatwaves is undertaken in Section 3.3.3.

The amount of OLR variability explained by the modes is clearly different between them. Figure 3.1 shows the variance of the mode-filtered anomalies of OLR during the MAMJ season. The MJO, EK and ER waves by decreasing order, have an intense activity over the Guinean sector in boreal spring. For the MJO and EK waves, the variance peaks at above 200 W^2m^{-4} near the Equator (Figs. 3.1a & 3.1c). The MJO is active over the entire sector between 10°S and 15°N. On the other hand, the EK

waves are active only within a band surrounding the Equator consistent with theory (the high variance of EK waves observed at the edges of the domain are mainly due to imperfections in the filtering technique which allows in noise from the mid-latitude eastward Rossby waves). As for the ER waves, they maintain a relatively important activity (peaks exceeding 150 W^2m^{-4}) over the eastern and central parts of the domain (Fig. 3.1b).

There is a slightly different seasonality between the modes during the spring season. The peak of convective activity related to the MJO occurs in March and April, that of EK waves in April and May whereas the ER is the most active in May (Fig. S3.1). The activity of these three modes decreases significantly in June, prior to the onset of the Sahelian phase of the West African monsoon (e.g. Fitzpatrick et al. 2015). This seasonality is further shown by the monthly count of active days of each mode at the reference longitude of 5°E (Fig. 3.2).

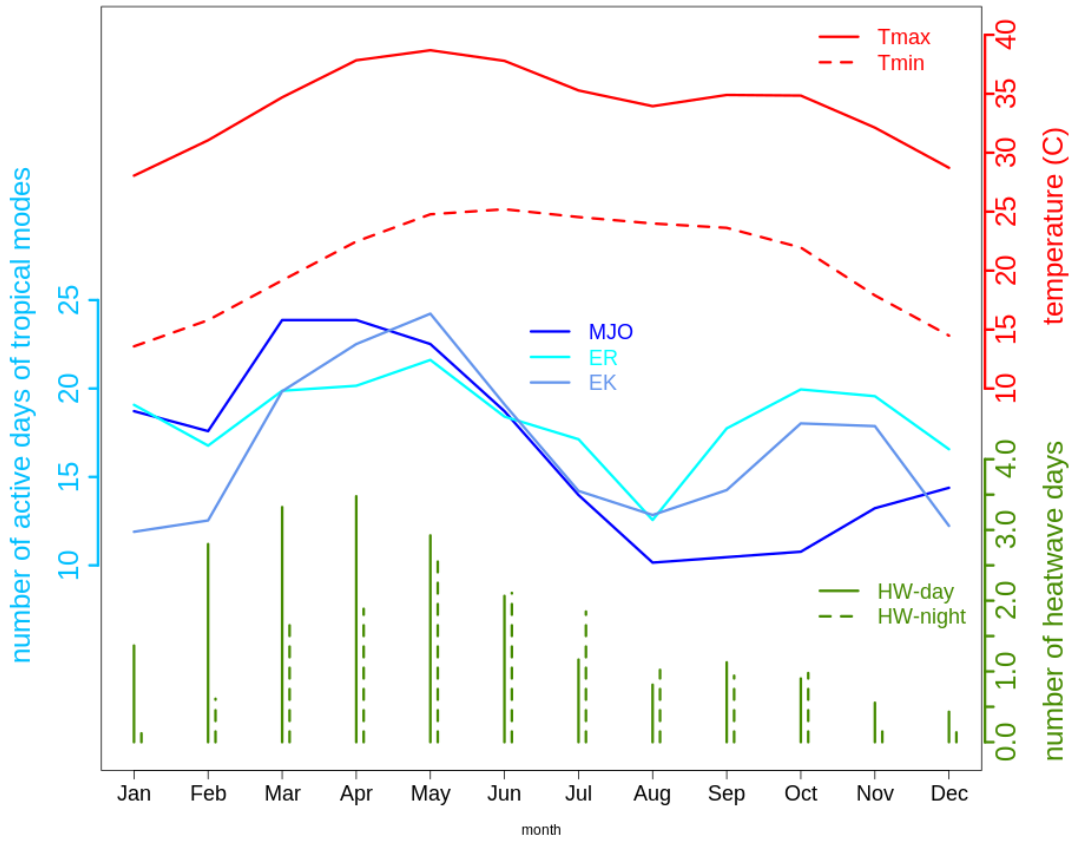

Fig. 3.2 Seasonality of the activity of tropical modes and heatwave occurrence. Bluish lines :monthly count of active days of the MJO, EK and ER waves as detected at the reference longitude of 5°E between the equator and 10°N (the definition of an active day is given in Section 3.2.3.). Green histograms: monthly count of the

number of daytime (solid bars) and nighttime (dashed bars) heatwave days spatially averaged over the Sahel domain. Red lines: Monthly values of Tmax (solid lines) and Tmin (dashed lines) spatially averaged over the Sahel domain.

3.3.2. Synoptic to intraseasonal heatwaves in the Sahel

Previous publications have already elaborated on the statistical characteristics of Sahelian heatwaves at different timescales. There is a general consensus on their short-lasting nature (e.g. Oueslati et al. 2017; Guigma et al. 2020) and their important intensity owing to the hot mean state of the region (red lines in Fig. 3.2). They are more frequent over the eastern and central Sahel, as shown by the count of springtime heatwave days at each grid-point over the 1980-2017 period in Fig. S3.2 (which provides the sampling basis of heatwaves for this study). As with tropical modes, the frequency of occurrence of synoptic to intraseasonal scale heatwaves has a moderate seasonality. Figure 3.2 shows that daytime heatwaves are mostly observed between February and June, with a peak in April. On the other hand, nighttime heatwaves occur mainly between March and July with May standing as the most heatwave-prone month. There is thus a shift of nighttime heatwaves with respect to their daytime counterparts. The main reason for this is probably the larger dependence of Tmin (and thus nighttime heatwaves) on low-level moisture whose penetrations into the Sahel are more frequent closer to the onset of the monsoon (Couvreux et al. 2010; Mera et al. 2014).

3.3.3. Modulation of heatwave probability of occurrence by tropical modes

This section first discusses the impact that each tropical mode, taken separately, has on heatwave occurrence, before analysing the outcome of the superposition of several modes.

1) Heatwave modulation by modes taken separately

Figure 3.3 shows the phase-longitude diagram of the modulation of heatwave probability (MP) averaged over the Sahel band (10°N-20°N) for the MJO, ER and EK waves during the spring season. Among these three investigated modes, the MJO stands as the lead modulator of heatwave occurrence in the Sahel (Figs. 3.3a & 3.3b) and its eastward propagation is clearly reflected in the modulation MP pattern. Overall, phases 1 to 4 are associated with higher heatwave probability than the climatological probability of occurrence. The values of MP, averaged over the Sahel band, can be as high as 1 (i.e. heatwaves are twice more likely under these phases than according to their climatology). Reversely for phases 5 to 8, the probability of heatwave occurrence is lower than usual.

For these phases, MP is typically below -0.5, meaning that the probability of occurrence is less than half of its climatological value. The patterns are relatively similar for daytime and nighttime heatwaves, but it is apparent that the stripe of positive MP values is wider in Tmin heatwaves than in Tmax (red stripe in Fig. 3.3a vs Fig. 3.3b), and reversely for the stripe of negative MP values (blue stripe in Fig. 3.3a vs Fig. 3.3b), especially over the western Sahel.

The modulation of Sahelian heatwaves by the ER wave (Figs. 3.3c & 3.3d) is less important than by the MJO. Heatwave probability of occurrence is mostly below normal when the ER wave is in phases 5 to 8 with values of MP generally higher than -0.5 (i.e. of lower intensity than observed for the MJO). In phases 1 to 4, there is a higher heatwave risk than normal over much of the Sahel, with positive MP values although usually lower than 1. It should be noted that the modulation by the ER wave is more sensitive to the diurnal cycle and geographic location than the two other modes. For example, daytime heatwaves over the eastern Sahel are only marginally affected by the activity of the ER wave

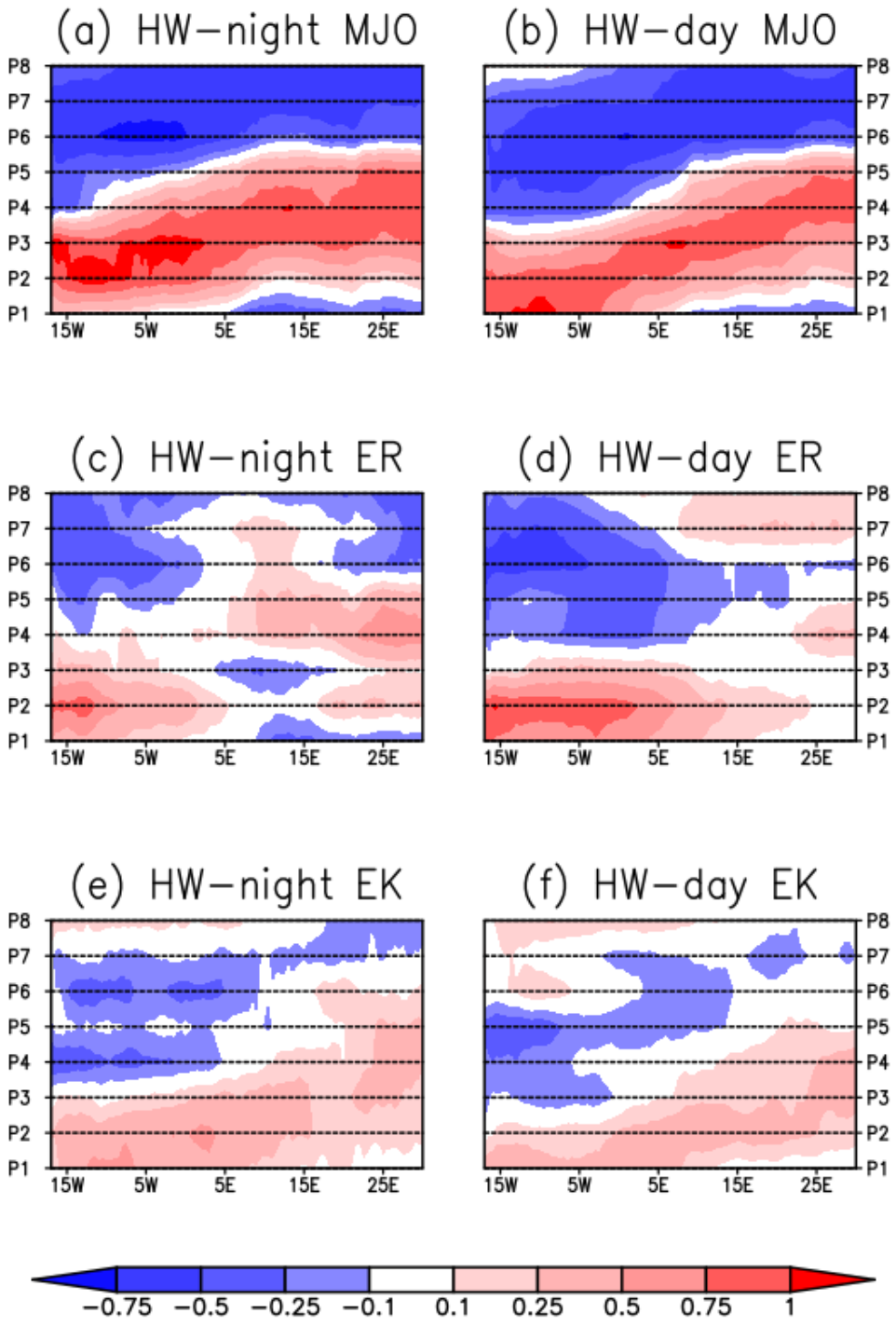

Fig. 3.3 Phase-longitude diagrams of the modulation of (left panel) nighttime and (right panel) daytime large-scale heatwave probability of occurrence by the MJO, ER and EK waves during MAMJ averaged over the Sahel band (10°N-20°N). The modulation corresponds to the variable MP defined in Section 3.2.4 (equation (4)) as a comparison of heatwave probability of occurrence in a given active phase versus the climatological probability. Significance was tested at the probability 0.05 level, using bootstrap resampling of tropical mode active days, with 1000 repetitions.

whereas nighttime heatwaves are much more impacted. On the other hand, over the western Sahel, the modulation is more important for daytime than nighttime heatwaves (this is valid for both positive and negative modulations).

The spatial patterns of the modulation of heatwaves by the EK wave (Figs. 3.3e & 3.3f) are similar to that of the MJO with marked eastward propagation in both cases. However, they present narrower stripes and lower magnitude than with the MJO. The values of MP are indeed in most cases absolutely below 0.5, making the EK wave the least important of the three modes for heatwave occurrence in the Sahel. They present only little sensitivity to the diurnal cycle.

The amplitude of tropical modes, as stated in Section 3.2.3, does not affect the spatial distribution of MP. On the other hand, with increasing amplitudes, the values of MP are slightly increased (without changing their sign). This is illustrated in Fig. S3.3, using a minimum amplitude of 2. Therefore, the stronger the amplitude of tropical modes, the more confident the changes of heatwave probability described above are.

The main reason why the MJO has a greater influence on heatwaves than the ER and EK waves is very likely related to its spectral properties. Heatwaves are slowly varying events whose minimum duration is set to three days here. Therefore, for a given mode to influence their occurrence, it should be able to sustain conditions which are favourable to the heating of the atmosphere for a long-enough amount of time. Evidently, the longer the period of a mode the higher its ability to develop such conditions. This sensitivity of the modulation to the temporal scale corroborates previous results by Schlueter et al (2019a) who investigated the modulation of precipitation in West Africa by tropical modes. Indeed, they found that, on the scale of three days, the MJO, ER and EK waves have an equal importance on precipitation while on the scale of a week, the effect of EK wave becomes marginal and beyond 20 days, the MJO is the only mode able to significantly contribute to precipitation variability. Besides, the additional constraint on the spatial extension of heatwaves may also favour the MJO. Consequently, the results of this study imply that the smaller the wavenumber of a mode, the more likely this mode can trigger heatwaves as it is also more able to promote warming conditions that spread over large areas.

It should be noted that the patterns of the modulation of heatwaves shown at the seasonal scale are generally consistent across the different months. However, some differences are noticeable, especially with nighttime heatwaves, for some modes. Thus, phases 1 to 4 of the ER wave lead to a

decreased probability of nighttime heatwave occurrence over the central Sahel (broadly between 0°E and 20°E) in early spring (March-April) whereas the probability is increased in late spring (May-June), and reversely for phases 5 to 8 (Fig. S3.4a vs Fig. S3.4b). For the EK wave, the decrease of heatwave probability observed in phases 5 to 8 is much more pronounced in late spring than in early spring (Fig. S3.4c vs Fig. S3.4d).

Table 3.3. Counts (in number of days) of co-occurrences of tropical modes in their most suppressed (phase 1) and most enhanced (phase 5) phases by pairs. The counts do not exclude the presence of a third mode.

	MJO		
		Phase 1	Phase5
EK	Phase1	44	29
	Phase 5	42	49

	MJO		
		Phase 1	Phase5
ER	Phase1	54	24
	Phase 5	25	56

	ER		
		Phase 1	Phase5
EK	Phase1	33	42
	Phase 5	31	28

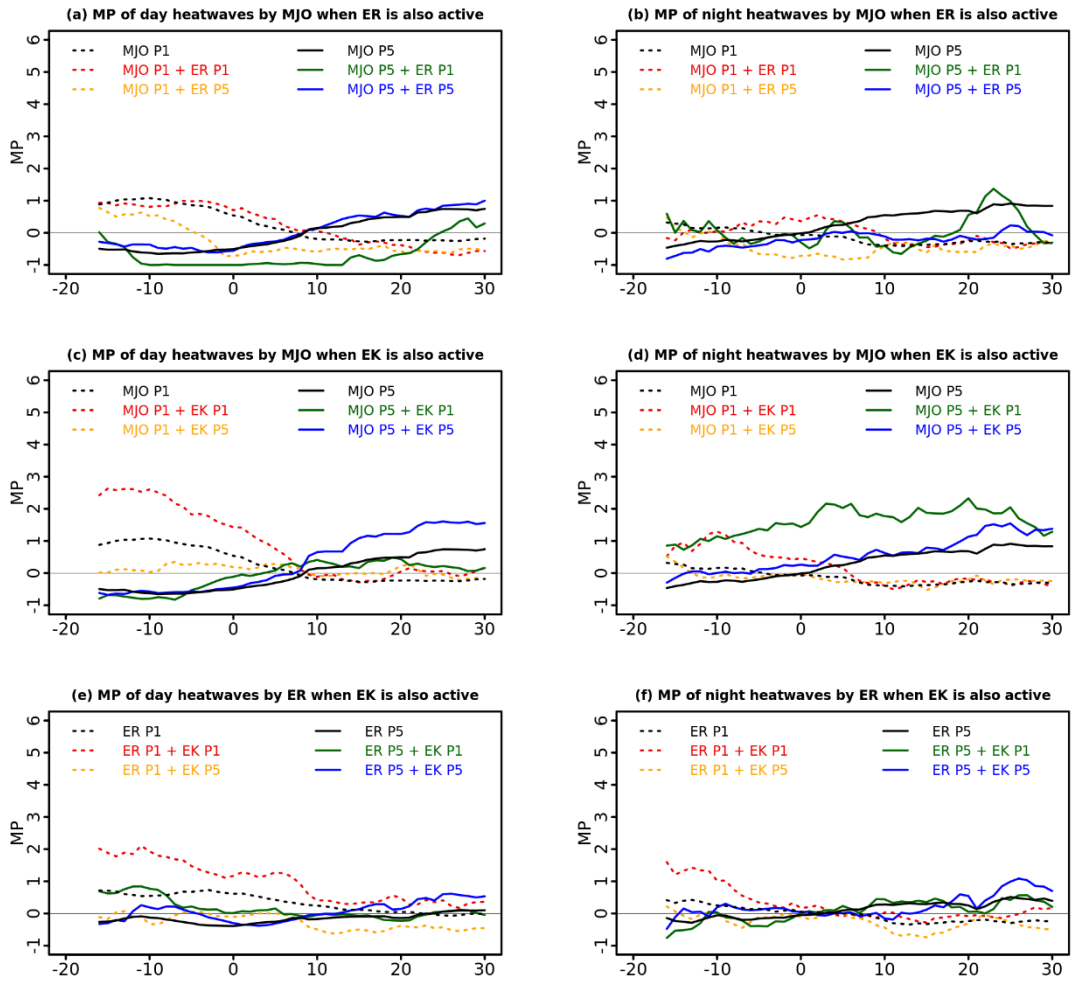

Fig. 3.4 Zonal averages (10°N-20°N) of the modulation of heatwave probability of occurrence (MP) by superposition of tropical modes during MAMJ. See Section 3.2.4 (equation (6)) for details regarding the method. Significance was tested at the 0.05 probability level, using bootstrap resampling of tropical mode active days, with 1000 repetitions.

2) Heatwave modulation by superposition of modes in various phases

Section 3.3.1 evidenced the need for special consideration of instances where multiple tropical modes are superposed. These superpositions may occur on any phase of the modes. For conciseness purpose, only the most convectively suppressed phase (phase 1) and the most convectively enhanced phase (phase 5) are investigated in the present section. However, it should be noted that, although these phases represent the extremes of the convective activity driven by the modes in the region, they do

not necessarily correspond to the peak of their effects on heatwaves as shown in Fig. 3.3. It is therefore possible to consider other phases when assessing the effect of the superposition of multiple modes on heatwaves.

Sample sizes of different combinations of modes in their phases 1 and 5 are relatively moderate, not exceeding 50 days (Table 3.3) but allow an insight as to how (much) these configurations impact Sahelian heatwave occurrence. The combinations can be mutually constructive (i.e. all modes on the same phase) or conflicting (e.g. one mode in an enhanced phase and another in a suppressed phase).

Figure 3.4 presents the zonal averages over the Sahel domain (10°N-20°N) of the modulations by pairs of tropical modes. The superposition of the ER wave and the MJO gives relatively similar results for daytime and nighttime, at least over the eastern Sahel (Figs. 3.4a & 3.4b). When these modes co-occur in a constructive way, the resulting MP pattern is comparable to the one obtained when they occur separately and mainly consists in dipolar MP structures: for the suppressed case, an increase of heatwave probability in the western Sahel and a decrease in the eastern Sahel (red dotted lines in Figs. 3.4a & 3.4b), and conversely for the enhanced phase (blue solid lines in Figs. 3.4a & 3.4b). When the MJO and the ER wave are conflictingly superposed, there is a decrease of heatwave probability in most cases (orange dotted lines and green solid lines in Figs. 3.4a & 3.4b). A few exceptions to this include an increase of daytime heatwave probability over the western Sahel when an enhanced ER wave and a suppressed MJO are superposed (orange dotted line in Fig. 3.4a), and an increase of both daytime and nighttime heatwave probability over the eastern Sahel when the ER wave is in a suppressed phase and the MJO in an enhanced phase (green solid lines in Figs. 3.4a & 3.4b).

The superposition of the EK wave onto the MJO (Figs. 3.4c & 3.4d) leads to modulations of relatively large magnitude which generally take the sign of a singular modulation by the MJO. Similarly to the combined MJO-ER modulation, dipolar patterns are observed as a result of constructive superpositions of the MJO and the EK wave. Heatwave probability is increased over the western Sahel (especially at daytime), in opposition to a relatively small decrease over the eastern Sahel when both modes are in their suppressed phases (red dotted lines in Figs. 3.4c & 3.4d). When they are both in their enhanced phases, heatwave occurrence is increased over the eastern Sahel whereas over the western Sahel it is either decreased (case of daytime heatwaves; blue solid lines in Fig. 3.4c) or unchanged (case of nighttime heatwaves; blue solid lines in Fig. 3.4d). The conflicting configuration in which the MJO is in phase 1 has only minor impacts on heatwave occurrence in the Sahel (orange dotted lines in Figs. 3.4c & 3.4d). On the other hand, in the contingency where the MJO is in phase 5 and the EK wave in phase 1, the modulation of daytime heatwaves is very close to that observed with

the MJO alone (green solid lines in Fig. 3.4c) whilst nighttime heatwave probability is significantly increased throughout the Sahel (MP often exceeds 2; green solid lines in Fig. 3.4d).

Finally the superposition of the ER and EK waves generally causes only minor changes to Sahelian heatwave probability (Figs. 3.4e & 3.4f). However when both modes are in a suppressed phase, the probability of heatwave occurrence is significantly augmented over the western Sahel (a modulation of up to 2).

In summary, the superposition of multiple modes over the African domain can substantially increase heatwave probability over the western Sahel when they are all in a convectively suppressed phase and over the eastern Sahel when they are all in a convectively enhanced phase, while the outcome for conflicting superpositions depends on the modes under consideration.

3.3.4. Modulation of heatwave intensity

Heatwave intensity is overall less sensible to tropical modes than the probability of occurrence. Some significant patterns are however obtained with the MJO and ER wave and are shown in Fig. 3.5. This figure reveals that the intensity of heatwaves is increased when the MJO and the ER waves are in phases 4 to 7, with the modulation MI often reaching 0.4. On the other hand, the intensity is decreased in phases 1 to 3 of the MJO and ER wave, and MI can also get below -0.4. Finally, the influence of EK waves on heatwave intensity is quite minor (Figs. 3.5e & 3.5f). Nighttime heatwave intensity is also more affected than daytime heatwave intensity (Figs. 3.5a & 3.5c vs Figs. 3.5b & 3.5d). From a spatial point of view, the modulation is more marked over the central and the eastern Sahel than over the western Sahel.

A comparative examination of the patterns of MP (Fig. 3.3) versus that of MI (Fig. 3.5) shows that the two do not match exactly, and this can have implications for heatwave risk management, especially for nighttime heatwaves whose intensity is more impacted by tropical modes. Thus, in phases 6 and 7 of the MJO, nighttime heatwaves are less probable but are more intense (Fig. 3.3a vs Fig. 3.5a). Conversely, they are more probable in phases 2 and 3 of the MJO but less intense. When the MJO is in phase 4, it poses a higher risk because heatwaves are both more probable and more intense. This is also the case when the ER wave is in phases 4 to 7 (Fig. 3.3c vs Fig. 3.5c).

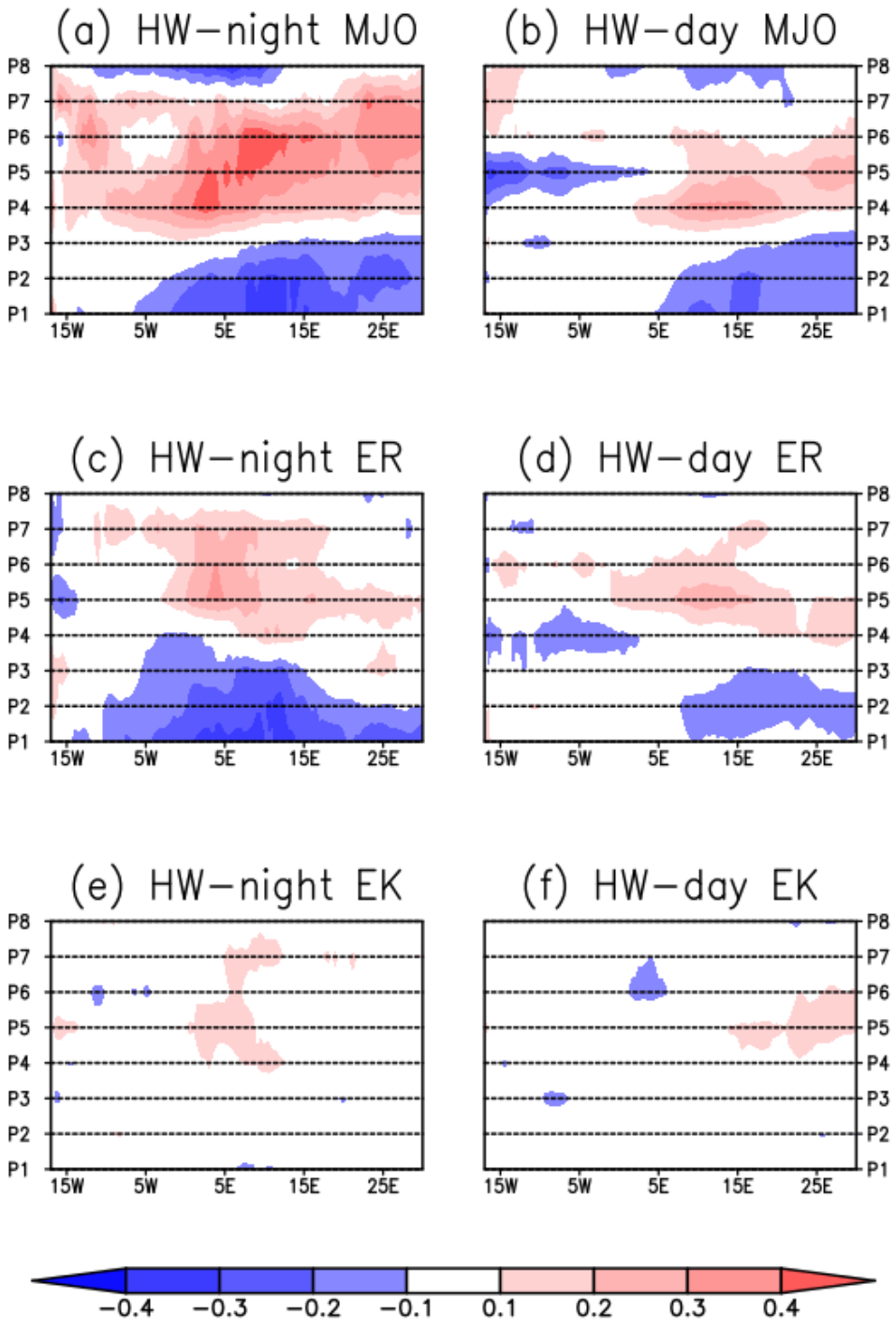

Fig. 3.5 Phase-longitude diagrams of the modulation of (left panel) nighttime and (right panel) daytime large-scale heatwave intensity by the MJO, ER and EK waves during MAMJ averaged over the Sahel band (10°N-20°N). The modulation corresponds to the variable MI defined in Section 3.2.4 (equation (5)) as a comparison of heatwave average intensity in a given active phase versus the climatological intensity of heatwaves. Significance was tested at the 0.05 probability level, using bootstrap resampling of tropical mode active days, with 1000 repetitions.

3.3.5. Potential mechanisms of modulation

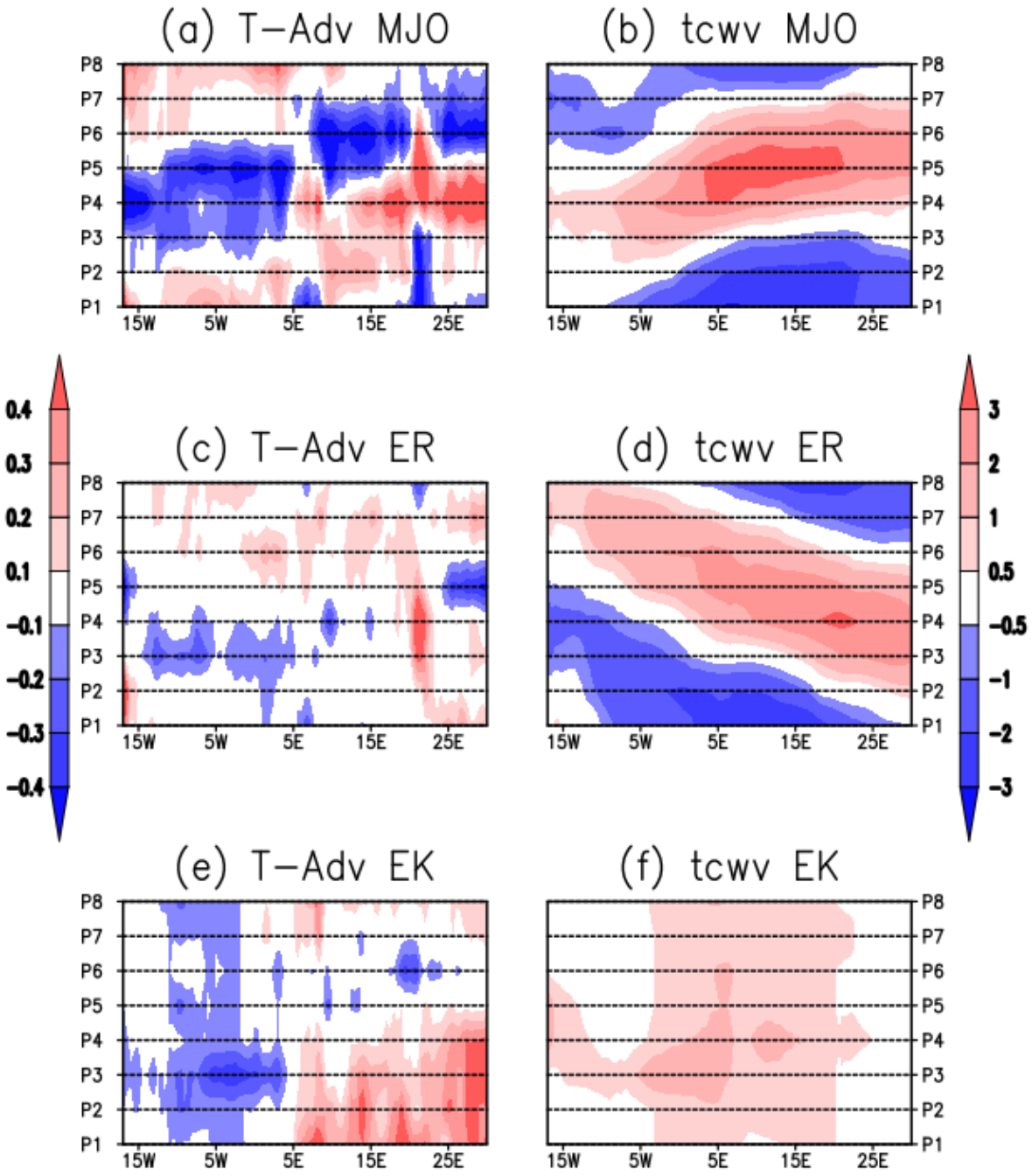

Fig. 3.6 Phase-longitude diagrams of the composite of daily anomalies of (left panel) heat advection in K day^{-1} and (right panel) precipitable water in mm over active phases of the MJO, ER and EK waves during MAMJ averaged over the Sahel band (10°N-20°N). Significance was tested using a Student t-test at the 0.05 probability level.

Previous studies (e.g. Oueslati et al. 2017; Guigma et al. 2020) have pointed to the increase of longwave radiation at the surface due to water vapour greenhouse effect, and hot air advection as processes underpinning Sahelian heatwaves. This motivates the composite analysis of thermodynamic and dynamical variables presented below for active phases of the modes. The aim here is to provide an insight as to how heatwave processes are impacted by the physical conditions created by tropical modes.

From Fig. 3.6a it is apparent that the patterns of the advection of heat into the Sahel, although patchy, are relatively consistent with that of the modulation of heatwave occurrence. Increased heatwave occurrence is indeed broadly associated with hotter air advection whereas cooler air advection goes with a decrease of heatwave probability (except over a narrow area around 20°E). The influence of tropical modes on heatwave occurrence is also due to their control on water vapour and its associated longwave radiative effect. As shown in Fig. 3.6b, over the eastern Sahel and in phases 4 and 5, the higher probability of heatwave coincides with a positive anomaly of precipitable water reaching 3 mm on zonal average (the longwave radiation and precipitable water patterns are very similar, not shown). However, the MJO-induced precipitable water anomaly has its greatest impact on heatwave intensity. Phases 4 to 7, which are associated with higher heatwave intensity, are also those for which the anomaly of precipitable water is positive; reversely, in phases 1 to 3 where heatwave intensity is lower, there is a dry anomaly especially marked over the eastern Sahel (Figs. 3.5a & 3.5b vs Fig. 3.6b). The stronger dependence of nighttime heatwaves on water vapour (Guigma et al. 2020; Largeron et al. 2020) likely explains why their intensity is more affected by the MJO (Fig. 3.5a vs Fig. 3.5b).

Associated with ER wave, an advection of hot air is present too, though mostly confined to the eastern Sahel (Fig. 3.6c) which could be linked to the increase of heatwave probability in phases 3 to 5 for nighttime heatwaves, and 7 to 8 for daytime heatwaves (Figs. 3.3c & 3.3d). Atmospheric water vapour itself is not directly linked to heatwave probability but its anomalies give an insight into other processes. Over the western Sahel, the increase of heatwave probability in phases 1 to 3 (Figs. 3.3c & 3.3d) can be connected to the negative anomaly of precipitable water (Fig. 3.6d), which is associated with reduced cloudiness and increased incoming solar radiation (not shown) which is a frequent underlying process of Sahelian heatwaves (Guigma et al. 2020). The reverse interpretation can be made for phases 5 to 8, where increased cloudiness and precipitable water (Fig. 3.6d) weaken incoming solar radiation (not shown) and are associated with a decrease of heatwave probability (Figs. 3.3c & 3.3d). As with the MJO, water vapour has a direct impact on heatwave intensity. The

patterns of precipitable water (Fig. 3.6d) and of the modulation of heatwave intensity (Figs. 3.5c & 3.5d) are indeed relatively close.

The links between the EK wave-modulated patterns of heatwave occurrence and physical processes are less evident given that the anomalies of the EK wave are predominantly confined to the equatorial region as per theory (not shown). Nonetheless, it is apparent that advection of hot air (which is important in magnitude) in phases 1 to 5 plays an important role especially over the eastern Sahel (Fig. 3.6e), where heatwave probability is increased. On the other hand, advection of cooler air over the western Sahel in phases 4 to 7 may also explain the decrease of heatwave probability there.

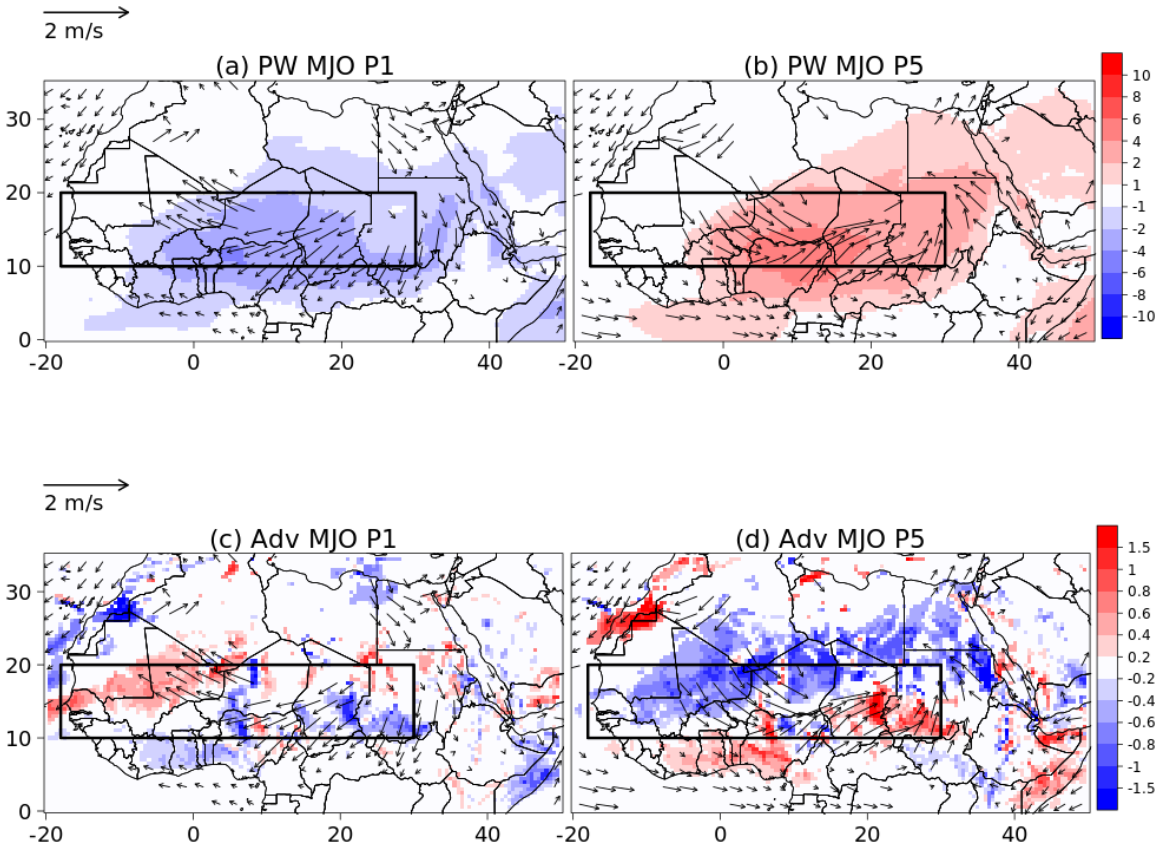

Fig. 3.7 Composite of daily anomalies of (a & b) precipitable water in mm and (c & d) 925 hPa heat advection in K day^{-1} over phases 1 and 5 of the MJO. Superimposed vectors are anomalies of horizontal wind at the 925 hPa level. Significance was tested using a Student t-test at the 0.05 probability level. The rectangular box delimits the Sahel region.

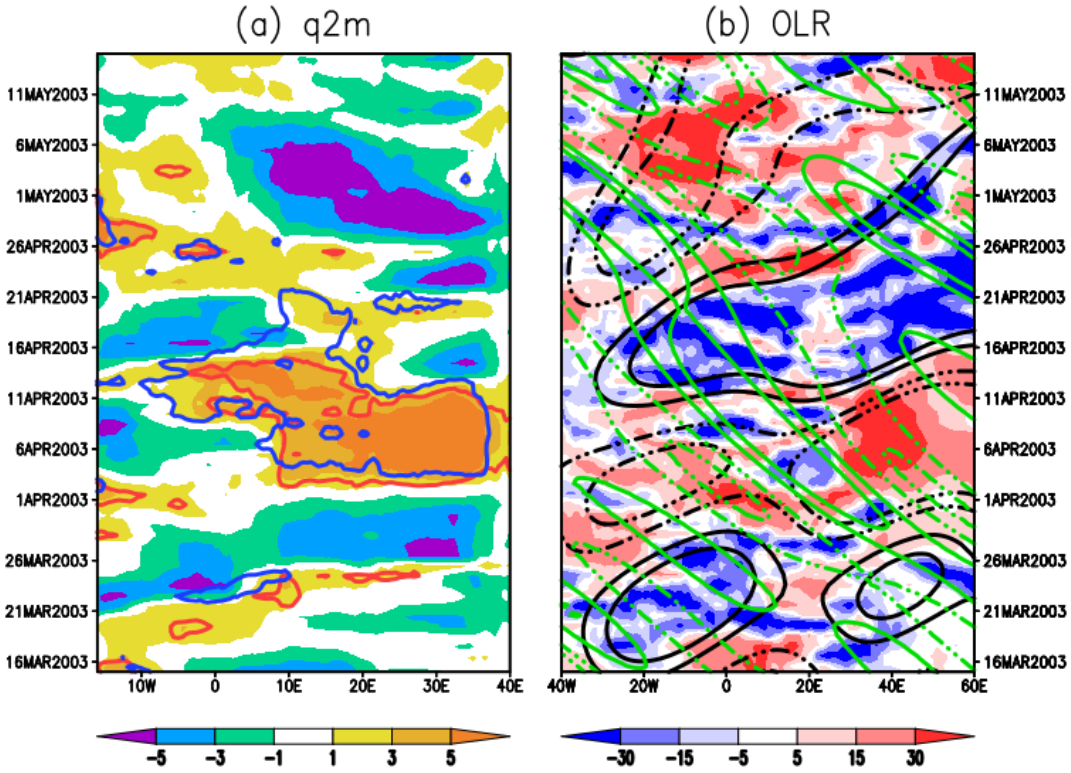

Fig. 3.8 Time-longitude diagrams of 90-day highpass filtered anomalies of (a) 2m specific humidity (shades; units in g Kg^{-1}), daily minimum (blue contours) and maximum (red contours) temperature averaged over the 10°-20°N band and (b) OLR (shades; units in Wm-2) superimposed with MJO (black contours) and ER (green contours) wave-filtered OLR anomalies averaged over the 0-10°N band between 15 March and 15 May 2003. In (a) the contour level is 2K for both the minimum and the maximum temperature. In (b), the contour levels for the MJO and ER-wave filtered anomalies are 5 and 10 W m^{-2} (-5 and -10 W m^{-2}) for the dashed (solid) lines.

While phase-longitude diagrams are efficient at summarising the physical conditions promoted by tropical modes in their different phases, they do not inform on their full horizontal distribution. To get around this issue, Fig. 3.7 shows for illustration purposes, the maps of these variables composited over the most convectively suppressed and enhanced phases (phases 1 and 5 respectively) of the MJO. They are superimposed with low-level (925 hPa) wind anomalies in order to assess the origins of the heat (whose climatological distribution is depicted in Lavaysse et al. 2009). The suppressed phase of the MJO is associated with a low-level northeasterly wind anomaly across the Sahel (which is part of an anticyclonic cell) carrying the drier and hotter air from the Sahara desert and the eastern Sahel towards the western Sahel (Figs. 3.7a & 3.7c). As a result, in the western part of the Sahel, advection of hotter air (with magnitude reaching 1.5 K day^{-1}), leads to an increase of heatwave probability (Figs. 3.3a & 3.3b). On the other hand the arrival of air masses from higher latitudes causes drying and

cooling over the eastern Sahel, reducing longwave radiation, hence the decline of heatwave probability in this region (Figs. 3.3a & 3.3b). Reversely, when the MJO is convectively enhanced, the low-level flow presents a cyclonic anomaly characterised by a northwesterly wind anomaly over the western Sahel/Sahara, which advects cooler air (Fig. 3.7d) leading to a decrease of heatwave probability (Figs. 3.3a & 3.3b). Over the eastern Sahel/Sahara, a southwesterly wind anomaly carries humid air from the equatorial region (Fig. 3.7b), causing an increase of heatwave probability (Figs. 3.3a & 3.3b) associated with increased longwave radiation.

These results agree with previous findings by Moron et al. (2018a) who also showed the importance of the modulation of low-level circulation by the MJO in increasing/decreasing temperature over tropical Africa. They also extend them further by documenting the associated physical processes.

3.4. Case-study of the April 2003 heatwave

3.4.1. Motivation and description of the heatwave

Guigma et al. (2020) showed that intraseasonal heatwaves over the Sahel are generally short-lived (average duration not exceeding five days), with only a small portion of them (about 10%) occurring concurrently at daytime and nighttime. Yet, in terms of impacts on health, longer lasting daytime events which persist during the nighttime are expected to be the most harmful (Schär 2016; Murage et al. 2017). Given their small sample size, the findings of the broad statistical analysis of heatwave modulation by tropical modes (Section 3.3) may not be directly applicable to them, especially since daytime and nighttime were dissociated. From this perspective, it is relevant to investigate them through a representative case study as also suggested by Guigma et al. (2020). This is the reason why the Sahelian heatwave which took place during the first half of April 2003 was selected. It is characterised by (i) a relatively long duration (more than 10 days) and (ii) a simultaneousness of daytime and nighttime heatwaves over a common wide domain. This event is also mentioned as a severe one in Oueslati et al. (2017) but, to the best of the authors' knowledge, it has never been investigated. The daytime heatwave started first, on 03 April, while the nighttime one started on 04 April, and they both ceased on 15 April. From a spatial point of view, the time-longitude diagram of temperature anomalies averaged over the Sahel band of 10°N-20°N (Fig. 3.8a) reveals that the heatwave kicked off over the eastern Sahel (in northern Chad/Sudan more precisely; not shown), stood there until approximately 08 April, moved towards the central Sahel before heading back to the east on its latest days. April 2003 was also marked by an important intraseasonal variability of temperature, as revealed by a wavelet decomposition of Tmin and Tmax (not shown). The variability of temperature at these scales is particularly relevant here as it suggests an important modulation by

the high-frequency modes of climate variability, including the MJO and equatorial waves. Finally in April 2003, there was no incursion of extratropical perturbations into West Africa, nor any strong interannual temperature anomaly (not shown), therefore allowing to get a "pure" modulation by tropical modes.

3.4.2. Activity of tropical modes in April 2003

Figure 3.8b shows a time-longitude diagram of highpass-filtered OLR anomalies averaged over the Guinean band to which the mode-filtered OLR anomalies (averaged over the same latitudinal band) are superimposed as contours. This is a common technique used in tropical mode investigations (e.g. Schreck and Molinari 2011; Ventrice and Thorncroft 2012; Lafore et al. 2017).

Over the heatwave period (i.e. first half of April), two MJO packets crossed West Africa (black contours in Fig. 3.8b). For the first packet, it is its convectively suppressed phase which is relevant to the heatwave. It penetrated West Africa during the second half of March 2003 and reached the Indian Ocean near 10 April. As for the second packet, its convectively enhanced phase (which is the one relevant to the heatwave) entered West Africa in early April, reached its maximum amplitude over Central West Africa (10°W-10°E) in mid-April before exiting the African domain after weakening at its eastern parts. An ER wave packet (green contours in Fig. 3.8b) also travelled westwards across West Africa during the first half of April 2003. The enhanced phase was the first to reach Africa from the eastern coast and was observed over Sahelian longitudes in early April. It eventually strengthened in mid-April, when it met with the enhanced phase of the second MJO packet. The suppressed phase reached West Africa after 15 April.

3.4.3. Overall physical processes during the event

An analysis of the thermodynamic budget emphasizes that two processes, namely longwave heating (Fig. 3.9a) and hot air advection (Fig. 3.9c) largely shaped the April 2003 heatwave. Indeed, during this period, the area covering Chad and Sudan is home to a strong hot air advection, reaching 1.5 K day^{-1} at some places. As a result, the thermal gradient between the atmosphere and the ground is weakened, leading also to a decrease of the sensible heat flux according to ERA5 (not shown). As for the net longwave heating, it is observed over the western and central Sahel/Sahara, and most importantly over the southeasternmost parts of the Sahel with a maximum exceeding 20 Wm^{-2}. This longwave anomaly results mostly from a greenhouse effect (GHE) of water vapour, as testified by the pattern of precipitable water which presents a similar anomaly (Fig. 3.9b). Dust aerosol (an

important constituent of the Sahelian atmosphere) was not significant in April 2003 according to MODIS data (not shown), precluding any significant contribution from this component to the observed warming.

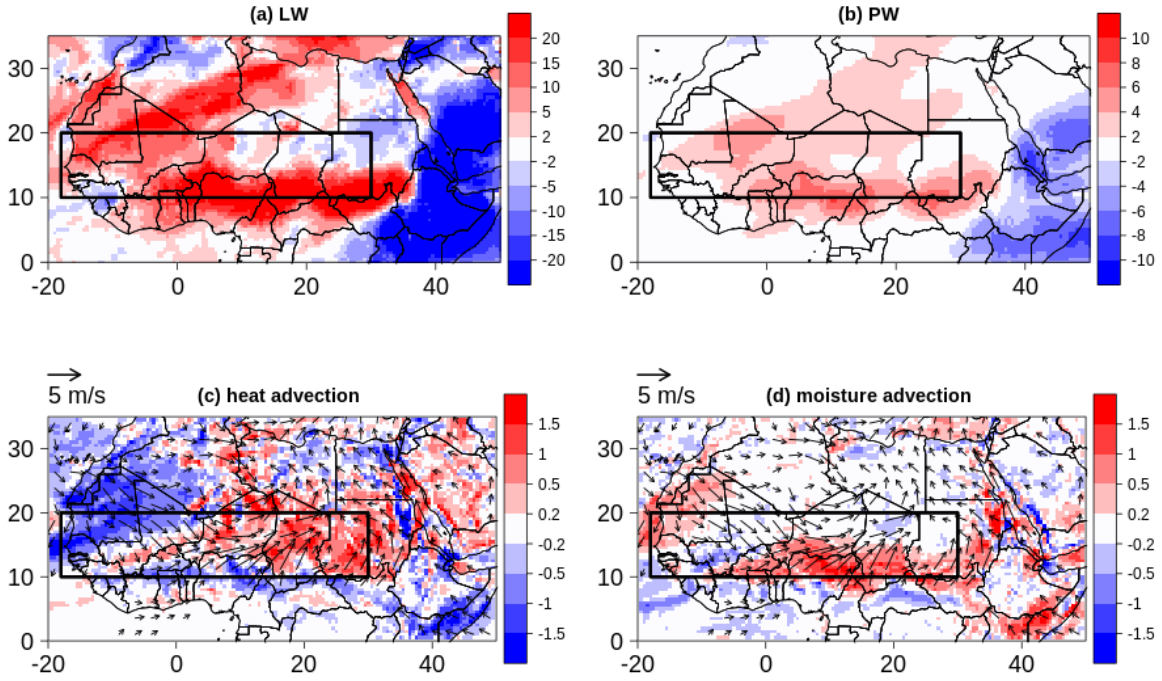

Fig. 3.9 Anomalies of (a) Net longwave radiation at the surface in Wm^{-2}, (b) Precipitable water in mm, (c) 925 hPa level heat advection in K day^{-1}, (d) 925 hPa level specific humidity advection (g kg^{-1} day^{-1}) averaged over the first half of April 2003. Vectors in (c) and (d) represent the 925 hPa level wind anomalies (only magnitudes greater than 1 m s^{-1} are shown). All quantities are obtained from ERA5. The rectangular box delimits the Sahel region.

The longwave warming anomaly at the surface is also a footprint of a reinforcement of convective activity over West Africa. Besides the positive anomaly of precipitable water, there is indeed a low-level cyclonic anomaly with monsoonal wind surges into the Sahel, advecting water vapour from the Gulf of Guinea (Fig. 3.9d). Furthermore, the patterns of low-level circulation, hot air advection and precipitable water observed during the heatwave period are very similar to their composite mean anomalies over the convectively enhanced phases of the MJO (Figs. 3.7b & 3.7d). As a reminder, heatwave probability is increased over the eastern Sahel when the MJO is in these phases (Figs. 3.3a & 3.3b). As such, the April 2003 event, despite being exceptional (by its length and daytime/nighttime concomitance), adheres to the general findings presented in Section 3.3, both in terms of the physical

conditions created by tropical modes and the outcome for heatwave occurrence. The next section emphasises this in more detail.

3.4.4. Day to day evolution of the heating processes and impact of tropical modes

A day to day analysis of the heatwave event further allows a deeper insight into the evolution of different processes shaping the heatwave and the role played by tropical modes.

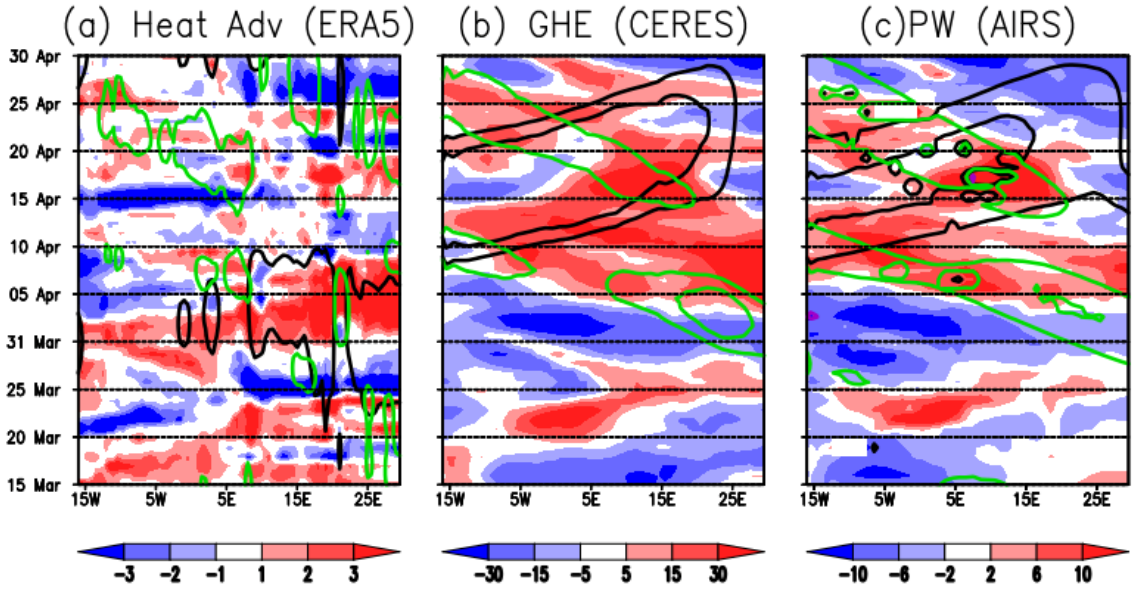

Fig. 3.10 Time-longitude diagram of (a) ERA5 heat advection at the 925 hPa level. Shades represent the daily highpass filtered anomalies and contours the regression of these anomalies on the MJO (black contours) and ER waves (green contours). Units are in K day^{-1} and the contour level is 0.1 (negative levels are omitted). (b) CERES incoming longwave radiation. Shades represent the daily highpass filtered anomalies and contours the regression of these anomalies on the MJO (black contours), the ER waves (green contours). Units are in Wm^{-2} and the contour levels are 2.5 and 5 (negative levels are omitted). (c) AIRS precipitable water. Shades represent the daily highpass filtered anomalies and contours the regression of these anomalies on the MJO (black contours) and ER waves (green contours). Units are in mm and the contour levels are 1 and 3 (negative levels are omitted). All the quantities are averaged over the 10°N-20°N latitudinal band between 15 March and 30 April 2003.

1) An initial role of heat advection fostered by the MJO (late March -04 April)

Figure 3.10a shows that the onset of the heatwave over the eastern Sahel was preceded by a sustained advection of hot air in late March and during the first days of April. The low-level wind pattern in

Fig. 3.9c shows that the hot air originated from the central and southern Sahel (approximately 10°N-13N°), where the West African Heat Low (WAHL) is typically located at this time of the year (Lavaysse et al. 2009). The projection of the activity of the different modes on this process (described in Section 3.2.4) shows that the MJO (which was in a convectively suppressed phase at that time; Fig. 3.8b) was its main driver. In Fig. 3.10a, the MJO-regressed anomalies (black contours) indeed encapsulate the heat advection. Therefore the MJO acted in suppressing convection over the WAHL area, causing a warming which is further advected to the northeastern Sahel and led to the heatwave initiation.

2) A progressive takeover by water vapour GHE led by the ER wave (05-08 April)

Despite a progressive decrease of heat advection after the onset, the heatwave was sustained mainly as a result of the arrival of moist air in the Sahel from the subequatorial region (Fig. 3.9d), causing a water vapour GHE as illustrated in Fig. 3.10b (using observed incoming longwave radiation at the surface, a proxy for GHE). In-situ observations at the Demokeya station (30.5°E; 13.3°N) also confirm the progressive increase of water vapour during this stage of the heatwave (Fig. S3.5). The regressed values of incoming longwave radiation (green contours in Fig. 3.10b) as well as of precipitable water (green contours in Fig. 3.10c) on the ER wave are positive and match relatively well the spatial structure of the anomalies of these variables, suggesting a preponderant role of this wave at this stage of the event. Thus, agreeingly with its expected impact on heatwaves discussed in early spring (Section 3.3), the convectively enhanced ER wave organised a low-level meridional transport of water vapour into the eastern Sahel, and, through longwave radiation, heated up the region. The statistical findings are further strengthened since consistency is shown here across different observational (satellite) datasets.

3) Final stage: a reinforcement of the GHE forced by the MJO (09-14 April)

The westward motion of the ER wave allowed the heating to reach the central and western parts of the Sahel. From 09 April, the convectively enhanced phase of the second MJO packet entered the West Africa sector (Section 3.4.2, Fig. 3.8b). It further increased moisture through a zonal transport of water vapour from the Atlantic into the Sahel. As a result, the GHE effect reached its peak (above 30 Wm^{-2}) leading to an intensification of temperature anomalies, especially at night (Fig. 3.8a). The leading role of the MJO on this stage of the heatwave is discernible from the regression of the relevant processes on its timeseries (black contours in Figs. 3.10b & 3.10c). Its eastward propagation also dragged the region of maximum heating back towards the eastern Sahel. Again this is predicted by the statistical analysis as it is shown that, through water vapour GHE (Figs. 3.6b & 3.7b), convectively

enhanced phases of the MJO heat up the eastern Sahel, augmenting heatwave probability therein (Figs. 3.3a & 3.3b). From approximately 15 April, the MJO-driven intensified convection caused organised rainfall events that watered large parts of the heatwave region (Fig. S3.6) and led to a decrease of temperature. This eventually ended the heatwave.

It should be noted that the evolution of GHE and precipitable water depicted by ERA5 is very similar to that of CERES and AIRS respectively. Furthermore, the influence of the modes on the evolution of the physical processes is also well captured by ERA5. This is shown by the daily evolution of the regressed fields of interest spatially averaged over grid-cells where the heatwave is detected (Fig. S3.7).

In summary, the April 2003 heatwave, from a large-scale point of view, was initiated by a convectively suppressed MJO that promoted hot air advection, and sustained through GHE of water vapour brought in, first by a convectively enhanced ER wave and later on by a convectively enhanced MJO. In addition to supporting the statistical characteristics of heatwave occurrence in the eastern Sahel, this case study also provided an insight on the organisation of the water vapour low-level flow by tropical modes which is an important driver of heatwaves. Thus, it appears that the MJO exerts its control mainly through zonal transport of water vapour whereas the ER wave mostly affects meridional transport.

3.5. Conclusion and perspectives

Extreme heat represents a growing threat for Sahelian populations, with the latest research stressing that by the end of the century, climate change would make the region reach worrying levels of thermal discomfort (Xu et al. 2020; Raymond et al. 2020). Therefore, undertaking actions which could mitigate this important issue is a top priority. This study contributes towards this through an analysis of the relationship between tropical modes and Sahelian heatwave events with the view of improving scientific understanding of these extremes. More precisely, it demonstrates that the MJO, ER and EK waves are important factors for the occurrence and - to a lesser extent - intensity of heatwaves in the region during the spring season. Their influence on heatwave occurrence is a function of their convective phase (enhanced or suppressed) and amplitude; it is also distinct for nighttime and daytime heatwaves and varies with the geographical location. Generally, in their convectively suppressed phases, they advect hot air from the climatological location of the WAHL towards the western coast of the Sahel, increasing heatwave probability there. When they are in convectively enhanced phases, they increase longwave warming especially over the eastern Sahel by bringing in water vapour from the Guinean region of Africa. Several tropical modes often overlap over the region. In these situations,

heatwaves are more likely to occur over the western Sahel when all modes are in a convectively suppressed phase, and over the eastern Sahel when they are convectively suppressed. The statistical findings were further illustrated by the detailed analysis of a strong Sahelian heatwave event which occurred in April 2003. Hot air advection and longwave radiation, driven by the MJO and ER waves were responsible for a relatively long lasting event that had the particularity of affecting both daytime and nighttime.

From an operational point of view, the heatwaves-tropical modes relationship is important since the wave activity can be used by forecasters as an additional relevant tool to prepare warnings. Moreover, there is a potential for further work aiming at building statistical models of heatwave predictability based on the activity of tropical modes and the interaction between them. The modulation patterns at 5°E shown in the present study can already be used to forecast the likelihood of heatwave occurrence at a given location in the Sahel, taking into account the spectral properties (wavenumber and period) of the modes. For example, when a convectively suppressed ER wave is detected at 30°E, a forecaster in Senegal can expect hot conditions over his/her region in the following 10 days. Better forecast recipes can be obtained from the monitoring of tropical mode activity by reassessing their impact when they are located at longitudes closer to the areas covered by the forecaster, but also at selected longitudes further away (because, given their wavenumbers, tropical modes can impact regions fairly remote from their central position). This therefore calls for more regional coordination between national meteorological services.

Besides, with the amelioration of weather observation networks, the increase of computational capacity and improvement of numerical models, tropical modes are now better represented and predicted (Dias et al. 2018; Janiga et al. 2018; Kim et al. 2018; Bengtsson et al. 2019). These skills can therefore be transferred to heatwave prediction at the intraseasonal scale and thus help to win time for preparedness actions. The authors are already engaged in research in that direction.

Other large-scale drivers of Sahelian heatwaves have been suggested by previous studies (Fontaine et al. 2013; Moron et al. 2018; Guigma et al. 2020). In particular, intrusions of extratropical Rossby waves often combined with tropical plumes can lead to significant increases of temperature and moisture in the Sahel as was the case in April 2010 (Largeron et al. 2020). It is therefore important that future studies also focus on the links between these large-scale features and heatwaves and on the interactions between them and tropical modes.

Finally, it may be important to assess whether the upward trend of Sahelian temperature and heatwave frequency and intensity over the recent past (Fontaine et al. 2013; Moron et al. 2016; Guichard et al.

2017; Ceccherini et al. 2017) is partly attributable to the global warming-induced increased activity of tropical modes over the same period (Song and Seo 2016; Adames et al. 2017). This has implications for future projections, as the accuracy of the simulation and future evolution of springtime convection over the Guinean region by climate models might have repercussions on Sahelian heatwave predictions.

Acknowledgments

Douglas J. Parker and four anonymous reviewers provided comments that substantially improved the manuscript. This research was supported through the (i) UK NERC/ESRC/DfID Science for Humanitarian Emergencies and Resilience (SHEAR) consortium project 'Towards Forecast-based Preparedness Action' (ForPAc, www.forpac.org), grant NE/P000673/1 and (ii) Future Climate for Africa (FCFA) regional consortium project 'AMMA-2050', grant NE/M02024X/1. KHG was supported by the Peter Carpenter Scholarship for African Climate Science at the University of Sussex, UK. The authors thank Jessica Barbier for assistance with the detection of large-scale heatwaves.

Data availability statement

All data used in this study are freely available at the following repositories:

ERA5: https://cds.climate.copernicus.eu/cdsapp#!/home

CERES: https://ceres.larc.nasa.gov/data/

AIRS: https://airs.jpl.nasa.gov/data/get-data/standard-data/

Demokeya observed data: http://downloads.hindawi.com/archive/2013/297973.item.1.xlsx and http://downloads.hindawi.com/archive/2013/297973.item.2.xlsx

Supplemental materials

This document provides supplementary figures to the main manuscript.

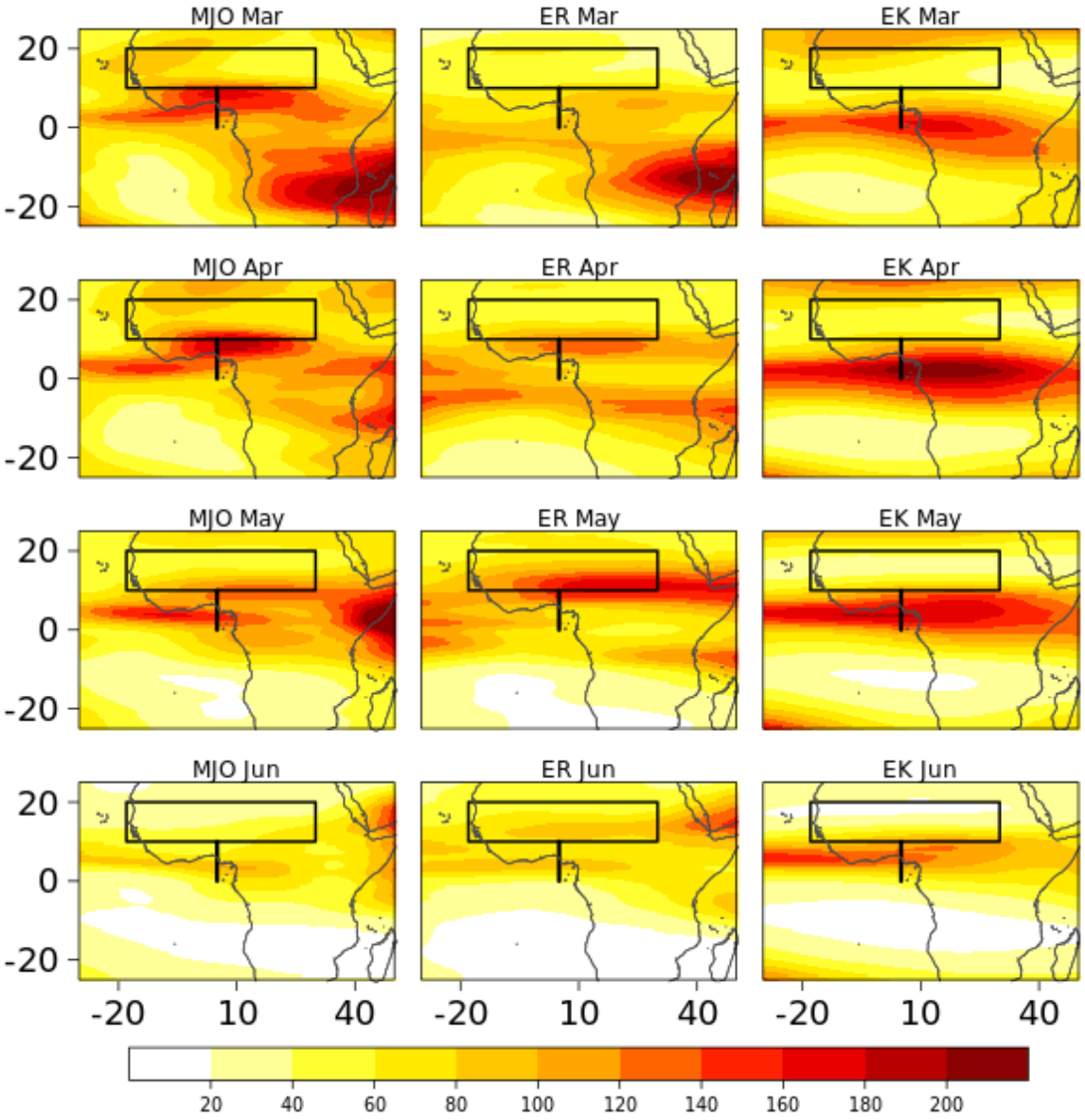

Fig. S3.1 Seasonality of the variance (in W^2m^{-4}) of mode-filtered OLR data during MAMJ. The rectangular box delimits the Sahel region. The vertical line marks the reference longitude (5°E) and latitudinal band over which the local activity of tropical modes is characterised (see Section 3.2.3).

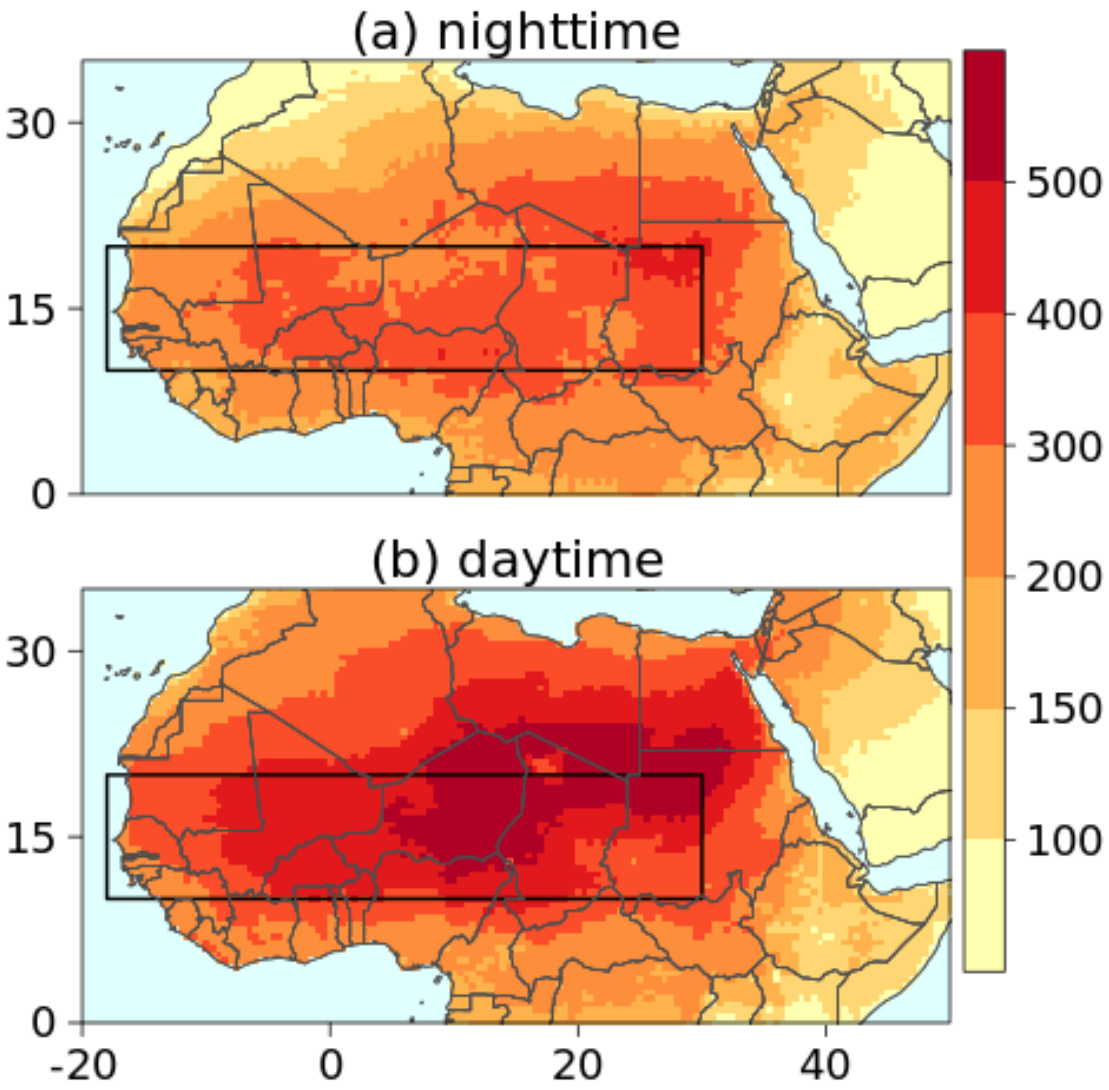

Fig. S3.2 Total number of (a) nighttime and (b) daytime heatwave days during MAMJ over the study period (1980-2017). The rectangular box delimits the Sahel region.

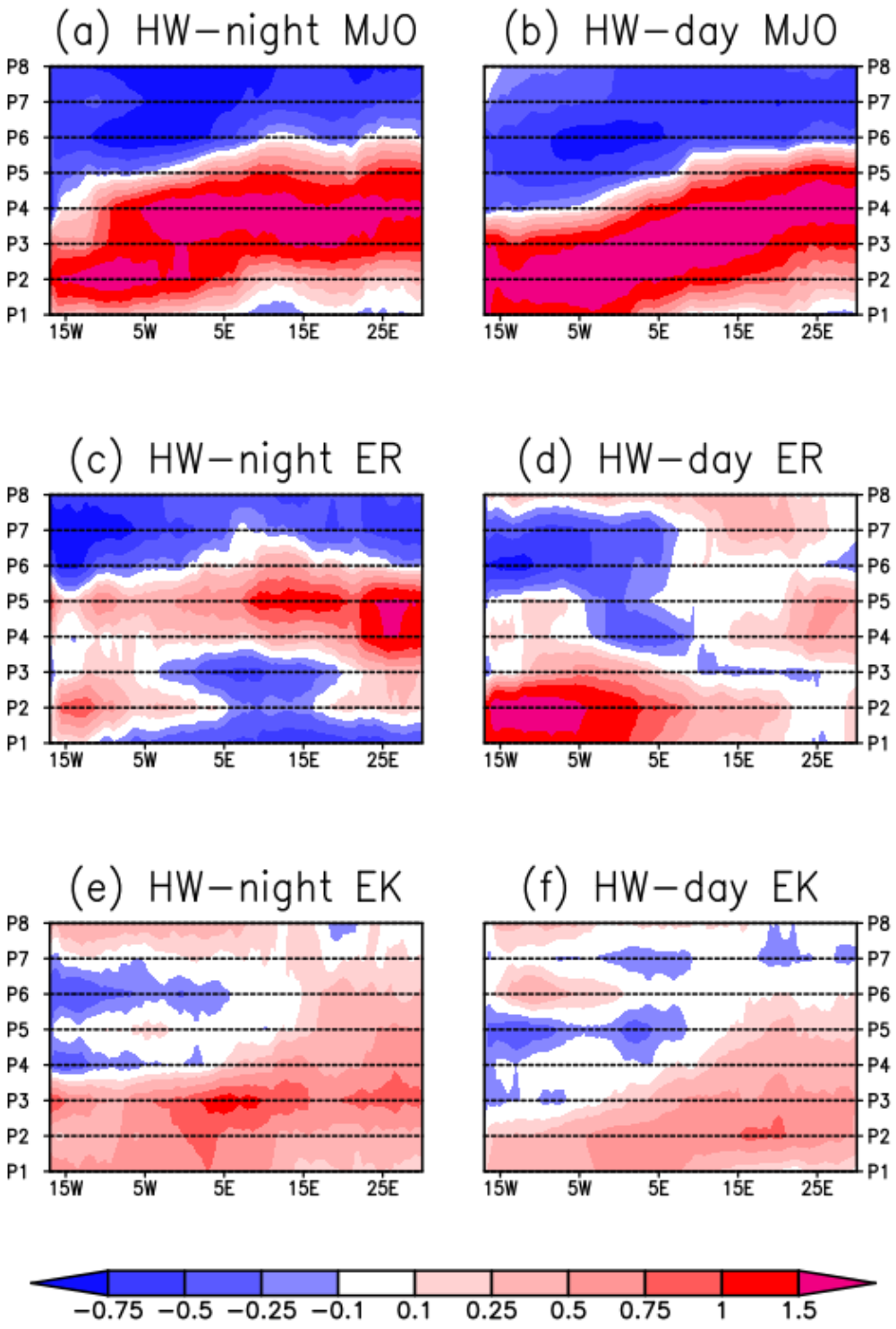

Fig. S3.3 Same as Fig. 3.3 in the main manuscript except using a minimum amplitude of 2 for active tropical mode detection.

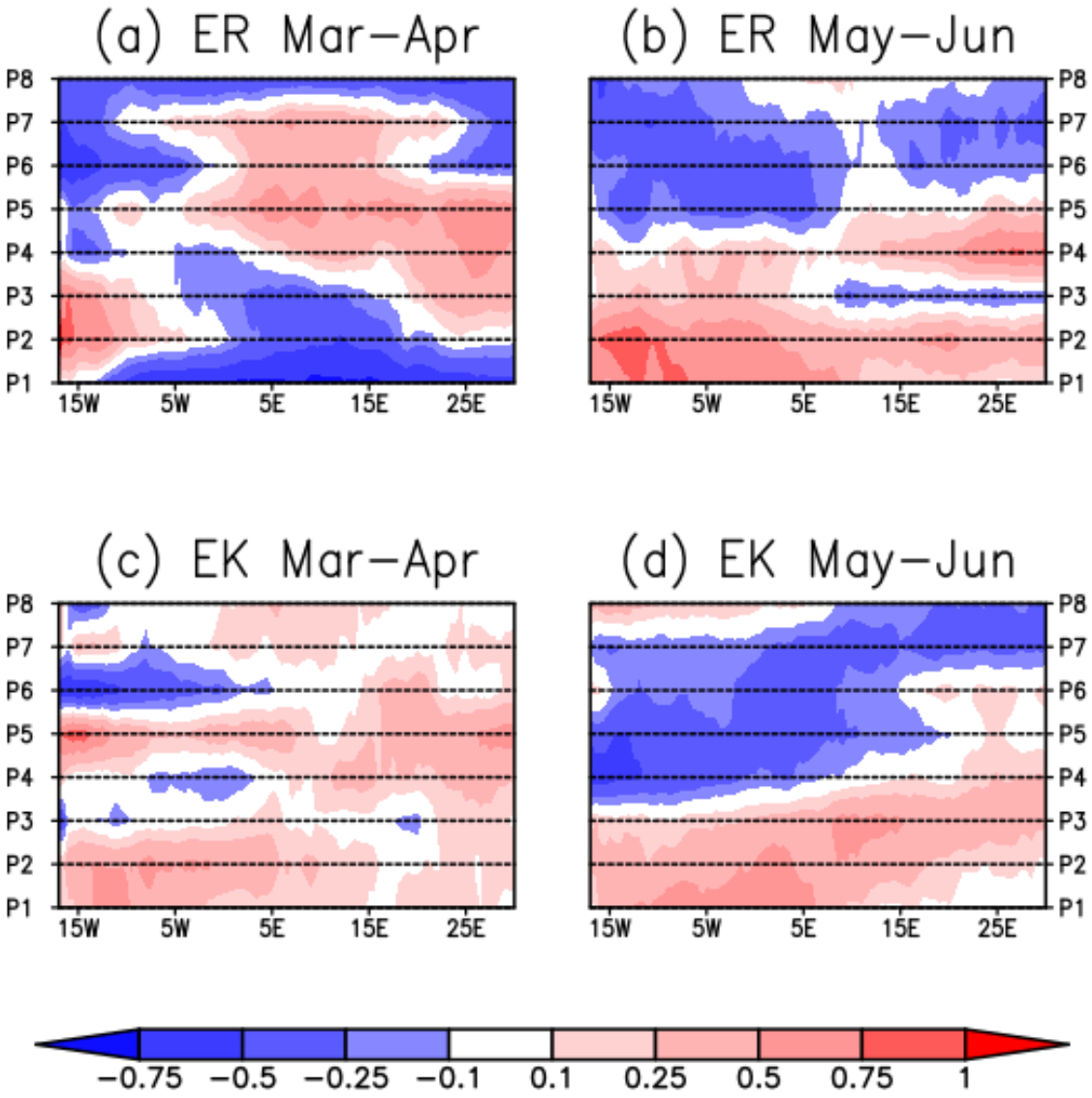

Fig. S3.4 Seasonality of the modulation of nighttime heatwave probability of occurrence by (top panels) ER and (bottom panels) EK waves. The left panels show the modulation for March-April, and the right panels that for May-June.

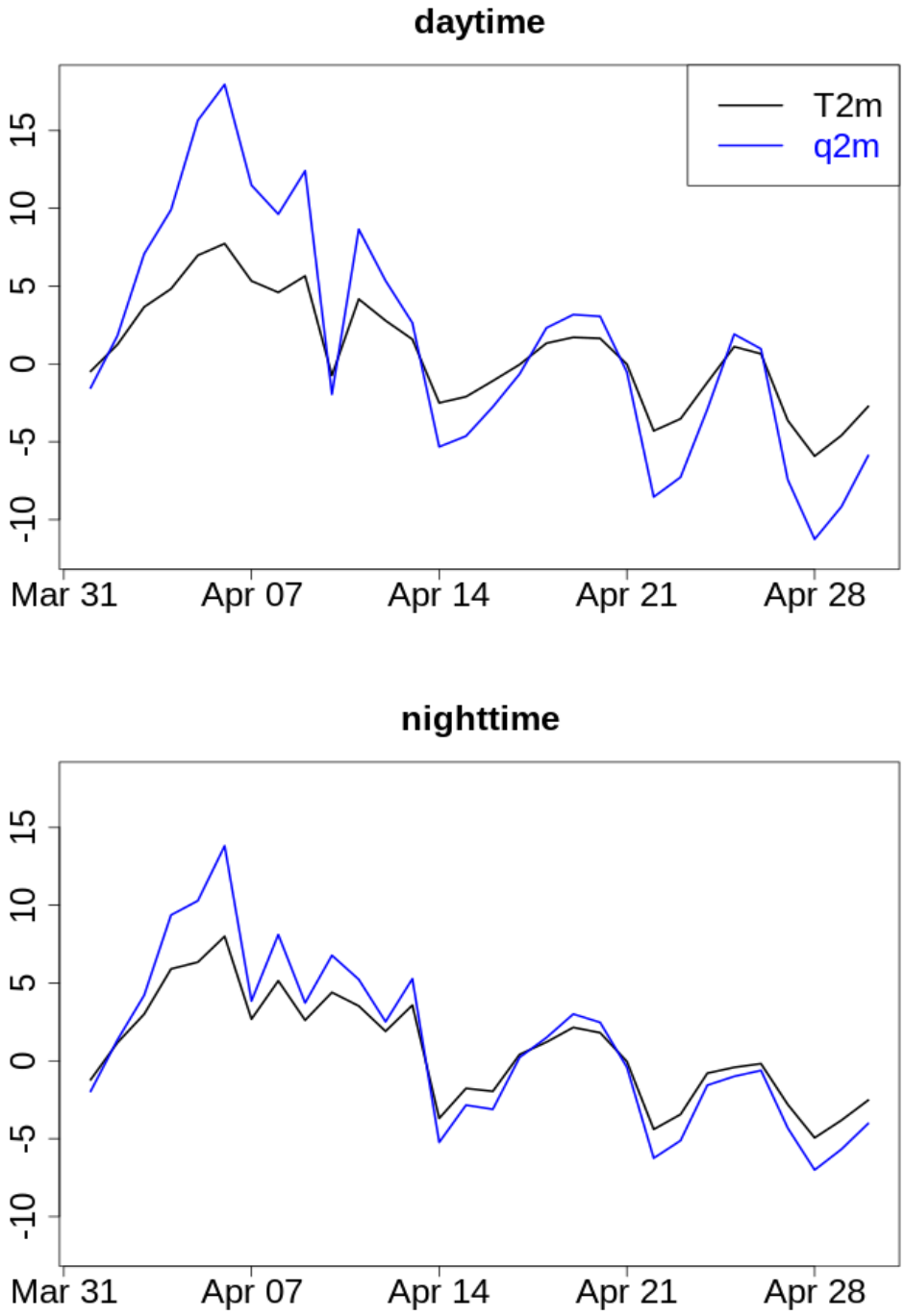

Fig. S3.5 Anomalies of 2m temperature (K) and relative humidity (%) observed at the Demokeya station (30.5°E-13.3°N) in April 2003.

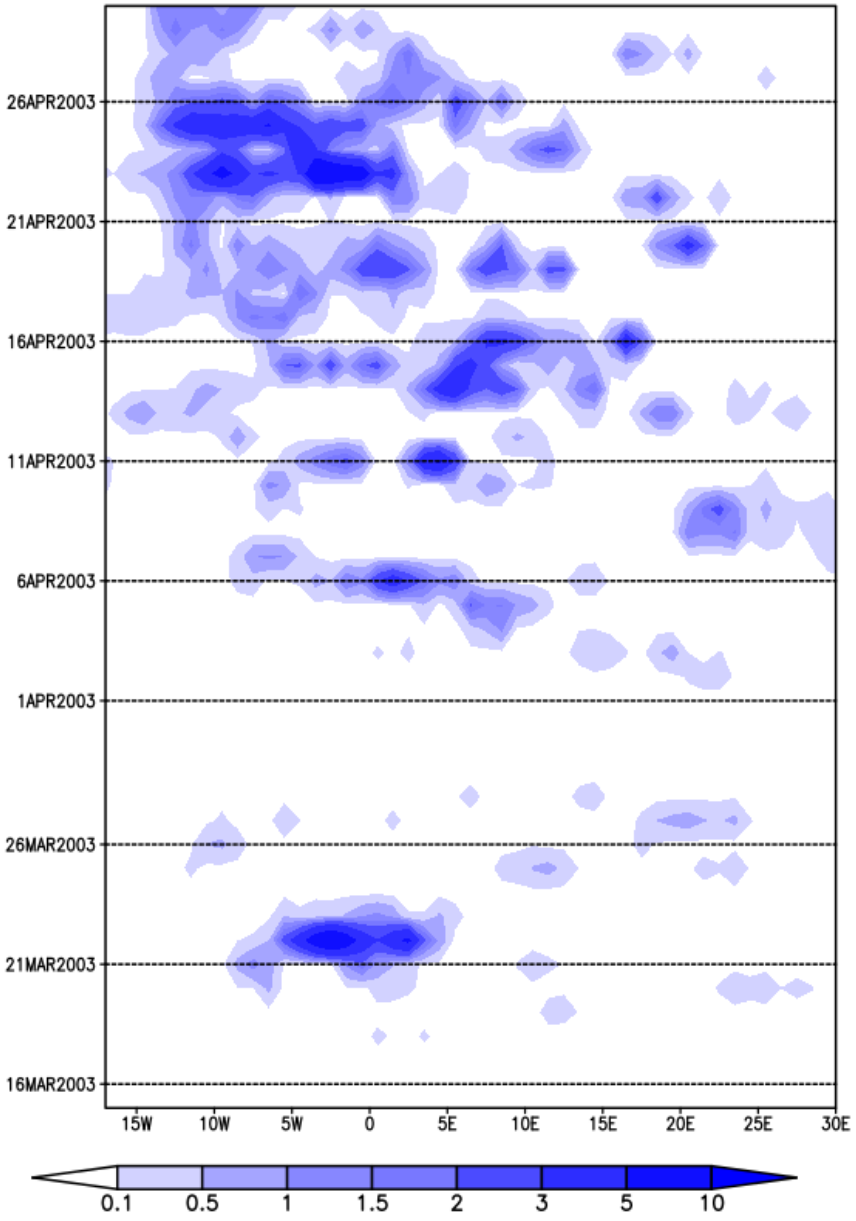

Fig. S3.6 Time-longitude diagram of GPCP daily precipitation in mm averaged over the 10°N-20°N latitudinal band between 15 March and 30 April 2003.

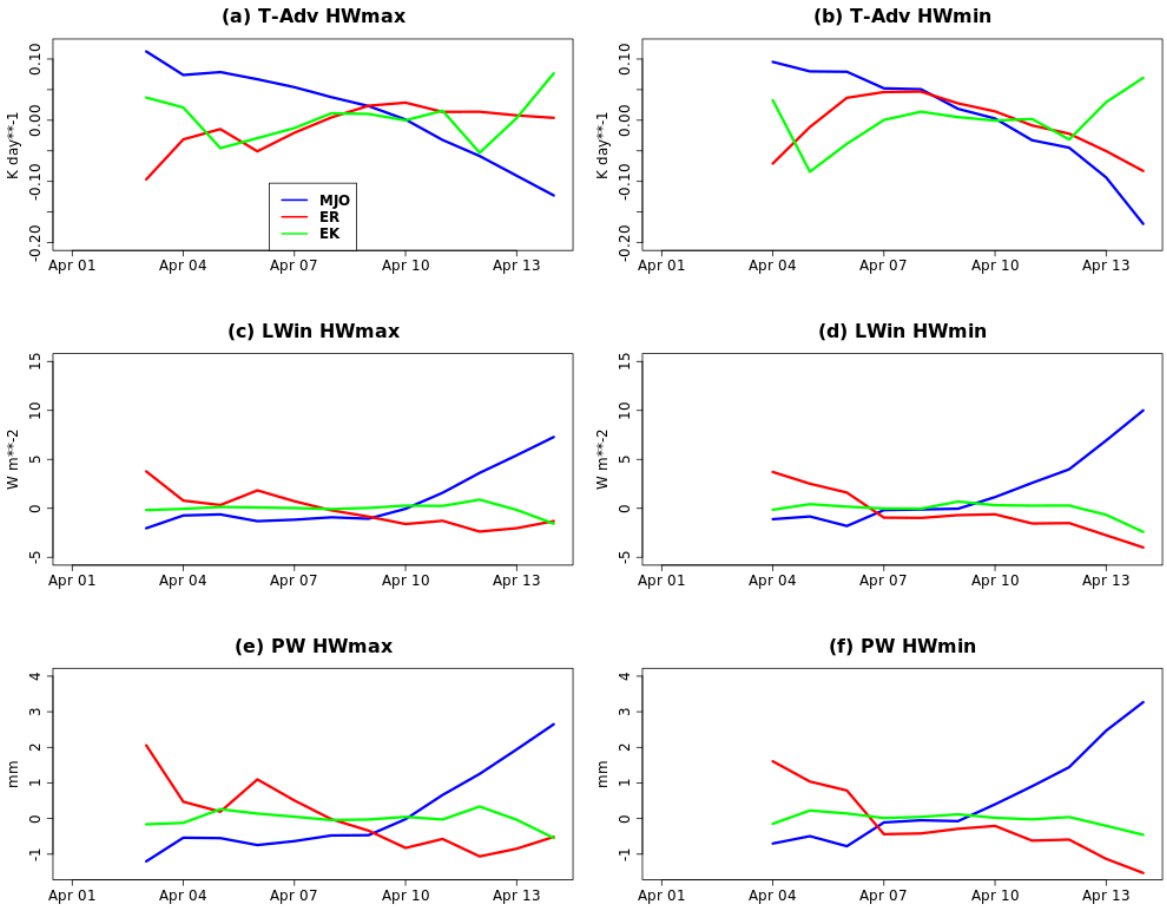

Fig. S3.7 Daily evolution of mode-regressed values of (a & b) heat advection in K day^{-1}, (c & d) incoming longwave radiation at the surface in Wm^{-2} and (e & f) precipitable water in mm averaged over grid-cells which are part of the heatwave. The MJO regressed variables are in blue, that of the ER wave in red and that of the EK wave in green.

Chapter 4. Prediction skill of Sahelian heatwaves out to subseasonal lead times and importance of atmospheric tropical modes of variability

Reproduced with the permission of Springer (https://link.springer.com/article/10.1007/s00382-021-05726-8)

Prediction skill of Sahelian heatwaves out to subseasonal lead times and importance of atmospheric tropical modes of variability

Kiswendsida H. Guigma[1*], David MacLeod[2], Martin Todd[1], Yi Wang[1]

[1]University of Sussex, Brighton. UK

[2]University of Bristol, Bristol. UK

[*]Corresponding author: k.guigma@sussex.ac.uk

Abstract

Global warming has increased the frequency of extreme weather events, including heatwaves, over recent decades. Heat early warning systems are being set up in many regions as a tool to mitigate their effects. Such systems are not yet implemented in the West African Sahel, partly because of insufficient knowledge on the skill of models to predict them. The present study addresses this gap by examining the skill of the ECMWF ENS extended-range forecasting system (ENS-ext) to predict Sahelian heatwaves out to subseasonal lead-times. It also assesses the importance of tropical modes of variability, which were previously identified as important large-scale drivers of heatwave occurrence in the Sahel. The results show that ENS-ext is able to predict Sahelian heatwaves with significant skill out to lead-week 2 to 3. With increasing lead-time, heatwaves are more predictable at nighttime than at daytime. Likewise, the pre-monsoon season heatwaves have a longer predictability than those occurring in late winter. The model is also able to relatively well simulate the observed relationship between heatwave occurrence and tropical mode activity. Furthermore, the prediction skill is better during the active phases of the modes, suggesting that they are good sources of heatwave predictability. Therefore, improving the representation of tropical modes in models will positively impact heatwave prediction at the subseasonal scale in the Sahel, and gain more time and precision for anticipatory actions.

Keywords: heatwaves, predictability, ECMWF, tropical modes, Sahel

4.1. Introduction

The recent developments in climate change are marked by an increased occurrence of extreme weather and climate events, including heatwaves (Stott 2016). There has indeed been an upward trend of heatwaves both at the global and regional levels (Perkins-Kirkpatrick and Lewis 2020), with future projections warning of even more severe thermal discomfort (Xu et al. 2020; Raymond et al. 2020) for the human community.

The West African Sahel, a climatologically hot region (e.g. Nicholson 2013), suffers from extreme heat events all year round (with peaks in boreal spring). The literature indicates that Sahelian heatwaves are relatively short-lived as compared to other regions, but are extremely severe in magnitude (e.g. Oueslati et al. 2017; Guigma et al. 2020a). Moreover, over the recent decades and in agreement with the global trend, they have been more frequent, more intense (especially at night) and longer lasting (Fontaine et al. 2013; Ringard et al. 2016; Moron et al. 2016; Oueslati et al. 2017; Barbier et al. 2018). Climate projections also anticipate an increase of the magnitude, spatial extent and frequency of extreme heat events (Russo et al. 2016; Dosio 2017; Sylla et al. 2018) that could only aggravate the thermal risk in the region.

The impacts of extreme heat in the region, as elsewhere in Africa, are largely unreported or underreported (Harrington and Otto 2020). A few studies have however elaborated on the topic, giving an insight into the adverse effects of heat across a range of sectors. Diboulo et al. (2012) and Azongo et al. (2012) showed strong associations between higher temperature and daily mortality in western Burkina Faso and northern Ghana respectively. The increase of death rates is especially important at the short-term (a few days after the heatwave events), with under-five children being the most hit. In the energy sector, Aissatou et al. (2017) evidenced a relatively strong correlation between extreme heat events and peaks of electricity consumption in two major Sahelian cities (Dakar and Niamey). Furthermore, the International Labour Office stresses in a recent report (ILO 2019) that, in Africa, seven of the 10 countries most severely affected by labour productivity loss due to heat stress are located in the Sahel. In this report, the working hours lost to heat stress in 1995 across West Africa, were estimated to be the equivalent of more than two million full-time jobs, which represents, in economic terms, 3.3% of the GDP of the region. With the projected increase of heat in the region, these losses are expected to reach more than eight million full-time jobs, or equivalently 4.77% of the GDP by just 2030. The agriculture and construction sectors, which employ an important portion of the work force, are the most severely affected.

Faced with this issue, it is urgent to undertake actions to alleviate the adverse effects of these extremes. In that regard, numerical weather prediction (NWP) models could provide information to help governments and humanitarian organisations in the region to trigger preventive actions. Such heat early warning systems (HEWSs), jointly recommended by the World Health Organisation (WHO) and the World Meteorological Organisation (WMO; WMO N°1142), are already implemented in several countries across North America (e.g. McElroy et al. 2020; Henderson et al. 2020), Europe (e.g. Morabito et al. 2019; Casanueva et al. 2019), Australia (e.g. Nicholls et al. 2008; Nitschke et al. 2016) and South Asia (e.g. Knowlton et al. 2014). A non-exhaustive global map of heat-action plans has been prepared by the Global Heat Health Information Network (GHHIN) and is accessible from http://ghhin.org/map/.

One prerequisite for HEWSs is skilful prediction from the NWP models at a reasonable lead-time for action. However, the skill of Sahelian heatwave forecasting has received only minor attention. The main work on this topic so far is an evaluation of two CNRM-CM forecasting systems in use at Météo-France by Batté et al. (2018). They found that, at the subseasonal scale, the skill of their forecasting systems is essentially restricted to the deterministic horizons (first 10 days). Coughlan de Perez et al. (2018) investigated the short-term (out to 10 days) predictability of temperature extremes at the global level, and found that while the NOAA model has limited skill, the ECMWF model instead presents a potential for the implementation of rapid preventive actions for heatwave impact mitigation. They also made the recommendation that further research be conducted to identify the drivers of heatwave predictability in regions including Africa. Likewise, Batté et al. (2018) mentioned that extended predictability may be provided by planetary waves and teleconnections.

These recommendations are in tune with previous work by Guigma et al. (2020b), who identified tropical modes of variability as important large-scale drivers of Sahelian heatwaves. Precisely, the activity of the Madden Julian Oscillation (MJO), the equatorial Rossby (ER) and Kelvin (EK) waves in the Equatorial West Africa sector (0-10°N), where convection peaks in spring, significantly modulates the frequency and spatial distribution of heatwaves in the Sahel. Given the spatio-temporal properties of these modes, Guigma et al. (2020b) suggested that they could provide heatwave predictability at subseasonal timescales. Subseasonal predictability has received increasing attention over recent years, given the range of new opportunities for risk management in several sectors (health, disaster preparedness, water management, energy and agriculture) that it brings (White et al. 2017).

This research seeks to address the gap in understanding of heatwave predictability in the Sahel and has two objectives: (i) to evaluate the skill of Sahelian heatwave prediction at the synoptic and subseasonal scales (i.e. up to ~45 days) and (ii) to assess the importance of tropical modes as a source of predictability. This is achieved through a statistical evaluation of a long record of hindcast (or re-forecast) data and a detailed examination of a case study heatwave event.

By building understanding of climate and predictability, this research seeks to pave the way for the development of HEWSs and the scaling of anticipatory forecast-based Actions/Financing (FbA/FbF) for such events (e.g. Coughlan de Perez et al. 2015). This is an especially relevant approach in developing countries, including the Sahel, where climate investments are currently principally directed to post-disaster recovery (Mirza 2003).

The remainder of this manuscript is structured as follows. Section 4.2 introduces the forecast and reference datasets used in this study as well as the different methods for tropical mode detection and skill evaluation. In Section 4.3, the results of both the statistical and the case studies are presented and discussed. Finally Section 4.4 summarises the findings, and elaborates on the next steps for future research on heatwaves in the Sahel.

4.2. Data and Method

The present research analyses heatwave prediction skill for forecasts initialised in two seasons, as in Guigma et al. (2020a): the February to March season (FM hereafter) and the pre-monsoon April to June season (AMJ hereafter), which marks the peak of heat in the region.

4.2.1. Description of the ECMWF ENS extended-range forecasting system

In this study, the ECMWF ENS extended-range forecasting system (ENS-ext hereafter) has been chosen to evaluate the prediction skill of Sahelian heatwaves at the synoptic to subseasonal lead-times. The main reason for this preference is that in most inter-model comparative studies, ECMWF has proved to be the most skilful (e.g. Janiga et al. 2018; de Andrade et al. 2019; Bengtsson et al. 2019). In addition, national meteorological services in the Sahel can freely access some of the ECMWF high-resolution real-time forecast data (including 2m temperature), thanks to a partnership between the African Centre for Meteorological Applications for Development (ACMAD) and the European Centre.

ENS-ext generates a hindcast twice a week (Monday and Thursday) in running an 11 member-ensemble (one control and 10 perturbed members) for the last 20 years, starting on the same weekday and month as the real time forecast. The present study uses all the hindcast data generated in 2018 (thus covering the 1998-2017 period), consisting of 105 different calendar days (initialisation dates). Note that 2018 covers two different versions of the model (CY43R3 and CY45R1) as an upgrade was implemented in June 2018. The hindcast, like the real-time forecast, has a time horizon of 46 days (output data are generated every six hours), with a native horizontal resolution of O640 (about 18km) up to day 15, degrading to O320 (about 36km) between day 16 and day 46.

Two main sets of variables are extracted. (i) Thermal variables consisting of temperature (T), maximum and minimum temperatures (Tmax and Tmin) and dewpoint temperature (Td), all at the screen level (2m height), from which are derived thermal indices (see Section 4.2.2). (ii) Outgoing longwave radiation (OLR) data which are used to assess the activity of tropical modes (see Section 4.2.4). The thermal variables are extracted as 06-hourly forecasts at a resolution of 0.5° x 0.5° over the Sahel domain (20°W-30°E ; 10°N-20°N), while the OLR data are downloaded as forecast 24-hour totals at a resolution of 2.5° x 2.5° over the global tropics (20°S-20°N). Both sets of variables extend up to the full 46-day forecast horizon.

The hindcasts are verified against the fifth generation of the European Reanalyses (ERA5, Hersbach et al. 2020), also produced by ECMWF. ERA5 has a native horizontal resolution of approximately 31km. The variables retrieved are those extracted from the hindcast, and the resolution chosen accordingly. In terms of the quality of near-surface temperatures in ERA5, Oueslati et al. (2017) and Barbier et al. (2017) assessed ERA-Interim, which ERA5 is an improvement of, against the Global Summary Of the Day (GSOD) observational dataset, and concluded that it was suitable for heatwave study in the Sahel. Furthermore, Gleixner et al. (2020) showed that in ERA5, near-surface temperatures are less climatologically biased, and their interannual variability better represented than in ERA-Interim across Africa, including in the Sahel band. Similarly, Wang et al. (2017), Tall et al. (2019), Wright et al. (2020) and Hersbach et al. (2020) proved that ERA5 represents relatively well the observed OLR over the tropical domain, confirming its suitability as reference dataset for the analysis of tropical modes. The Berkeley Earth Surface Temperatures (BEST; Muller et al. 2014; Rohde et al. 2016) dataset is used as a second reference dataset to provide an independent evaluation of thermal indices (given that ERA5 is created using the same model as ENS-ext). BEST data consist

of daily Tmax and Tmin (no moisture data is available) at a native resolution of 1° x 1°, regridded to 0.5° x 0.5° to match the hindcast grid.

4.2.2. Thermal index derivation

Guigma et al. (2020a) showed that in the Sahel, heatwaves defined using different thermal indices over the same diurnal period, or the daytime versus nighttime heatwaves of a same index are not synchronous, and often result from different underlying thermodynamic processes. Their predictability could therefore also differ, and to account for this eventuality, two distinct measures of heat are used in this paper: Temperature (T) and the heat index (HI). Considering their daytime and nighttime components separately gives a total of four thermal indices.

For temperature, the nighttime (daytime) component is taken as the daily minimum (maximum) value of the 06-hourly forecasts of minimum (maximum) temperature and is hereafter referred to as T-night (T-day).

The formula for HI derivation (Steadman 1979) is as follows:

$$HI = -42.37 + 2.04T + 10.14RH - 0.22\,T.RH\ - 6.83\ \times 10^{-3}T^2 - 5.48 \times 10^{-2}RH^2 + 1.22 \times 10^{-3}T^2.RH + 8.52 \times 10^{-4}T.RH^2 - 1.99 \times 10^{-6}T^2.RH \quad (1)$$

Where T is temperature, and RH relative humidity computed from temperature and dewpoint temperature.

The nighttime (daytime) component of HI, hereafter referred to as HI-night (HI-day), is computed by replacing T from (1) by T-night (T-day) and RH by the averages of the 06-hourly forecasts of relative humidity valid at 00 and 06 UTC (12 and 18 UTC).

Similarly, T-night, T-day, HI-night and HI-day are derived from the ERA5 dataset using the corresponding timesteps. T-night and T-day are directly available in BEST.

4.2.3. Heatwave definition and forecast probability

Using the method of Guigma et al. (2020a), heatwaves in the ERA5 dataset are defined for each thermal index and at each grid-cell, as spells of at least three consecutive days where the daily index value exceeds both the 75th percentile of its total distribution over all days, and the 90th percentile of

its calendar day distribution computed over a 31-day centred window. Binary data of heatwave occurrence (coded 1) or non-occurrence (coded 0) are thus obtained.

Heatwaves are also defined in the hindcast dataset at each grid-cell and for each thermal index using several steps. As a reminder, for each thermal index, a given grid-cell has a total of 1062600 data records, broken down into 105 initialisation dates each year, 46-day integrations (or forecast horizons), 20 years of forecasts (covering 1998-2017) and 11 ensemble members. Pooling all the 11 members together, the 75th percentile of the total distribution and the 90th percentile of each calendar day are calculated. Both thresholds are derived as a function of lead-time, giving a total of 46 values for the 75th percentile and 4830 values for the 90th percentile (46 lead-times x 105 calendar days). The latter is smoothed through averaging over a window of 10 initialisation dates (including the date of interest, the four initialisation dates before, and the five initialisation dates after). For example, to calculate the 90th percentile of forecasts initialised on 15 January 2018, the forecasts initialised on 01, 04, 08, 11, 15, 18, 22, 25, 29 January and 01 February are used.

Once the magnitude thresholds are defined, heatwaves are detected in each member as spells of three or more consecutive days where the thermal index exceeds both the two thresholds defined above. In order to account for events which start before the first day of the forecast but run into the forecast time, each 46 day-long forecast integration is padded at its beginning with the two days of reference heatwave occurrence binary data immediately before the forecast. These extra two days are removed after the detection step. The forecast data thus turn binary to indicate the occurrence or non-occurrence of heatwaves.

Then, on a given day and at a given grid-cell, the forecast probability of heatwave occurrence is given by the ratio of the sum of the ensemble members' binary heatwave values to the ensemble size of 11 (ranging from 0 to 1 in 1/11 increments).

4.2.4. Predicted tropical mode activity and link with heatwaves

In order to assess whether tropical modes can be a source of skill for heatwave prediction, their activity in each of the ENS-ext individual members, as well as in the ensemble mean (EM) (mainly for the case study purposes) is filtered, using the same method as in Janiga et al. (2018), which consists of several steps.

(i) First, besides the 11 individual members, daily values of the EM forecast OLR for each grid-cell across the global tropics are derived. For each of the 11 individual members and the EM, there is a total of 96600 data points (105 initialisation dates x 20 years, each with a forecast horizon of 46 days).

(ii) The ends of each 46-day long forecast integration are padded: the heads with the 730 days (two years) of reference (ERA5) OLR immediately prior to the forecast first day, and the tails with zeros (zero-padding) to a length of 730 days also. This results in new data segments of length 1506 days each (46 days of forecast plus 2 x 730 days of padded data) for each individual member and the EM, from which the mean and first four harmonics of the reference OLR are subtracted.

(iii) Then, each segment undergoes a wavenumber frequency filtering similarly to (Wheeler and Kiladis 1999), to retain the harmonics of the MJO, ER and EK waves. The exact characteristic wavenumbers, periodicities and equivalent depths used to detect each of these three modes of tropical variability are the same as those used in Guigma et al. (2020b), and are shown in Table 4.1. The outcome of the filtering for each mode and for each segment is a 1506-day long timeseries of filtered OLR data at each of the global tropics grid-cell. For verification purposes, the 46 days of forecast in each segment are replaced by the corresponding analysed ERA5 data, and the same filtering is applied. This gives to each forecast mode-filtered data segment an equivalent observed mode-filtered data segment, which it can be verified against.

Table 4.1. Characteristics of the tropical modes analysed in this study.

Mode	Equivalent depth (m)	Wavenumber	Period band (days)	References
MJO	Not specified	0 to 9	20 to 100	Kiladis et al. (2005);
ER	1 to 90	-10 to -1	9.7 to 72	Kiladis et al (2009)
EK	8 to 90	1 to 14	2.5 to 20	Straub & Kiladis (2002) (Mekonnen et al. 2008)

MJO: Madden Julian Oscillation; ER: Equatorial Rossby wave; EK: Equatorial Kelvin wave.

Then, another set of methods is used to assess the activity of tropical modes locally over the Equatorial West Africa sector (this set of methods is not applied to the EM data). The forecast and observed 1506-day long mode-filtered data segments are each averaged at the characteristic 5°E longitude between the equator and 10°N (this band of latitudes corresponds to the region of maximum convection over West Africa in spring; Guigma et al. 2020b). For each segment, the resulting unidimensional timeseries and its first order time derivative are standardised (using the standard

deviation from ERA5 for both the forecast and observed segments), and, through trigonometric operations, they are combined to identify wave angle and amplitudes for each day. The angles are further binned into eight 45° wide phases labelled 1 to 8. A mode is considered active on a given day only if its amplitude reaches or exceeds one. If not, the corresponding phase takes the value 0. The composite anomalies of observed OLR against these phases are shown in Fig. S4.1 for each mode of variability. The reader is referred to Guigma et al. (2020b) for a thorough description of the method. At the end of this process, the days corresponding to padded data (a total of 1460 days for each segment) are removed from the data segments, such that only the mode phases of the effective 46 days of the forecast and the corresponding observation are retained. The final outcome for each mode of variability is then 12 arrays (11 forecast and one observation) of filtered OLR data, each of dimensionality 46 (forecast horizons) x 105 (initialisation dates) x 20 (years).

4.2.5. Forecast evaluation metrics

4.2.5.1. General evaluation

To evaluate the skill of ENS-ext, a set of evaluation metrics has been used. The complete description of each metric is presented in Joliffe and Stephenson (2012).

1) Anomaly correlation coefficients

The strength of the association between the observed versus predicted values of thermal indices is evaluated using the anomaly correlation coefficients (ACCs), i.e. correlation coefficients between the anomalies of observed versus the anomalies of predicted values of the indices. The ACCs for the four thermal indices are discussed in Section 4.3.1.

2) Symmetric Extremal Dependency Index

Heatwaves are relatively rare events. Many common measures of forecast quality struggle to give real indications of model skill for extreme events, as they degenerate to trivial values with increasingly rare events (Ferro and Stephenson 2011). For this reason, non-degenerate metrics have been specifically designated to assess the skill associated with rare events. This study uses the

Symmetric Extremal Dependence Index (SEDI), suggested by Hogan and Mason (2012) to be the best choice, and successfully used in similar heatwave studies (e.g. Marshall et al. 2014; Mandal et al. 2019). SEDI itself is based on two simple scores: the hit rate (H) and false alarm rate (F) which are derived from a two-by-two contingency table (Table 4.2) between a deterministic forecast and observation of heatwave occurrence:

$$H = \frac{hits}{hits + misses} \quad (2)$$

$$F = \frac{false\ alarms}{false\ alarms + correct\ negatives} \quad (3)$$

In (2) and (3), hits are instances where heatwaves were forecast and did occur indeed, misses instances where heatwaves were not forecast but occurred, false alarm instances where heatwaves were forecast but did not occur, and correct negatives instances where heatwaves were not forecast and did not occur (see Table 4.2).

From H and F, SEDI is obtained by applying this logarithmic formula:

$$SEDI = \frac{\ln F - \ln H - \ln(1-F) + \ln(1-H)}{\ln F + \ln H + \ln(1-F) + \ln(1-H)} \quad (4)$$

The possible values for SEDI range from -1 to 1, with 1 being the perfect score and positive values indicating that the model is better than random.

Table 4.2. Contingency table of heatwave occurrence between a deterministic forecast and the observation.

		Observed	
		yes	no
Forecast	yes	hits	False alarms
	no	misses	Correct negatives

In the present research, the SEDI calculation proceeds similarly to Marshall et al. (2014) as follows: contingency tables are first built separately for each of the 11 individual members before pooling them as a single table to calculate H and F, and SEDI subsequently. To assess the significance of the SEDI scores, their standard errors are derived using the following formula (Ferro and Stephenson 2011):

$$SE_{SEDI} = \frac{2\left|\frac{(1-H)(1-F)+HF}{(1-H)(1-F)}\log[F(1-H)]+\frac{2H}{1-H}\log[H(1-F)]\right|}{H\{\log[F(1-H)]+\log[H(1-F)]\}^2}\sqrt{\frac{H(1-H)}{pn}} \quad (5)$$

Where H is the hit rate, F the false alarm rate, n the sample size and p the base rate (relative frequency of heatwave occurrence).

At a given grid-cell, the SEDI score is considered significant if the confidence interval (i.e. $[SEDI - 2SE_{SEDI}; SEDI + 2SE_{SEDI}]$) does not include zero.

4.2.5.2. Evaluation of heatwave prediction skill taking into account the modulation by tropical modes

To assess the skill of the ENS-ext in simulating the activity of tropical modes, the forecast local phases are verified against those detected from ERA5 (local phases are defined in Section 4.2.4), using hit rates. As with the SEDI scores, the contingency tables are first built separately before pooling them to calculate the hit rates. They are discussed in Section 4.3.3.1.

To assess how well the model represents the relationship between tropical modes and heatwaves, the frequency of heatwave occurrence conditioned on the phase of tropical modes (also termed as modulation of heatwave occurrence by the modes) is evaluated in both the model and the reference datasets, using the same formula as in Guigma et al. (2020b):

$$M = \frac{P_x - P_a}{P_a} \quad (6)$$

Where P_x is the conditional frequency of heatwaves over an active phase x of a given mode, and P_a the frequency derived from all days, irrespectively of the activity of the mode.

The results for this modulation are presented in Section 4.3.3.2.

Finally, a given tropical mode is considered to be a source of heatwave predictability if the SEDI scores are higher under its forecast active phases than its inactive phase. This assessment considers

(i) all the eight active phases altogether (i.e. the comparison is made between instances where the mode amplitude is greater than one versus instances where it is equal to or less than one) as in Hudson et al. (2011) and (ii) each phase separately in order to determine precisely which phases contribute the most to the skill. At each grid-cell, statistical significance at a 95% level is tested using a nonparametric bootstrap resampling, with 1000 repetitions as in Guigma et al. (2020b).

4.2.6. Additional methods for the case study

To understand the causes of the heatwave case-study event analysed in Section 4.3.4, the patterns of net radiation (shortwave and longwave) and turbulent fluxes (sensible heat flux SHF and latent heat flux LHF) at the surface are analysed from the ERA5 data. For each of these terms, the anomalies are derived by subtracting the calendar day mean and are subsequently averaged over the heatwave period. The fluxes are, by convention, counted positively when directed from the atmosphere towards the surface.

The activity of the tropical modes during this period is visualised through a time-longitude diagram of the mode-filtered OLR averaged between the Equator and 20°N, a commonly used technique in tropical meteorology (e.g. Schreck et al. 2011, Guigma et al. 2020b).

4.3. Results and discussion

4.3.1. Skill of thermal index prediction by ENS-ext

ENS-ext has a relatively good skill in predicting the four thermal indices under investigation. Figure 4.1 shows the ACCs averaged over the Sahel across the 46 lead days for the FM and AMJ seasons (see Section 4.2.5.1 for method description). For the first week of the forecast for example, the ACCs of all the four thermal indices exceed 0.6. There is then a fast decrease of the forecast skill out to week 3-4 of the forecast bringing the ACC values down to about 0.2. The fast decrease of ACCs beyond the first week is also noticed by Batté et al. (2018) using the Météo-France S2S system, but the drop is much sharper there. A diurnal dependence in thermal index prediction skill is noticeable for both seasons. For the shortest lead-times (out to about day 7), daytime indices slightly outperform their nighttime counterparts and conversely for longer lead-times (exception for HI-day in AMJ). The prediction skill also presents a relatively marked seasonality. Thus in the FM season (Fig. 4.1a) the

ACCs are generally better than during AMJ (Fig. 4.1b) but only for the shortest lead-times. There is indeed a reversal at longer lead-times such that the more humid season of AMJ presents higher skill than FM (even though ACC values are low). Figure 4.1 also shows that ENS-ext clearly outperforms persistence forecast (black dashed lines in Fig. 4.1), even at the shortest lead-times.

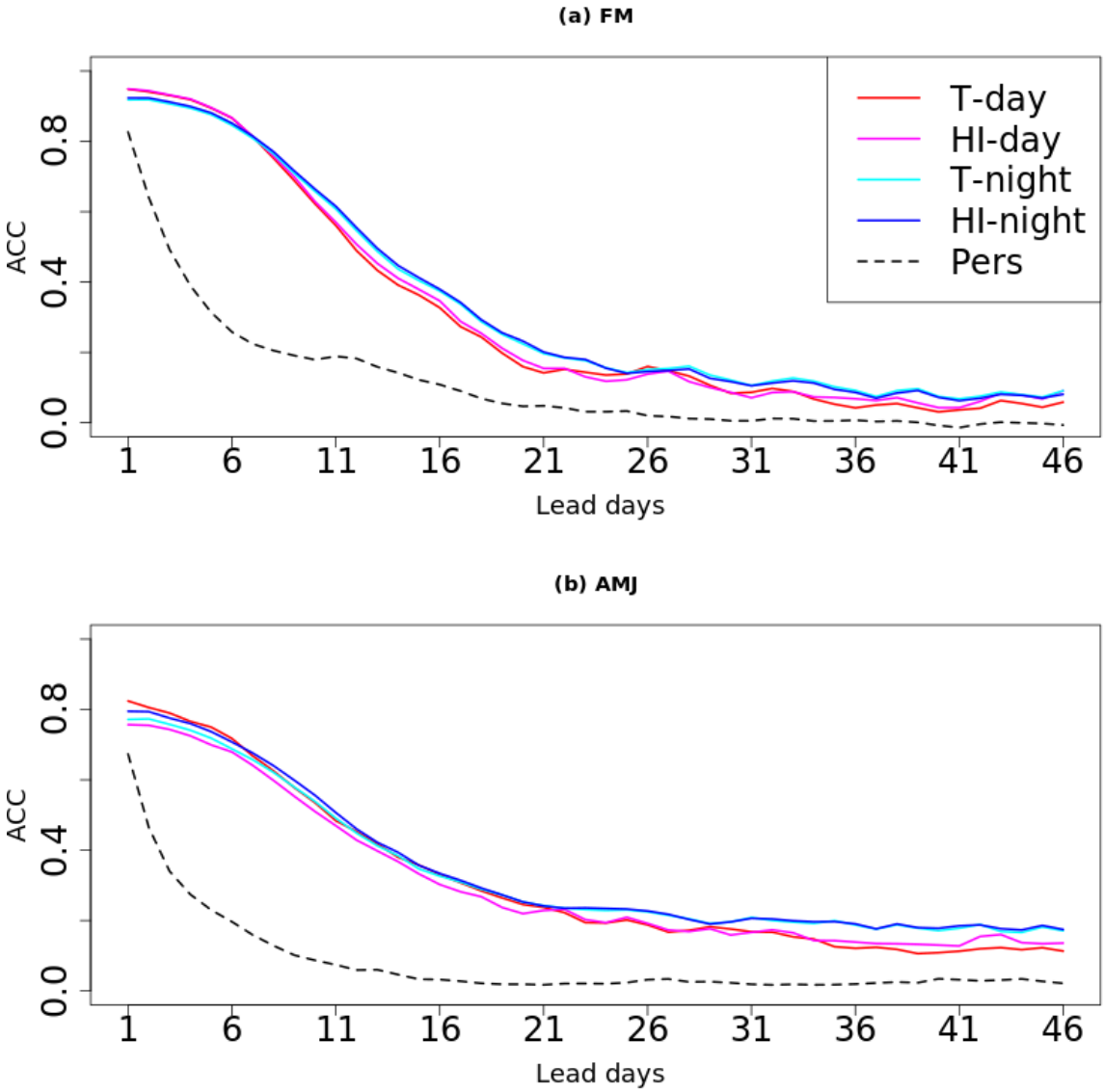

Fig. 4.1 Anomaly correlation coefficients (ACCs) between the ENS-ext forecasts and the ERA5 reference averaged over the Sahel for the four thermal indices over the (a) February-March and (b) April to June seasons. The black dotted lines represent the average ACCs of the persistence forecast across the four indices.

The examination of the spatial distribution of the ACCs reveals differences across the Sahel (Fig. S4.2 using T-day for illustration). For the shortest horizons, the skill is higher in the north than in the

south of the Sahel (irrespectively of the season), whereas at longer forecast lead-times, there is increasingly higher skill in the south than in the north (where the correlation becomes insignificant).

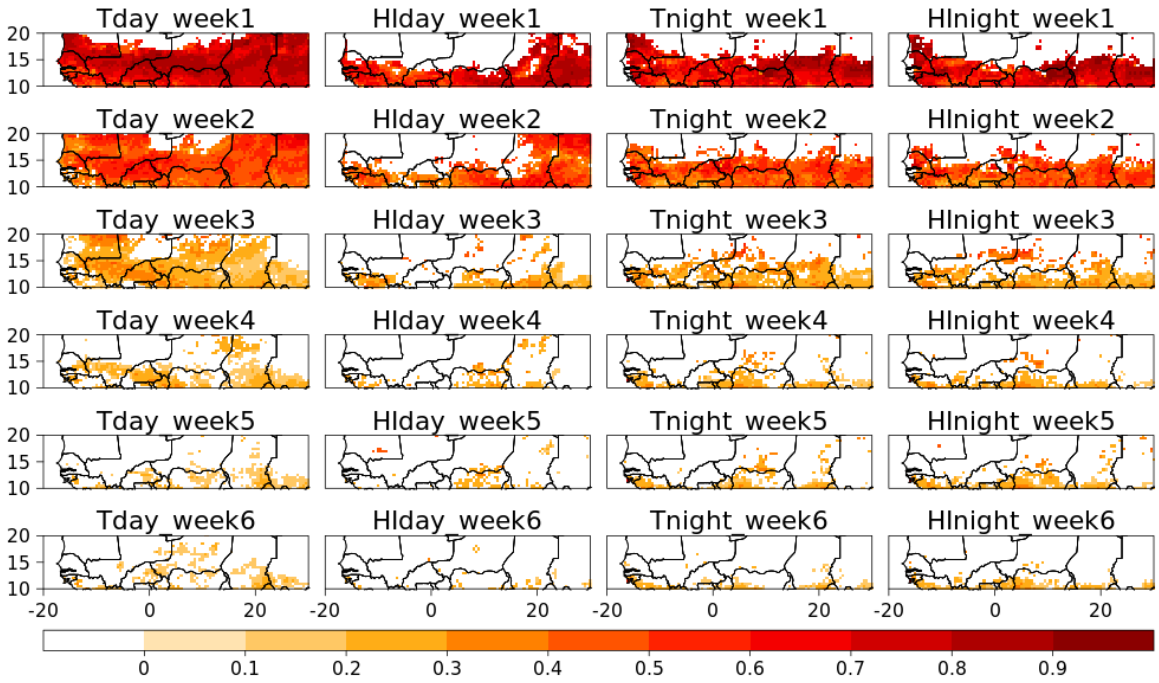

Fig. 4.2 SEDI scores in the FM seasons for each of the four heatwave indices using ERA5 as reference dataset. Each panel represents a specific week of the forecast with the first week at the top. White areas are not significant at the 95% probability level.

4.3.2. Heatwave prediction skill and potential for early action

The skill of ENS-ext in predicting Sahelian heatwaves is assessed using the SEDI score (described in Section 4.2.5.1). Similarly to the ACCs of the indices, the FM season offers larger SEDI scores of heatwave prediction than the AMJ season at short lead-times. Thus, with ERA5 as reference, for the first and second weeks of forecast, the scores are respectively above 0.8 and 0.5 (0.6 and 0.3) in the FM (AMJ) seasons across much of the region as shown in Fig. 4.2 (Fig. 4.3). The skill vanishes quicker in the subsequent lead-weeks in FM than in AMJ such that, after week 3, there is almost no skill (SEDI scores below zero means random forecast better than the model) in forecasts initialised in FM, whereas some scarce areas still have positive (though very weak) SEDI scores in AMJ at lead-week 6. As is also observed with the ACCs, the SEDI scores are initially higher in the northern half of the domain, but a reversal is observed at longer lead-times (this is less evident in FM as heatwaves are not detected in northern Sahel at that season). The seasonality and the evolution with lead-time of

the skill are similar across all four heatwave indices. It should be noted however, that in AMJ, the decrease of skill of nighttime heatwave indices (T-night and HI-night) is slower than that of their daytime counterparts, especially in the southern Sahel, consistently with previous findings by Batté et al. (2018). HI-day has the fastest rate of skill decrease, with only limited areas showing positive SEDI scores after week 2. This marks a contrast to HI-night which is the best forecast heatwave index at the longest lead-times. The lower skill observed in HI-day may be related to the differential diurnal cycle between Tmax and the relative humidity (the two variables from which it is derived) in the Sahel. Whilst Tmax peaks in the early hours of the afternoon and increases with clear skies, moisture reaches its minimum at the same time, with cloudier skies tending to increase it (Guichard et al. 2009; Bourgeois et al. 2018).

The verification using BEST as reference is shown in Fig. S4.3 and it shows mainly similar patterns as using ERA5 with however slightly lower SEDI scores.

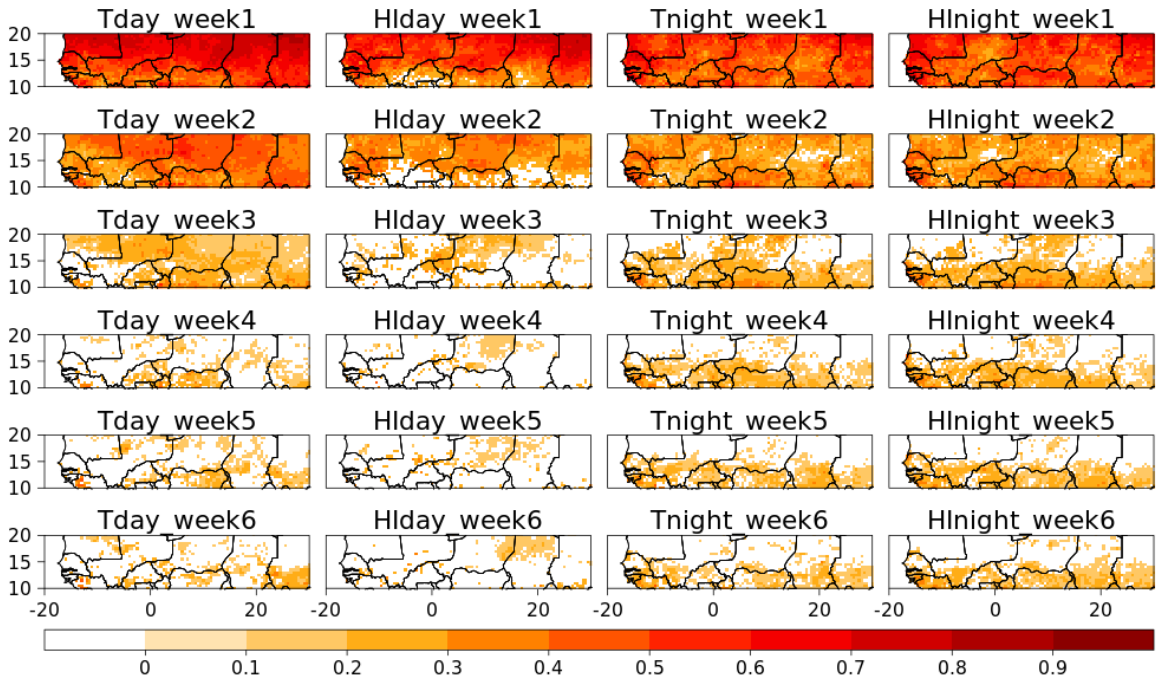

Fig. 4.3 Same as Fig. 4.2 but for the AMJ season.

Compared with other regions across the globe, it can be said that the Sahel enjoys at least the same degree of heatwave predictability at the subseasonal scale. Thus, European heatwaves are found by Lavaysse et al. (2019) to be predictable mostly up to two weeks in advance using ENS-ext. In

Australia, the Bureau of Meteorology's POAMA-2 ensemble model is able to well predict heatwaves two to three weeks ahead with SEDI scores reaching 0.5 at these lead-times under some weather regimes (Hudson et al. 2011; Marshall et al. 2014). In India, a region with a closer climate system to that of the Sahel, the skill of heatwave prediction by the Indian Institute of Tropical Meteorology's ensemble prediction system is found to still be significant at lead-week 3, with comparable SEDI scores as those of the Sahel during the pre-monsoon season (Mandal et al. 2019). As such, the Sahel can also benefit from HEWSs as currently implemented in these regions (e.g. Lowe et al. 2011; Nitschke et al. 2016; Hess et al. 2018; Casanueva et al. 2019).

One potential explanation for the spatiality/seasonality of the ACC and heatwave prediction skill can be found in the large-scale circulation controlling the Sahelian atmosphere. The FM season experiences a large influence from extratropical weather systems coming from the northern edge of the domain (Knippertz and Martin 2005), which are known for their large synoptic-scale predictability (e.g. Knippertz and Fink 2009; Wheeler et al. 2017). On the other hand, AMJ is characterised by an increasing activity of the MJO and equatorial waves, which are by then more active in the equatorial sector of Africa (e.g. Berhane et al. 2015; Guigma et al. 2020b). These modes of variability, since they are less inclined to forecast error growth with lead-time than extratropical disturbances, confer higher subseasonal predictability to the tropics (Judt 2020).

While the verification is so far based on strict comparison of forecast and observed heatwaves at the exact grid-cell and day, it may also be relevant, for operational purposes, to include a window of flexibility in which the forecast still has some potential for action (e.g. Coughlan de Perez et al. 2016). Such a "tolerant" evaluation is assessed here from the temporal point of view through considering that a positive forecast of heatwave (i.e. heatwave forecast to occur) is considered to be a hit if it occurs within a time window of three days centred on the forecast validity date, i.e. between a day earlier and a day after. Given the three-day minimum duration constraint used in this paper, the tolerance only affects the onset and cessation of heatwave events. The comparison between the Sahel-wide average SEDI scores of strict and tolerant evaluation is shown in Fig. 4.4. It is apparent that the gain in skill obtained through the tolerant evaluation is more important in AMJ than in FM (Figs. 4.4c & 4.4d vs Figs. 4.4a & 4.4b). Moreover, the gain is the largest at the longest lead-times, with difference of SEDI scores from the strict evaluation reaching a value close to 0.2 in AMJ (Figs.4.4c & 4.4d). As a matter of comparison, the tolerant evaluation shows a heatwave prediction skill at lead-week 6 similar or better than that of the strict evaluation at lead-week 3 (or at lead-week 2 if a five-day window of tolerance is used instead, not shown). Providing forecasts with such a tolerance for

the longest lead-times could prove relevant for heat-health early actions in the region. With long lead-times, the preparedness actions likely do not need daily accuracy in the forecast. An operational scheme could adopt the 'Ready-Set-Go!' approach of the Red Cross in which various inexpensive actions are implemented at long lead-times, and different more specific or costly actions are then invoked based on more accurate shorter-lead forecasts (Bazo et al. 2019). In this sense, the tolerant verification statistics show that the skill at long lead-times is meaningful to risk managers.

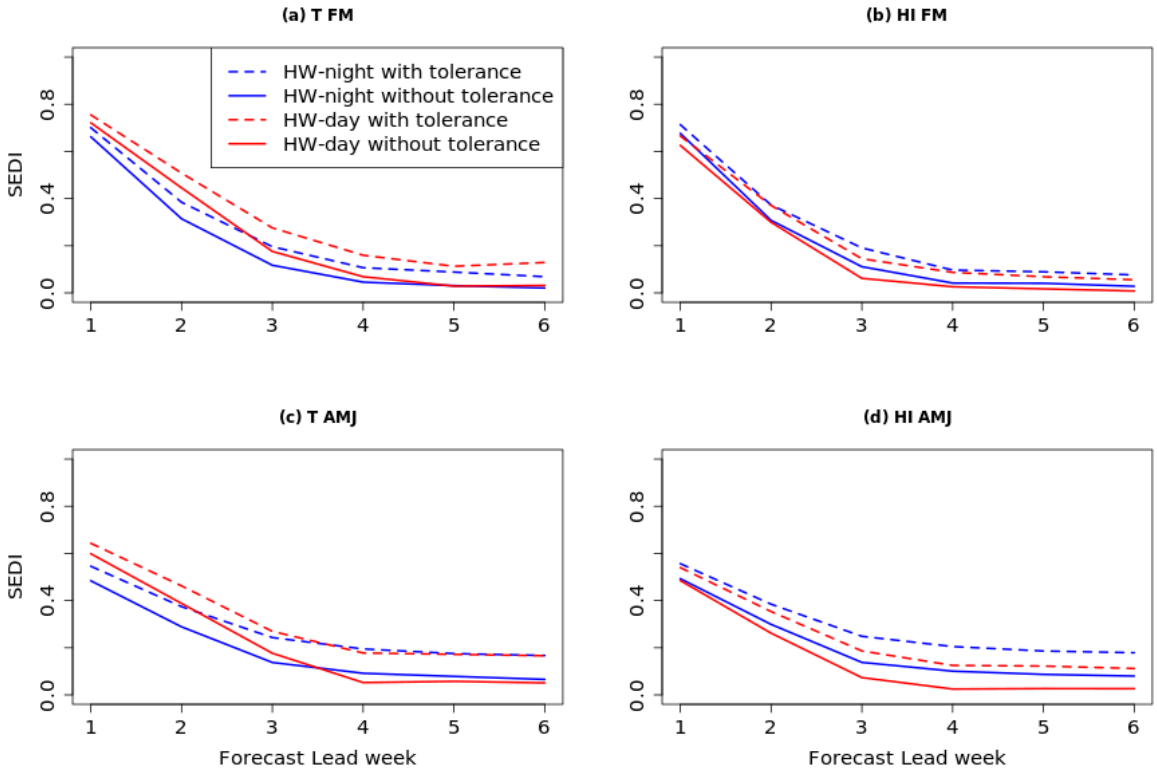

Fig. 4.4 SEDI scores spatially averaged over the Sahel domain for (a & b) the FM and (c & d) the AMJ seasons. Daytime (nighttime) heatwaves are shown in red (blue) with the strict (tolerant) verification in solid (dotted) lines. Strict and tolerant verifications are defined in Section 4.3.2.1.

4.3.3. Tropical modes as a source of predictability for Sahelian heatwaves

Guigma et al. (2020b) showed that at the subseasonal scale, heatwaves in the Sahel are modulated by tropical modes of variability, namely the MJO, the ER and EK waves. Furthermore, in Section 4.3.1, the higher skill at subseasonal scale in the AMJ season than in the FM season could be related to the greater activity of tropical modes in the former season. The present section aims at assessing whether,

in addition to being important drivers of heatwave occurrence, tropical modes also constitute a significant source of predictability. Marshall et al. (2014) mentioned two conditions that any model should a priori meet to be able to predict a hazard in association with its climatic driver: (i) well predict the climatic driver, and (ii) well simulate the relationship between the climatic driver and the hazard. These two conditions will first be assessed, before considering whether tropical modes indeed provide skill for heatwave prediction in the Sahel. The analysis is restricted to the first three weeks of the forecast, beyond which the SEDI scores become relatively low (Fig. 4.3), and covers only the AMJ season.

4.3.3.1. How well does ENS-ext predict tropical modes?

At the global level, Janiga et al. (2018) discussed the predictability of the mode-filtered OLR across the tropics and found ECMWF to be the model with the lowest bias for forecasts of the mean state and activity of tropical modes. Furthermore, investigations by Dias et al. (2018) revealed that ECMWF is relatively skilful at propagating tropical modes for longer lead-times. Here the focus is on the Equatorial West Africa Sector (the region just south of the Sahel, i.e. 20°W-30°E; 0°-10°N) where convection is shown to modulate heatwave occurrence in the Sahel (Guigma et al. 2020b). To assess the skill of the model in capturing the local activity of tropical modes, the forecast phases are compared against observation using hit rates (defined in Section 4.2.5.2).

Among the three investigated modes, the MJO (blue histograms in Fig. 4.5) stands clearly as the most skilfully predicted. At week 1 for example, the hit rate is above 0.4 in most active phases. This value decreases to 0.3 at week 2 and slightly above 0.2 at week 3. As for the ER wave, it has hit rates which are on average 0.1 point lower than that of the MJO, being about 0.3, 0.2 and above 0.1 at weeks 1, 2 and 3 respectively. The EK wave shows the lowest hit rates. They indeed always remain below 0.2, even at week 1, and at weeks 2 and 3, stand below 0.1. Note that the lower skill associated with the EK wave has already been highlighted by previous work (e.g. Li and Stechmann 2020). For each mode, the hit rates are generally comparable across the eight phases, with however slightly higher values in the central phases (phases 3 through 6). The differences observed between the different modes are in agreement with their spectral properties summarised in Table 4.1. The MJO and ER wave indeed have a longer periodicity than the EK wave. This provides them with a longer "memory" and leads to slower error growth.

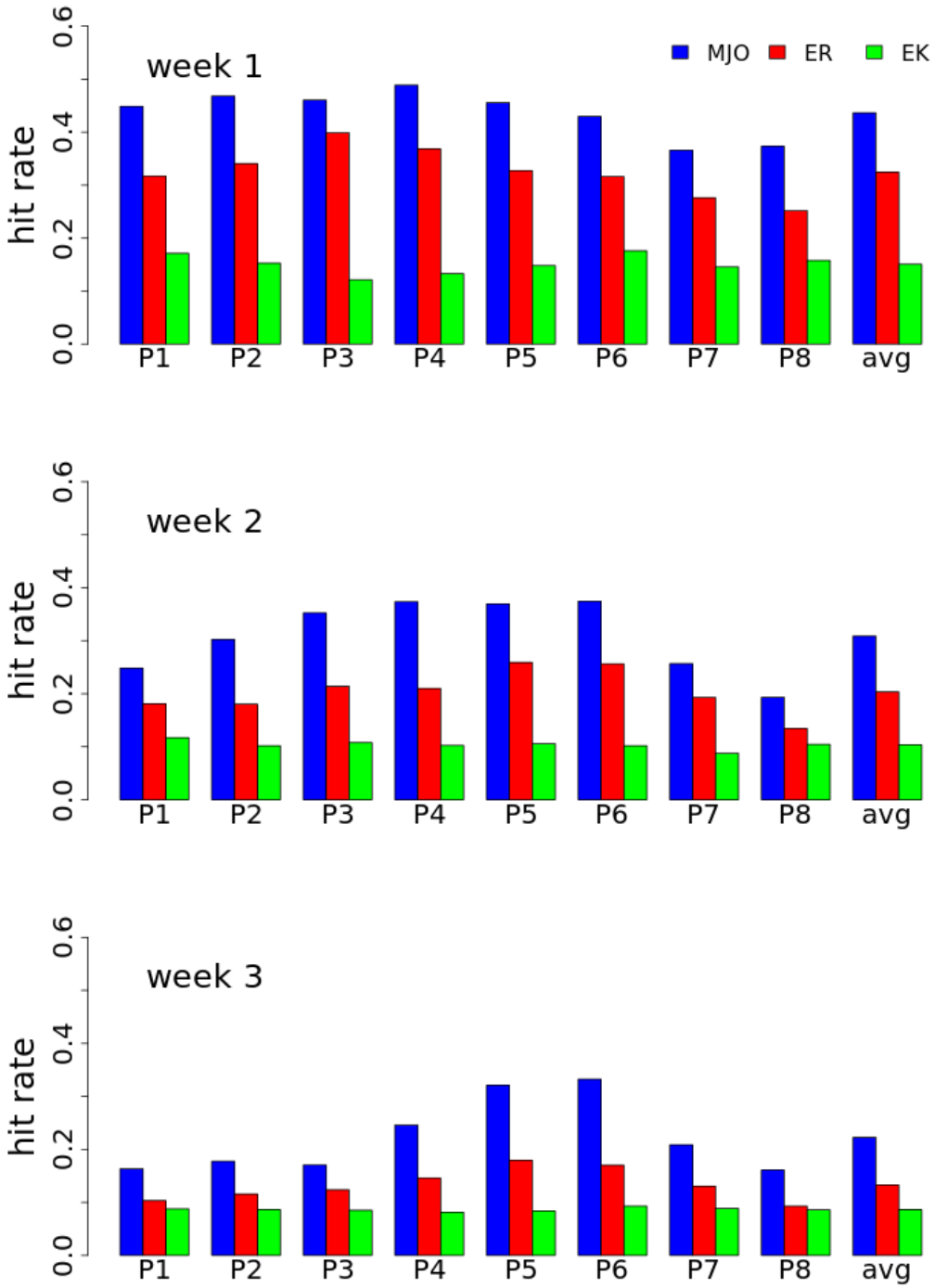

Fig. 4.5 Hit rates of predicted tropical mode phases at the reference longitude of 5°E for the first three weeks of the forecast. The rightmost histograms in each panel represent the average hit rates across the eight active phases. The blue, red and green bars represent the MJO, ER and EK waves respectively.

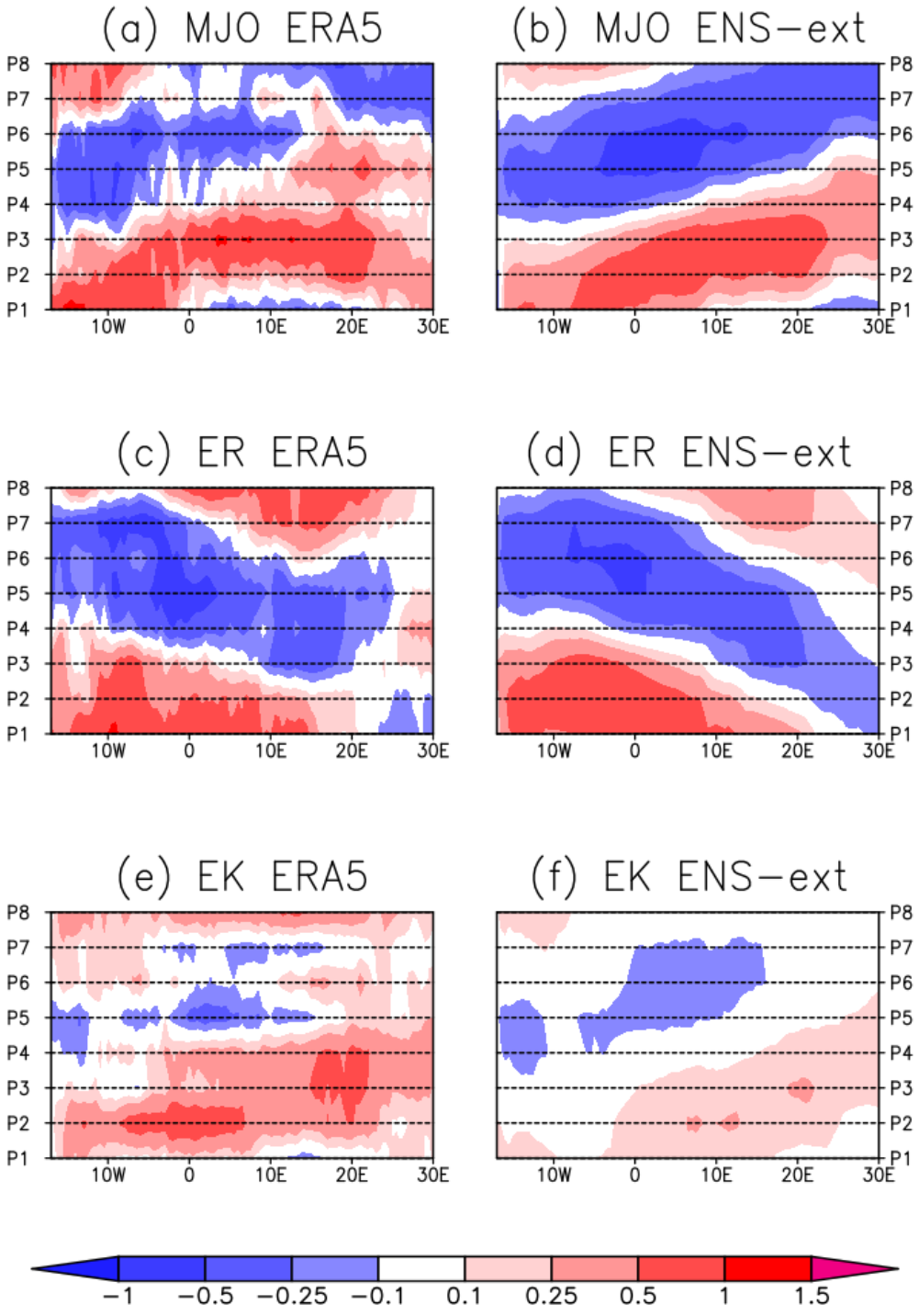

Fig. 4.6 Modulation of T-day heatwave probability of occurrence by active phases of tropical modes in observation (left panels) and ENS-ext (right panels). The modulation is the variable M defined in Section 4.2.5.2 (equation (6)).

4.3.3.2. How well does the model simulate the link between tropical modes and heatwaves?

Guigma et al. (2020b) already elaborated on the modulation of heatwave occurrence by tropical modes from an observational perspective, with a discussion of the underlying physical mechanisms. This modulation, as described in Section 4.2.5.2, compares heatwave occurrence under active phases of the modes to the climatological occurrence. The quality of the replication of this modulation by ENS-ext is a function of the mode under consideration, and is discussed here using T-day heatwaves for illustration. As shown in the left panels of Fig. 4.6, observed phases 1 to 3 of tropical modes (which roughly correspond to a suppression of convection, Fig. S4.1) are overall favourable to heatwaves, whereas phases 5 to 7 (enhancement of convection) obstruct heatwave occurrence. It is apparent that in ENS-ext, the influence of the MJO and ER wave on heatwaves is well simulated. Both the zonal propagation (eastward for the MJO and westward for the ER wave) and the magnitude of the modulation (with M values absolutely reaching 1.5) are well captured by the model (Figs. 4.6b & 4.6d). On the other hand, for the EK wave (Fig. 4.6f), whilst there is a relatively acceptable simulation of the propagation of the modulation across phases, ENS-ext struggles to get the magnitude correct. There is indeed an underestimation of the forcing that EK waves exert on heatwave occurrence. This is however not a surprise, given that the model also has difficulty to predict the activity of this mode (Section 4.3.3.1). For the three other thermal indices (T-night, HI-night and HI-day), similar conclusions are drawn, i.e. a skilful representation of the impact of the MJO and the ER wave on heatwaves versus a limited skill for the EK wave (not shown).

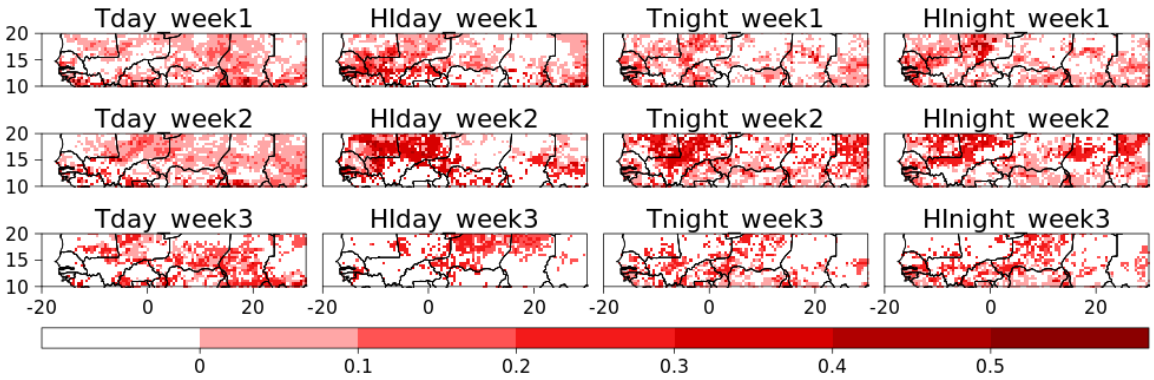

Fig. 4.7 Difference of SEDI scores between forecasts falling on active versus inactive phases of the MJO. All active phases are pooled together and the significance of the SEDI differences is tested by bootstrap resampling (see Section 4.2.5.2).

4.3.3.3. Heatwave prediction skill in active versus inactive phases of the modes

The previous two sections have shown that ENS-ext meets the two necessary conditions (according to Marshall et al. 2014) to be able to draw heatwave predictability from tropical modes, especially from the MJO and ER wave (much less for the EK wave). This section addresses whether there is indeed an enhancement of prediction skill associated with the activity of tropical modes during the AMJ season. This is done through stratifying the forecast (not observation) into active versus inactive phases, as described in Section 4.2.5.2, and assessing the SEDI differences between the two instances. Out of the three modes of variability, the MJO is the largest source of prediction skill. For T-night, HI-night and HI-day, the MJO-related skill reaches values of 0.4, mainly over the central Sahel (Mali, Burkina Faso and western Niger) and extends out to week 2 to 3 of the forecast (Fig. 4.7). For T-day, the skill is mainly observed over the eastern Sahel. The main phases responsible for the positive SEDI differences are phases 3 and 4 (Fig. S4.4). For the ER wave, the improvement of skill, limited to 0.3, is mostly found over the eastern (western) Sahel for T-night, HI-night and HI-day (T-day) at week 1 (Fig. 4.8) and comes essentially from phases 7 and 8 (Fig. S4.5). At longer lead-times, the ER-related skill is relatively marginal, apart from T-day and HI-day which show some skill over the central Sahel (Burkina Faso and western Niger) at week 2-3 (Fig. 4.8). As for the EK wave, the skill, analysed only for week 1 of the forecast (beyond which the model cannot well predict it, Section 4.3.3.1) originates mostly from phase 3 and is generally not much in excess of 0.1 (Fig. S4.6).

These results therefore show that the MJO, the ER wave and, to a lesser extent, the EK wave provide predictability to Sahelian heatwaves. This implies that heatwave predictions are more reliable when an intense activity of tropical modes is also (skilfully) forecast. Such a conclusion is especially interesting for operational forecasters in the region. They can indeed rely on the local activity of tropical modes to estimate the confidence levels of their heatwave warnings.

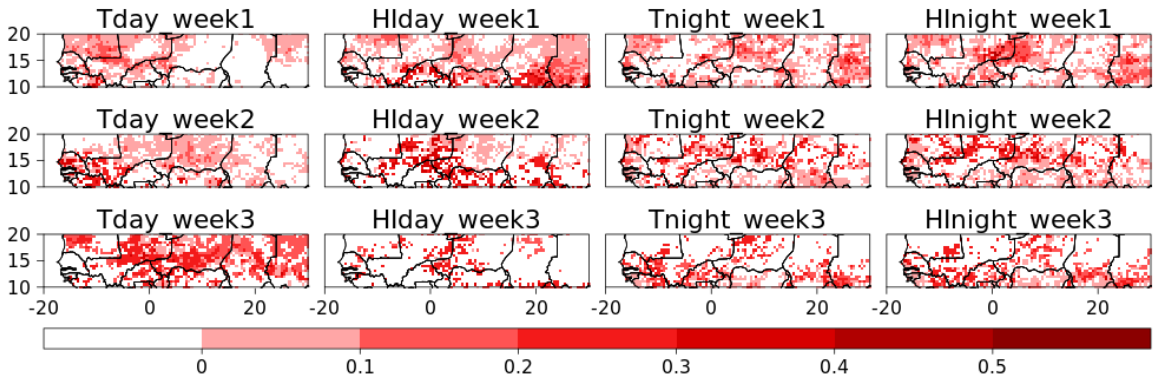

Fig. 4.8 Same as Fig.4.6 but for the ER wave.

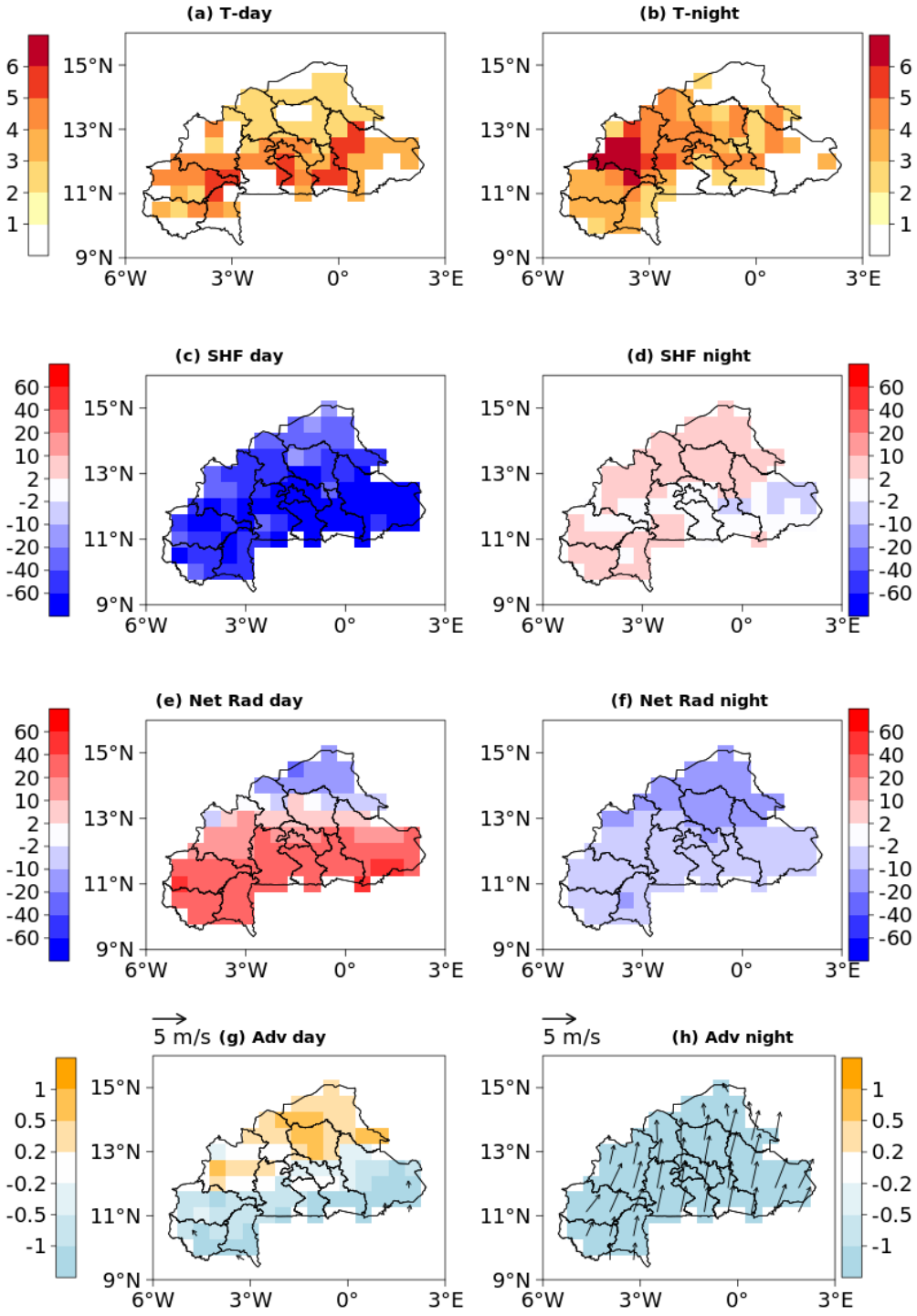

Fig. 4.9 Heatwave occurrence and thermodynamic conditions between 27 May and 02 June 2015. a & b show the number of heatwave days sampled by T-day and T-night respectively. c & d (e &f) show the average anomalies of sensible heat flux (net radiation) at the surface in Wm^{-2} for daytime and nighttime respectively. They are conventionally counted positively when oriented from the atmosphere towards the surface. g & h display the average anomalies of heat advection at the 925 hPa pressure level superimposed with wind anomalies at the same level respectively for daytime and nighttime.

4.3.4. Case study of a tropical mode-driven heatwave over Burkina Faso

In this section, the detailed analysis of the prediction of a heatwave event over Burkina Faso, in the central Sahel, by ENS-ext is undertaken with the objective of assessing, in a real case, how the activity of tropical modes can impact the skill of the model. The choice of this event is justified mainly by the fact that it was physically favoured by tropical modes, and also because of its relatively large spatial extent.

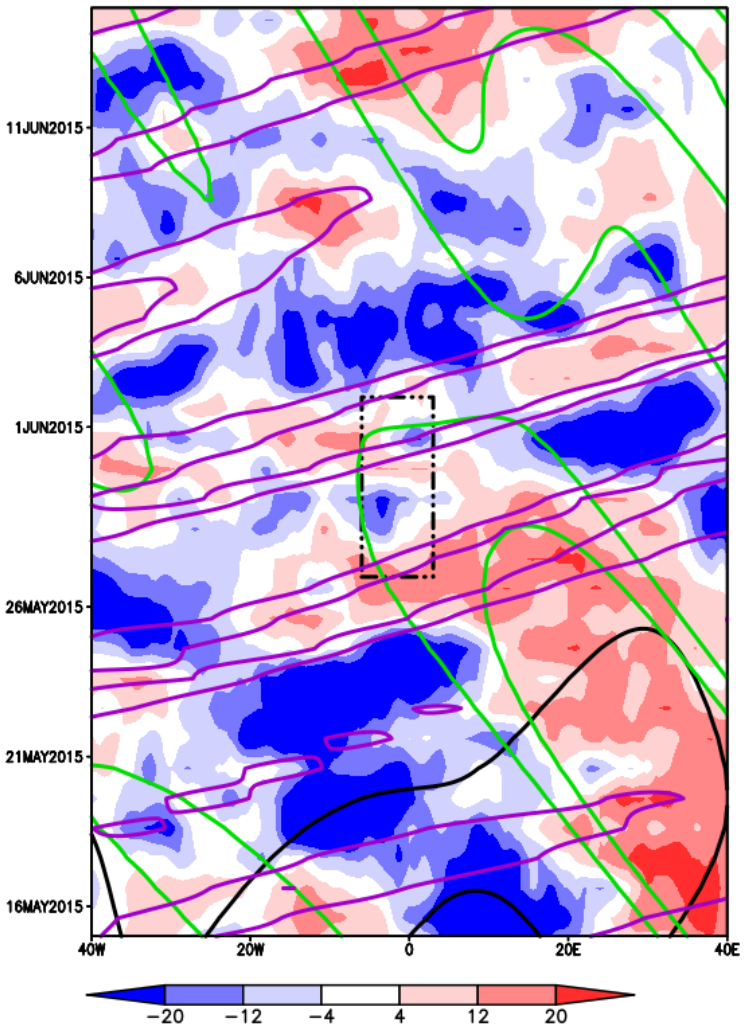

Fig. 4.10 Time-longitude diagram of high-pass filtered OLR averaged between the Equator and 20°N from 15 May to 15 June 2015 in Wm^{-2}. The MJO, ER and EK wave-filtered OLR averaged over the same domain are superimposed as black, green and purple contours respectively. Contour levels are 2 and 8 Wm^{-2} (only positive contours, representing convectively suppressed phases are shown). The rectangular black box in the middle of the plot delimits the longitudinal domain of Burkina Faso (6°W-3°E) and the heatwave period (27 May-02June).

4.3.4.1. Description of the heatwave and thermodynamic conditions

The heatwave event under scrutiny took place mainly in Burkina Faso between 27 May and 02 June 2015. Figures 4.9a and 4.9b show the spatial distribution and the length of the event across the country. Both daytime and nighttime were affected (which is unusual in the Sahel; Guigma et al. 2020a) over the whole country. It should be noted that the event was less marked in HI-day and HI-night than in T-day and T-night (not shown).

The analysis of some thermodynamic variables over the heatwave period reveals that the daytime event was chiefly shaped by a strong sensible flux from the ground towards the atmosphere (a magnitude above 40 Wm^{-2} in some areas; Fig. 4.9c) which was anomalously dryer than usual (not shown), an increased incoming solar radiation in the south of the country (Fig. 4.9e) and heat advection in the north (Fig. 4.9g). At night, the heat resulted mainly from a longwave radiation emission from the ground (Fig. 4.9f) which was overheated during the day (a relatively cool air was however advected, reducing the heat load, Fig. 4.9h).

4.3.4.2. Evolution of tropical modes during the event

The increase of incoming solar radiation during the day and longwave loss during the night were favoured by large-scale conditions that suppressed convection over the region. To find out the origins of this convective inhibition, the time-longitude diagram of the ERA5 mode-filtered OLR is shown in Fig. 4.10. It is apparent that an ER wave originating from the Indian Ocean was the main mode suppressing convection over the domain surrounding Burkina Faso (green lines in Fig. 4.10) during the heatwave period. Besides, the initial and last days of the heatwave are also affected by EK waves on convectively suppressed phases which also promoted the heating. An eventual contribution from the MJO is ruled out since it was instead on a convectively enhanced phase (not shown).

4.3.4.3. Skill of the model over the heatwave period

The average anomalies of T-day and T-night over the heatwave period in the ENS-ext EM forecasts and in the ERA5 analysis, as well as the average anomalies in ERA5 over the week preceding the heatwave (persistence) are shown in Fig. 4.11. The first remark is the relatively good spatial coherence between the forecasts at different lead-times and the observation, valid for both T-day and

T-night. The model was therefore able to predict the anomalously hot conditions that prevailed over Burkina Faso between 27 May and 02 June 2015, even at the longest lead-times.

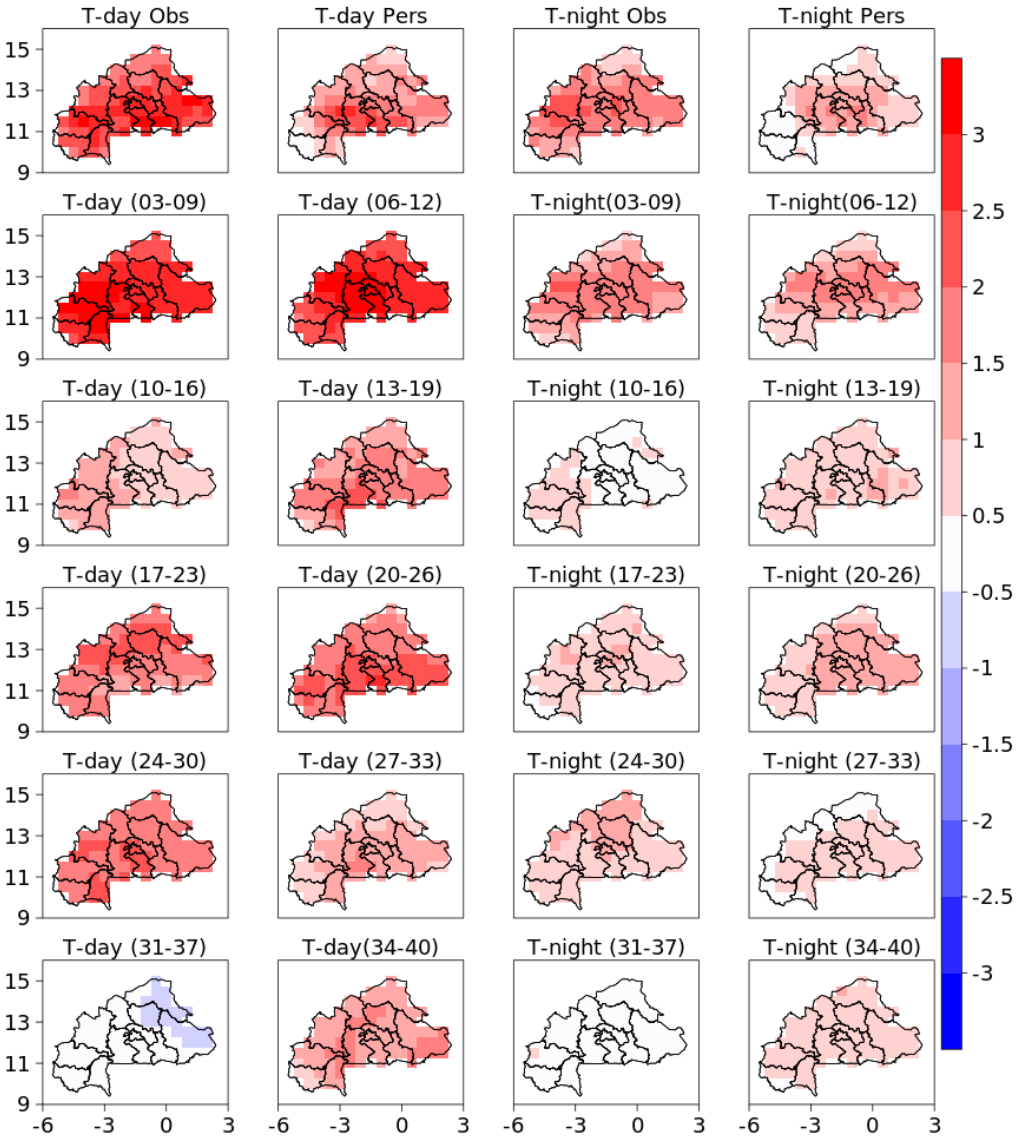

Fig. 4.11 Average anomalies of T-day and T-night over the 27 May - 02 June 2015 period in (top panels) ERA5 analysis and persistence and (subsequent panels) in ENS-ext ensemble mean forecasts at different start dates. The persistence ('Pers') is taken as the average of ERA5 anomalies over the period from 20 to 26 May 2015. The numbers between brackets indicate the lead-times in days from the forecast start dates to the onset and cessation of the heatwave.

Better, on the last two initialisations before the event, the model beat persistence, notwithstanding that for T-day there is a slight overestimation of the magnitude of the anomalies. Two forecasts, namely those initialised at lead-times 31 days and 10 days to the onset, are however characterised by

less accuracy than the rest, especially in comparison with forecasts initialised at longer lead-times than them.

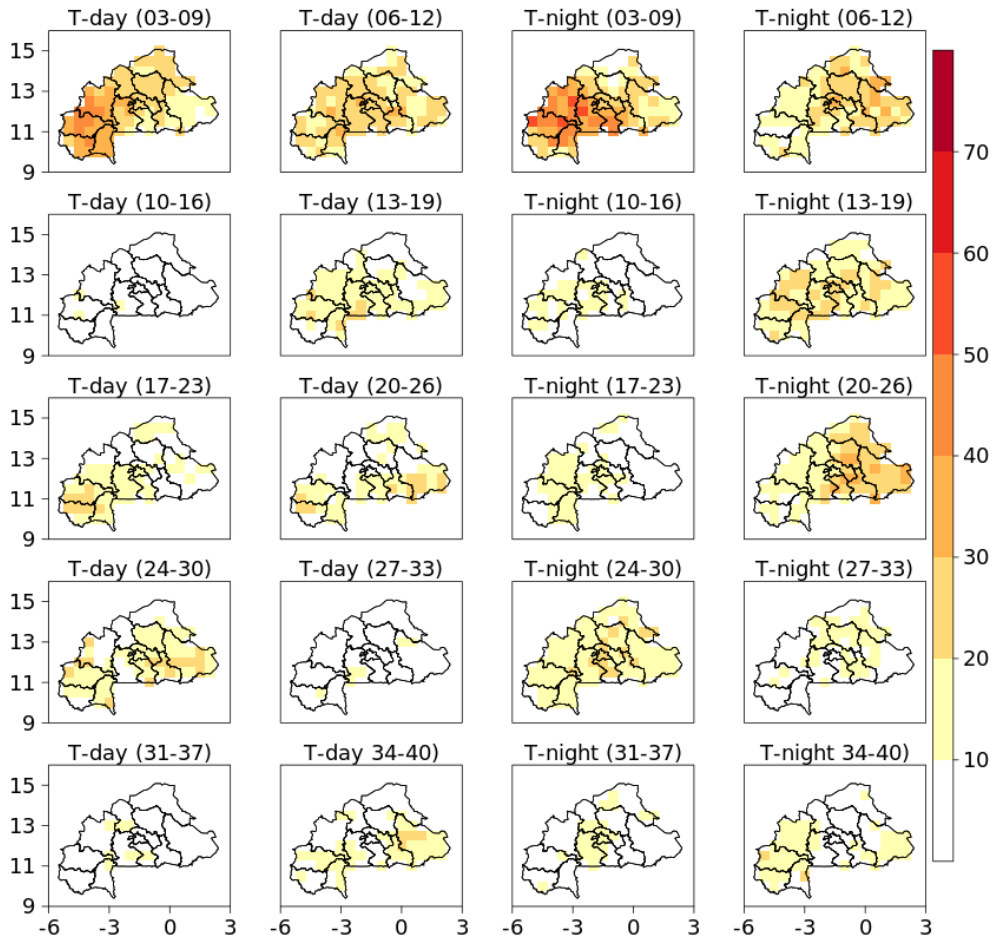

Fig. 4.12 T-day and T-night average heatwave forecast probabilities (in %) over the 27 May - 02 June 2015 period at different start dates. The numbers between brackets indicate the lead-times in days from the forecast start dates to the onset and cessation of the heatwave.

Figure 4.12 shows the heatwave forecast probabilities at different lead-times for T-day and T-night. The flavour of the heatwave was already perceptible at lead-time 24 days to the onset (i.e. more than three weeks in advance) with at least one individual member predicting the event over the vast majority of the country, consistently in both T-day and T-night (note that the climatological forecast probability is below 0.1 over the heatwave period; not shown). The forecast probabilities increased on the following initialisation dates to eventually reach 50% three days prior to the onset. However, as with the index anomalies, some initialisation days "lost" the heatwave signal in the run-up. Thus, forecast probabilities at lead-times 17 and 10 days to the onset are lower than that at the respective longer lead-times.

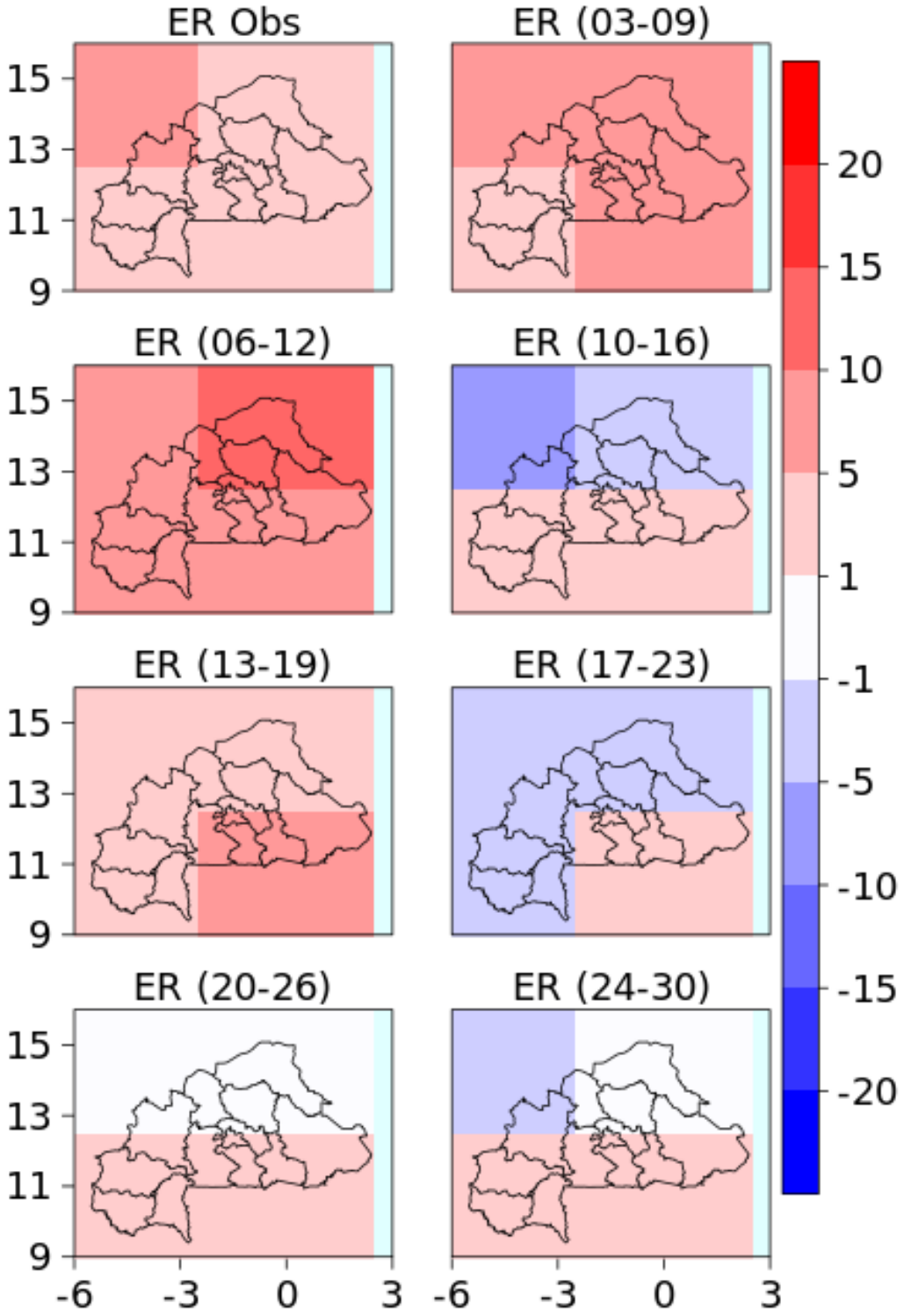

Fig. 4.13 ER wave-filtered OLR observed in ERA5 (top left) and predicted by ENS-ext averaged over the 27 May- 02 June 2015 period. The numbers between brackets indicate the lead-times in days from the forecast start dates to the onset and cessation of the heatwave.

To understand the weakening of the forecast probabilities at these dates, the EM forecast of tropical mode activity is examined, knowing that the heatwave was associated with a convectively suppressed ER wave (Section 4.3.4.2). Figure 4.13 thus shows observed and EM-predicted ER wave-filtered OLR, starting from lead-time 24 days to the onset where the heatwave was first significantly predicted. It is apparent that at lead-time 17 and 10 days to the onset, the forecast of the ER wave activity over Burkina Faso was less accurate than at other lead-times. While the entire country was under the influence of a convectively suppressed phase of the ER wave during the heatwave period, at lead-times 17 and 10 days, the model was predicting a convectively enhanced phase across at least half of the country. Therefore it can be said that the wrong forecast of the physical driver also led to a less accurate forecast of the heatwave itself, with the reverse being true.

Previous studies have already highlighted similar cases where the misrepresentation of subseasonal variability by models also caused misses in heatwave forecasts (e.g. QI and YANG 2019; Hsu et al. 2020). As a result, improving the skill of prediction of tropical modes in models could also be beneficial for heatwave prediction in the Sahel as well as in other regions.

4.4. Conclusion

The ECMWF ENS extended-range forecasting system shows significant skill for heatwave prediction across most parts of the Sahel in the first two to three weeks of the forecast. The AMJ season has a longer lead-time predictability than the FM season, likewise nighttime heatwaves are better predicted at longer lead-times than their daytime counterparts. This study has also demonstrated that atmospheric tropical modes of variability, mostly the MJO and ER waves, are effective sources of skill for heatwave prediction in the Sahel. The forecast skill is indeed higher when they are active in the region than when they are weak. The case study of the prediction of a heatwave event driven by tropical modes in 2015 over Burkina Faso further illustrated this, by showing that the forecasts of heatwaves are more skilful when that of the tropical modes are accurate. Information on the predicted activity of tropical modes can thus be useful to forecasters in their heatwave warnings.

In addition, as already highlighted by Guigma et al. (2020b), a more accurate simulation of tropical modes will have a positive repercussion on heatwave prediction in the region. This will likely improve the current skill and extend it to longer lead-times, thus winning more time and precision for preparedness actions. In this context and given the connection between convection and tropical

modes, convection-permitting models can play an important role as they reduce model errors, and likely offer a better representation of tropical modes (Judt 2020). It has indeed been shown that the parameterisation of moist convective processes and their links to the large-scale flow is an important source of errors in the tropics (Dias et al. 2018).

But even with the current level of predictability, there is a potential for HEWSs. With a predictability of two to three weeks, there is indeed a range of actions that can be triggered in advance (e.g. Matthies and Menne 2009; Lowe et al. 2016; Nissan et al. 2017). As evidenced in other regions of the globe, many socio-economic sectors (especially public health) can benefit from such systems (e.g. Knowlton et al. 2014). The scaling up of HEWSs actually emerges as a pressing necessity given the future projections of global warming (Xu et al. 2020; Raymond et al. 2020) and could therefore serve as an efficient tool to mitigate its adverse effects. Furthermore, since the predictability is extendible when the verification criteria are relaxed, low-cost preparedness actions can be taken at even longer lead-times, following the "Red-Set-Go!" approach of the Red Cross.

However to get the best of such systems, it is important to have a clear understanding of how the heat hazard affects populations (e.g. WMO N°1142; Casanueva et al. 2019). This includes identifying the most affected social groups, the most lethal heat thresholds, the most relevant thermal indices, the most recurrent heat-related illnesses in the region etc. Such a research area is still in its infancy in the Sahel and should therefore receive more attention now that the potential for anticipatory action is evidenced. Furthermore the investigations can extend to other sectors like energy and water management which are heat-sensitive in this semi-arid region. This will allow a holistic approach to the heat issue and contribute to save many lives and protect livelihoods in the Sahel.

Acknowledgements

Two anonymous reviewers helped to improve the manuscript through insightful comments. KHG was supported by the Peter Carpenter Scholarship for African Climate Science at the University of Sussex, UK. Further support was provided through the (i) UK NERC/ESRC/DfID Science for Humanitarian Emergencies and Resilience (SHEAR) consortium project 'Towards Forecast-based Preparedness Action' (ForPAc, www.forpac.org), grant number NE/P000673/1 and (ii) Future Climate for Africa (FCFA) regional consortium project 'AMMA-2050', grant number NE/M02024X/1.

Data availability statement

The verification data are freely available at the following repositories:

ERA5: https://cds.climate.copernicus.eu/cdsapp#!/home

BEST: http://berkeleyearth.org/data-new/

The hindcast data are freely available to ECMWF member states at the following address: https://www.ecmwf.int/en/forecasts/accessing-forecasts.

Supplemental materials

This supplement to the article provides additional results.

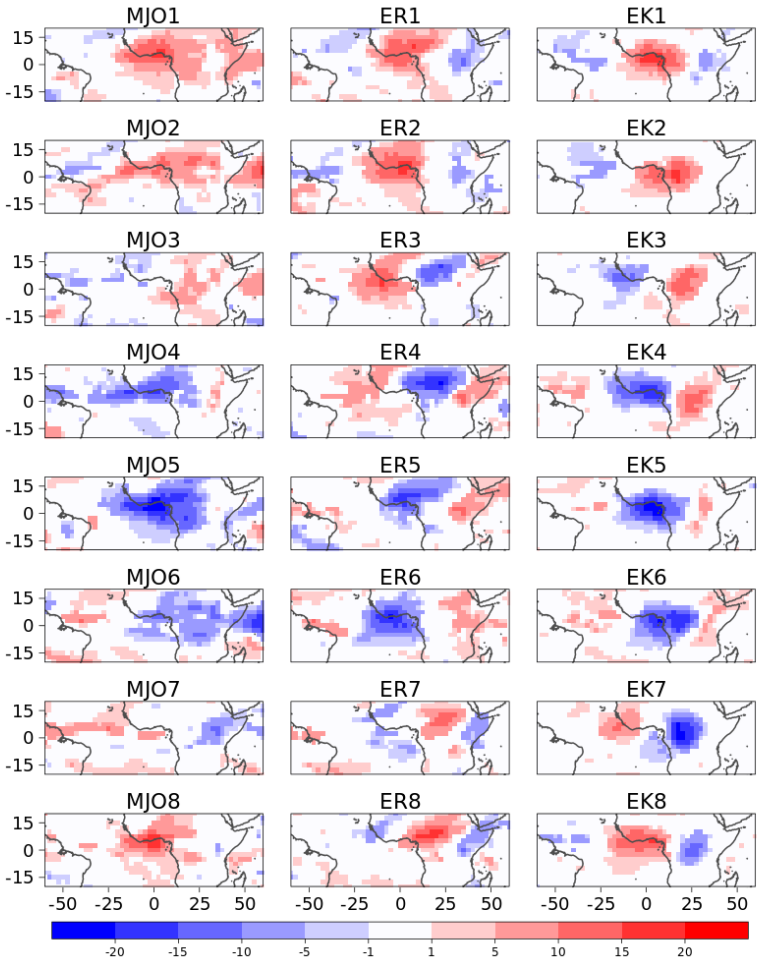

Fig. S4.1 Composite of ERA5 OLR anomalies against each active phase of the MJO (left panels), the ER (middle panels) and the EK waves (right panels) detected at the reference longitude of 5°E. White areas are not significant at the 95% probability level.

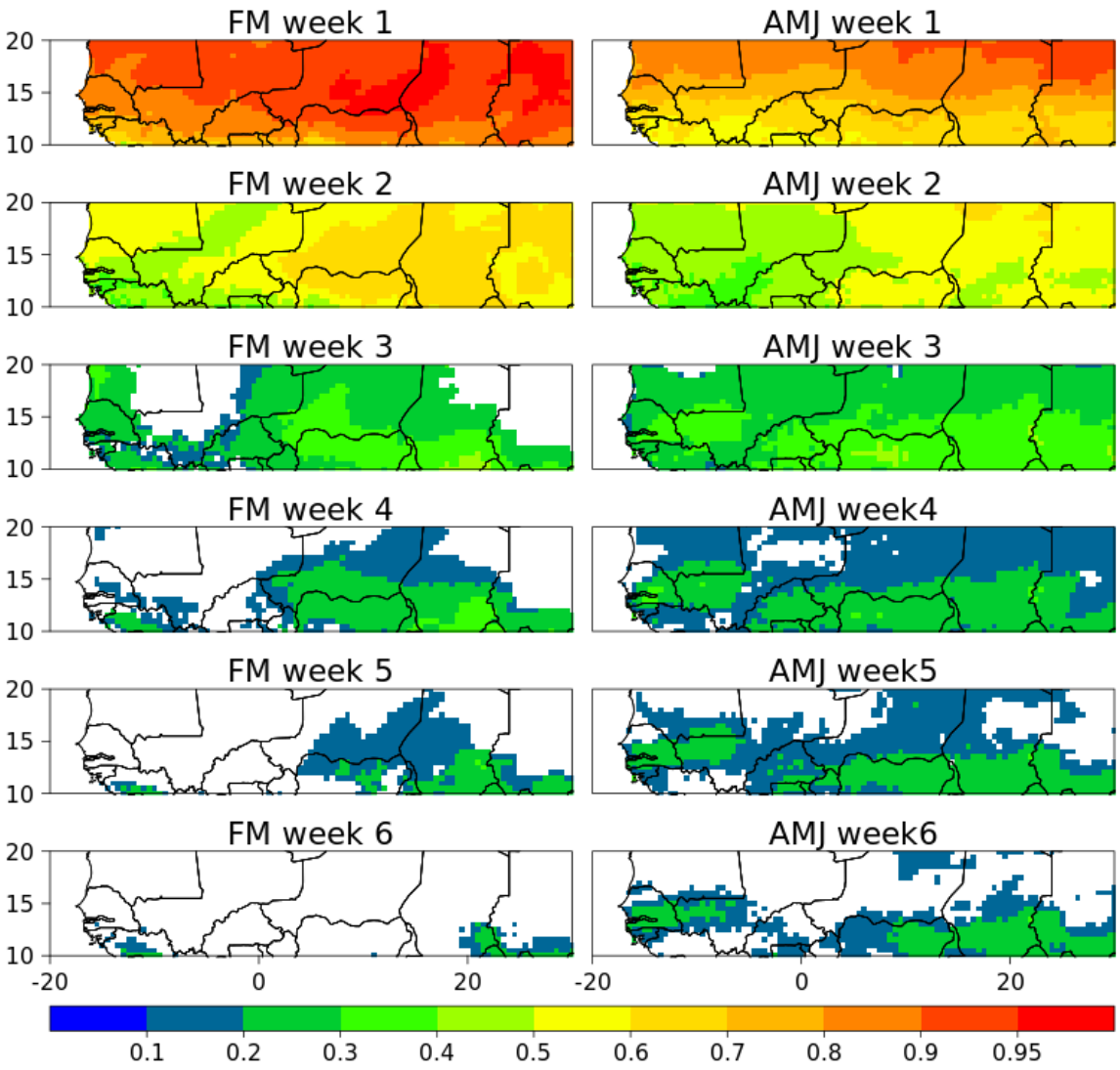

Fig. S4.2 Anomaly correlation coefficients of T-day. Each panel represents a specific week of the forecast with the first week at the top. White areas over land are not significant at the 95% probability level.

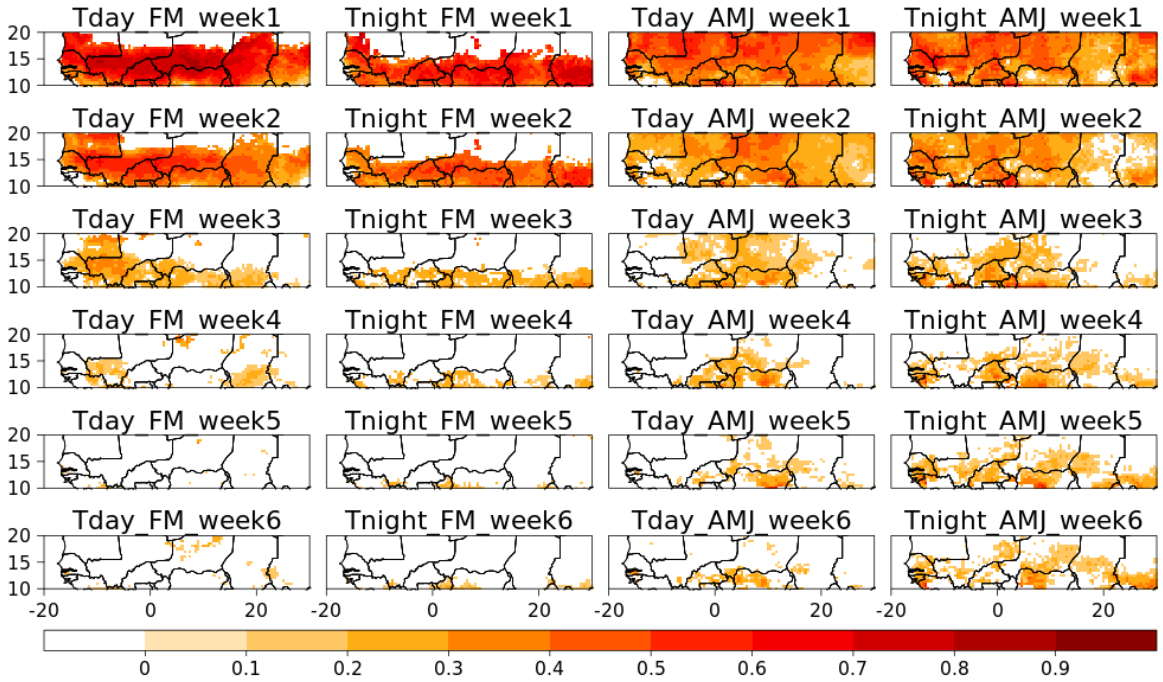

Fig. S4.3 SEDI scores in the (two leftmost panels) FM and (two rightmost panels) AMJ seasons for T-day and T-night heatwaves using BEST as reference dataset. Each panel represents a specific week of the forecast with the first week at the top panel. White areas are not significant at the 95% probability level.

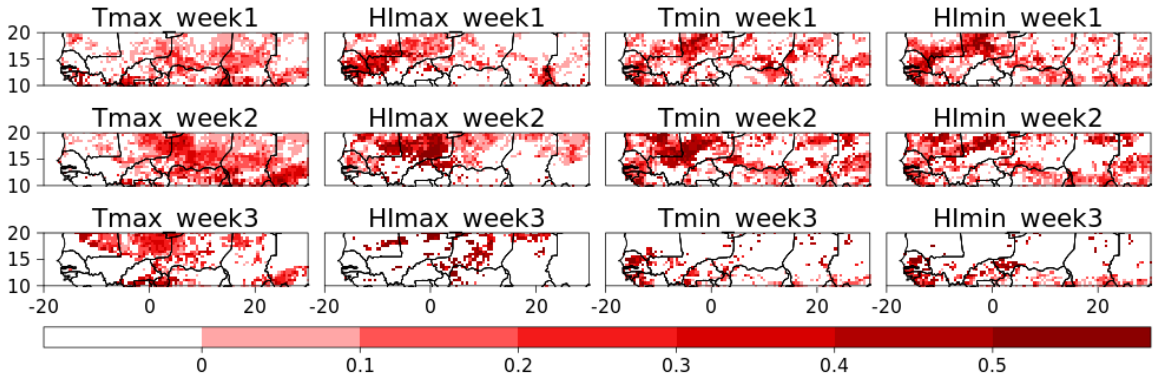

Fig. S4.4 Difference of SEDI scores between forecasts falling on active phase 3 versus inactive phase of the MJO. The significance of the SEDI differences is tested by bootstrap resampling (see Section 4.2.5.2).

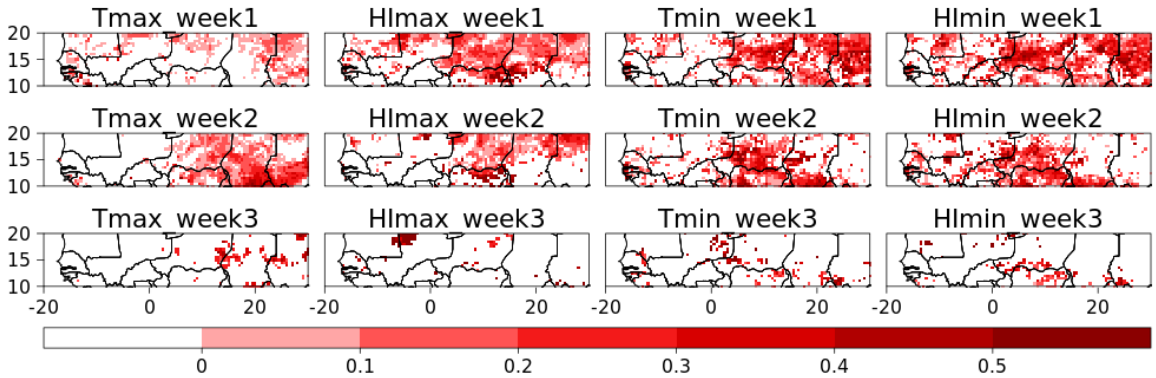

Fig. S4.5 Difference of SEDI scores between forecasts falling on active phase 7 versus inactive phase of the ER wave. The significance of the SEDI differences is tested by bootstrap resampling (see Section 4.2.5.2).

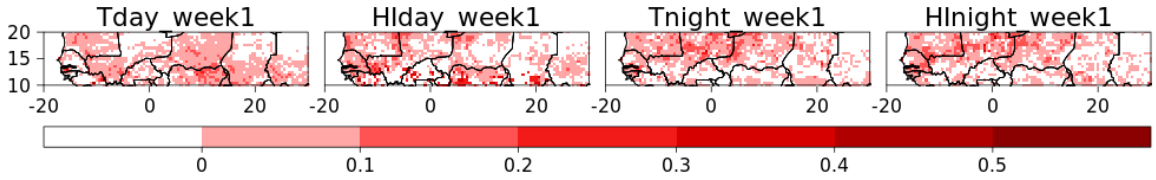

Fig. S4.6 Same as Fig. 4.6 but for the EK wave and for the first two weeks of the forecast.

Chapter 5. Conclusion

This thesis has advanced knowledge on the physical science of heatwaves in the Sahel. The focus was on weather and intraseasonal scales which have been overlooked by previous research although being crucial for risk management. This piece of work was built on three specific areas of climate research namely the nature, drivers and predictability of heatwaves at the aforementioned timescales. Each of these areas has been explored in a scientific paper in order to reach a wide community of scientists and stakeholders. These papers contain important new findings that are summarised below.

5.1. What is now known about Sahelian heatwaves thanks to this thesis?

Characteristics and underlying thermodynamic processes

In the first paper (characteristics and thermodynamics of Sahelian heatwaves analysed using various thermal indices), the key objectives were to evaluate the statistical characteristics of Sahelian heatwaves and explore the thermodynamic processes that shape them. To achieve this, a fundamental task consisted of defining heatwaves which arise as a result of the intraseasonal variability of the Sahelian atmosphere while being also potentially harmful to people. For this reason two magnitude thresholds were used. The first one seeks to identify days where the temperature at a given location is absolutely hot irrespectively of the period of the year. It has been defined as the 75^{th} percentile of the total distribution of thermal indices. The second magnitude threshold, seeking to identify relatively hot events that result from the variability at the intraseasonal scale, is defined as the 90^{th} percentile of the calendar day distribution of 90-day highpass filtered anomalies of the thermal indices. Five thermal indices were used, accounting for different ways to measure the heat load (through combining different environmental variables), and for each of them, the daytime and nighttime components were analysed separately. The results show that, overall, heatwaves in the Sahel are relatively short-lasting (mean duration of three to five days) and with a low frequency of occurrence (less than two events a year). However, with the absolute magnitude constraint (75^{th} percentile of the total distribution), the sampled events are of high magnitude, given that the region itself has a hot climate. From a spatial point of view, heatwaves are slightly longer lasting and more frequent over the eastern and central Sahel than in the western Sahel. Likewise daytime heatwaves also have longer duration and higher frequency than their nighttime counterparts. These statistics are relatively similar across the different thermal indices. However, an analysis of the simultaneity of heatwave events revealed that the thermal indices do not sample the same heatwave events. There is on average less than 50% chance that a heatwave detected by a given index be also captured by

another index. This low coincidence is explained by the parameterisation of the indices but also by the constraints of heatwave definition (magnitude and duration thresholds). Furthermore, it has been found that the concomitance of nighttime and daytime heatwave events is a relatively rare situation in the Sahel. The analysis revealed indeed that only around 10% of daytime heatwaves persist at night. To assess the thermodynamics at play during Sahelian heatwave events, high-pass filtering of diverse physical variables was performed as the focus is on the intraseasonal modulation. The results show that the asynchronicity between daytime and nighttime heatwave events chiefly owes to different underlying processes. Thus, the nighttime heatwaves are mainly the result of a greenhouse effect of water vapour that prevents the temperature from dropping at night. On the other hand, the daytime heatwaves are often caused by heat advection from hotter regions (e.g. hot air advected from the hinterland towards the western coast causes heatwave events in the western Sahel) as well as sensible heat flux from the ground and increased downward solar radiation (on days where cloudiness decreases significantly). For a given diurnal period and from an index to another, the identified processes may slightly change or be of different magnitudes, but overall the leading thermodynamics remain similar across the indices (as opposed to the low co-occurrence of their heatwave samples). The analysis of the low-level circulation during heatwaves as well as moisture distribution revealed large-scale anomalies that involved the whole Northern Africa domain. Large heatwave events are indeed associated with harmattan reinforcement or monsoon surges depending on the affected region. Moreover, significant convection and rainfall anomalies are especially detected in the Guinean region of West Africa where the monsoon is at its peak during the spring season. This came in support of previously published papers which implicitly suggested a possible connection between thermal conditions in the Sahel and convection in the Gulf of Guinea region. This also oriented the investigation of large-scale drivers of Sahelian heatwaves toward the drivers of Guinean convection.

Large-scale drivers: importance of tropical modes of variability

Since the timescale of interest in this thesis is the intraseasonal scale, the connection between convection in the Guinean region of West Africa and heatwaves in the Sahel is assessed using the intraseasonal drivers of this convection as a proxy for it. The investigated drivers are the tropical modes of variability including the MJO, ER and EK waves. They were detected from the intraseasonal anomalies of OLR, a proxy for convection. Using a method initially developed by Riley et al. (2011), the magnitude and phase of their local activity were evaluated. The results showed that from a statistical point of view, heatwaves in the Sahel are indeed significantly modulated by the tropical modes of variability. They can lead, depending on their convective phase and the Sahelian subregion

under consideration, to a decrease or an increase of the likelihood of heatwaves. Among the analysed modes, the MJO proved to be the most important driver of heatwaves. This is explained by its longer periodicity and smaller wavenumbers that allows it to maintain slowly varying atmospheric conditions for a sustained period of time over relatively large areas. During its active phases, Sahelian heatwaves can be twice more likely than usual in the region. The ER and EK waves are also found to be significant to heatwave occurrence in the region, although with notably less importance than the MJO. In addition, it is common to have many of these modes overlapping over the region. The outcome of such instances in terms of heatwave occurrence is ultimately a function of the nature and intensity of the overlapping modes as well as their respective convective phases. Unlike on the frequency of occurrence, tropical modes have a limited effect on heatwave intensity. The mechanisms through which this modulation takes place are linked to the underlying thermodynamic causes of Sahelian heatwaves identified in the first paper. Tropical modes exert a control on large-scale circulations in the region, allowing them to also control the transport and distribution of heat and moisture. For example, on their convectively enhanced phases, they advect moisture in the eastern Sahel, favouring (mostly) nighttime heatwaves therein whereas the western Sahel is cooled off (with then less chance for heatwave occurrence) by the arrival air masses from northern latitudes. A case study of a two-week duration heatwave event in April 2003 over the Sahel was conducted to further emphasize the role played by tropical modes on Sahelian heatwaves. The event was initiated by the MJO, which, through sustainably suppressing convection, allowed heat advection towards the northeasternmost parts of Sahel. The warming was maintained thanks to the arrival of a convectively enhanced ER wave which brought in moisture, creating a greenhouse effect. This longwave warming was reinforced when the convectively enhanced phase of the MJO reached the region before a cessation of the heatwave caused by the rainy events that followed, due to the intensification of convection. Therefore in the second paper it has been established that tropical modes of variability, namely the MJO, ER and EK waves are important to Sahelian heatwaves. This comes in support of other drivers that were suggested by the literature, notably the mid-latitude weather systems whose intrusions into the tropics also lead to hot weather events in the Sahel. Unlike the mid-latitude drivers which are active mainly at the synoptic scale, the MJO, ER and EK waves are intraseasonal modes of variability. As such, they also present the potential to provide heatwave predictability at the intraseasonal scale which is a relevant timeframe for heat risk management. Heatwave predictability and potential role of tropical modes are the object of the third research paper of this thesis.

Skill of Sahelian heatwave prediction

The predictability of heatwaves in the Sahel has been assessed at weather and intraseasonal scale (out to forecast day 46) using ENS-ext. The predictions of ENS-ext were verified against its own analysis i.e. ERA5 and the Berkeley Earth Surface Temperature (BEST) dataset. Considering the asynchronicity of heatwaves defined from different thermal indices (in the first paper), the eventuality of an index-sensitive predictability was accounted for by considering two distinct thermal indices, temperature (T) and the heat index (HI, which adds moisture effect). Daytime and nighttime heatwave prediction skills were also assessed separately since they are not concomitant, and, most importantly, are driven by different thermodynamic processes. The results show that in the Sahel, heatwave prediction has a significant skill out to lead-week two to three and is extendible to subsequent weeks when the verification is conducted with flexibility. There is a marked seasonality with heatwaves having a longer predictability in the pre-monsoon AMJ season than in the FM season. However, for the first week of the forecast, the FM season heatwaves show higher skill than their AMJ counterparts. It has also been shown that, at long lead-times, heatwaves are more predictable at nighttime than at daytime. Regarding the sensitivity to the thermal indices, the nighttime component of HI offers the longest predictability of all analysed indices whereas its daytime component has limited skill. The importance of tropical modes (which were found in the second paper to be important drivers of heatwaves) as sources of predictability has also been assessed in the AMJ season, since it is in this season that they are the most active in the region. For this, the skill of ENS-ext in predicting their local activity was first analysed. It was found that the model shows fairly good skill in predicting the MJO and ER wave out to the third week of forecast, whereas this is limited to the first week for the EK wave. Then, the observed modulation of Sahelian heatwave frequency by tropical modes has also been found to be well simulated by the model. Finally a regime-dependent analysis was conducted to determine whether tropical modes indeed provide skill to heatwave prediction. This was done through stratifying the ENS-ext forecasts into instances where the forecast tropical modes are active versus instances where they are inactive. The results show that active phases of tropical modes are associated with higher heatwave prediction skill than inactive phases. By mode, the MJO is the most important source of predictability, followed by the ER wave. Their contribution to the skill of heatwave prediction extends out to the third week of the forecast and covers much of the Sahel. The EK wave also enhances the prediction skill during its active phases, but this is restricted mostly to the first week of the forecast. The main reason for the lower skill associated with the EK wave is the lesser ability of the model to predict it, inherent to the shorter periodicity of this wave. As a consequence, a better representation of tropical mode activity by numerical models will help improve the skill of heatwave prediction. The analysis of the evolution of the prediction skill with lead-time of a major heatwave event in 2015 further confirmed this potential for improvement. The heatwave itself was driven

primarily by the ER wave. At lead-times for which ENS-ext was able to correctly forecast the activity of the ER wave, it was also able to give a good forecast of the heatwave event. On the other event, at lead-times for which the model struggled to capture the activity of the ER wave, it was neither able to give a skilful forecast of the heatwave.

5.2. What are the implications for operational management of heatwave risk in the Sahel?

In addition to their contribution to the purely scientific knowledge, the findings of this thesis are also of interest for heatwave risk management.

Thus, the low concomitance between daytime and nighttime heatwaves is a significant relief for Sahelian populations in terms of health. Previous research has indeed demonstrated that such concomitance exacerbates human discomfort, causing high morbidity and mortality (e.g. Schär 2016; Murage et al. 2017; Mukherjee and Mishra 2018). Therefore, most heat-related actions in the Sahel will address either a daytime or a nighttime event and are thus likely less costly. Besides, even though some heatwave events can last up to two weeks, the average duration is generally below six days. As compared to other regions of the globe, this is another attenuating factor for heatwave risk in the Sahel. Short-lived heatwaves doubtlessly harm less than if they last longer. For risk managers, this also means that their action can be focused on a relatively short period of time and be more efficient. For example, during heatwaves, various mitigation actions including public awareness campaigns, increasing access to water and setting-up of cooling centres are recommended by humanitarian organisations such as the Red Cross Climate Centre[2]. The sustainability of these actions for a prolonged time in low-income countries, like those of the Sahel, could be problematic. With the relatively short duration of heatwaves however, they become more conceivable, such that maximum assistance is made available over a couple of days to relieve the most vulnerable people. This perspective is also more likely to motivate governments and organisations in the region to invest in HEWSs.

The low coincidence of heatwaves detected from different thermal indices also has implications for risk management. It suggests that an HEWS should priorly make clear which socio-economic group(s) are on target. This targeting should be carefully undertaken, taking into account the exposure

[2] Red Cross Red Crescent Climate Centre (2019). Heatwave guide for cities. Retrieved from https://www.climatecentre.org/downloads/files/IFRCGeneva/RCCC%20Heatwave%20Guide%202019%20A4%20RR%20ONLINE%20copy.pdf

and vulnerability aspects. It should consider various aspects such as professional activity, geographic location, age and gender, housing facilities etc. Once this is done, the thermal index (es) for heatwave detection should be chosen accordingly in order to ensure capturing the actual heat threat for the identified groups. It could be relevant for a HEWS to utilise many different thermal indices if it intends to reach distinct groups.

The fact that tropical modes drive heatwave occurrences in the Sahel is especially interesting for operational forecasters in the region. In a HEWS, they will be in charge of issuing the alerts which different stakeholders will act upon. The monitoring of tropical modes activity can therefore be an additional tool to assist in that regard. For this, they can make use of the forecasts of tropical modes activity out to a month ahead, which are generated and freely distributed by institutions such as the North Carolina Institute for Climate Studies (https://ncics.org/portfolio/monitor/mjo/). Strong events of tropical mode passages will help provide more confidence to their forecasts. They can even further their expertise by characterising the local specificities of the modulation of heatwaves by the modes in the area covered by their alerts. Taking into account the extratropical drivers as well, they will be able to develop empirical heatwave forecasting schemes to guide them in their daily tasks. Evaluating and communicating these schemes to researchers will eventually lead to more progress in the scientific understanding of Sahelian heatwaves, especially at the local scale.

The prediction skill, as highlighted in the third research paper, evidences more tangibly the potential for heatwave preparedness action. With similar prediction skill, i.e. two to three week predictability, other regions have set up their HEWSs, proving that such systems are also possible in the Sahel. In the joint WMO-WHO guidance on heat-health warning systems (WMO N°1142), it is indicated that subseasonal forecasts are relevant for such systems as it allows an optimisation of financial, logistic and human resource management, as well as being convenient for public awareness-raising activities. Furthermore the “Ready-Set-Go!” approach of the Red Cross introduced in the third paper can well be implemented in the Sahel at long lead-time. With information on the possible occurrence of a heatwave one month before for example, and even without precision on the exact days that will be affected, several general and relatively inexpensive actions can already be triggered. They will eventually be reinforced by more decisive actions as the certainty improves closer to the heatwave. This also calls for the development of more probabilistic multi-week heat-related forecasts by global and regional meteorological centres. With the continual improvement of the representation of tropical modes in models (e.g. Hirons et al. 2013), these multi-week forecasts are expected to improve (it was shown in the third paper that a good representation of tropical modes also leads to good skills of

heatwave prediction). Of particular use will be the forecasts of different thermal indices, to account for the hazard posed to different socio-economic groups. From these forecasts, meteorological services at national and subnational levels will be able to use their expertise to develop tailored products for their areas. These products can include clear and concise indications of the likelihood of the occurrence of extreme heat conditions for targeted socio-economic groups, taking care to specify the affected administrative domains and the expected severity. Co-producing them with other experts and institutions involved in the heat risk management will also guarantee more practical usability to these products. Such efforts are expected to significantly relieve Sahelian populations from the heatwave threat. However there is still more to find about heatwaves and their effects in the Sahel.

5.3. What still needs to be addressed by future work?

This thesis leaves open many research gaps that need to be addressed by future works in order to advance knowledge on Sahelian heatwaves. These gaps concern the physical science of heatwaves but also their impacts on different socio-economic sectors.

Future projections in relation to convection and thermal indices

The thesis has established a link between convection variability and heatwaves in the Sahel at the weather and intraseasonal scales. As a result, future projections of convection in the region also have profound implications for future heatwaves. With global warming, an increase of precipitation is expected in much of West Africa (although with large uncertainty given contradictions between models) owing to an intensification of convection at all timescales (Berthou et al. 2019; Dosio et al. 2019; Akinsanola et al. 2020). The explicit link between this increased convection and extreme heat events in the Sahel should thus be addressed, taking into account the relative uncertainty around future convection. In addition, with global warming, atmospheric moisture increases (Clausius-Clapeyron equation) and should therefore impact some thermal indices which have been investigated in this study. Consequently, the future behaviour of heatwaves in the Sahel may also differ depending on which thermal indices (considering the diurnal cycle as well) are used for the projections. This is an important point to investigate as it also relates to how different socio-economic groups will be affected.

Interaction between extratropical Rossby waves and tropical modes

Extratropical weather systems have been suggested by previous studies (Fontaine et al. 2013) as drivers of Sahelian heatwaves and Largeron et al. (2020) identified them as the main large-scale factor

behind the April 2010 nighttime heatwave. However, there has been so far no systematic analysis of their role on the occurrence of heatwaves in the Sahel. There is thus a need to conduct a characterisation study to identify the statistics of this modulation, and a dynamic analysis to understand the mechanisms through which it takes place. A comparative study between the modulation by tropical modes and that of extratropical weather systems is also relevant to determine which is the most important. Furthermore, it will be interesting to investigate the interactions between these two drivers. Their timescales of activity often overlap and previous studies have already shown that they often interact in West Africa (Chauvin et al. 2010; Roehrig et al. 2011; Hall et al. 2017). However, these studies only cover the boreal summer as the interest is generally on the impact on rainfall. It is therefore important to extend them to the FM and AMJ seasons to assess how these interactions contribute to the modulation of Sahelian heatwave occurrence.

Heat-health research

For an effective management of heatwave risk, major efforts should be made to understand how they affect populations. In the Sahel, the social and economic impacts have been largely overlooked with only scare papers on the topic (Diboulo et al. 2012). One potential reason for this, as suggested by (Harrington and Otto 2020) is the lack of reports of heatwave casualties. Therefore the first step towards understanding the effects of heatwaves in the region could be the establishment of a database of heat-related casualties. Public health organisations in the Sahel can encourage systematic recording of consultations, hospital admissions and mortality that may be related to the heat. This necessitates an awareness-raising among health practitioners and demographers. In addition, given the fragility of health systems (Adair et al. 2020), it is important to associate community leaders and local administrations to promote death notifications. The gathering of such statistics will favour the setting up of solid databases that can be used not only for heatwave studies but also for other socio-economic analyses.

In terms of health studies, several elements can be considered. The first is to analyse whether heatwaves indeed pose specific health issues to populations. Hot conditions prevail most of the year, and it may be the case that, by acclimatisation, heatwaves do not threaten the Sahelians as much as in mid-latitude regions. Likewise, the very concept of heatwaves may not be relevant in the region. With daytime temperatures regularly above 40C in spring, it may be the case that short periods of time where they exceed these values (the mean duration is generally less than six days) do not have pronounced impacts. Rather, the seasonal mean heat load could be more significant in terms of health.

These are relevant questions to address before setting to scale up early warning systems. Profound investigations are thus necessary to elucidate these unknown aspects of heatwaves in the Sahel.

In the instance where heatwaves are found to significantly cause health issues in the region, it will be interesting to characterise this impact. For example, thermal thresholds are key factors in HEWS. In this study, they were arbitrarily set, but for an efficient operational system, they should be associated with an important health landmark. Across many countries that have functioning HEWSs, the thresholds are generally defined based on death rates, the reason being that mortality data are generally the most collected and standardised of all health metrics (WMO N°1142). However, it is also relevant to take into account hospital admissions or morbidity data in order to determine different thresholds accounting for different levels of severity.

The setting-up of thresholds should go along with the identification of vulnerable groups as well as the pathologies that are the most recurrent during heatwaves. Diboulo et al. (2012) found that the mortality of under-five children is strongly affected by extreme heat at short-term (lag 0-1 day) in Nouna, western Burkina Faso. However these results are based on 10-year data from a single health centre. There is thus a need to extend that to other health districts across the Sahel for a statistically meaningful generalisation. Furthermore, establishing a list of heat-related pathologies (including diseases that are aggravated by the heat) in the region is very helpful when it comes to alerting health professionals of heatwave risks. They would in that case be forewarned about potential changes in causes and numbers of consultations and thus prepare to provide an adequate response. Another benefit is that people susceptible to be affected by these diseases can also be forewarned when heatwaves are imminent, stimulating preventive actions among them. Given that the measure of heat itself is important as underlined in the first paper, it is relevant that all these studies play with different thermal indices in a logic to determine for each pathology the index (es) with the strongest sensitivity.

Impact on water and energy

Apart from health, many other socio-economic sectors could be affected by heatwaves and future studies should assess these impacts as well. In terms of energy for example, there is preliminary evidence that, at the interannual level, the trends of power consumption match that of extreme heat in some of the largest Sahelian cities (Aissatou et al. 2017). It is thus plausible that at the intraseasonal level, extreme heat events put substantial pressure on energy demand in the region. The same strain is also observable on water demand and extreme heat is often pointed as one of the major causes of

power and water shortages which have multiplied and become longer lasting in recent years[3]. It is thus important that future research addresses the actual impact of heatwaves on the water and energy sectors for a better management. These studies should also account for the predicted worsening of heatwaves in future decades such that mitigation actions be taken. It should however be noted that heatwaves may also have positive impacts on energy. The Sahel is known for its important potential for solar energy (e.g. Azoumah et al. 2010), and, as shown throughout the three papers of the thesis, some heatwaves are associated with a decrease of cloudiness and an increase of incoming radiation. As such, promoting the use of solar energy can be a good mitigation strategy. This "green" energy can indeed be used to cool off households without negative impacts on the environment and climate, as opposed to conventional sources of energy. The practical feasibility however requires more in depth studies.

Impact on labour productivity

Labour productivity in a range of important sectors of the Sahelian economy such as street selling, market gardening and agriculture, construction and mining industry can also be affected by heatwaves. In many regions, the impact of heat on these sectors is often assessed by quantifying the equivalent economic losses. For example, Watts et al. (2018) estimated that, at the global level, 153 billion hours of labour were lost in 2017 because of heat. Conducting similar studies in Sahelian countries at local levels (e.g. in major cities) will therefore draw attention to the negative impact of heatwaves on the economy and could convince different actors to invest in mitigating them.

Once the impact of heatwaves on all these sectors will be quantified, it will be possible to move toward heat impact-based forecasting which will add substantial value to the HEWS.

[3] http://amediaagency.com/burkina-faso-drought-triggers-water-and-power-shortages/

References

Adair T, Rajasekhar M, Bo KS, et al (2020) Where there is no hospital: improving the notification of community deaths. BMC Med 18:. https://doi.org/10.1186/s12916-020-01524-x

Adames, Á. F., D. Kim, A. H. Sobel, A. D. Genio, and J. Wu, 2017: Characterization of Moist Processes Associated With Changes in the Propagation of the MJO With Increasing CO2. Journal of Advances in Modeling Earth Systems, 9, 2946–2967, https://doi.org/10.1002/2017MS001040.

Adeniyi MO, Oyekola SO (2017) Assessment of heat and cold wave events over West Africa using three regional climate models. Ann Geophys 60:0322. https://doi.org/10.4401/ag-7039

AIRS Science Team/Joao Teixeira (2013), AIRS/Aqua L3 Daily Standard Physical Retrieval (AIRS-only) 1 degree x 1 degree V006, Greenbelt, MD, USA, Goddard Earth Sciences Data and Information Services Center (GES DISC). doi:10.5067/Aqua/AIRS/DATA303

Aissatou N, Rabani A, Moussa G, Arona D (2017) Global Warming and Heat Waves in West-Africa: Impacts on Electricity Consumption in Dakar (Senegal) and Niamey (Niger). International Journal of Energy and Environmental Science 2:16. https://doi.org/10.11648/j.ijees.20170201.13

Akinsanola AA, Zhou W, Zhou T, Keenlyside N (2020) Amplification of synoptic to annual variability of West African summer monsoon rainfall under global warming. npj Climate and Atmospheric Science 3:1–10. https://doi.org/10.1038/s41612-020-0125-1

Alamirew NK, Todd MC, Ryder CL et al (2018) The early summertime Saharan heat low: sensitivity of the radiation budget and atmospheric heating to water vapour and dust aerosol. Atmos Chem Phys 18:1241–1262

Anderberg MR (1973) Cluster analysis for applications. Academic Press, New York

Anderson GB, Dominici F, Wang Y, et al (2013) Heat-related Emergency Hospitalizations for Respiratory Diseases in the Medicare Population. Am J Respir Crit Care Med 187:1098–1103. https://doi.org/10.1164/rccm.201211-1969OC

Añel JA, Fernández-González M, Labandeira X et al (2017) Impact of cold waves and heat waves on the energy production sector. Atmosphere 8:209. https://doi.org/10.3390/atmos8110209

Arbuthnott KG, Hajat S (2017) The health effects of hotter summers and heat waves in the population of the United Kingdom: a review of the evidence. Environ Health 16:119. https://doi. org/10.1186/s12940-017-0322-5

Ardö, J., 2013: A 10-Year Dataset of Basic Meteorology and Soil Properties in Central Sudan. Dataset Papers in Geosciences, 2013, e297973, https://doi.org/10.7167/2013/297973.

Arkin PA, Ardanuy PE (1989) Estimating Climatic-Scale Precipitation from Space: A Review. J

Climate 2:1229–1238. https://doi.org/10.1175/1520-0442(1989)002<1229:ECSPFS>2.0.CO;2

Azoumah Y, Ramdé EW, Tapsoba G, Thiam S (2010) Siting guidelines for concentrating solar power plants in the Sahel: Case study of Burkina Faso. Solar Energy 84:1545–1553. https://doi.org/10.1016/j.solener.2010.05.019

Balarabe MK, Sahin M (2020) Metaspace, mobility and resistance: understanding vendors' movement pattern as a resistive strategy in Kano, Nigeria. J Asian Afr Stud. https://doi.org/10.1177/00219 09620905055

Barbier, J., F. Guichard, D. Bouniol, F. Couvreux, and R. Roehrig, 2018: Detection of Intraseasonal Large-Scale Heat Waves: Characteristics and Historical Trends during the Sahelian Spring. J. Climate, 31, 61–80, https://doi.org/10.1175/JCLI-D-17-0244.1.

Barriopedro D, Fischer EM, Luterbacher J et al (2011) The hot summer of 2010: redrawing the temperature record map of Europe. Science 332:220–224. https://doi.org/10.1126/science.1201224

Batté L, Ardilouze C, Déqué M (2018) Forecasting West African heat waves at subseasonal and seasonal time scales. Mon Weather Rev 146:889–907. https://doi.org/10.1175/MWR-D-17-0211.1

Batté, L., C. Ardilouze, and M. Déqué, 2018: Forecasting West African Heat Waves at Subseasonal and Seasonal Time Scales. Mon. Wea. Rev., 146, 889–907, https://doi.org/10.1175/MWR-D-17-0211.1.

Bazo, J., R. Singh, M. Destrooper, and E. Coughlan de Perez, 2019: Chapter 18 - Pilot Experiences in Using Seamless Forecasts for Early Action: The "Ready-Set-Go!" Approach in the Red Cross. Sub-Seasonal to Seasonal Prediction, A.W. Robertson and F. Vitart, Eds., Elsevier, 387–398.

Bengtsson L, Dias J, Gehne M, et al (2019) Convectively Coupled Equatorial Wave Simulations Using the ECMWF IFS and the NOAA GFS Cumulus Convection Schemes in the NOAA GFS Model. Mon Wea Rev 147:4005–4025. https://doi.org/10.1175/MWR-D-19-0195.1

Berhane, F., B. Zaitchik, and H. S. Badr, 2015: The Madden–Julian Oscillation's Influence on Spring Rainy Season Precipitation over Equatorial West Africa. J. Climate, 28, 8653–8672, https://doi.org/10.1175/JCLI-D-14-00510.1.

Berman A, Horovitz T, Kaim M, Gacitua H (2016) A comparison of THI indices leads to a sensible heat-based heat stress index for shaded cattle that aligns temperature and humidity stress. Int J Biometeorol 60:1453–1462. https://doi.org/10.1007/s0048 4-016-1136-9

Berthou S, Kendon EJ, Rowell DP, et al (2019) Larger Future Intensification of Rainfall in the West

African Sahel in a Convection-Permitting Model. Geophysical Research Letters 46:13299–13307. https://doi.org/10.1029/2019GL083544

Black H (2010) When to Warn? Comparing heat indices to evaluate public health risks. Environ Health Perspect 118:A35

Blazejczyk K, Epstein Y, Jendritzky G, Staiger H, Tinz B (2012) Comparison of UTCI to selected thermal indices. Int J Biometeorol 56:515–535. https://doi.org/10.1007/s00484-011-0453-2

Borg M, Bi P, Nitschke M, et al (2017) The impact of daily temperature on renal disease incidence: an ecological study. Environ Health 16:. https://doi.org/10.1186/s12940-017-0331-4

Bourgeois, E., D. Bouniol, F. Couvreux, F. Guichard, J. H. Marsham, L. Garcia-Carreras, C. E. Birch, and D. J. Parker, 2018: Characteristics of mid-level clouds over West Africa. Quarterly Journal of the Royal Meteorological Society, 144, 426–442, https://doi.org/10.1002/qj.3215.

Bröde P, Fiala D, Błażejczyk K, Holmér I, Jendritzky G, Kampmann B, Tinz B, Havenith G (2012) Deriving the operational procedure for the Universal Thermal Climate Index (UTCI). Int J Biom-eteorol 56:481–494. https://doi.org/10.1007/s00484-011-0454-1

Burpee, R. W., 1972: The Origin and Structure of Easterly Waves in the Lower Troposphere of North Africa. Journal of the Atmospheric Sciences, 29, 77–90, https://doi.org/10.1175/1520-0469(1972)029<0077:TOASOE>2.0.CO;2.

Campbell S, Remenyi TA, White CJ, Johnston FH (2018) Heatwave and health impact research: a global review. Health Place 53:210–218. https://doi.org/10.1016/j.healthplace.2018.08.017

Casanueva, A., and Coauthors, 2019: Overview of Existing Heat-Health Warning Systems in Europe. Int J Environ Res Public Health, 16, https://doi.org/10.3390/ijerph16152657.

Ceccherini G, Russo S, Ameztoy I et al (2017) Heat waves in Africa 1981–2015, observations and reanalysis. Nat Hazards Earth Syst Sci 17:115–125. https://doi.org/10.5194/nhess-17-115-2017

Cerne SB, Vera CS, Liebmann B (2007) The nature of a heat wave in Eastern Argentina occurring during SALLJEX. Mon Weather Rev 135:1165–1174. https://doi.org/10.1175/MWR3306.1

Cerne, S. B., and C. S. Vera, 2011: Influence of the intraseasonal variability on heat waves in subtropical South America. Clim Dyn, 36, 2265–2277, https://doi.org/10.1007/s00382-010-0812-4.

Chapman L, Azevedo JA, Prieto-Lopez T (2013) Urban heat and critical infrastructure networks: a viewpoint. Urban Clim 3:7–12. https://doi.org/10.1016/j.uclim.2013.04.001

Charney JG (1975) Dynamics of deserts and drought in the Sahel. Quarterly Journal of the Royal Meteorological Society 101:193–202. https://doi.org/10.1002/qj.49710142802

Chauvin F, Roehrig R, Lafore J-P (2010) Intraseasonal Variability of the Saharan Heat Low and Its Link with Midlatitudes. J Climate 23:2544–2561. https://doi.org/10.1175/2010JCLI3093.1

Chen X, Li N, Liu J et al (2019) Global heat wave hazard considering humidity effects during the 21st century. Int J Environ Res Public Health. https://doi.org/10.3390/ijerph16091513

Cheng J, Xu Z, Bambrick H, et al (2018) Heatwave and elderly mortality: An evaluation of death burden and health costs considering short-term mortality displacement. Environment International 115:334–342. https://doi.org/10.1016/j.envint.2018.03.041

Cheng Y, Niu J, Gao N (2012) Thermal comfort models: a review and numerical investigation. Build Environ 47:13–22. https://doi. org/10.1016/j.buildenv.2011.05.011

Coates L, Haynes K, O'Brien J et al (2014) Exploring 167 years of vulnerability: an examination of extreme heat events in Australia 1844–2010. Environ Sci Policy 42:33–44. https://doi. org/10.1016/j.envsci.2014.05.003

Collins M, Knutti R, Arblaster J et al (2013) Long-term climate change: projections, commitments and irreversibility. Climate change 2013—the physical science basis: contribution of working group I to the fifth assessment report. Intergovernmental Panel on Climate Change, Geneva, pp 1029–1136

Cook KH (2008) The mysteries of Sahel droughts. Nature Geoscience 1:647–648. https://doi.org/10.1038/ngeo320

Cook MA, King CW, Davidson FT, Webber ME (2015) Assessing the impacts of droughts and heat waves at thermoelectric power plants in the United States using integrated regression, thermodynamic, and climate models. Energy Reports 1:193–203. https://doi.org/10.1016/j.egyr.2015.10.002

Copernicus Climate Change Service (C3S) (2017): ERA5: Fifth generation of ECMWF atmospheric reanalyses of the global climate. Copernicus Climate Change Service Climate Data Store (CDS). https://cds.climate.copernicus.eu/cdsapp#!/home

Coughlan de Perez, E., and Coauthors, 2016: Action-based flood forecasting for triggering humanitarian action. Hydrology and Earth System Sciences, 20, 3549–3560, https://doi.org/10.5194/hess-20-3549-2016.

Coughlan de Perez, E., B. van den Hurk, M. K. van Aalst, B. Jongman, T. Klose, and P. Suarez, 2015: Forecast-based financing: an approach for catalyzing humanitarian action based on extreme weather and climate forecasts. Natural Hazards and Earth System Sciences, 15, 895–904, https://doi.org/10.5194/nhess-15-895-2015.

Couvreux F, Guichard F, Bock O, Campistron B, Lafore J-P, Redel-sperger J-L (2010) Synoptic variability of the monsoon flux over West Africa prior to the onset. Q J R Meteorol Soc

136:159–173. https://doi.org/10.1002/qj.473

Cowan T, Purich A, Perkins S, et al (2014) More Frequent, Longer, and Hotter Heat Waves for Australia in the Twenty-First Century. J Climate 27:5851–5871. https://doi.org/10.1175/JCLI-D-14-00092.1

Cuxart J, Conangla L, Jiménez MA (2015) Evaluation of the surface energy budget equation with experimental data and the ECMWF model in the Ebro Valley. J Geophys Res Atmos 120:1008–1022. https://doi.org/10.1002/2014JD022296

Davidson, O., K. Halsnæs, S. Huq, M. Kok, B. Metz, Y. Sokona, and J. Verhagen, 2003: The development and climate nexus: the case of sub-Saharan Africa. Climate Policy, 3, S97–S113, https://doi.org/10.1016/j.clipol.2003.10.007.

Davis RE, Novicoff WM (2018) The Impact of Heat Waves on Emergency Department Admissions in Charlottesville, Virginia, U.S.A. Int J Environ Res Public Health 15:. https://doi.org/10.3390/ijerph15071436

de Andrade, F. M., C. A. S. Coelho, and I. F. A. Cavalcanti, 2019: Global precipitation hindcast quality assessment of the Subseasonal to Seasonal (S2S) prediction project models. Clim Dyn, 52, 5451–5475, https://doi.org/10.1007/s00382-018-4457-z.

de Freitas CR, Grigorieva EA (2015a) A comprehensive catalogue and classification of human thermal climate indices. Int J Biom-eteorol 59:109–120. https://doi.org/10.1007/s00484-014-0819-3

de Freitas CR, Grigorieva EA (2015b) Role of acclimatization in weather-related human mortality during the transition seasons of autumn and spring in a thermally extreme mid-latitude continental climate. Int J Environ Res Public Health 12:14974–14987. https://doi.org/10.3390/ijerph121214962

de Freitas CR, Grigorieva EA (2017) A comparison and appraisal of a comprehensive range of human thermal climate indices. Int J Biometeorol 61:487–512. https://doi.org/10.1007/s0048 4-016-1228-6

de Perez EC, van Aalst M, Bischiniotis K et al (2018) Global predictability of temperature extremes. Environ Res Lett 13:054017. https://doi.org/10.1088/1748-9326/aab94a

Dee DP, Uppala SM, Simmons AJ et al (2011) The ERA5nterim reanalysis: configuration and performance of the data assimilation system. Q J R Meteorol Soc 137:553–597. https://doi.org/10.1002/qj.828

Depietri Y, Welle T, Renaud FG (2013) Social vulnerability assessment of the Cologne urban area (Germany) to heat waves: links to ecosystem services. International Journal of Disaster Risk Reduction 6:98–117. https://doi.org/10.1016/j.ijdrr.2013.10.001

Déqué M, Calmanti S, Christensen OB, et al (2017) A multi-model climate response over tropical Africa at +2C. Climate Services 7:87–95. https://doi.org/10.1016/j.cliser.2016.06.002

Dezfuli, Amin (2017) Climate of Western and Central Equatorial Africa. Oxford University Press. https://doi.org/10.1093/acrefore/9780190228620.013.511

Dias, J., M. Gehne, G. N. Kiladis, N. Sakaeda, P. Bechtold, and T. Haiden, 2018: Equatorial Waves and the Skill of NCEP and ECMWF Numerical Weather Prediction Systems. Monthly Weather Review, 146, 1763–1784, https://doi.org/10.1175/MWR-D-17-0362.1.

Diboulo E, Sié A, Rocklöv J, et al (2012) Weather and mortality: a 10 year retrospective analysis of the Nouna Health and Demographic Surveillance System, Burkina Faso. Global Health Action 5:19078. https://doi.org/10.3402/gha.v5i0.19078

Diffenbaugh NS, Singh D, Mankin JS, et al (2017) Quantifying the influence of global warming on unprecedented extreme climate events. PNAS 114:4881–4886. https://doi.org/10.1073/pnas.1618082114

Doelling, D. R., Haney C. O., Scarino B. R., Gopalan A., and Bhatt R., 2016: Improvements to the Geostationary Visible Imager Ray-Matching Calibration Algorithm for CERES Edition 4. J. Atmos. Oceanic Technol., 33, 2679–2698, https://doi.org/10.1175/JTECH-D-16-0113.1.

Doelling, D. R., and Coauthors, 2013: Geostationary Enhanced Temporal Interpolation for CERES Flux Products. J. Atmos. Oceanic Technol., 30, 1072–1090, https://doi.org/10.1175/JTECH-D-12-00136.1.

Dore MHI (2005) Climate change and changes in global precipitation patterns: What do we know? Environment International 31:1167–1181. https://doi.org/10.1016/j.envint.2005.03.004

Dosio A (2017) Projection of temperature and heat waves for Africa with an ensemble of CORDEX Regional Climate Models. Clim Dyn 49:493–519. https://doi.org/10.1007/s00382-016-3355-5

Dosio A, Jones RG, Jack C, et al (2019) What can we know about future precipitation in Africa? Robustness, significance and added value of projections from a large ensemble of regional climate models. Clim Dyn 53:5833–5858. https://doi.org/10.1007/s00382-019-04900-3

Duchon CE (1979) Lanczos filtering in one and two dimensions. J Appl Meteor 18:1016–1022. https://doi.org/10.1175/1520-0450(1979)018<1016:LFIOAT>2.0.CO;2

Ebi KL, Teisberg TJ, Kalkstein LS et al (2004) Heat watch/warning systems save lives: estimated costs and benefits for Philadelphia 1995–98. Bull Am Meteorol Soc 85:1067–1074. https://doi. org/10.1175/BAMS-85-8-1067

Everitt B, Landau S, Leese M, Stahl D (2011) Cluster analysis. Wiley, Hoboken

Ferro, C. A. T., and D. B. Stephenson, 2011: Extremal Dependence Indices: Improved Verification

Measures for Deterministic Forecasts of Rare Binary Events. Wea. Forecasting, 26, 699–713, https://doi.org/10.1175/WAF-D-10-05030.1.

Fink AH, Knippertz P (2003) An extreme precipitation event in southern Morocco in spring 2002 and some hydrological implications. Weather 58:377–387. https://doi.org/10.1256/wea.256.02

Fink, A. H., and A. Reiner, 2003: Spatiotemporal variability of the relation between African Easterly Waves and West African Squall Lines in 1998 and 1999. Journal of Geophysical Research: Atmospheres, 108, https://doi.org/10.1029/2002JD002816.

Fischer EM, Schär C (2010) Consistent geographical patterns of changes in high-impact European heatwaves. Nat Geosci 3:398– 403. https://doi.org/10.1038/ngeo866

Fitzpatrick, R. G. J., C. L. Bain, P. Knippertz, J. H. Marsham, and D. J. Parker, 2015: The West African Monsoon Onset: A Concise Comparison of Definitions. J. Climate, 28, 8673–8694, https://doi.org/10.1175/JCLI-D-15-0265.1.

Foken T (2008) The energy balance closure problem: an overview. Ecol Appl 18:1351–1367. https://doi.org/10.1890/06-0922.1

Fontaine B, Janicot S, Monerie P-A (2013) Recent changes in air temperature, heat waves occurrences, and atmospheric circulation in Northern Africa. J Geophys Res 118:8536–8552. https://doi. org/10.1002/jgrd.50667

Gachon P, Bussières L, Gosselin P, Raphoz M, Bustinza R, Martin P, Dueymes G, Gosselin D, Labrecque S, Jeffers S, Yagouti A (2016) Guide to identifying alert thresholds for heat waves in Canada based on evidence. Co-edited by Université du Québec à Montréal, Environment and Climate Change Canada, Institut National de Santé Publique du Québec, and Health Canada, Mon-tréal, Québec, Canada, p 71.

García-Herrera R, Díaz J, Trigo RM et al (2010) A review of the European summer heat wave of 2003. Crit Rev Environ Sci Technol 40:267–306. https://doi.org/10.1080/10643380802238137

Gasparrini A, Armstrong B (2011) The impact of heat waves on mortality. Epidemiology 22:68–73. https://doi.org/10.1097/ EDE.0b013e3181fdcd99

Ghatak D, Zaitchik B, Hain C, Anderson M (2017) The role of local heating in the 2015 Indian Heat Wave. Sci Rep 7:7707. https:// doi.org/10.1038/s41598-017-07956-5

Gleixner, S., T. Demissie, and G. T. Diro, 2020: Did ERA5 Improve Temperature and Precipitation Reanalysis over East Africa? Atmosphere, 11, 996, https://doi.org/10.3390/atmos11090996.

Goldie J, Alexander L, Lewis SC, Sherwood S (2017) Comparative evaluation of human heat stress indices on selected hospital admissions in Sydney, Australia. Australian and New Zealand

Journal of Public Health 41:381–387. https://doi.org/10.1111/1753-6405.12692

Gounou A, Guichard F, Couvreux F (2012) Observations of diurnal cycles over a west african meridional transect: pre-monsoon and full-monsoon seasons. Bound Layer Meteorol 144:329–357. https://doi.org/10.1007/s10546-012-9723-8

Gronlund CJ, Zanobetti A, Schwartz JD, et al (2014) Heat, heat waves, and hospital admissions among the elderly in the United States, 1992-2006. Environ Health Perspect 122:1187–1192. https://doi.org/10.1289/ehp.1206132

Gu G, Adler RF (2004) Seasonal evolution and variability associated with the West African Monsoon System. J Clim 17:3364–3377. https://doi.org/10.1175/1520-0442(2004)017<3364:SEAVA W>2.0.CO;2

Guichard F (2014) Thermodynamic processes shaping Sahelian heat waves: analysis of selected case studies. AGU, Washington

Guichard F., L. Kergoat, E. Mougin, F. Timouk, F. Baup, P. Hiernaux, and F. Lavenu, 2009: Surface thermodynamics and radiative budget in the Sahelian Gourma: Seasonal and diurnal cycles. Journal of Hydrology, 375, 161–177, https://doi.org/10.1016/j.jhydrol.2008.09.007.

Guichard F, Kergoat L, Mougin E, Hourdin F (2012) The annual cycle of temperature in the Sahel and its climatic sensitivity. AGU Fall Meeting Abstracts 33:GC33A-1004

Guichard F., L.Kergoat, F. Hourdin, C. Léauthaud, J. Barbier, E. Mougin and B. Diarra (2017) Climate warming observed in the Sahel since 1950 , In 'Rural societies in the face of climatic and environmental changes in West Africa'. pp 23-42. Ed. B. Sultan, R. Lalou, M. A. Sanni, A. Oumarou, M. A. Soumaré. AN13: 9782709924245 and 9782709924269.

Guigma, K. H, Todd, M., Wang, Y., 2020a: Characteristics and thermodynamics of Sahelian Heatwaves analysed using various thermal indices, submitted to Climate Dynamics

Guigma, K. H., F. Guichard, M. Todd, P. Peyrille, and Y. Wang, 2020b: Atmospheric tropical modes are important drivers of Sahelian springtime heatwaves. Clim Dyn, https://doi.org/10.1007/s00382-020-05569-9.

Guirguis K, Gershunov A, Tardy A, Basu R (2013) The impact of recent heat waves on human health in California. J Appl Meteorol Climatol 53:3–19. https://doi.org/10.1175/JAMC-D-13-0130.1

Hall NMJ, Thibaut S, Marchesiello P (2017) Impact of the observed extratropics on climatological simulations of the MJO in a tropical channel model. Clim Dyn 48:2541–2555. https://doi.org/10.1007/s00382-016-3221-5

Hannachi A, Jolliffe IT, Stephenson DB (2007) Empirical orthogonal functions and related

techniques in atmospheric science: a review. Int J Climatol 27:1119–1152. https://doi.org/10.1002/ joc.1499

Hannachi A, Jolliffe IT, Stephenson DB, Trendafilov N (2006) In search of simple structures in climate: simplifying EOFs. Int J Climatol 26:7–28. https://doi.org/10.1002/joc.1243

Hansen J, Johnson D, Lacis A, et al (1981) Climate Impact of Increasing Atmospheric Carbon Dioxide. Science 213:957–966. https://doi.org/10.1126/science.213.4511.957

Harrington LJ, Otto FEL, Cowan T, Hegerl GC (2019) Circulation analogues and uncertainty in the time-evolution of extreme event probabilities: evidence from the 1947 Central European heatwave. Clim Dyn 53:2229–2247. https://doi.org/10.1007/s00382-019-04820-2

Harrington, L. J., and F. E. L. Otto, 2020: Reconciling theory with the reality of African heatwaves. Nature Climate Change, 1–3, https://doi.org/10.1038/s41558-020-0851-8.

Hartmann DL, Tank AMGK, Rusticucci M, et al (2013) Observations: atmosphere and surface. Climate Change 2013 the physical science basis. In: Working group I contribution to the fifth assessment report of the Intergovernmental Panel on Climate Change, pp 159–254. https://doi.org/10.1017/CBO9781107415324.008

Henderson, D., and Coauthors, 2020: Developing a harmonized heat warning and information system for Ontario: a case study in collaboration. Can J Public Health, 111, 426–432, https://doi.org/10.17269/s41997-020-00337-y.

Hentschel G (1987) A human biometeorology classification of climate for large and local scales. In Proceedings of WMO/HMO/UNEP symposium on climate and human health, Leningrad 1986, vol 1, WCPA—No. 1, WMO. K

Heo S, Bell ML (2019) Heat waves in South Korea: differences of heat wave characteristics by thermal indices. Journal of Exposure Science & Environmental Epidemiology 29:790–805. https://doi.org/10.1038/s41370-018-0076-3

Herrmann A, Sauerborn R (2018) General practitioners' perceptions of heat health impacts on the elderly in the face of climate change— a qualitative study in Baden-Württemberg, Germany. Int J Envi-ron Res Public Health. https://doi.org/10.3390/ijerph15050843

Hersbach, H., and Coauthors, 2020: The ERA5 global reanalysis. Quarterly Journal of the Royal Meteorological Society, 146, 1999–2049, https://doi.org/10.1002/qj.3803.

Hess, J. J., and Coauthors, 2018: Building Resilience to Climate Change: Pilot Evaluation of the Impact of India's First Heat Action Plan on All-Cause Mortality. Journal of Environmental and Public Health, 2018, e7973519, https://doi.org/10.1155/2018/7973519.

Hirons LC, Inness P, Vitart F, Bechtold P (2013) Understanding advances in the simulation of intraseasonal variability in the ECMWF model. Part I: The representation of the MJO.

Quarterly Journal of the Royal Meteorological Society 139:1417–1426. https://doi.org/10.1002/qj.2060

Hogan, R. J., and I. B. Mason, 2012: Deterministic Forecasts of Binary Events. Forecast Verification, John Wiley & Sons, Ltd, 31–59.

Hopp S, Dominici F, Bobb JF (2018) Medical diagnoses of heat wave-related hospital admissions in older adults. Prev Med 110:81–85. https://doi.org/10.1016/j.ypmed.2018.02.001

Hsu, P.-C, Qian Y., Liu Y., Murakami H., and Gao Y., 2020: Role of Abnormally Enhanced MJO over the Western Pacific in the Formation and Subseasonal Predictability of the Record-Breaking Northeast Asian Heatwave in the Summer of 2018. J. Climate, 33, 3333–3349, https://doi.org/10.1175/JCLI-D-19-0337.1.

Hsu, P.-C., J.-Y. Lee, K.-J. Ha, and C.-H. Tsou, 2017: Influences of Boreal Summer Intraseasonal Oscillation on Heat Waves in Monsoon Asia. J. Climate, 30, 7191–7211, https://doi.org/10.1175/JCLI-D-16-0505.1.

Hudson, D., A. G. Marshall, and O. Alves, 2011: Subseasonal Forecasting of the 2009 Summer and Winter Australian Heat Waves Using POAMA. Wea. Forecasting, 26, 257–279, https://doi.org/10.1175/WAF-D-10-05041.1.

Im E-S, Pal JS, Eltahir EAB (2017) Deadly heat waves projected in the densely populated agricultural regions of South Asia. Science Advances 3:e1603322. https://doi.org/10.1126/sciadv.1603322

International Labour Office 2019: Working on a warmer planet: The impact of heat stress and on labour productivity and decent work – Geneva, ILO, 2019. ISBN 978-92-2-132968-8

Jacques-Coper M, Brönnimann S, Martius O et al (2016) Summer heat waves in southeastern Patagonia: an analysis of the intraseasonal timescale. Int J Climatol 36:1359–1374. https://doi.org/10.1002/ joc.4430

Janicot S, Moron V, Fontaine B (1996) Sahel droughts and Enso dynamics. Geophysical Research Letters 23:515–518. https://doi.org/10.1029/96GL00246

Janiga, M. A., C. J. Schreck, J. A. Ridout, M. Flatau, N. P. Barton, E. J. Metzger, and C. A. Reynolds, 2018: Subseasonal Forecasts of Convectively Coupled Equatorial Waves and the MJO: Activity and Predictive Skill. Mon. Wea. Rev., 146, 2337–2360, https://doi.org/10.1175/MWR-D-17-0261.1.

Johnson H, Kovats S, McGregor G, et al (2005) The impact of the 2003 heat wave on daily mortality in England and Wales and the use of rapid weekly mortality estimates. Eurosurveillance 10:15–16. https://doi.org/10.2807/esm.10.07.00558-en

Jolliffe, I.T. and Stephenson, D.B. (2012) Forecast Verification: A Practitioner's Guide in

Atmospheric Science. 2nd Edition, Wiley-Blackwell, Oxford.

Judt, F., 2020: Atmospheric Predictability of the Tropics, Middle Latitudes, and Polar Regions Explored through Global Storm-Resolving Simulations. Journal of Atmospheric Sciences, 77, 257–276, https://doi.org/10.1175/JAS-D-19-0116.1.

Kalapureddy, M. C. R., M. Lothon, B. Campistron, F. Lohou, and F. Saïd, 2010: Wind profiler analysis of the African Easterly Jet in relation with the boundary layer and the Saharan heat-low. Quarterly Journal of the Royal Meteorological Society, 136, 77–91, https://doi.org/10.1002/qj.494.

Kamsu-Tamo PH, Janicot S, Monkam D, Lenouo A (2014) Convection activity over the Guinean coast and Central Africa during northern spring from synoptic to intra-seasonal timescales. Clim Dyn 43:3377–3401. https://doi.org/10.1007/s00382-014-2111-y

Keatinge WR (2003) Death in heat waves. BMJ 327:512–513

Keellings D, Bunting E, Engström J (2018) Spatiotemporal changes in the size and shape of heat waves over North America. Climatic Change 147:165–178. https://doi.org/10.1007/s10584-018-2140-3

Kiladis GN, Straub KH, Haertel PT (2005) Zonal and Vertical Structure of the Madden–Julian Oscillation. J Atmos Sci 62:2790–2809. https://doi.org/10.1175/JAS3520.1

Kiladis, G. N., C. D. Thorncroft, and N. M. J. Hall, 2006: Three-Dimensional Structure and Dynamics of African Easterly Waves. Part I: Observations. J. Atmos. Sci., 63, 2212–2230, https://doi.org/10.1175/JAS3741.1.

Kim Y-M, Kim S, Cheong H-K, Kim E-H (2011) Comparison of temperature indexes for the impact assessment of heat stress on heat-related mortality. Environ Health Toxicol. https://doi. org/10.5620/eht.2011.26.e2011009

Kim, H., F. Vitart, and D. E. Waliser, 2018: Prediction of the Madden–Julian Oscillation: A Review. J. Climate, 31, 9425–9443, https://doi.org/10.1175/JCLI-D-18-0210.1.

Klose M, Shao Y, Karremann MK, Fink AH (2010) Sahel dust zone and synoptic background. Geophysical Research Letters 37:. https://doi.org/10.1029/2010GL042816

Knippertz P (2003) Tropical-extratropical interactions causing precipitation in Northwest Africa: statistical analysis and seasonal variations. Mon Weather Rev 131:3069–3076. https://doi. org/10.1175/1520-0493(2003)131<3069:TICPIN>2.0.CO;2

Knippertz P, Martin JE (2005) Tropical plumes and extreme precipitation in subtropical and tropical West Africa. Q J R Meteorol Soc 131:2337–2365. https://doi.org/10.1256/qj.04.148

Knippertz P, Martin JE (2007) The role of dynamic and diabatic processes in the generation of cut-off lows over Northwest Africa. Meteorol Atmos Phys 96:3–19.

https://doi.org/10.1007/s0070 3-006-0217-4

Knippertz P, Todd MC (2012) Mineral dust aerosols over the Sahara: meteorological controls on emission and transport and implications for modeling. Rev Geophys. https://doi.org/10.1029/2011R G000362

Knippertz, P, and A. H. Fink, 2009: Prediction of Dry-Season Precipitation in Tropical West Africa and Its Relation to Forcing from the Extratropics. Wea. Forecasting, 24, 1064–1084, https://doi.org/10.1175/2009WAF2222221.1.

Knowlton, K., and Coauthors, 2014: Development and Implementation of South Asia's First Heat-Health Action Plan in Ahmedabad (Gujarat, India). International Journal of Environmental Research and Public Health, 11, 3473–3492, https://doi.org/10.3390/ijerph110403473.

Koutroulis AG, Grillakis MG, Tsanis IK, Jacob D (2018) Mapping the vulnerability of European summer tourism under 2 C global warming. Climatic Change 151:157–171. https://doi.org/10.1007/s10584-018-2298-8

Krstić G (2011) Apparent temperature and air pollution vs elderly population mortality in metro vancouver. PLoS ONE. https:// doi.org/10.1371/journal.pone.0025101

Kueh M-T, Lin C-Y, Chuang Y-J, et al (2017) Climate variability of heat waves and their associated diurnal temperature range variations in Taiwan. Environ Res Lett 12:074017. https://doi.org/10.1088/1748-9326/aa70d9

Lafore, J.-P., and Coauthors, 2017: A multi-scale analysis of the extreme rain event of Ouagadougou in 2009. Quarterly Journal of the Royal Meteorological Society, 143, 3094–3109, https://doi.org/10.1002/qj.3165.

Lam CKC, Loughnan M, Tapper N (2013) An exploration of temperature metrics for further developing the heat-health weather warning system in Hong Kong. In: International Scholarly Research Notices. https://www.hindawi.com/journals/isrn/2013/930238/. Accessed 8 Jan 2019

Largeron, Y., F. Guichard, R. Roehrig, F. Couvreux, and J. Barbier, 2020: The April 2010 North African heatwave: when the water vapor greenhouse effect drives nighttime temperatures. Clim Dyn, 54, 3879–3905, https://doi.org/10.1007/s00382-020-05204-7.

Lavaysse, C., C. Flamant, S. Janicot, D. J. Parker, J.-P. Lafore, B. Sultan, and J. Pelon, 2009: Seasonal evolution of the West African heat low: a climatological perspective. Clim Dyn, 33, 313–330, https://doi.org/10.1007/s00382-009-0553-4.

Lavaysse, C., G. Naumann, L. Alfieri, P. Salamon, and J. Vogt, 2019: Predictability of the European heat and cold waves. Clim Dyn, 52, 2481–2495, https://doi.org/10.1007/s00382-018-4273-5.

Lavender, S. L., and A. J. Matthews, 2009: Response of the West African Monsoon to the Madden–Julian Oscillation. J. Climate, 22, 4097–4116, https://doi.org/10.1175/2009JCLI2773.1.

Lee H-J, Lee W-S, Yoo JH (2016) Assessment of medium-range ensemble forecasts of heat waves. Atmos Sci Lett 17:19–25. https ://doi.org/10.1002/asl.593

Lélé, M. I., and P. J. Lamb, 2010: Variability of the Intertropical Front (ITF) and Rainfall over the West African Sudan–Sahel Zone. Journal of Climate, 23, 3984–4004, https://doi.org/10.1175/2010JCLI3277.1.

Lemonsu A, Viguié V, Daniel M, Masson V (2015) Vulnerability to heat waves: Impact of urban expansion scenarios on urban heat island and heat stress in Paris (France). Urban Climate 14:586–605. https://doi.org/10.1016/j.uclim.2015.10.007

Leuning R, van Gorsel E, Massman WJ, Isaac PR (2012) Reflections on the surface energy imbalance problem. Agric For Meteorol 156:65–74. https://doi.org/10.1016/j.agrformet.2011.12.002

Lhotka O, Kyselý J, Plavcová E (2018) Evaluation of major heat waves' mechanisms in EURO-CORDEX RCMs over Central Europe. Clim Dyn 50:4249–4262. https://doi.org/10.1007/s0038 2-017-3873-9

Li PW, Chan ST (2000) Application of a weather stress index for alerting the public to stressful weather in Hong Kong. Meteorol Appl 7:369–375. https://doi.org/10.1017/S1350482700001602

Li, Y., and S. N. Stechmann, 2020: Predictability of tropical rainfall and waves: Estimates from observational data. Quarterly Journal of the Royal Meteorological Society, 146, 1668–1684, https://doi.org/10.1002/qj.3759.

Liebmann B, Smith CA (1996) Description of a Complete (Interpolated) Outgoing Longwave Radiation Dataset. Bulletin of the American Meteorological Society 77:1275–1277

Liss A, Wu R, Chui KKH, Naumova EN (2017) Heat-Related Hospitalizations in Older Adults: An Amplified Effect of the First Seasonal Heatwave. Scientific Reports 7:39581. https://doi.org/10.1038/srep39581

Lowe, D., K. L. Ebi, and B. Forsberg, 2011: Heatwave Early Warning Systems and Adaptation Advice to Reduce Human Health Consequences of Heatwaves. Int J Environ Res Public Health, 8, 4623–4648, https://doi.org/10.3390/ijerph8124623.

Lowe, R., M. García-Díez, J. Ballester, J. Creswick, J.-M. Robine, F. R. Herrmann, and X. Rodó, 2016: Evaluation of an Early-Warning System for Heat Wave-Related Mortality in Europe: Implications for Sub-seasonal to Seasonal Forecasting and Climate Services. International Journal of Environmental Research and Public Health, 13, 206,

https://doi.org/10.3390/ijerph13020206.

Luo M, Lau N-C (2018) Synoptic characteristics, atmospheric controls, and long-term changes of heat waves over the Indochina Peninsula. Clim Dyn 51:2707–2723. https://doi.org/10.1007/s0038 2-017-4038-6

Macpherson RK (1962) The assessment of the thermal environment. Rev Occup Environ Med 19:151–164. https://doi.org/10.1136/ oem.19.3.151

Madden, R. A., and P. R. Julian, 1971: Detection of a 40–50 Day Oscillation in the Zonal Wind in the Tropical Pacific. J. Atmos. Sci., 28, 702–708, https://doi.org/10.1175/1520-0469(1971)028<0702:DOADOI>2.0.CO;2.

Madden, R. A., and P. R. Julian, 1972: Description of Global-Scale Circulation Cells in the Tropics with a 40–50 Day Period. J. Atmos. Sci., 29, 1109–1123, https://doi.org/10.1175/1520-0469(1972)029<1109:DOGSCC>2.0.CO;2.

Madden, R. A., and P. R. Julian, 1994: Observations of the 40–50-Day Tropical Oscillation—A Review. Mon. Wea. Rev., 122, 814–837, https://doi.org/10.1175/1520-0493(1994)122<0814:OOTDTO>2.0.CO;2.

Mandal, R., S. Joseph, A. K. Sahai, R. Phani, A. Dey, R. Chattopadhyay, and D. R. Pattanaik, 2019: Real time extended range prediction of heat waves over India. Scientific Reports, 9, 9008, https://doi.org/10.1038/s41598-019-45430-6.

Mann ME, Rahmstorf S, Kornhuber K, et al (2017) Influence of Anthropogenic Climate Change on Planetary Wave Resonance and Extreme Weather Events. Scientific Reports 7:45242. https://doi.org/10.1038/srep45242

Marshall, A. G., D. Hudson, M. C. Wheeler, O. Alves, H. H. Hendon, M. J. Pook, and J. S. Risbey, 2014: Intra-seasonal drivers of extreme heat over Australia in observations and POAMA-2. Clim Dyn, 43, 1915–1937, https://doi.org/10.1007/s00382-013-2016-1.

Martens, B., D. L. Schumacher, H. Wouters, J. Muñoz-Sabater, N. E. C. Verhoest, and D. G. Miralles, 2020: Evaluating the surface energy partitioning in ERA5. Geoscientific Model Development Discussions, 1–35, https://doi.org/10.5194/gmd-2019-315.

Masato G, Bone A, Charlton-Perez A et al (2015) Improving the health forecasting alert system for cold weather and heat-waves in eng-land: a proof-of-concept using temperature-mortality relationships. PLoS ONE 10:e0137804. https://doi.org/10.1371/journ al.pone.0137804

Matthies, F., and B. Menne, 2009: Prevention and management of health hazards related to heatwaves. International Journal of Circumpolar Health, 68, 8–12, https://doi.org/10.3402/ijch.v68i1.18293.

May JF, Guengant J-P, Barras V (2017) Demographic Challenges of the Sahel Countries. In: Groth

H, May JF (eds) Africa's Population: In Search of a Demographic Dividend. Springer International Publishing, Cham, pp 165–177

Mazdiyasni O, AghaKouchak A (2015) Substantial increase in concurrent droughts and heatwaves in the United States. Proc Natl Acad Sci U S A 112:11484–11489. https://doi.org/10.1073/pnas.1422945112

McElroy, S., L. Schwarz, H. Green, I. Corcos, K. Guirguis, A. Gershunov, and T. Benmarhnia, 2020: Defining heat waves and extreme heat events using sub-regional meteorological data to maximize benefits of early warning systems to population health. Science of The Total Environment, 721, 137678, https://doi.org/10.1016/j.scitotenv.2020.137678.

Meehl GA, Zwiers F, Evans J, et al (2000) Trends in Extreme Weather and Climate Events: Issues Related to Modeling Extremes in Projections of Future Climate Change. Bull Amer Meteor Soc 81:427–436. https://doi.org/10.1175/1520-0477(2000)081<0427:TIEWAC>2.3.CO;2

Meillassoux C (1974) Development or exploitation: is the Sahel famine good business? Review of African Political Economy 1:27–33. https://doi.org/10.1080/03056247408703235

Mekonnen A, Thorncroft CD, Aiyyer AR, Kiladis GN (2008) Convectively Coupled Kelvin Waves over Tropical Africa during the Boreal Summer: Structure and Variability. J Climate 21:6649–6667. https://doi.org/10.1175/2008JCLI2008.1

Mera, R., A. G. Laing, and F. Semazzi, 2014: Moisture Variability and Multiscale Interactions during Spring in West Africa. Mon. Wea. Rev., 142, 3178–3198, https://doi.org/10.1175/MWR-D-13-00175.1.

Meredith MP, Naveira Garabato AC, Hogg AM, Farneti R (2012) Sensitivity of the Overturning Circulation in the Southern Ocean to Decadal Changes in Wind Forcing. J Climate 25:99–110. https://doi.org/10.1175/2011JCLI4204.1

Middleton NJ (1985) Effect of drought on dust production in the Sahel. Nature 316:431–434. https://doi.org/10.1038/316431a0

Miralles DG, Teuling AJ, van Heerwaarden CC, Vilà-Guerau de Arel-lano J (2014) Mega-heatwave temperatures due to combined soil desiccation and atmospheric heat accumulation. Nat Geosci 7:345–349. https://doi.org/10.1038/ngeo2141

Mirza, M. M. Q., 2003: Climate change and extreme weather events: can developing countries adapt? Climate Policy, 3, 233–248, https://doi.org/10.1016/S1469-3062(03)00052-4.

Moore TR, Matthews HD, Simmons C, Leduc M (2015) Quantifying Changes in Extreme Weather Events in Response to Warmer Global Temperature. Atmosphere-Ocean 53:412–425. https://doi.org/10.1080/07055900.2015.1077099

Morabito M, Crisci A, Messeri A et al (2014) Environmental temperature and thermal indices: what

is the most effective predictor of heat-related mortality in different geographical contexts? Sci World J 2014:961750. https://doi.org/10.1155/2014/961750

Morabito, M., and Coauthors, 2019: An Occupational Heat–Health Warning System for Europe: The HEAT-SHIELD Platform. International Journal of Environmental Research and Public Health, 16, 2890, https://doi.org/10.3390/ijerph16162890.

Moreno A (2010) Mediterranean Tourism and Climate (Change): A Survey-Based Study. Tourism and Hospitality Planning & Development 7:253–265. https://doi.org/10.1080/1479053X.2010.502384

Moron, V., B. Oueslati, B. Pohl, S. Rome, and S. Janicot, 2016: Trends of mean temperatures and warm extremes in northern tropical Africa (1961–2014) from observed and PPCA-reconstructed time series. Journal of Geophysical Research: Atmospheres, 121, 5298–5319, https://doi.org/10.1002/2015JD024303.

Moron, V., B. Oueslati, B. Pohl and S. Janicot, 2018a: Daily Weather Types in February–June (1979–2016) and Temperature Variations in Tropical North Africa. J. Appl. Meteor. Climatol., 57, 1171–1195, https://doi.org/10.1175/JAMC-D-17-0105.1.

Moron, V, A. W. Robertson, and F. Vitart, 2018b: Editorial: Sub-seasonal to Seasonal Predictability and Prediction of Monsoon Climates. Front. Environ. Sci., 6, https://doi.org/10.3389/fenvs.2018.00083.

Mukherjee S, Mishra V (2018) A sixfold rise in concurrent day and night-time heatwaves in India under 2 C warming. Scientific Reports 8:16922. https://doi.org/10.1038/s41598-018-35348-w

Muller, R. A., and Coauthors, 2014: A New Estimate of the Average Earth Surface Land Temperature Spanning 1753 to 2011. Geoinformatics & Geostatistics: An Overview, 2013, https://doi.org/10.4172/2327-4581.1000101.

Murage P, Hajat S, Kovats RS (2017) Effect of night-time temperatures on cause and age-specific mortality in London. Environmental Epidemiology 1:e005. https://doi.org/10.1097/EE9.0000000000000005

Murari, K. K., A. S. Sahana, E. Daly, and S. Ghosh, 2016: The influence of the El Niño Southern Oscillation on heat waves in India. Meteorological Applications, 23, 705–713, https://doi.org/10.1002/met.1594.

Nairn J, Fawcett R (2013) Defining heatwaves: heatwave defined as a heat-impact event servicing all community and business sectors in Australia. Centre for Australian Weather and Climate Research, Sydney, p 96

Nangombe SS, Zhou T, Zhang W, Zou L, Li D (2019) High-temperature extreme events over

Africa under 1.5 and 2 C of global warming. J Geophys Res Atmos 124:4413–4428. https://doi. org/10.1029/2018JD029747

Napoli CD, Barnard C, Prudhomme C, Cloke HL, Pappenberger F (2020) ERA5-HEAT: A global gridded historical dataset of human thermal comfort indices from climate reanalysis. Geosci Data J. https://doi.org/10.1002/gdj3.102

Nerem RS, Beckley BD, Fasullo JT, et al (2018) Climate-change–driven accelerated sea-level rise detected in the altimeter era. PNAS 115:2022–2025. https://doi.org/10.1073/pnas.1717312115

New M, Hewitson B, Stephenson DB, et al (2006) Evidence of trends in daily climate extremes over southern and west Africa. Journal of Geophysical Research: Atmospheres 111:. https://doi.org/10.1029/2005JD006289

Nguyen, H., C. D. Thorncroft, and C. Zhang, 2011: Guinean coastal rainfall of the West African Monsoon. Quarterly Journal of the Royal Meteorological Society, 137, 1828–1840, https://doi.org/10.1002/qj.867.

Nicholls L, Strengers Y (2018) Heatwaves, cooling and young children at home: Integrating energy and health objectives. Energy Research & Social Science 39:1–9. https://doi.org/10.1016/j.erss.2017.10.002

Nicholls, N., C. Skinner, M. Loughnan, and N. Tapper, 2008: A simple heat alert system for Melbourne, Australia. Int J Biometeorol, 52, 375–384, https://doi.org/10.1007/s00484-007-0132-5.

Nicholson, S. E., 2013: The West African Sahel: A Review of Recent Studies on the Rainfall Regime and Its Interannual Variability. ISRN Meteorology, 2013, e453521, https://doi.org/10.1155/2013/453521.

https://www.hindawi.com/journals/isrn/2013/453521/. Accessed 26 Aug 2020

Nicholson, S. E., 2011: *Dryland Climatology.* Cambridge University Press, 516 pp.

Nicholson, S. E., 2018: Climate of the Sahel and West Africa. Oxford Research Encyclopedia of Climate Science, https://doi.org/10.1093/acrefore/9780190228620.013.510.

Nicholson SE, Webster PJ (2007) A physical basis for the interannual variability of rainfall in the Sahel. Quarterly Journal of the Royal Meteorological Society 133:2065–2084. https://doi.org/10.1002/qj.104

Nissan, H., K. Burkart, E. Coughlan de Perez, M. Van Aalst, and S. Mason, 2017: Defining and Predicting Heat Waves in Bangladesh. J. Appl. Meteor. Climatol., 56, 2653–2670, https://doi.org/10.1175/JAMC-D-17-0035.1.

Nitschke, M., G. Tucker, A. Hansen, S. Williams, Y. Zhang, and P. Bi, 2016: Evaluation of a heat

warning system in Adelaide, South Australia, using case-series analysis. BMJ Open, 6, e012125, https://doi.org/10.1136/bmjopen-2016-012125.

NOAA National Centers for Environmental Information, State of the Climate: Global Climate Report for Annual 2020, published online January 2021, retrieved on January 20, 2021 from https://www.ncdc.noaa.gov/sotc/global/202013.

Olauson, J., 2018: ERA5: The new champion of wind power modelling? Renewable Energy, 126, 322–331, https://doi.org/10.1016/j.renene.2018.03.056.

Oppermann E, Brearley M, Law L et al (2017) Heat, health, and humidity in Australia's monsoon tropics: a critical review of the prob-lematization of 'heat' in a changing climate. Wiley Interdiscip Rev Clim Change 8:e468. https://doi.org/10.1002/wcc.468

Oudin Åström D, Bertil F, Joacim R (2011) Heat wave impact on morbidity and mortality in the elderly population: A review of recent studies. Maturitas 69:99–105. https://doi.org/10.1016/j.maturitas.2011.03.008

Ouedraogo LS, Mundler P (2019) Local Governance and Labor Organizations on Artisanal Gold Mining Sites in Burkina Faso. Sus-tainability 11:616. https://doi.org/10.3390/su11030616

Oueslati, B., B. Pohl, V. Moron, S. Rome, and S. Janicot, 2017: Characterization of Heat Waves in the Sahel and Associated Physical Mechanisms. J. Climate, 30, 3095–3115, https://doi.org/10.1175/JCLI-D-16-0432.1.

Palin EJ, Thornton HE, Mathison CT et al (2013) Future projections of temperature-related climate change impacts on the railway network of Great Britain. Clim Change 120:71–93. https://doi. org/10.1007/s10584-013-0810-8

Palmer TN, Doblas-Reyes FJ, Weisheimer A, Rodwell MJ (2008) Toward Seamless Prediction: Calibration of Climate Change Projections Using Seasonal Forecasts. Bull Amer Meteor Soc 89:459–470. https://doi.org/10.1175/BAMS-89-4-459

Panda DK, AghaKouchak A, Ambast SK (2017) Increasing heat waves and warm spells in India, observed from a multiaspect framework. J Geophys Res Atmos 122:3837–3858. https://doi. org/10.1002/2016JD026292

Pappenberger F, Jendritzky G, Staiger H et al (2015) Global forecasting of thermal health hazards: the skill of probabilistic predictions of the Universal Thermal Climate Index (UTCI). Int J Biometeorol 59:311–323. https://doi.org/10.1007/s00484-014-0843-3

Parker DJ, Burton RR, Diongue- Niang A, et al (2005) The diurnal cycle of the West African monsoon circulation. Quarterly Journal of the Royal Meteorological Society 131:2839–2860. https://doi.org/10.1256/qj.04.52

Parker, T. J., G. J. Berry, M. J. Reeder, and N. Nicholls, 2014: Modes of climate variability and heat

waves in Victoria, southeastern Australia. Geophysical Research Letters, 41, 6926–6934, https://doi.org/10.1002/2014GL061736.

Pearson KJ, Hogan RJ, Allan RP, et al (2010) Evaluation of the model representation of the evolution of convective systems using satellite observations of outgoing longwave radiation. Journal of Geophysical Research: Atmospheres 115:. https://doi.org/10.1029/2010JD014265

Pechan A, Eisenack K (2014) The impact of heat waves on electricity spot markets. Energy Economics 43:63–71. https://doi.org/10.1016/j.eneco.2014.02.006

Perez EC de, Aalst M van, Bischiniotis K, et al (2018) Global predictability of temperature extremes. Environ Res Lett 13:054017. https://doi.org/10.1088/1748-9326/aab94a

Perkins, S. E., 2015: A review on the scientific understanding of heatwaves—Their measurement, driving mechanisms, and changes at the global scale. Atmospheric Research, 164–165, 242–267, https://doi.org/10.1016/j.atmosres.2015.05.014.

Perkins SE, Alexander LV (2012) On the measurement of heat waves. J Clim 26:4500–4517. https://doi.org/10.1175/JCLI-D-12-00383.1

Perkins SE, Alexander LV, Nairn JR (2012) Increasing frequency, intensity and duration of observed global heatwaves and warm spells. Geophysical Research Letters 39:. https://doi.org/10.1029/2012GL053361

Perkins-Kirkpatrick SE, Gibson PB (2017) Changes in regional heat-wave characteristics as a function of increasing global temperature. Sci Rep 7:12256. https://doi.org/10.1038/s41598-017-12520-2

Perkins-Kirkpatrick SE, Lewis SC (2020) Increasing trends in regional heatwaves. Nature Communications 11:3357. https://doi.org/10.1038/s41467-020-16970-7

Perry A (2000) Impacts of climate change on tourism in the mediter-ranean: adaptive responses. Social Science Research Network, Rochester

Poan ED, Gachon P, Dueymes G, et al (2016) West African monsoon intraseasonal activity and its daily precipitation indices in regional climate models: diagnostics and challenges. Clim Dyn 47:3113–3140. https://doi.org/10.1007/s00382-016-3016-8

Potter SH, Kreft PV, Milojev P et al (2018) The influence of impact-based severe weather warnings on risk perceptions and intended protective actions. Int J Disaster Risk Reduct 30:34–43. https:// doi.org/10.1016/j.ijdrr.2018.03.031

QI, X., and J. YANG, 2019: Extended-range prediction of a heat wave event over the Yangtze River Valley: role of subseasonal signals. Atmospheric and Oceanic Science Letters, 12, 451–457, https://doi.org/10.1080/16742834.2019.1669408.

Quak E (2018) Drivers, challenges and opportunities for job creation in the Sahel: K4D helpdesk report 455. Institute of Development Studies, Brighton

Ramon, J., L. Lledó, V. Torralba, A. Soret, and F. J. Doblas-Reyes, 2019: What global reanalysis best represents near-surface winds? Quarterly Journal of the Royal Meteorological Society, 145, 3236–3251, https://doi.org/10.1002/qj.3616.

Raymond, C., T. Matthews, and R. M. Horton, 2020: The emergence of heat and humidity too severe for human tolerance. Science Advances, 6, eaaw1838, https://doi.org/10.1126/sciadv.aaw1838.

Reed, R. J., E. Klinker, and A. Hollingsworth, 1988: The structure and characteristics of African easterly wave disturbances as determined from the ECMWF operational analysis/forecast system. Meteorl. Atmos. Phys., 38, 22–33, https://doi.org/10.1007/BF01029944.

Richman MB (1986) Rotation of principal components. J Climatol 6:293–335. https://doi.org/10.1002/joc.3370060305

Riley, E. M., B. E. Mapes, and S. N. Tulich, 2011: Clouds Associated with the Madden–Julian Oscillation: A New Perspective from CloudSat. J. Atmos. Sci., 68, 3032–3051, https://doi.org/10.1175/JAS-D-11-030.1.

Ringard J, Dieppois B, Rome S, et al (2016) The intensification of thermal extremes in west Africa. Global and Planetary Change 139:66–77. https://doi.org/10.1016/j.gloplacha.2015.12.009

Roberts AJ, Marsham JH, Knippertz P (2014) Disagreements in low-level moisture between (re)analyses over summertime West Africa. Mon Weather Rev 143:1193–1211. https://doi.org/10.1175/MWR-D-14-00218.1

Roberts AJ, Marsham JH, Knippertz P et al (2017) New Saharan wind observations reveal substantial biases in analysed dust-generating winds. Atmos Sci Lett 18:366–372. https://doi.org/10.1002/ asl.765

Robinson PJ (2001) On the definition of a heat wave. J Appl Meteorol 40:762–775. https ://doi.org/10.1175/1520-0450(2001)040<0762:OTDOAH>2.0.CO;2

Roehrig R, Chauvin F, Lafore J-P (2011) 10–25-Day Intraseasonal Variability of Convection over the Sahel: A Role of the Saharan Heat Low and Midlatitudes. J Climate 24:5863–5878. https://doi.org/10.1175/2011JCLI3960.1

Rohat G, Flacke J, Dosio A, Dao H, van Maarseveen M (2019) Projections of human exposure to dangerous heat in African cities under multiple socioeconomic and climate scenarios. Earth's Future 7:528–546. https://doi.org/10.1029/2018EF001020

Rohde, R., and Coauthors, 2016: Berkeley Earth Temperature Averaging Process. Geoinformatics & Geostatistics: An Overview, 2013, https://doi.org/10.4172/2327-4581.1000103.

Rohini P, Rajeevan M, Mukhopadhay P (2019) Future projections of heat waves over India from CMIP5 models. Clim Dyn 53:975–988. https://doi.org/10.1007/s00382-019-04700-9

Russo S, Dosio A, Graversen RG, et al (2014) Magnitude of extreme heat waves in present climate and their projection in a warming world. Journal of Geophysical Research: Atmospheres 119:12,500-12,512. https://doi.org/10.1002/2014JD022098

Russo S, Marchese AF, Sillmann J, Immé G (2016) When will unusual heat waves become normal in a warming Africa? Environ Res Lett 11:054016. https://doi.org/10.1088/1748-9326/11/5/054016

Salack S, Saley IA, Bliefernicht J (2018) Observed data of extreme rainfall events over the West African Sahel. Data in Brief 20:1274–1278. https://doi.org/10.1016/j.dib.2018.09.001

Sambou M-JG, Janicot S, Pohl B, Badiane D, Dieng AL, Gaye A (2020) Heat wave occurrences over Senegal during spring: regionalization and synoptic patterns. Int J Climatol 40:440–457. https://doi.org/10.1002/joc.6220

Sarath Chandran MA, Subba Rao AVM, Sandeep VM, et al (2017) Indian summer heat wave of 2015: a biometeorological analysis using half hourly automatic weather station data with special reference to Andhra Pradesh. Int J Biometeorol 61:1063–1072. https://doi.org/10.1007/s00484-016-1286-9

Schamm, K., M. Ziese, A. Becker, P. Finger, A. Meyer-Christoffer, U. Schneider, M. Schröder, and P. Stender, 2014: Global gridded precipitation over land: a description of the new GPCC First Guess Daily product. Earth System Science Data, 6, 49–60, https://doi.org/10.5194/essd-6-49-2014.

Schär C (2016) The worst heat waves to come. Nat Clim Change 6:128–129. https://doi.org/10.1038/nclimate2864

Schlueter, A., A. H. Fink, P. Knippertz, and P. Vogel, 2019a: A Systematic Comparison of Tropical Waves over Northern Africa. Part I: Influence on Rainfall. J. Climate, 32, 1501–1523, https://doi.org/10.1175/JCLI-D-18-0173.1.

Schlueter, A., A. H. Fink, and P. Knippertz, 2019b: A Systematic Comparison of Tropical Waves over Northern Africa. Part II: Dynamics and Thermodynamics. J. Climate, 32, 2605–2625, https://doi.org/10.1175/JCLI-D-18-0651.1.

Schoof JT, Ford TW, Pryor SC (2017) Recent changes in US regional heat wave characteristics in observations and reanalyses. J Appl Meteor Climatol 56:2621–2636. https://doi.org/10.1175/ JAMC-D-16-0393.1

Schreck, C. J, J. Molinari, and K. I. Mohr, 2011: Attributing Tropical Cyclogenesis to Equatorial Waves in the Western North Pacific. J. Atmos. Sci., 68, 195–209,

https://doi.org/10.1175/2010JAS3396.1.

Schreck, C. J., and J. Molinari, 2011: Tropical Cyclogenesis Associated with Kelvin Waves and the Madden–Julian Oscillation. Mon. Wea. Rev., 139, 2723–2734, https://doi.org/10.1175/MWR-D-10-05060.1.

Sfîcă L, Croitoru A-E, Iordache I, Ciupertea A-F (2017) Synoptic conditions generating heat waves and warm spells in Romania. Atmosphere 8:50. https://doi.org/10.3390/atmos8030050

Sharma S, Mujumdar P (2017) Increasing frequency and spatial extent of concurrent meteorological droughts and heatwaves in India. Scientific Reports 7:15582. https://doi.org/10.1038/s41598-017-15896-3

Slingo, A., H. E. White, N. A. Bharmal, and G. J. Robinson, 2009: Overview of observations from the RADAGAST experiment in Niamey, Niger: 2. Radiative fluxes and divergences. Journal of Geophysical Research: Atmospheres, 114, https://doi.org/10.1029/2008JD010497.

Smith TT, Zaitchik BF, Gohlke JM (2013) Heat waves in the United States: definitions, patterns and trends. Clim Change 118:811– 825. https://doi.org/10.1007/s10584-012-0659-2

Smoyer-Tomic KE, Kuhn R, Hudson A (2003) Heat wave hazards: an overview of heat wave impacts in Canada. Nat Hazards 28:465– 486. https://doi.org/10.1023/A:1022946528157

Song, E.-J., and K.-H. Seo, 2016: Past- and present-day Madden-Julian Oscillation in CNRM-CM5. Geophysical Research Letters, 43, 4042–4048, https://doi.org/10.1002/2016GL068771.

Sossa, A., B. Liebmann, I. Bladé, D. Allured, H. H. Hendon, P. Peterson, and A. Hoell, 2017: Statistical Connection between the Madden–Julian Oscillation and Large Daily Precipitation Events in West Africa. J. Climate, 30, 1999–2010, https://doi.org/10.1175/JCLI-D-16-0144.1.

Souch C, Grimmond S (2006) Applied climatology: urban climate. Prog Phys Geogr Earth Environ 30:270–279. https://doi. org/10.1191/0309133306pp484pr

Stammerjohn SE, Martinson DG, Smith RC, Iannuzzi RA (2008) Sea ice in the western Antarctic Peninsula region: Spatio-temporal variability from ecological and climate change perspectives. Deep Sea Research Part II: Topical Studies in Oceanography 55:2041–2058. https://doi.org/10.1016/j.dsr2.2008.04.026

Steadman, R. G., 1979: The Assessment of Sultriness. Part I: A Temperature-Humidity Index Based on Human Physiology and Clothing Science. J. Appl. Meteor., 18, 861–873, https://doi.org/10.1175/1520-0450(1979)018<0861:TAOSPI>2.0.CO;2.

Steadman RG (1994) Norms of apparent temperature in Australia. Aust Meteorol Mag 43:1–16

Stott, P., 2016: How climate change affects extreme weather events. Science, 352, 1517–1518,

https://doi.org/10.1126/science.aaf7271.

Straub KH, Kiladis GN (2002) Observations of a Convectively Coupled Kelvin Wave in the Eastern Pacific ITCZ. J Atmos Sci 59:30–53. https://doi.org/10.1175/1520-0469(2002)059<0030:OOACCK>2.0.CO;2

Sultan B, Janicot S, Diedhiou A (2003) The West African Monsoon Dynamics. Part I: Documentation of Intraseasonal Variability. J Climate 16:3389–3406. https://doi.org/10.1175/1520-0442(2003)016<3389:TWAMDP>2.0.CO;2

Sylla MB, Gaye AT, Jenkins GS (2012) On the Fine-Scale Topography Regulating Changes in Atmospheric Hydrological Cycle and Extreme Rainfall over West Africa in a Regional Climate Model Projections. In: International Journal of Geophysics. https://www.hindawi.com/journals/ijge/2012/981649/. Accessed 26 Aug 2020

Sylla, M. B., A. Faye, F. Giorgi, A. Diedhiou, and H. Kunstmann, 2018: Projected Heat Stress Under 1.5 C and 2 C Global Warming Scenarios Creates Unprecedented Discomfort for Humans in West Africa. Earth's Future, 6, 1029–1044, https://doi.org/10.1029/2018EF000873.

Tall M, Albergel C, Bonan B, et al (2019) Towards a Long-Term Reanalysis of Land Surface Variables over Western Africa: LDAS-Monde Applied over Burkina Faso from 2001 to 2018. Remote Sensing 11:735. https://doi.org/10.3390/rs11060735

Taylor CM, Belušić D, Guichard F, et al (2017) Frequency of extreme Sahelian storms tripled since 1982 in satellite observations. Nature 544:475–478. https://doi.org/10.1038/nature22069

Tazen F, Diarra A, Kabore RFW, et al (2019) Trends in flood events and their relationship to extreme rainfall in an urban area of Sahelian West Africa: The case study of Ouagadougou, Burkina Faso. Journal of Flood Risk Management 12:e12507. https://doi.org/10.1111/jfr3.12507

Thorncroft CD, Nguyen H, Zhang C, Peyrillé P (2011) Annual cycle of the West African monsoon: regional circulations and associated water vapour transport. Q J R Meteorol Soc 137:129–147. https ://doi.org/10.1002/qj.728

Toloo GS, Yu W, Aitken P, et al (2014) The impact of heatwaves on emergency department visits in Brisbane, Australia: a time series study. Crit Care 18:R69. https://doi.org/10.1186/cc13826

Trang PM, Rocklöv J, Giang KB, et al (2016) Heatwaves and Hospital Admissions for Mental Disorders in Northern Vietnam. PLOS ONE 11:e0155609. https://doi.org/10.1371/journal.pone.0155609

Tschakert, P., 2007: Views from the vulnerable: Understanding climatic and other stressors in the

Sahel. Global Environmental Change, 17, 381–396, https://doi.org/10.1016/j.gloenvcha.2006.11.008.

Tulet P, Mallet M, Pont V, et al (2008) The 7–13 March 2006 dust storm over West Africa: Generation, transport, and vertical stratification. Journal of Geophysical Research: Atmospheres 113:. https://doi.org/10.1029/2008JD009871

van der Velde M, Wriedt G, Bouraoui F (2010) Estimating irrigation use and effects on maize yield during the 2003 heatwave in France. Agriculture, Ecosystems & Environment 135:90–97. https://doi.org/10.1016/j.agee.2009.08.017

van Loenhout JAF, Delbiso TD, Kiriliouk A, et al (2018) Heat and emergency room admissions in the Netherlands. BMC Public Health 18:108. https://doi.org/10.1186/s12889-017-5021-1

Ventrice, M. J., and C. D. Thorncroft, 2012: The Role of Convectively Coupled Atmospheric Kelvin Waves on African Easterly Wave Activity. Mon. Wea. Rev., 141, 1910–1924, https://doi.org/10.1175/MWR-D-12-00147.1.

Wang H, Loeb NG, Su W, Rose FG, Kato S, Doelling DR (2017) Evaluating Radiative Fluxes in Current Reanalyses using CERES EBAF-TOA and EBAF-Surface Ed4.0. 23. Presented at the Fall 2017 CERES Science Team Meeting, September 2017. https://ceres.larc.nasa.gov/documents/STM/2017-

Wang, Y., M. Notaro, Z. Liu, R. Gallimore, S. Levis, and J. E. Kutzbach, 2008: Detecting vegetation-precipitation feedbacks in mid-Holocene North Africa from two climate models. Climate of the Past, 4, 59–67, https://doi.org/10.5194/cp-4-59-2008.

Watts N, Amann M, Arnell N, et al (2018) The 2018 report of the Lancet Countdown on health and climate change: shaping the health of nations for centuries to come. The Lancet 392:2479–2514. https://doi.org/10.1016/S0140-6736(18)32594-7

Webster PJ, Jian J (2011) Environmental prediction, risk assessment and extreme events: adaptation strategies for the developing world. Philos Trans A Math Phys Eng Sci 369:4768–4797. https://doi.org/10.1098/rsta.2011.0160

Weyrich P, Scolobig A, Bresch DN, Patt A (2018) Effects of impact-based warnings and behavioral recommendations for extreme weather events. Weather Clim Soc 10:781–796. https://doi.org/10.1175/WCAS-D-18-0038.1

Wheeler MC and Nguyen H (2015) TROPICAL METEOROLOGY AND CLIMATE | Equatorial Waves. In: North GR, Pyle J, Zhang F (eds) Encyclopedia of Atmospheric Sciences (Second Edition). Academic Press, Oxford, pp 102–112

Wheeler, M. C, H. Zhu, A. H. Sobel, D. Hudson, and F. Vitart, 2017: Seamless precipitation prediction skill comparison between two global models. Quarterly Journal of the Royal

Meteorological Society, 143, 374–383, https://doi.org/10.1002/qj.2928.

Wheeler, M. C., and H. H. Hendon, 2004: An All-Season Real-Time Multivariate MJO Index: Development of an Index for Monitoring and Prediction. Mon. Wea. Rev., 132, 1917–1932, https://doi.org/10.1175/1520-0493(2004)132<1917:AARMMI>2.0.CO;2.

Wheeler, M., and G. N. Kiladis, 1999: Convectively Coupled Equatorial Waves: Analysis of Clouds and Temperature in the Wavenumber–Frequency Domain. J. Atmos. Sci., 56, 374–399, https://doi.org/10.1175/1520-0469(1999)056<0374:CCEWAO>2.0.CO;2.

White, C. J., and Coauthors, 2017: Potential applications of subseasonal-to-seasonal (S2S) predictions. Meteorological Applications, 24, 315–325, https://doi.org/10.1002/met.1654.

Wielicki, B. A., B. R. Barkstrom, E. F. Harrison, R. B. Lee, G. L. Smith, and J. E. Cooper, 1996: Clouds and the Earth's Radiant Energy System (CERES): An Earth Observing System Experiment. Bull. Amer. Meteor. Soc., 77, 853–868, https://doi.org/10.1175/1520-0477(1996)077<0853:CATERE>2.0.CO;2.

Wilkinson, E., L. Weingärtner, R. Choularton, M. Bailey, M. Todd, D. Kniveton, and C. Cabot Venton, 2018: Forecasting hazards, averting disasters: Implementing forecast-based early action at scale. Overseas Development Institute (ODI), http://lib.riskreductionafrica.org/handle/123456789/1501 (Accessed January 3, 2019).

Willett KM, Sherwood S (2012) Exceedance of heat index thresholds for 15 regions under a warming climate using the wet-bulb globe temperature. Int J Climatol 32:161–177. https://doi.org/10.1002/ joc.2257

Woltering L, Pasternak D, Ndjeunga J (2011) The African market garden: the development of a low-pressure drip irrigation system for smallholders in the sudano sahel. Irrig Drain 60:613–621. https ://doi.org/10.1002/ird.610

World Meteorological Organization (2015) Guidelines on multi-hazard impact-based forecast and warning services. WMO-No.1150, Geneva

World Meteorological Organization and World Health Organization (2015) Heatwaves and health: guidance on warning-system development. WMO-No. 1142, Geneva.

Wright, J. S., and Coauthors, 2020: Differences in tropical high clouds among reanalyses: origins and radiative impacts. Atmospheric Chemistry and Physics, 20, 8989–9030, https://doi.org/10.5194/acp-20-8989-2020.

Xavier, P., R. Rahmat, W. K. Cheong, and E. Wallace, 2014: Influence of Madden-Julian Oscillation on Southeast Asia rainfall extremes: Observations and predictability. Geophysical Research Letters, 41, 4406–4412, https://doi.org/10.1002/2014GL060241.

Xu J, Grumbine RE, Shrestha A, et al (2009) The Melting Himalayas: Cascading Effects of Climate

Change on Water, Biodiversity, and Livelihoods. Conservation Biology 23:520–530. https://doi.org/10.1111/j.1523-1739.2009.01237.x

Xu Z, Crooks JL, Black D et al (2017) Heatwave and infants' hospital admissions under different heatwave definitions. Environ Pollut 229:525–530. https://doi.org/10.1016/j.envpol.2017.06.030

Xu Z, FitzGerald G, Guo Y et al (2016) Impact of heatwave on mortality under different heatwave definitions: a systematic review and meta-analysis. Environ Int 89–90:193–203. https://doi.org/10.1016/j.envint.2016.02.007

Xu Z, Sheffield PE, Su H, et al (2014) The impact of heat waves on children's health: a systematic review. Int J Biometeorol 58:239–247. https://doi.org/10.1007/s00484-013-0655-x

Xu, C., T. A. Kohler, T. M. Lenton, J.-C. Svenning, and M. Scheffer, 2020: Future of the human climate niche. PNAS, 117, 11350–11355, https://doi.org/10.1073/pnas.1910114117.

Yang, G.-Y., J. Methven, S. Woolnough, K. Hodges, and B. Hoskins, 2018: Linking African Easterly Wave Activity with Equatorial Waves and the Influence of Rossby Waves from the Southern Hemisphere. J. Atmos. Sci., 75, 1783–1809, https://doi.org/10.1175/JAS-D-17-0184.1.

Yin Q, Wang J (2017) The association between consecutive days' heat wave and cardiovascular disease mortality in Beijing, China. BMC Public Health 17:223. https://doi.org/10.1186/s12889-017-4129-7

Zhang K, Rood RB, Michailidis G et al (2012) Comparing exposure metrics for classifying "dangerous heat" in heat wave and health warning systems. Environ Int 46:23–29. https://doi.org/10.1016/j. envint.2012.05.001